Universidade de Aveiro Departamento de Engenharia Mecânica
Ano 2020

CLÁUDIA PATRÍCIA CÂNDIDO DO AMARAL

A NANOTECNOLOGIA NA CONSTRUÇÃO: ESTUDO EXPERIMENTAL E NUMÉRICO DE SOLUÇÕES CONSTRUTIVAS COM MATERIAIS DE MUDANÇA DE FASE

NANOTECHNOLOGY APPLIED TO CONSTRUCTION: EXPERIMENTAL AND NUMERICAL STUDY OF BUILDING SOLUTIONS WITH PHASE CHANGE MATERIALS

Universidade de Aveiro Departamento de Engenharia Mecânica
Ano 2020

CLÁUDIA PATRÍCIA CÂNDIDO DO AMARAL

A NANOTECNOLOGIA NA CONSTRUÇÃO: ESTUDO EXPERIMENTAL E NUMÉRICO DE SOLUÇÕES CONSTRUTIVAS COM MATERIAIS DE MUDANÇA DE FASE

Tese apresentada à Universidade de Aveiro para cumprimento dos requisitos necessários à obtenção do grau de Doutor em Nanociências e Nanotecnologia, realizada sob a orientação científica do Doutor Romeu da Silva Vicente, Professor Associado do Departamento de Engenharia Civil da Universidade de Aveiro e coorientação da Doutora Paula Alexandrina de Aguiar Pereira Marques, Investigadora Principal do Departamento de Engenharia Mecânica da Universidade de Aveiro e da Doutora Ana Margarida Madeira Viegas de Barros Timmons, Professora Auxiliar do Departamento de Química da Universidade de Aveiro.

Dedico este trabalho ao meu marido e aos meus filhos

o júri

presidente

Prof. Doutor Armando Domingos Batista Machado
professor catedrático da Universidade do Aveiro

vogais

Prof. Doutor Victor Miguel Carneiro de Sousa Ferreira
professor catedrático da Universidade do Aveiro

Prof. Doutor Romeu da Silva Vicente
professor associado da Universidade do Aveiro

Prof. Doutor José Joaquim da Costa
professor auxiliar da Faculdade de Ciências e Tecnologia da Universidade de Coimbra

Prof. Doutor Nuno Albino Vieira Simões
professor auxiliar da Faculdade de Ciências e Tecnologia da Universidade de Coimbra

Prof. Doutora Olinda Coelho Monteiro
investigadora da Universidade de Lisboa

agradecimentos

Concluir uma tese de doutoramento implica uma longa jornada, em grande medida individual e solitária, difícil de levar a "bom porto" sem o apoio de uma rede de pessoas e instituições a quem quero aqui deixar os meus sinceros agradecimentos. E muitos participaram nesta longa jornada, por vezes incerta, outras vezes desafiante e divertida, dando apoio nas horas certas, oferecendo ajuda, sem o saber, e muitas vezes direcionando determinados caminhos.

Em primeiro lugar, agradeço ao meu orientador, professor Doutor Romeu Vicente, pela orientação, apoio e contribuição científica, ajuda e pela relação de proximidade, que se traduziu em muitos momentos de reflexão e crescimento pessoal e profissional. À minha coorientadora, professora Doutora Paula Marques pela disponibilidade, discussão de ideias e acima de tudo pelas oportunidades de aprendizagem. Á minha coorientadora, professora Doutora Ana Barros, pela seu empenho, leituras minuciosas e questões pertinentes que contribuíram de forma decisiva para o bom rumo desta tese.

À Universidade de Aveiro, em especial ao Departamento de Engenharia Civil e ao Departamento de Engenharia Mecânica, pelo acolhimento, e aos seus professores e funcionários pelo apoio e ajuda. Em especial ao professor Doutor Victor Ferreira, à engenheira Maria Carlos e ao técnico Vítor Rodrigues pela ajuda prestada no laboratório e pela disponibilidade apresentada durante a campanha experimental. Ao Doutor Nuno Gama pela ajuda, motivação e apoio.

Ao Instituto Fraunhofer na Alemanha (Fraunhofer Institute for Chemical Technology, ICT laboratory) pela disponibilidade de serviços e ajuda, em especial ao engenheiro Kristian Kowollik.

Agradeço a todos os meus amigos e colegas de trabalho, em especial ao André, ao António, à Márcia e ao Flávio pela sua amizade e apoio, bem como todas as vezes que me incentivaram a sair do "meu canto isolado" para fazer pausas recheadas de conversas animadas e aliciantes.

Um agradecimento especial à minha família, em particular aos meus pais, ao meu irmão e aos meus sobrinhos, a quem foram retiradas muitas horas da minha presença, que me apoiaram incondicionalmente e me incentivaram para continuar.

Ao meu marido Tiago, companheiro de sempre, pelo amor e alegria com que preenche a minha vida, pela paciência e força com que me amparou, não me deixando vacilar. Aos meus filhos, Iara e Santiago, o meu maior orgulho e felicidade, por serem como são e por fazerem questão de me mimar. Pelos momentos que lhes roubei, espero ter tempo para lhes retribuir o tempo que não vivemos. Porém estou certa de que a minha valorização pessoal será um contributo precioso na sua educação.

palavras-chave

armazenamento de energia térmica (TES), conforto térmico interior, eficiência energética, material de mudança de fase (PCM), *nanofillers*, soluções construtivas.

resumo

Os sistemas de armazenamento de energia térmica (TES), usando materiais de mudança de fase (PCM) no setor da construção, são tecnologias amplamente investigadas e uma área de estudo em rápido desenvolvimento. O uso de PCM em soluções e componentes construtivas aparece como uma potencial solução para aumentar a eficiência energética de edifícios novos e reabilitados, uma vez que eles podem armazenar mais energia, de forma latente, do que a típica energia sensível armazenada por materiais comuns utlizados na construção. No entanto, a baixa condutividade térmica dos PCM limita o seu potencial uso, pois diminui a resposta da transferência de calor associada aos processos de carga e descarga. O presente trabalho aborda essa fragilidade, explorando o desenvolvimento de soluções construtivas que incorporam PCM sintetizados com base em *nanofillers* e outros aditivos para aumentar a sua condutividade térmica. Foi estudada a avaliação em termos de desempenho térmico de diferentes formulações de espumas de poliuretano (PUFs) incorporando, primeiro PCM microencapsulado de origem comercial, e um segundo PCM sintetizado à base de parafina e carbonato de cálcio para comparação. Foi realizada uma análise comparativa de três abordagens de ensaio para a caracterização e determinação da condutividade térmica em função da temperatura. Em seguida, foi construído um modelo numérico, com o objetivo de validar o mesmo, com recurso aos dados experimentais, para posteriormente realizar um estudo paramétrico para avaliar o desempenho térmico de painéis de PUFs rígidos incorporando PCM comercial e PCM sintetizado com carbonato de cálcio. Finalmente, foi avaliado o desempenho térmico de uma alternativa aos painéis de PUFs rígida, especificamente o de uma "*layer*" estrutural de poli (cloreto de vinila) (PVC) incorporando PCM microencapsulado comercial e os dois PCM sintetizados.
Este trabalho apresenta resultados promissores para o PCM sintetizado em comparação com o PCM comercial e a sua incorporação nas diferentes matrizes poliméricas (PUFs e PVC) mostrando possíveis aplicações de LHTES. Além disso, de acordo com os critérios de validação analisados, os resultados do modelo numérico foram considerados calibrados e validados. Os resultados obtidos provam o potencial dos materiais de mudança de fase na regulação térmica e na otimização da eficiência energética de espaços interiores.

keywords

Building solutions, energy performance, indoor thermal comfort, phase change material (PCM), nanofillers, thermal energy storage (TES).

abstract

Thermal Energy Storage systems (TES), using phase change materials (PCM) in building sector, are widely investigated technologies and a fast developing research area. The use of PCM in building solutions and components appear as a potential solution to increase the thermal efficiency in buildings, either new or refurbished, since they can storage more energy, in latent form, than the typical sensible energy stored by common construction materials. However, the low thermal conductivity of PCM limits their full potential use because it slows down the heat transfer response associated to the charging and discharging processes. The present work approaches this frailty exploring the development of building solutions which incorporate synthetized PCM based on nanofillers and other additives to enhance the thermal conductivity. The evaluation in terms of thermal performance of different polyurethane foams (PUFs) formulations incorporating first, commercial microencapsulated PCM and a second, synthetized PCM based on paraffin and calcium carbonate. For comparison comparative analysis of three thermal conductivity testing procedures to characterize and determine the thermal conductivity. Next, a numerical model was developed to be calibrated resourcing to experimental data to then carry out a parametric study to assess the thermal performance of rigid PUFs panels incorporating PCM. Finally, the thermal performance of an alternative to rigid PUFs, specifically that of a poly(vinyl chloride) (PVC) structural layer incorporating commercial microencapsulated PCM and the two synthetized PCM was evaluated.

This work presents promising results of the synthesized PCM in comparison to the commercial PCM and their incorporation into the different polymeric matrices (PUFs and PVC) revealing potential in LHTES applications. In addition, according the used acceptance criteria, the results of the numerical model presented a good agreement and reliability and were considered calibrated with well prediction data. The results reveal the PCM potential for the thermal regulation of indoor spaces as well as improving the energy efficiency of the indoor spaces.

TABLE OF CONTENTS

LIST OF FIGURES

LIST OF TABLES

CHAPTER 1

1. Introduction and thesis scope

1.1. Scope and Motivation

In the last two decades, the European Union (EU) has been working on new and stricter legislation to control the energy consumption in buildings. This sector is responsible for consuming around 40% of the total final energy use of the EU and produces nearly 40% of the total CO_2 emissions [1,2]. This sector generates pollution, and wastes natural resources, being one of the major energy consumers [3,4]. It is necessary that the energy consumption of this sector decreases, but without compromising thermal comfort and indoor air quality in the buildings, which is the concept of energy efficiency [5].

To minimize the energy consumption in this sector, many new and optimized solutions with passive cooling and heating strategies, have been developed by researchers and passed on to commercial based solutions by companies which are already implemented on the market. Existing controlling devices and appliances to keep the temperature within the comfort range consume a large amount of energy. For that reason, in the last decade, thermal energy storage systems arouse as a good approach and have gained much attention.

In this context, the phase change materials (PCM) appear as a potential solution to increase the thermal efficiency in buildings, either new or refurbished, since they can storage more energy, in the latent form, than the typical sensible energy stored by common materials, as for example: clay, brick, wood, concrete and others [6,7]. The integration of LHTES (latent heat thermal energy storage system) using PCM in buildings increases the thermal inertia, increases the efficiency of energy use and is expected to solve the time mismatch between the energy supply and the consumption. The main advantage is their high storage density for small temperature intervals from storage to release energy. In consequence, it is demanding to contribute to solve the time mismatch between the energy supply and demand of these systems the energy is storage during melting and released during freezing of a PCM [7–10].

A fundamental action to increase the energy efficiency of the buildings is improving the external building envelop fabric. PCM incorporated into the building envelope, can decrease the building energy demand and improve the thermal comfort through enhancing the thermal energy storage capacity of building envelope, consequently reducing the temperature peaks, decreasing the temperature swing through the PCM capacity to store and release energy. In other words, this potential thermal regulator effect of the PCM of indoor spaces to assure less energy consumption to guarantee good comfort levels is a passive benefit, as is the case of hotter climates, in which PCM potentially reduce the overheating time during the summer period [9,11].

However, the low thermal conductivity of PCM limits the full potential use of these materials because it slows down the heat transfer response associated to the charging and discharging processes. The solution for this problem may be tackled by the addition of high thermal conductivity substances such as carbon nanostructures or other additives that can positively affect the overall thermal conductivity of PCM. Among the various nanofillers reported in literature (inorganic and organic fillers), carbon materials have been preferred due their extremely high thermal conductivity and relatively low density [12–14]. This research describes the importance of the nanotechnology and nanoscience sib the material science applied to sustainable construction solutions through the: *i)* incorporation of carbon materials that can increase the thermal conductivity of PCM; *ii)* development of shape stability of synthesized PCM prevent leakage of molten paraffin during the structural layer production; *iii)* ensure no or low bursting risk of microencapsulated PCM when incorporated into other material matrices (foams and polymers).

1.2. Objectives

The main goal of this thesis is to improve typical building solution layers by incorporating synthetized phase change materials (PCM) based on nanofillers and other additives to enhance the thermal conductivity and thus achieve a more effective charging and discharging process. The main objectives are next summarized:

- Development of two types of synthesized PCM, one based on paraffin and calcium carbonate and the other on paraffin, silica and graphene oxide to enhance the thermal conductivity and thus achieve a more effective charging and discharging process;
- Evaluation the thermal performance of different polyurethane foams (PUFs) formulations incorporating first, commercial PCM and second, synthetized PCM based on paraffin and calcium carbonate, for comparison;
- Carry out comparative analysis of three thermal conductivity characterization approaches to determine the thermal conductivity of rigid polyurethane foams (RPU) with and without PCM;
- Comparison of experimental and numerical analysis of the thermal performance of RPU panels incorporating PCM;
- Evaluation the thermal performance of an alternative to RPU, specifically that of a poly(vinyl chloride) (PVC) structural layer incorporating commercial PCM and the two synthetized PCM.

1.3. Thesis structure

This section aims to systematize the thesis organization and the explain the link between the research activities. Thus, and to clearly expose all the work developed, in the scope of the thesis, a flow chart is presented in Figure 1. The thesis is structured into seven chapters.

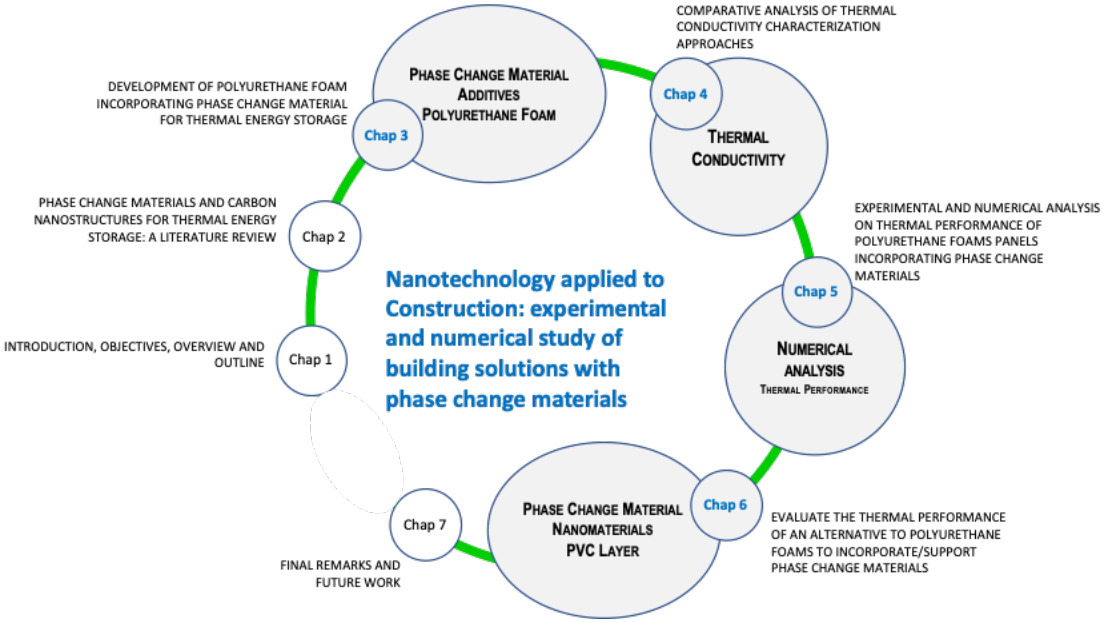

Figure 1: Flowchart of the thesis

As shown in Figure 1, the thesis starts (Chapter 1) with an overall introduction followed by the objectives and a general overview. Chapter 2 consists in a literature review about experimental research studies regarding the enhancement of the thermal properties (thermal conductivity and the latent heat capacity) of PCM obtained by the addition of carbon nanostructures or other additives. Chapter 3 presents the development of synthesized PCM based on paraffin and calcium carbonate, to enhance the thermal conductivity of different material matrices, focusing on PUFs. Then, three different approaches (flux meter approach, the guarded hot plate approach and the transient plane source approach) are presented in Chapter 4 to determine the thermal conductivity of RPU panels incorporating PCM based on steady state methods and on a transient method. This chapter also presents and discusses the comparison between the three approaches revealing the important factors that should be considered to determine the thermal conductivity of the RPU panels with PCM, particularly in the temperature range during PCM phase change transition (solid/liquid state). Chapter 5 is dedicated to the experimental and numerical analysis evaluation of the thermal performance of RPU panels incorporating PCM. Next in Chapter 6, similar to Chapter 3 is presented the

development of synthesized PCM based on paraffin, silica and graphene oxide, and discussed the thermal performance of polymer (PVC) based layers incorporating different types of PCM. Finally, Chapter 7 sums up the main findings of the thesis and presents proposals for future work.

CHAPTER 2

2. Phase change materials and carbon nanostructures for thermal energy storage: A literature review

This chapter was published in the Journal of Renewable & Sustainable Energy Reviews.

Amaral, C.; Vicente, R.; Marques, P.A.A.P.; Barros-Timmons, A. (2017) – Phase change materials and carbon nanostructures for thermal energy storage: A literature review – Journal of Renewable & Sustainable Energy Reviews, Elsevier, 10.1016/j.rser.2017.05.093, Vol. 79, pp. 1212-1228 (IF2017=9.184; IF5y=10.093)
https://doi.org/10.1016/j.rser.2017.05.093

Abstract

The high thermal conductivity of carbon based nanostructures (CNs) has been recognized appropriate to be integrated into phase change materials (PCM) to enhance the overall thermal properties of the obtained nanocomposites. The equilibrium of the possibility to enhance the thermal conductivity of the PCM and the latent heat capacity are the key for their ability to store or dissipate a large amount of energy in a short period of time. This chapter gives an update overview summarizing the state-of-the-art concerning nanocomposites prepared using PCM and CNs with emphasis on the improvement of the latent heat capacity and of the thermal conductivity. Focus is directed towards experimental research studies regarding the enhancement of the thermal properties (thermal conductivity and the latent heat capacity) of PCM obtained by the addition of the CNs by means of the encapsulation method.

The majority of the reported research studies focus mainly on the thermal characterization of PCM nanocomposites, however there is scarce information about the mechanisms explaining why/how the thermal properties are enhanced. This review outlines the results of the thermal conductivity and the latent heat capacity of PCM/CNs nanocomposites, trying to identify the features that lead to the improvement of their thermal properties.

Keywords: Phase change materials (PCM); Carbon nanostructures (CNs); Latent heat capacity; Thermal conductivity; Thermal energy storage (TES)

Abbreviations list

AC	Acetamide
CA	Capric acid
CNFs	Carbon nanofibers
CNs	Carbon nanostructures
CNTs	Carbon nanotubes
EG	Expanded graphite
EU	European Union
GNPs	Graphene nanoplatelets
GNs	Graphite nanosheets
GO	Graphene oxide
HD	Hexadecane
HP	Heptadecane
HVAC	Heating, ventilation and air conditioning
LA	Lauric acid
LHTES	Latent heat thermal energy storage

L-MWCNTs	Long multi-wall carbon nanotubes
MA	Myristic acid
MF	Melamine-formaldehyde
MWCNTs	Multi-wall carbon nanotubes
NDG	Nitrogen doped graphene
NG	Nano graphite
O-GNs	Oriented graphite nanosheets
PA	Palmitic acid
PA6	Polyamide 6
PCM	Phase change materials
PD	Pentadecane
PEG	Polyethylene glycol
PMMA	Poly(methyl metracrylate)
PU	Polyurethane
PVP	Dispersing agent
R-GNs	Randomly distributed graphite nanosheets

SA	Stearic acid
S-MWCNTs	Short multi-wall carbon nanotubes
SSPCM	Shape-stabilized phase change materials
SWCNTs	Single-wall carbon nanotubes
TD	Tetradecane
TES	Thermal energy storage
UF	Urea-formaldehyde
UMF	Urea-melamine- formaldehyde
xGNPs	Exfoliated graphite nanoplatelets

2.1. Introduction

For the two last decades, the European Union (EU) has been working on new and stricter legislation to reduce energy consumption in all sectors and promote the use of renewable energy sources. In particular, the building sector is responsible for consuming around 40 % of the total final energy and producing nearly 40 % of the total CO_2 emissions [1,2]. Indeed, this sector is one of the major energy consumers [3,4].

In what regards the building sector, the basic premise of energy efficiency is to decrease energy consumptions, without compromising thermal comfort and indoor air quality in buildings [5]. Considering that buildings active systems for cooling and heating consume a large amount of energy to keep the indoor temperature within the comfort range, many new and optimized solutions based on passive cooling and heating strategies , such as latent heat thermal energy storage (LHTES) systems, have been developed in order to minimize the energy consumption. In fact, some have been passed onto commercial solutions are presently available on the market.

Amongst the strategies mentioned above, Thermal Energy Storage (TES) systems have gained much attention in the last decade, particularly as a potential approach to improve the energy efficiency in buildings. In this context, PCM appear as a potential solution to increase the energy efficiency in new and refurbished constructions, since they can store more energy, in the latent form, than the typical sensible energy stored by common materials, as for example: clay, brick, wood, concrete and others [6,7]. The integration of LHTES systems using PCM increases the thermal inertia, and when coupled with other active systems can increase the energy efficiency in new and refurbished buildings. The main advantage of LHTES systems is the high storage density for small temperature intervals. In consequence, it is demanding to contribute to solve the time mismatch between the energy supply and demand of these systems, the energy is storage during melting and released during freezing of the PCM [7–10].

A simple way to increase the energy efficiency of new and existing buildings is to incorporate PCM in the building external envelope wall solutions, as well as in other components such as glazing, enclosure facade and partitions walls, ceiling, and active HVAC (heating, ventilation and air conditioning) systems. In addition to the increase of energy storage, PCM help to reduce the temperature peaks and attenuate the comfort asymmetry and temperature swing in building spaces through storing and releasing energy, functioning as a thermal regulator. Additionally, for hot climates, PCM potentially reduce the overheating during the summer period [9,11].

However, the low thermal conductivity of PCM limits the use of the full potential of these materials since it slows down the heat transfer process associated with the charging and discharging processes. The solution to this problem may be tackled by the incorporation of high thermal conductivity nanofillers such as CNs or other additives that can increase the thermal conductivity of the final composites [12,13]. Other strategies have been studied, in order to improve the thermal properties of PCM, for example, shape stabilization of the PCM [15–17] and the PCM microencapsulation [18,19]. Among the various nanofillers reported in literature (inorganic and organic fillers), CNs have been preferred due their extremely high thermal conductivity and relatively low density [12–14]. Improvement of energy storage capacity of PCM/CNs nanocomposites inevitably requires the increase of the thermal conductivity whilst minimizing the variation of the latent heat capacity of the nanocomposite and ideally increases it. In other words, materials should be able to store or dissipate a large amount of energy in a short period of time. The equilibrium between these parameters (thermal conductivity and latent heat capacity) in PCM/CNs nanocomposites is the key factor for the development of many TES applications such as energy storage and thermal insulation systems as well as in active and passive cooling of electronic devices, for thermal management of computers clusters, solar energy storage use, energy saving constructions, electrical engines, recovery of waste heat, smart textiles and heat transfer media.

Several reviews have been published regarding the characterization and applications of PCM composites for thermal energy storage. However, there are just a few reviews focusing on methods developed to enhance the thermal properties of the PCM composites by the addition of nanoparticles using encapsulation methods. Liu et al. [20] summarized and listed experimental and theoretical methods to enhance the thermal conductivity of the PCM by the incorporation of additives such as CNs and metals or their oxides. These authors discussed and compared several methods to enhance the thermal conductivity of PCM. Ibrahim et al. [21] reviewed separately the thermal conductivity enhancement strategies of the PCM using porous materials, nanoparticles and low density materials, and the heat transfer enhancement of the PCM with fins, heat pipes and using multiple PCM. Huang et al. [22] focused their review on ways to improve the thermal conductivity and heat transfer of the PCM using the incorporation of nanomaterials and porous materials, as well as encapsulation methods. Qiu et al. [23] presented an extensive review about the characterization of the microencapsulated PCM slurries with the identification of the increase/decrease of thermal conductivity and latent heat capacity enhancement of microencapsulated PCM slurries under the laminar and turbulent flow conditions. Milián et al. [24] summarized the encapsulation and characterization techniques for two types of encapsulated inorganic PCM: core-shell PCM and shape-stabilized PCM. In addition, this review presents the effects of

materials used for encapsulation and the parameters of encapsulation methods on PCM thermal conductivity and on PCM latent heat capacity. Al-Maghalseh and Hahkamov [25] published results and discussions on the heat transfer intensification methods including application of fins, filling materials, nano-fluids, nano-particles, microencapsulation and the thermal conductivity enhancement method. Additionally, this review summarised the experimental and mathematical methods available to enhance the thermal conductivity of PCM. Rodríguez-Cumplido et al. [26] have reviewed some strategies to modify the composition of the microencapsulated and nanoencapsulated PCM developed in the last decade can be useful to improve the characteristics of these materials (like their thermal conductivity). Gao et al. [27] presented a review which highlighted recent progress in the research of nanoporous shape-stabilized PCM, such as the design concept of porous support, fabrication and characterization techniques, and especially the nanoconfinement effects of the porous support on the thermal properties of the PCM confined in the nanopores. Umair et al. [28] reported research studies focused mainly on the shape stability that can be achieved by entrapping the organic phase change materials in a shell through microencapsulation and by integrating into the supporting materials' matrix or by developing phase change materials with solid-solid phase change. This work also described the synthesis routes, structural features and PCM encapsulation capacity of different supporting materials.

Despite of the contributions referred above, a comprehensive review focusing on the enhancement of the thermal properties (thermal conductivity and the latent heat capacity) of PCM as a result of the addition of the CNs using the encapsulation method has not yet been carried out. This review gives an overview of the experimental research that has been reported concerning the improvement of the energy storage capacity and thermal conductivity of PCM/CNs nanocomposites and the factors that determine the thermal performance of these nanocomposites. Therefore, and for a better understanding of this issue, this review focuses primarily on the fundamental properties of the individual PCM and CNs and after on the PCM/CNs nanocomposites. Next, the enhancement of the thermal properties (thermal conductivity and the latent heat capacity) of PCM/CNs obtained from macro, micro and nano encapsulation methods, including shape stabilized methodologies are discussed.

This review is organized as follows:

- Discussion and identification of the most relevant parameters that can influence the enhancement of the thermal properties of PCM/CNs composites using the referred methods.

- Organization of the relevant information in tables: for the enhancement of the thermal properties of PCM/CNs , the tables contain the variance of the latent heat capacity and the thermal conductivity increase for different types of PCM and CNs (with different loading content); for the enhancement of the thermal properties of PCM by the encapsulation method, the tables contain the latent heat capacity and the thermal conductivity values for different shell materials.
- Detailed description of the most relevant experimental studies regarding innovative results, and identification of the critical reason(s) for the observed increase of the thermal conductivity and of the latent heat capacity, are separately presented.

Therefore, the present work gives an overview of different ways to improve the thermal properties of the PCM, by enumerating in detail the most relevant experimental research studies to enhance the thermal conductivity and the latent heat capacity of the PCM. Thus, this work helps identifying the current status, potential existing problems and future directions in relation to research.

2.2. Phase Change Materials (PCM)

2.2.1. Definition and operation principles

Materials with solid-liquid phase change, which are suitable for heat or cold storage applications, are commonly referred to as phase change materials (PCM). In this context, PCM appear as a potential solution to increase the thermal regulation in buildings since they can storage more energy, in the latent form, than typical sensible energy stored by common building materials [29–31].

The sensible heat storage is the most common method for heat storage (ΔQ) [32], and this process can be expressed by equation (1):

$$\Delta Q = C.\ \Delta T = m.\ c.\ \Delta T \qquad (1)$$

Where, the heat capacity, C, is given by the amount of material, m, and by the specific heat of the material, c, and ΔT represents the thermal amplitude between the final and initial temperature. Each material has a different heat capacity, C, so the sensible heat is influenced by the materials properties and by the imposed temperature [32].

Another method for thermal energy storage determination is the latent heat physical process. This method uses the phase change process of the material to store energy, in the latent form. Usually this type of materials suffers a small volume change, less than 10%, when the phase change process occurs. As Figure 2 shows, for a solid-liquid phase change, when the melting temperature of the phase change is reached, the temperature of the PCM is constant and the stored heat increases.

The latent heat storage for the solid-liquid case, maintains the temperature constant throughout the phase changing state of the storage material. In turn, below and above the temperature range at which the phase change occurs, heat is stored as sensible heat but the temperature of the material increases.

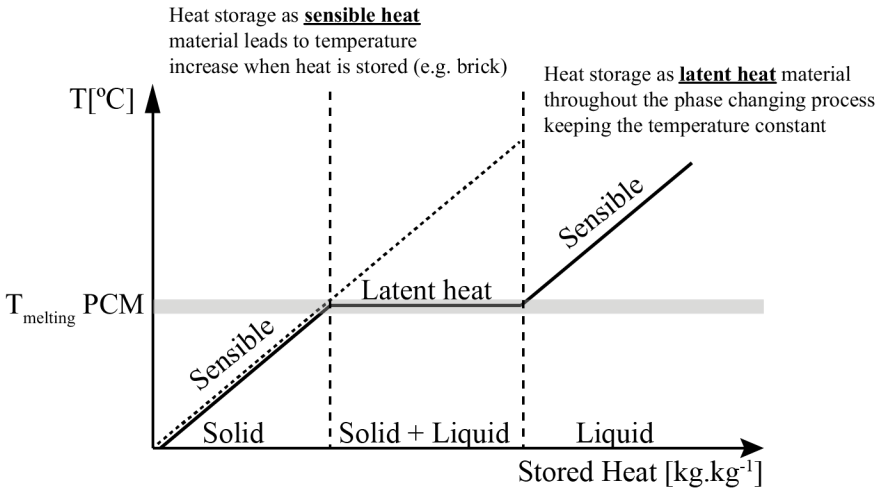

Figure 2: Latent heat storage for the case solid-liquid (adapted from [33]).

In the case of PCM, these materials change from solid to liquid when heated, thus absorbing energy in the endothermic process. When the ambient temperature drops, the liquid PCM will turn into solid state materials again while releasing the earlier absorbed heat in an exothermic process [33,34]. The stored heat associated with the phase change process is calculated from the enthalpy difference, ΔH, between the solid and liquid phase, at constant pressure, given by:

$$\Delta Q = \Delta H \tag{2}$$

Outside the temperature range of the phase change process, the PCM behaviour is the same of a common material, storing sensible heat. The two potential fields of application of PCM can be divided into (see Figure 2) [32]:

- temperature control: heat can be supplied to, or extracted from a PCM without a significant change of its temperature. Therefore, PCM can be used to stabilize the temperature.
- storage and supply of energy with small temperature change: large amounts of energy can be stored at comparatively small temperature change and range.

2.2.2. Classification of PCM types

Many types of energy storage materials have been studied during the last 40 years, mainly hydrated salts, paraffin waxes, fatty acids and eutectics mixtures of organic and inorganic compounds (see Figure 3).

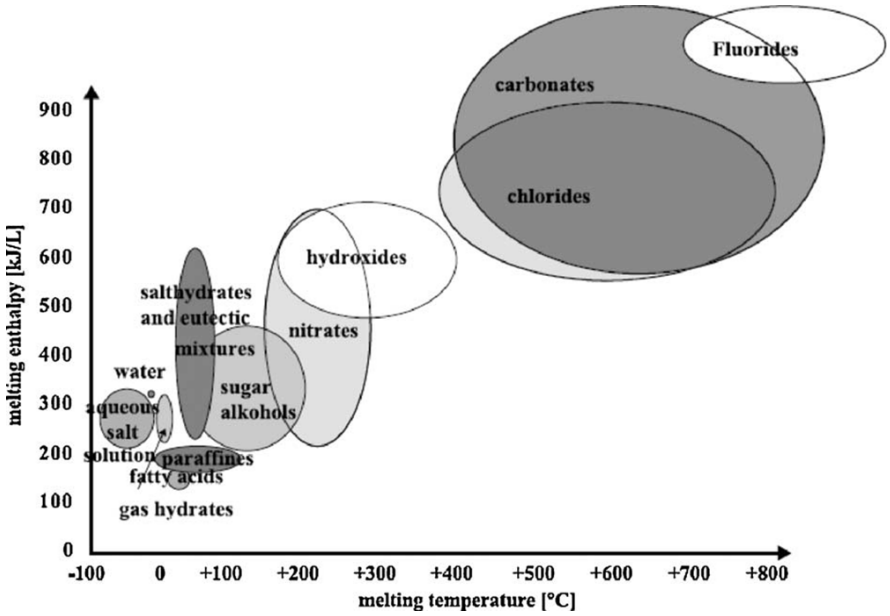

Figure 3: Classes of materials that can be used as thermal storage materials. Reproduced with permission from Elsevier [9]

Literature reviews on PCM divide the energy storage materials into two main categories according to their characteristics: Organic and Inorganic. These two main categories are divided into two sub-categories: the eutectics single temperature and the mixtures temperature interval (see Figure 4) [35–37]. The most commonly used are organic PCM in the form of paraffin, fatty acids and polyethylene glycol (PEG).

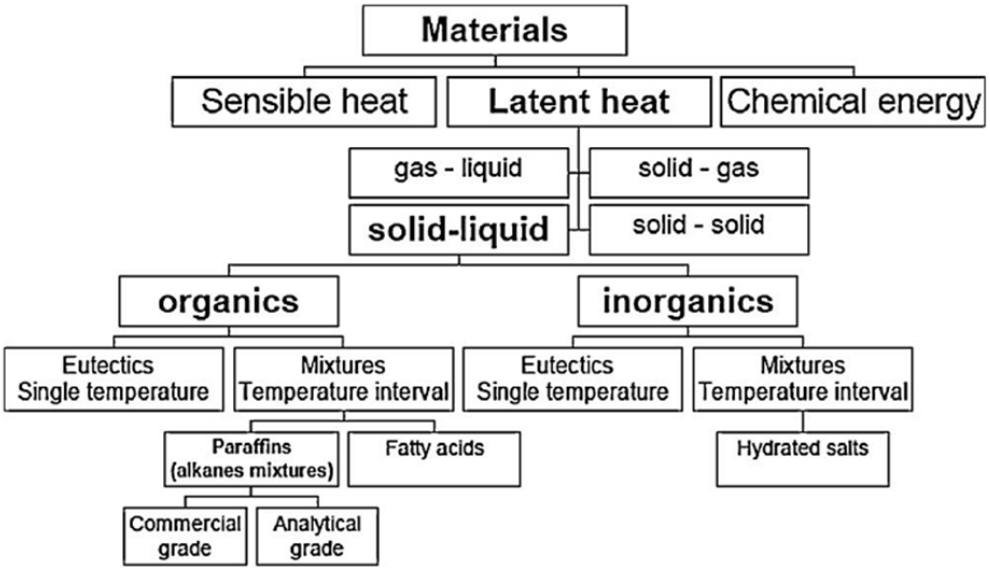

Figure 4: Classification of energy storage materials. Reproduced with permission from Elsevier [9].

Several authors [1,7,9,38–41] have presented a comparison of the advantages and disadvantages of organic and inorganic materials including eutectics and mixtures, as synthetized and shown in Table 1, 2 and 3.

Table 1: Comparison of organic, inorganic and eutectics mixtures for energy storage [1,7,9,40,41]

	ADVANTAGES	**DISADVANTAGES**
ORGANIC	Non corrosive Low or no supercooling effects Chemical and thermal stability Good thermal behaviour Adjustable transition zone Availability in a large temperature range No segregation Good nucleation rate No dangerous (chemically) Recyclable Compatibility with conventional construction materials	Low phase change enthalpy Low thermal conductivity, density and melting point Flammability Highly volatile Volume change during phase change Expensive
EUTECTIC	Sharp melting temperature Volumetric thermal storage density slightly above organic compounds No segregation and congruent phase-change	Limited data are available on their thermophysical properties Quite strong odour

	ADVANTAGES	DISADVANTAGES
INORGANIC	Great phase change enthalpy High energy storage density and thermal conductivity No flammable Less expensive (Low cost) comparative to the organic Low volume change Sharp phase-change	Supercooling effect Corrosion Decomposition and phase separation Phase segregation and lack of thermal stability No compatible with some building materials Slightly toxic Incongruent melting and dehydration in the process of thermal cycling Their application could require the use of some nucleating and thickening agents (poor nucleating properties)

Table 2:Comparison of different types of organic PCM [1,9,38,39]

	ADVANTAGES	DISADVANTAGES
PARAFFINS	Quite a wide range of phase change temperature Moderate thermal storage densities Chemically inert Stable with no phase segregation Good storage density with respect to mass Vapour pressure is not significant Good compatibility with metals Few safety constraints No supercooling effect Commercially available at a reasonable cost	Insoluble in water Water repellent No reactive with most common chemical reagents Burn easily Low phase change enthalpy Low thermal conductivity, density and melting point Flammability
FATTY ACIDS	Proper melting temperature range High heat capacity Little or no supercooling during phase change Low vapour pressure No toxic Good chemical and thermal stability Small volume change Stable upon cycling High heat of fusion Easily producible from common vegetable and animal oils	Low phase change enthalpy Low thermal conductivity, density and melting point Flammability No compatibility with metals Much more expensive (about three times) than paraffin PCM
ESTERS, ALCOHOL, GLYCOLS	High volumetric storage density High thermal conductivity	Slight supercooling effect High melting temperatures

Table 3: Comparison of different types of inorganic PCM [1,9,39]

	ADVANTAGES	DISADVANTAGES
HYDRATED SALTS	High volumetric storage density High thermal conductivity Moderate costs No flammable nature	Chemical instability Degradation (heating cycle) Chemically aggressive towards materials High degree of supercooling effect Inoperative characteristic after repeated phase change cycles No compatible with most construction materials
METALLICS	High heat of fusion per unit volume High conductivity	High weight High degree of supercooling effect

Comparing the PCM types, commercial paraffin is the less expensive and has a considerable thermal storage density (200 kJ/kg or 150 MJ/m^3). Furthermore, it has low or negligible supercooling effect, and is chemically, physically and thermally stable. PCM with these characteristics are available within a range of temperatures and can be incorporated into building solutions [42]. The main problem is the low thermal conductivity (mean value for paraffin is 0.2 W/mK even though some commercial organic PCM solutions present thermal conductivity values up to 0.8 W/mK).

Hydrated salts have the highest thermal storage capacity comparatively to paraffin based solutions, however they are chemically unstable and when they are heated to high temperatures, they degrade losing a percentage of their water content for every heating cycle [40].

2.3. Carbon Nanostructures (CNs)

Nanostructures are low-dimensional systems with length scales down to a few nanometres (typically under 100 nm). The discovery and understanding of nanoscale phenomena and the assembly of nanostructures into different devices are among the most promising fields of material science research. Materials included in this term are: structures that have nanometric dimensions in all directions, such as nanoparticles and quantum dots, crystalline materials such as metals where the crystals are distributed at the nanoscale, nanoscale containers such as capsules and materials with nanoscale holes [43].

Among CNs, carbon nanotubes (CNTs) are allotropes of carbon with a cylindrical nanostructure with diameters that can be as small as one nanometre [44,45]. There are two basic types of CNTs: single-wall carbon nanotubes (SWCNTs) which are the fundamental cylindrical structure and multi-wall carbon nanotubes (MWCNTs) which are coaxial cylinders that have interlayer spacing close to that of the interlayer distance in graphene (0.34 nm). These cylindrical structures have only a few nanometres of diameter, but the cylinder length can be ten times higher. The name MWCNT is restricted to nanostructures with outer diameter of less than 15 nm, above which the structures are designated as carbon nanofibers. CNTs are distinct from carbon fibers, which are not single molecules but strands of layered-graphite sheets.

In what concerns CNs, nowadays the most outstanding material being explored is graphene and its derivatives (Figure 5).

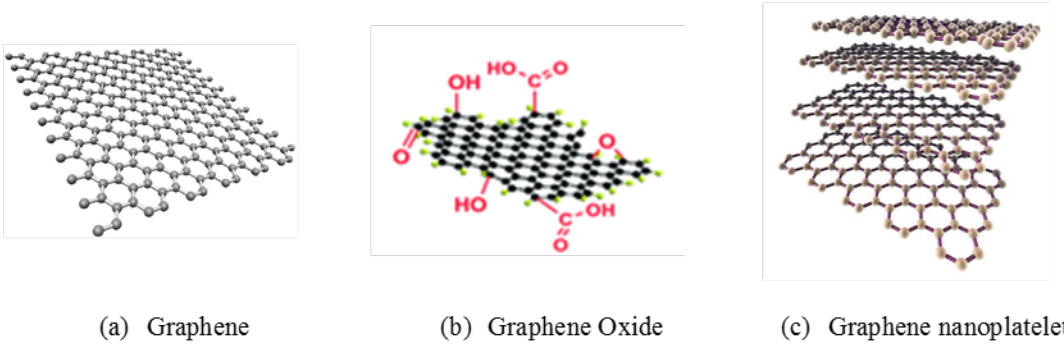

Figure 5: Carbon nanostructures: Graphene and its derivatives

Graphene (Figure 5a), has been studied for more than 6 decades, conceptually it represents a new class of material that is only one atom thick, and the long-range π-conjugation in graphene yields extraordinary thermal, mechanical, and electrical properties. Graphene is one-atom-thick planar sheet of sp^2 bonded carbon atoms that are densely packed in a honeycomb crystal lattice [45–48]. However, it was only in 2004 that it was isolated for the first time by Geim et al. [49,50], using a procedure based on the repeated peeling of highly oriented pyrolyzed graphite using scotch-tap. Other members of the graphene family of 2D materials include related materials with significant variations in layer number, thickness, lateral dimension, crystal structure, and chemical modification of the monolayer graphene [51,52].

Graphene oxide (GO) is receiving the attention of a considerable number of researchers as it retains much of the properties of the highly valued super material pristine graphene, but it is much easier, and cheaper, to prepare in bulk quantities,

easier to process, and its significant oxygen content has been demonstrated to be very attractive to grow chemical structures at its surface [53,54]. GO is decorated by several oxygenated functional groups (carboxylic, hydroxyl and epoxy) on its basal planes and at its edges, resulting in a hybrid structure comprising a mixture of sp^2 and sp^3 hybridized carbon atoms (Figure 5b). This material is obtained by the chemical exfoliation of graphite[55].

Graphene nanoplatelets (GNPs) are another type of graphene derivative obtained from the mechanical exfoliation of bulk graphite and consist of small stacks of platelet graphene sheets (Figure 5c). The use of GNP is desirable as they are cheaper and easier to produce than single layer graphene or CNTs and owing to their unique 2D planar structure, have been identified to even outperform the other wire-shaped CNs in enhancing the thermal conductivity for engineered suspensions [13,56]. Enhanced barrier properties and improved mechanical properties (stiffness, strength, and surface hardness) can be achieved with graphene nanoplatelets due to their unique size and morphology.

Table 4 summarizes some properties of graphite in comparison with graphene, GO and CNTs.

Table 4: Carbon structures properties

Property	Unit	Graphite[a]	Graphene[b]	GO[b]	CNTs[a]
Density	g cm^{-3}	1.9-2.3	-	-	0.8 (SWCNTs) 1.8 (MWCNTs)
Elastic modulus	TPa	1 (in-plane)	1	0.2	~1 (SWCNTs) ~0.3-1 (MWCNTs)
Yield strength	GPa	130	130	120	50-500 (SWCNTs) 10-60 (MWCNTs)
Thermal conductivity	W mK^{-1}	3000 (in-plane) 6 (z-axis)	5000	2000	3000
Electrical conductivity	S cm^{-1}	4000 (in-plane) 3.3 (z-axis)	10^4	10^{-1}	10^2–10^6 (SWCNTs) 10^3–10^5 (MWCNTs)

[a] From Refs: [45,57]; [b] From Refs: [58,59].

Other carbon based materials such as expanded graphite (EG) and carbon nanofibers (CNFs) have also been widely used in this type of studies even though due to their dimensions, they cannot accurately be classified as nanostructures. Nevertheless, in view of their importance they shall be also considered later in this review.

2.4. Enhancement of the thermal properties of PCM by the addition of CNs

As previously referred, one of the ways to improve the thermal properties of the PCM, namely latent heat capacity and thermal conductivity, involves the addition of the CNs to the pristine PCM. In general, the nanocomposites are prepared by dispersing CNs into pristine PCM (mixture) or the incorporation of CNs as the material matrix into pristine PCM that results in shape-stabilized PCM. In the following sub-sections information of the various experimental studies on thermal properties enhancement of PCM as well as highlights on the possible future research directions are discussed.

2.4.1. Mixtures (PCM with carbon nanostructures)

Many research studies have reported the enhancement of thermal conductivity of nanocomposites prepared by the addition of CNs to liquid PCM, namely CNTs (SWCNTs and MWCNTs), CNFs (carbon nanofibers), GNPs and EG. Basically, the nanocomposites are prepared by dispersing CNs into liquid PCM with different loadings with or/without surfactants using vigorous stirring and intensive sonication [60]. Globally, the studies report the boost of thermal conductivity of the final PCM/CNs nanocomposites when compared with the pristine PCM. As regards the effect on the latent heat capacity of the ensuing composites, the addition of CNs to the PCM matrix is frequently associated with some decrease but the values are still acceptable for LHTES applications. In fact, the combined effect of increased thermal conductivity and reasonable values of latent heat capacity improves the rate of response of the resulting materials making these composite interesting for LHTES applications. Among CNs, GNPs and EG seem to have the greatest beneficial effect over thermal conductivity. In the case of the GNPs, this is due to the 2D planar structure which decreases filler/matrix thermal interface resistance, and in the case of the EG, its worm-like structure create more heat conductions links. Furthermore the enhancement depends strongly on the shape, size and loading content of CNs. However, the majority of research has focused exclusively on the quantitative increase on the thermal properties of the PCM/CNs nanocomposites without discussing the reason(s) for that increase. In fact, it is not clear whether the enhancement depends of the type CNs, the dispersion of the CNs into the PCM matrix, intermolecular forces or other reasons.

The main achievements regarding the thermal conductivity and latent heat capacity enhancement in PCM/CNs nanocomposites are summarized in Table 5. In order to establish a direct comparison, this table was filled with information

taken directly from the references but in some cases it was necessary to estimate the thermal conductivity and latent heat capacity increase with information taken indirectly from those references. The variance on the latent heat capacity (%) of the composites is in relation to pristine PCM. In some researches, the information on thermal conductivity and latent heat capacity enhancement of the composites promoted by the addition of CNs in PCM is not available.

For composite materials the variance latent heat capacity (%) was calculated using equation (3).

$$Variance\ Latent\ heat\ capacity\ (\%) = \frac{\Delta H_{composite}}{\Delta H_{PCM}} \times 100\% \quad (3)$$

Where $\Delta H_{composite}$ represents the latent heat capacity of PCM/CNs nanocomposites (melting or cooling) and ΔH_{PCM} indicates the latent heat capacity of pristine PCM (melting or cooling).

Table 5: Main thermal properties of the mixtures (PCM with CNs)

PCM	NCs	Loading content (%)	Variance latent heat capacity (%)	Thermal conductivity increase (%)	Reference of research
Paraffin wax	MWCNTs	0.6 vol	Melting: -2.0; Cooling: 5.0	40-45	[61]
Paraffin wax	SWCNTs MWCNTs CNFs	1.0 vol	13 10 6.8	-	[62]
Paraffin wax	xGnPs	7.0 wt	No changes	200	[63]
Paraffin wax	R (random) GNs O (oriented) GNs	5.0 wt	-16.4 -	390 1210	[64]
Paraffin wax	SMWCNTs	5.0 wt	Melting: -15; Cooling: -14	30	[13]
	LMWCNTs		Melting: -15; Cooling: -12	15	
	CNFs		Melting: -10; Cooling: -9	15	
	GNPs		Melting: -10; Cooling: -9	164	

PCM	NCs	Loading content (%)	Variance latent heat capacity (%)	Thermal conductivity increase (%)	Reference of research
Paraffin wax	S-MWCNTs	4.0 wt	-	20	[65]
	C-S-MWCNTs			20	
	L-MWCNTs			7	
	CNFs			20	
	GNPs			93	
Paraffin wax Soy wax	CNFs	10.0 wt	-	Paraffin wax/CNFs: 40	[66]
	CNTs			Soy wax/CNFs: 45	
				Soy wax/CNTs: 24	
Paraffin wax	MWCNTs	2.0 wt	-1	35-45	[67]
Paraffin wax	CNFs	4.0 wt	-	45	[68]
Paraffin wax	EG	25.0 wt	-26	2150-5350	[69]
		35.0 wt	-33	2800-7000	
Paraffin wax	Graphene	0.1 wt	Melting: -1.4; Cooling: -2.6	16	[70]
		0.2 wt	Melting: -2.9; Cooling: -3.1	32	
		0.3 wt	Melting: -6.4; Cooling: -6.1	38	
		0.4 wt	Melting: -9.3; Cooling: -9.6	58	
		0.5 wt	Melting: -12.3; Cooling: -12.9	60	
1-octadecanol	Graphene	4.0 wt	-15	140	[71]
1-Hexadecanol ($C_{16}H_{34}O$)	MWCNTs	3.0 wt	-	31	[72]
	GNPs			170	
Erythritol ($C_4H_8O_4$)	GNPs	0.1 wt	Melting: 3.9; Cooling: -6.6	Solid: 19; Liquid: 47	[73]
		0.5 wt	Melting: -7.2; Cooling: -27.4	Solid: 33; Liquid: 49	
		1.0 wt	Melting: -14.2; Cooling: -36.4	Solid: 37; Liquid: 53	
N-octadecane	Graphene	4.0 wt (solid)	-	52-87	[74]
	CNTs	5.0 vol (liquid)		48-66	
Eicosane	GNPs	10.0 wt	-16	400	[75]
Palmitic acid	Treated MWCNTs	1.0 wt	-	24-50 (depends on the treatment)	[76]
Stearic acid	MWCNTs	1.0 vol	-2	9 (with dispersing agent)	[77]

PCM	NCs	Loading content (%)	Variance latent heat capacity (%)	Thermal conductivity increase (%)	Reference of research
Bio based PCM	GNPs	5.0 wt	Melting: -2.2; Cooling: -6.6	336	[78]
	CNTs		Melting: -11.3; Cooling: - 9.1	248	
Palmitic-stearic acid	GNPs	8.0 wt	Melting: -20.9; Cooling: -23.9	373	[79]
	EG		Melting: -25.2; Cooling: - 27.0	1684	
Myristic acid	GNPs	1.0 wt	Melting: -2.9; Cooling: -2.2	Solid: 102; Liquid: 25	[80]
		2.0 wt	Melting: -3.9; Cooling: -2.8	Solid: 127; Liquid: 45	
		3.0 wt	Melting: -4.0; Cooling: -3.4	Solid: 176; Liquid: 60	
	MWCNTs	1.0 wt	Melting: -1.5; Cooling: -1.5	Solid: 34; Liquid: 4	
		2.0 wt	Melting: -2.5; Cooling: -2.1	Solid: 37; Liquid: 10	
		3.0 wt	Melting: -3.3; Cooling: -3.6	Solid: 47; Liquid: 13	
	NG	1.0 wt	Melting: -1.9; Cooling: -2.0	Solid: 15; Liquid: 3	
		2.0 wt	Melting: -2.2; Cooling: -2.1	Solid: 26; Liquid: 6	
		3.0 wt	Melting: -3.1; Cooling: -3.2	Solid: 44; Liquid: 12	

wt – weight; vol - volume

Although the experimental studies dedicated to the thermal properties enhancement of the PCM by addition of CNs is very extensive, in this review, only the most relevant experimental research studies that have achieved innovative results are listed and discussed in detail. Identification of the critical reason(s) for the increase of the thermal conductivity and of the latent heat capacity, are discussed separately.

Kumaresan et al. [61] prepared a novel class of nanofluid PCM by dispersing MWCNTs in liquid paraffin with volume fractions of 0.15, 0.3, 0.45 and 0.6 vol.% without using any dispersing agents. The results obtained showed an enhancement of the thermal conductivity of 30–45% of the nanocomposites both in the liquid and solid states, when the content of CNTs was about 0.6 vol.%. Increasing the concentration of the MWCNTs steadily increased the thermal conductivity of the composites without a significant change of the latent heat capacity (decrease 2%

for melting and increase 5% for cooling for 0.6 vol.% of MWCNTs). This could be due to the continuous network of the MWCNTs and the greater stability of MWCNTs in the PCM, resulting in high intermolecular attraction between them.

An experimental and theoretical study was conducted by Shaikh et al. [62] in order to evaluate the change in latent heat capacity of PCM samples doped with CNs. Three types of nanocomposites were prepared by doping paraffin wax with SWCNTs, MWCNTs and CNFs, with nominal diameters of about 1, 10, and 100 nm, respectively. A maximum experimental enhancement of approximately 13, 10 and 7% was observed for the wax/SWCNTs, wax/MWCNTs and wax/CNFs sample, respectively, corresponding to 1.0 vol.% loading by volume of CNs. The authors concluded that the higher molecular density of the SWCNTs in comparison to MWCNTs and CNFs and its larger surface area due to its smaller size were the reasons for a relatively higher latent heat capacity. However, the effect on the thermal conductivity of the PCM samples doped with CNs is not presented.

Kim and Drzal [63] used GNPs and paraffin to prepare a latent heat material with high thermal and electric conductivity. The thermal conductivity of paraffin/GNPs nanocomposites increased with the GNPs loading content increase and an enhancement of more than 200% was achieved for 7.0 wt.% of GNPs. On the other hand, the latent heat capacity did not decrease as GNPs loading content decreased, partially due to the good dispersion of GNPs in the paraffin as a result of high surface area of the nanoparticles.

The thermal properties and structural characteristics of two paraffin composites filled separately with randomly distributed graphite nanosheets (R-GNs) and oriented graphite nanosheets (O-GNs) were investigated by Chen et al. [64]. The thermal conductivity of these nanocomposites was respectively 20 and 7.5 times higher than that of pristine paraffin, when 5.0 wt.% GNs were introduced. Comparatively, the thermal conductivity of the O-GNs/paraffin nanocomposites is lower than that of the R-GNs/paraffin nanocomposites under the same GN loading. For the oriented nanostructures, the layer structure with an orientation roughly parallel to the laser beam, increases phonon scattering at the GNs/paraffin interfaces due to the reduced contact among the GNs. The latent heat capacity of GNs/paraffin composites decreased as the GN loading increased due to the rise of the inner pressure in the paraffin and the replacement of some of the paraffin by GNs.

Fan et al. [13] studied the effects of adding various CNs over the thermal conductivity and latent heat capacity of paraffin-based nanocomposite PCM. The CNs tested included short and long MWCNTs, CNFs and GNPs. For each type of CNs,

nanocomposite PCM samples with CNs mass concentrations of 1.0–5.0 wt.% with an increment of 1.0 wt.% were prepared. It was shown that the presence of CNs enhanced the thermal conductivity of the nanocomposites and the enhancement strongly depended on the size and shape of the CNs. Among the three wire-shaped fillers, the short S-MWCNTs demonstrated best dispersion and hence most pronounced enhancement. An improvement up to 164% at the loading of 5.0 wt.% of GNPs was obtained, due to their two-dimensional planar structure that led to reduced filler/matrix thermal interface resistance. However, the presence of CNs led to the reduction of the latent heat capacity with the increasing loading of all the CNs. At the constant loading, the PCM/CNFs composite presented the highest latent heat capacity, may be because of the size and shape filler (the higher size and the type shape helps the heat conduction connections).

The effect of adding CNs with various sizes and shapes on the thermal conductivity of liquid paraffin based suspensions was also explored by Yu et al. [65]. The various CNs involved were pristine and carboxyl-functionalized short MWCNTs, long MWCNTs, CNFs, and GNPs, with the 3 types of CNTs being hereafter coined as C-S-MWCNTs, S-MWCNTs, GNPs and L-MWCNTs, respectively. The use of mass fractions of 1, 2, 3 and 4.0 wt.% was evaluated and no dispersing agents were used. The suspensions with L-MWCNTs demonstrated a small increase of the absolute value of thermal conductivity by 0.012 W/mK for the highest loading of 4.0 wt.% in comparison with pristine paraffin value. The S-MWCNTs, C-S-MWCNTs, and CNFs caused a similar increase, which was more significant than that of the L-MWCNT samples with the greatest absolute increase being slightly above 0.03 W/mK for a 4.0 wt.% loading, i.e., a relative increase of about 20% in comparison with pristine paraffin value. For the sample prepared using 4.0 wt.% GNPs, the thermal conductivity was as high as 0.29 W/mK, which was nearly double that of pristine paraffin. In other words, a nearly 100% thermal conductivity increase was achieved by adding only 4.0 wt.% GNPs. This significant difference was attributed to the particular structure of GNPs which led to larger contact area, and in turn smaller thermal interface resistance, between the additives and matrix materials. However, the effect on the latent heat capacity was not discussed.

Research carried out by Cui et al. [66] led to the improvement of the thermal conductivity of two composites with PCM materials (soy wax and paraffin wax), using CNFs and CNTs. The composites were prepared by the stirring CNFs or CNTs in liquid wax, using CNs loading levels of 1.0, 2.0, 5.0, and 10.0 wt.%. The experimental results showed that the thermal conductivity of nanocomposite PCM increased with higher CNFs or CNTs loading. Yet, CNFs proved to be more effective than CNTs as thermal conductive fillers due to their better dispersion in the matrix (CNFs have weaker Van der Waals forces between fibres thus it is easier for this

material to be uniformly dispersed in the wax matrix). For a loading level of 10.0 wt.% in soy wax, the thermal conductivity enhancement was about 43.5% for CNFs and 32.7% for CNTs. On the other hand, the latent heat capacity did not decrease with the CNFs or CNTs loading content when paraffin was used. However, the reasons for those results are not discussed nor are the values for latent heat capacity presented. The argument is based on the comparison of the corresponding DSC (differential scanning calorimeter) thermograms.

Wang et al. [67] prepared four heat storage nanocomposites samples consisting of paraffin wax and MWCNTs (0.2, 0.5, 1.0, and 2.0 wt.%) and investigated their thermal properties. The enhancement of the thermal conductivity of nanocomposites raised with increasing of MWCNTs loading. For the composite with 2.0 wt.%, the thermal conductivity enhancement reached 35% and 40% in solid and liquid states, respectively. The latent heat capacity increased with the increase in the mass fraction of MWCNTs, due to the interaction between the paraffin wax molecules and the MWCNTs.

Elgafy and Lafdi [68] dispersed different mass ratios (1.0, 2.0, 3.0 and 4.0 wt.%.) of CNFs in paraffin and a significant enhancement of the thermal conductivity of the modified PCM was achieved (45%) when 4.0 wt.% of CNFs were used. The comparative study to investigate the effect of CNFs surface characteristics on the thermal performance of paraffin nanocomposite showed that heat transfer phenomena at the nanoscale seem to be surface dependent. Conversely, the latent heat capacity decreased with increasing CNFs ratio, which means that nanocomposites displayed less ability to store energy but high ability/propensity to conduct energy. The variation in latent heat capacity was not referred, instead a plot of heat capacity versus temperature was presented which clearly illustrated that the heat capacity decreased with increasing load of CNFs.

The effects of different EG mass fractions on the thermal properties of the PCM/EG composites was studied by Ling et al. [69]. The experimental results showed that the increase of EG mass fraction increased the thermal conductivity of the PCM/EG composite but decreased their latent heat capacity. Also, this research presented other factors (besides the EG mass fraction) that affect the thermal conductivity of an PCM/EG composite, namely the composite temperature and the composite density. For the same EG mass fraction, the thermal conductivity of PCM/EG composite increased with the increase of the composite density, because increasing density compacted the thermal conducting network and shortened the heat conduction pathway. Outside melting range, there weren't significant differences in the thermal conductivity of PCM/EG composite, but during the phase

change the thermal conductivity increased sharply because the PCM have the capacity of keeping the temperature constant.

Joseph and Sajith [70] investigated experimentally the enhanced thermal conductivity effect of paraffin/graphene composite in a hybrid cooling system with low loading graphene levels *i.e.* the range of 0.1–0.5 wt%. The results illustrate that much higher relative enhancement in thermal conductivity of composite in the range 16–60 % is obtained with these low loadings of graphene then the pristine paraffin. The increased thermal conductivity for paraffin/graphene composite are mainly attributed to the 2D-structure of the graphene and low resistance at the graphene-paraffin interface. However, the latent heat capacity of the composite paraffin/graphene was reduced by 12.3 % at low graphene loading of 0.5 wt% due to weakened bond structure. The lack of strong supporting network structure reduced the latent heat capacity with graphene loading. As loading increased, the clustering of graphene and weakened bond structure reduced the availability of active nucleating sites and inhibited complete crystallization. Hence, due to the change in the local steric hindrance of paraffin molecules induced by graphene fillers and incomplete crystallization the solidification latent heat capacity of the composite was found to be slightly lower than the melting latent heat capacity.

Yavari et al. [71] experiments have shown that adding different mass ratios (1.0, 2.0, 3.0 and 4.0 wt.%.) of GNPs to 1-octadecanol significantly boosted the thermal conductivity without experiencing a large reduction of their latent heat capacity. An addition of 4.0 wt.% of GNPs to 1-octadecanol led to 140% increase of the thermal conductivity. This increase can be attributed to the high thermal conductivity of the GNPs fillers network that provides a path of lower resistance for phonons to travel. Also, the high aspect ratio and large interfacial contact area of GNPs as well as strong interface between GNPs and the PCM may help increasing the thermal performance of GNPs/PCM nanocomposites.

Fan et al. [72] prepared nanocomposites using 1-hexadecanol ($C_{16}H_{34}O$) as the base PCM and MWCNTs or multi-layered GNPs, with three mass fractions of 0.3, 1.0 and 3.0 wt.%. At a constant loading of 3.0 wt.%, the thermal conductivity of MWCNTs based nanocomposite increased by 31%, whereas that of GNPs based nanocomposite increased by 170%. The difference of the performance of these nanocomposites was attributed to the much higher thermal conductivity of GNPs. This results from the geometry of this type of CNs (size and shape) which presents lower thermal interface when compared to the MWCNTs. This outperformance was also reported by Yu et al. [65]. Yet, the effect on the latent heat capacity is not discussed.

Mayilvelnathan and Valan Arasu [73] dispersed GNPs in three different mass fractions (0.1, 0.5 and 1.0 wt.%) in the erythritol base PCM for enhancing the thermo-physical properties of the base PCM. The experimental results showed that adding 1.0 wt. % GNPs led to 53 % increase in thermal conductivity with 36.4 % decrease in latent heat capacity during the fusion process. The GNPs structure helps to form a proper molecular alignment in PCM which leads to proper phonon motion in the matrix of PCM in a particular direction over a long distance, thus increasing thermal conductivity. The reason for the decrease in latent heat capacity of fusion could be attributed to the difference in melting points of graphene and erythritol. As the graphene does not go through any phase transformation during the melting of composite erythritol and it is responsible for the reduction of heat of fusion of composite erythritol.

The effect of incorporating CNTs and graphene in *n*-octadecane molecules in terms of the thermal conductivity was investigated by Babaei, H. et al. [74]. An addition of 4.0 wt.% of the CNTs to *n*-octadecane (solid) exhibited an enhancement of 66% when compared to the pristine solid. The enhancement for the 5.0 vol% of CNTs to *n*-octadecane (liquid) suspension was 48%. Also, for the graphene–octadecane mixture, the enhancement of the solid phase (87%) is higher than the liquid phase (52%) for the same loading content (4.0 wt% for solid state and 5.0 vol% for liquid state). The fact that the solid mixture showed greater thermal conductivity enhancement was due to significant ordering brought about by directed crystallization. However, the effect of incorporating CNTs and graphene in *n*-octadecane molecules in terms of the latent heat capacity is not presented.

Fang et al. [75] investigated the influence of adding GNPs to *n*-eicosane. The nanocomposites were prepared by dispersing GNPs in liquid *n*-eicosane using various loadings (0.0, 1.0, 2.0, 5.0, and 10.0 wt.%), using vigorous stirring and intensive sonication and without the aid of any surfactants. It was shown that for the highest loading tested (10.0 wt.%), the relative thermal conductivity enhancement was above 400% at 10°C. The reduced thermal interface resistance, related to the unique two-dimensional planar morphology of the GNPs, was considered responsible for their high thermal performance. Nevertheless, the presence of GNPs decreased slightly the energy storage capacity. This drop of the latent heat capacity below the simple linear correlation was attributed to the realignment of molecules of the PCM matrix in the presence of high loading of nanostructures.

Other studies performed by Wang et al. [81] reported an increase of thermal conductivity values higher than 30% when 1.0 wt.% of CNTs, which had been previously mechano-chemically treated, were added to palmitic acid (PA). These

results were significantly better than those obtained using CNTs that had been treated with strong oxidizing acid mixtures, highlighting the importance of CNTs surface treatment on the thermal properties of the ensuing composites. Indeed, this group has also published an extensive study of the effect of surface treatment of CNTs on the thermal conductivity of CNT/PA composites. In that work [69] four different methods were used to treat MWCNTs: (i) acid oxidation, (ii) mechano-chemical reaction, (iii) ball milling, and (iv) grafting following acid oxidation. The results obtained have shown that the thermal conductivity of the composites is highly dependent on the MWCNTs pre-treatment process and conclude that the nanocomposite containing MWCNTs functionalized with hydroxyl groups, treated by a mechano-chemical reaction, revealed the highest thermal conductivity increase, which, at room temperature, is up to 50% for a MWCNTs load of 1.0 wt.%. Furthermore, it also concluded that the thermal performance is associated with two main issues: (i) the lower intrinsic tube conductivity after treatment, possibly due to scattering of heat carrying phonons by interactions with the surroundings or from defects and (ii) the thermal contact resistance at the MWCNTs surfaces. As MWCNTs have much higher thermal conductivity than the PA matrix and MWCNTs are at a very small fraction in the nanocomposite, the thermal conductivity enhancement of the composites is dominated by the thermal resistance of the surfaces of MWCNTs. Yet, the effect on the latent heat capacity was not discussed.

Li et al. [77] prepared a latent heat nanocomposite made of stearic acid (SA) and MWCNTs for thermal energy storage application. The experimental results showed that addition of MWCNTs improved the thermal conductivity. For a content of 1.0 vol.% of MWCNTs, an enhancement of the thermal conductivity of approximately 9.0% was obtained (when dispersing agent was used) and 5.0% (without dispersing agent) for the nanocomposite. This increase was attributed to the high thermal conductivity of MWCNTs that in combination with the high surface area of the MWCNTs provides a large heat transfer area for SA. Moreover, it was observed that the addition of a dispersing agent (PVP) improved the thermal conductivity of SA/MWCNTs nanocomposites. Moreover, increasing the MWCNTs ratio led to a reduction of the latent heat capacity of SA/MWCNT nanocomposite, e.g., the latent heat capacity of pristine SA is 200.2 kJ/kg, and it decreased from 199.9 to 186.7 kJ/kg when the volume fraction of MWCNT was increased from 0.1 to 5.0 vol.% in SA/MWCNT nanocomposites. In relation to pristine SA, the latent heat capacity of SA/1.0%MWCNT nanocomposite was reduced by about 2%. This resulted from the relatively small mass of SA in the nanocomposite when compared to pristine SA for a fixed total mass of different samples, in which a portion of the PCM volume was replaced by the additive which does not undergo phase change in the operating temperature range.

A bio-based PCM not specified by the authors [78] with a melting temperature of 28.13 °C and latent heat capacity of 149.2 J/g was loaded with GNPs and CNTs using different mass ratios (0.0, 1.0, 3.0 and 5.0 wt.%). As the CNs loading contents were increased, the thermal conductivity increased significantly. The bio-based PCM/GNPs 5.0 wt.% showed the greatest increase in thermal conductivity by 336%. In the case of bio-based PCM/CNTs composites, an increase of 248%, for loading contents of 5.0 wt.% was registered. The latent heat capacity of bio-based PCM/GNPs composites was practically the same as the pristine bio-based PCM, due to good dispersion of GNPs into bio-based PCM matrix, with a high surface area and nanoparticle size. However, in the case of the bio-based PCM/CNTs nanocomposites, the latent heat capacity was reduced upon addition of CNTs. This reduction was attributed to the fact that the 3-D network structure confines heat flow in PCM composites.

Yuan et al. [79] studied the effects of the GNPs and EG addition on the thermal properties (latent heat capacity and thermal conductivity) of the palmitic-stearic acid (as the PCM) using poly(vinyl pyrrolidone) as stabilizer of CNs. The results showed that the latent heat capacity of the composite decreased with increasing loading content (mass fraction) for both CNs. This significant reduction was attributed to the lower degree of crystallinity resulting from the presence of CNs and the stabilizer which may hinder chain mobility and thus crystallization. As regards the effect of the two types of fillers, using the same mass fraction (for example 2.0 wt.%), the latent heat capacity of the PCM/EG composite was higher than that of the PCM/GNPs composite as a result of the higher specific surface of EG. As regards the effect of these CNs on the thermal conductivity of the ensuing composites, the presence of both CNs, led to improvements with, EG being more effective due to its worm-like structure. In fact, whilst the large microstructure of EG allows more heat conductions links, the thin sheet morphology and small size of GNPs limits heat conduction links and promotes agglomeration.

He et al. [80] presented the preparation and thermal characterization of myristic acid (MA - the PCM) enhanced by carbon-based nanoparticles, including GNPs, MWCNTs and NG with different weight concentrations (1.0, 2.0 and 3.0 wt.%). The results showed that the thermal conductivity of the MA was enhanced by adding the nanoparticles, in particular GNPs as additives, to the PCM. However, the increasing rate of the thermal conductivity tended to reduce with the increase of the GNPs concentration. This can be attributed to the agglomeration or even sedimentation phenomena which were likely to occur in the PCM composites under high nanoparticle concentrations. Besides the thermal conductivity enhancement, the addition of nanoparticles also modified the phase change process reducing the

phase change temperature range and eliminated supercooling while maintaining the high latent heat capacity.

2.4.2. Shape-stabilized PCM (SSPCM) with carbon nanostructures

In the late 1990s, a novel type of materials was developed, shape-stabilized PCM (SSPCM). SSPCM consist of a working substance and a supporting material, which can keep the shape of materials and prevent leakage throughout the phase change process. The interest of this type of materials is due to their large apparent specific heat, suitable thermal conductivity, the ability to keep the shape of PCM stabilized during the phase-change process and a good performance over long-term multiple thermal cycles [1,16].

For common PCM, some latent storage device or containers to encapsulate the PCM are necessary in order to store and release the latent heat. However, SSPCM keep shape during the phase change process and there is no need for containers [15]. Most shape-stabilized PCM are prepared by physical methods, such as blending, adsorption, impregnation or chemical methods, including graft copolymerization and sol gel methods [82]. Many research studies have reported that SSPCM composite matrix showed enhanced thermal conductivity with the incorporation of CNs as material matrix, namely EG (expanded graphite), CENG (compressed expanded natural graphite), NG (nano graphite), xGNPs (exfoliated graphite nanoplatelets), graphene, NDG (nitrogen doped graphene), GO, MWCNTs and GNPs [27,28].

The majority of research exclusively focuses on the quantitative increase of the thermal properties (thermal conductivity and latent heat capacity) of the stabilized PCM/CNs composites without identifying the reasons for which the increase was due. It is not clear whether the enhancement depends of the type carbon structures, their dispersion in the PCM matrix, intermolecular forces or other reasons (as stated in section 2.4.1 of this literature review).

Table 6 summarizes the results of some studies regarding shape-stabilized PCM/CNs. This table was prepared in some cases with information taken directly from each reference and in other cases, once again, it was necessary to estimate the thermal conductivity and latent heat capacity increase with information taken indirectly from the corresponding reference for a clear comparison of the different composites. The variance latent heat capacity (%) of the composites is in respect to pristine PCM. In general, the SSPCM composites with CNs reveal high thermal conductivity compared to pristine PCM (an increase of 40% to 8000%) and do not affect significantly the latent heat capacity.

For composite materials the variance latent heat capacity (%) is calculated using equation (3).

Table 6: Main thermal properties of shape-stabilized PCM with carbon structures

PCM	CNs (material matrix)	Content loading (wt.%)	Variance Latent heat capacity (%)	Thermal Conductivity increase (%)	Reference of research
Paraffin	EG	25	15.6	8200	[83]
Paraffin	EG	10	-8.3	172	[84]
Paraffin	EG	14.4	-14.4	-	[85]
Paraffin	EG	10	-10	1155	[86]
Paraffin	EG MWCNTs	25 25	Melting: -20; Cooling: -24	576 41	[14]
Paraffin	CENG	8	-15.5	2250	[87]
Paraffin	NG	10	-13.1	741	[88]
Paraffin	xGNPs Graphene	10	-	980 100	[89]
Paraffin	xGNPs-1 xGNPs-15	2	1.5	-	[90]
Paraffin	GO sheets	51.7	-51	223	[17]
Paraffin	GO	3	Melting: -3.5; Cooling: 0	32	[91]
PEG	GO	4	Melting: -9.5; Cooling: -10	-	[16]
PEG	GNPs	0.5 1.0 1.5 2.0	Melting: -1.0; Cooling: -1.6 Melting: -1.5; Cooling: -2.5 Melting: -2.0; Cooling: -3.0 Melting: -2.8; Cooling: -3.6	45 83 110 131	[92]
PA	NDG	3	-3.3	250	[93]
PA	GO sheets	50	-50	386	[94]
Acetamide	EG	10	-16	507	[95]
Steric acid(SA)	GO	1	-40	-	[96]
Capric and lauric acid **Capric and palmitic acid**	PA6/EG	10	Melting: -19.2; Cooling: -18.4 Melting: -5.0; Cooling: -3.0 Melting: -11.6;	-	[97]

PCM	CNs (material matrix)	Content loading (wt.%)	Variance Latent heat capacity (%)	Thermal Conductivity increase (%)	Reference of research
Capric and stearic acid			Cooling: -8.7		
Capric and lauric acid	EG	6.3	Melting: -5.8; Cooling: -1.5	1400	[98]

As in section 2.4.1 of this review, the most relevant experimental research studies regarding innovative results and identification of the critical reason(s) for the observed increase of the thermal conductivity and of the latent heat capacity, are separately presented.

Mills et al. [83] prepared SSPCM composites with EG (SSPCM/EG) through capillary forces between liquid PCM and the EG. The thermal conductivity of the composite (16.6 W/mK) was roughly 8200% higher than the thermal conductivity of the RT-24 paraffin (0.2 W/mK). In turn, the latent heat capacity of the composite increased by 15.6% (160J/g for the paraffin and 185J/g for the composite SSPCM/EG).Notice should be made that the thermal conductivity of the composite became increasingly anisotropic for higher bulk densities, presenting greater values in the direction perpendicular to the direction of compaction.

SSPCM were prepared by the simple impregnation of paraffin through the porous of EG structure by Sari et al. [84]. They found that the optimum mass fraction of the EG in the composite was 10.0 wt.% (with no leakage), corresponding to an increase in thermal conductivity of 276.2% and a slight decrease of 8% in the latent heat capacity. Due to its form-stable property, direct usability without the need for an extra storage container was envisaged.

Zhang and Fang [85] prepared a SSPCM (paraffin/EG composite) with thermal energy storage properties. The paraffin was absorbed onto the EG network providing the latent heat storage ability whilst EG acted as the supporting material preventing leakage of the melted paraffin from its porous structure due to the capillary and surface tension forces. The total latent heat of the pristine paraffin was 188.69 J/g and the total latent heat of the composite PCM was 161.45 J/g, i.e., a 85.6% increase relative to pristine paraffin was achieved.

Two studies were reported by Xia et al. [86,95] involving the preparation of PCM/EG composites. Paraffin and acetamide were chosen as PCM and different mass fractions of EG were used in both systems. The system paraffin/EG provided thermal conduction paths which enhanced the thermal conductivity of the composite PCM. For example, the addition of 10.0 wt.% of EG resulted in a significant improvement

in the thermal conductivity compared to that of pristine paraffin (more than 1000% for [86] and more than 500% for [95]). The acetamide/EG composite with 10.0 wt% EG as the effective heat transfer promoter led to an improvement of the thermal conductivity of more than 500%. The results obtained indicated that the thermal conductivity of PCM nanocomposite is greatly influenced by the gradually formed EG networks and increases with the increase of the mass fraction of EG. As regards the effect on latent heat capacity, these authors have identified different responses depending on the mass fraction of PCM used. Besides the direct effect that a higher load of EG has on the percentage of the PCM on the composite and consequently on the amount of latent heat involved, in the case of paraffin /EG composite, the effect of intermolecular forces between the PCM and support have been discussed. For lower loadings of EG, the latent heat of the composite increased as the interactions between the PCM and the support become stronger than those between bulk paraffin hence, more energy was required to overcome those interactions. As a result of this, the latent heat was higher. However, for higher loadings of EG, the ensuing 3-D structure that was formed, limited the molecular thermal motion of paraffin causing a decrease in latent heat. In what concerns the acetamide/EG nanocomposite, the performance of these materials seemed to be associated with similar issues as discussed above. However, the reduction observed in the heat transfer rate of the nanocomposites was attributed to the fact that the natural convection in the melted form was limited in the presence of higher percentages of EG.

Gilart et al. [14] developed an innovative SSPCM with paraffin/carbon based (EG and MWCNTs) composite materials by a simple, efficient and robust system based on the slow adsorption of PCM, working at liquid–vapour equilibrium conditions. Using a mass fraction of CNs in the composite, the ensuing materials showed higher thermal conductivity than that of pristine PCM (an increase of up to 576% in the case of EG and 41% in the case of MWCNTs). The lower thermal conductivity of the SSPCM prepared using MWCTNs was distributed to the fact that nanotubes form bundles or a rope structure, randomly oriented, thus jeopardising the heat flow. The latent heat capacity of the SSPCM prepared using EG (120.7 kJ/kg for SSPCM with paraffin RT-50) was lower than that of pristine paraffin RT-50 (150.9 kJ/kg). However, for the SSPCM prepared using MWCNTs hardly any difference was observed between pristine paraffin and the SSPCM composite. Nevertheless, the authors did not identify, nor discuss the causes associated with the results obtained for this property.

SSPCM with CENG/paraffin composites were prepared by Zhong et al. [87]. The CENG matrices with different densities were wrapped by the paraffin wax, and then heated above the melting point of the paraffin wax, in a vacuum oven. The results

obtained indicated a great boost in the thermal conductivity of the composites. The improvement effect of CENG (8.0 wt%) over the thermal conductivity was 2250% (0.35 W/mK for the paraffin and 8.22W/mK for the composite SSPCM/CENG). This spectacular increase was attributed to the extensive contact area between the paraffin wax and the ligaments of the CENG matrix during the heat transfer process. Therefore, the high thermal conductivity of the graphite ligaments of CENG allowed heat to transfer throughout the paraffin wax rapidly. Studies using CENG samples with different bulk densities revealed a pretty linear relationship between the thermal conductivity and the bulk density of the CENG matrix. Moreover, different melting rates have been observed as a result of the anisotropy of the pore structure and the occurrence of heat transport both by conduction and convection. In turn, the composite prepared using 8.0 wt.% exhibited a decrease of 15.5% of the latent heat capacity compared to the pristine paraffin which is associated with the higher density of CENG (2.24 g/cm^3) in comparison with that of paraffin wax (0.91 g/cm^3). Additionally, an almost linear relationship between the latent heat capacity of the composite and the mass ratio of paraffin wax in the CENG matrix has been verified indicating there is no reaction involved between these two materials during the preparation of the composite.

The study carried out by Li [88] focused on the preparation of composites containing NG and PCM. The nano-layers of NG (1.0-10.0 wt.%) were dispersed in paraffin in a random orientation. The improvement brought by the addition of NG (10.0 wt%) over the thermal conductivity was approximately 165%. As the NG content increased, the thermal conductivity of the NG/paraffin composite increased while the latent heat capacity gradually decreased due to the reduction in paraffin content.

Shi et al. [89] compared the enhancement of the thermal conductivity of two shape-stabilized PCM systems (paraffin/xGnP and paraffin/graphene). The composites were prepared by mixing paraffin with xGnP or graphene in hot toluene, followed by solvent evaporation and vacuum drying. A larger increase of the thermal conductivity was observed for paraffin/xGnP, with a 5.0 wt.% xGnP (750%) loading when compared to that achieved by the paraffin/graphene (75%). These results were attributed to the small size of the graphene which resulted in a large number of contacts thus compromising the advantageous high thermal conductivity of this material as the heat flow was significantly blocked. By contrast, the larger size for xGnP reduces the negative impact of thermal contacts and led to a better thermal conduction network. However, the effect of these CNs on the latent heat capacity was not discussed.

Xiang and Drzal [90] prepared PCM composites for latent heat thermal energy storage by mixing two different kinds of CNs namely, exfoliated graphite (xGnP-15 μm) and nanoplatelets (xGnP-1, 1 μm) in paraffin wax. Direct casting and two roll milling were used to prepare samples. The investigation of the thermal and electrical conductivity of nanocomposites with these two types of nanoplatelets was performed. Higher thermal conductivity of composite PCM was achieved using nanostructures of larger aspect ratio, better orientation and lower interface density. Nanocomposites prepared using xGnP-15 showed higher thermal conductivity than xGnP-1 counterparts due to the higher interface density. Two roll milling enabled the platelet particles to orient uniformly in the matrix enhancing the in-plane thermal conductivity of the nanocomposites. However, the milling process also separated the particles disrupting the percolated network and increasing polymer graphite interfaces. It was found that the latent heat capacity of the nanocomposites was not adversely affected by the presence of xGnP nanoplatelets and the thermal stability improved.

Mehrali et al. [17] studied a new form-stable composite PCM prepared by vacuum impregnation of paraffin within GO sheets (see Figure 6). The composite PCM contained 48.3 wt.% of paraffin without leakage of melted PCM and therefore this composite was found to be a form-stable composite PCM with a thermal conductivity enhancement of 230%. The decrease in latent heat capacity values was 50% (an acceptable level for LHTES applications for composite PCM in this experimental study).

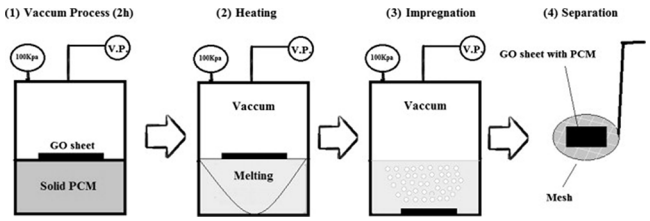

Figure 6: Vacuum impregnation procedure for shape stabilized PCM. Reproduced with permission from Elsevier [17].

Ye et al. [91] developed a SSPCM material by a modified hydrothermal method, in which GO sheets were reduced and self-assembled into 3D graphene aerogels (consisting of numerous hollow graphene cells) and paraffin was simultaneously encapsulated into the cells in the form of micrometer-scale droplets. The resulting core-shell-like structured composite PCM exhibited a high encapsulation ratio of paraffin and large latent heat capacity (no significant values change in comparison with the pristine paraffin). For these PCM filled with CNs, the increase of the latent heat capacity independent of the paraffin content was generally attributed to the interactions between paraffin and the CNs. In addition, the composites showed

enhanced thermal and electrical conductivity compared to pristine paraffin (about 32%). The hydrothermal process leads to an efficient removal of oxygenated groups and partial recovery of the conjugated structures of the GO sheets, which regains the intrinsic thermally conductive nature of graphene. Therefore, the presence of graphene networks has a positive influence on the thermal conductivity of SSPCM. The good shape stability prevents the leakage above paraffin's melting point, as well as, enhanced thermal conductivity compared with pristine paraffin.

Qi et al. [16] used GO sheets to stabilize the shape of PEG during the solid–liquid phase change process. GO contents ranged from 0.5 to 8.0 wt.% and a maximum weight percentage of PEG as high as 96% without any leakage was achieved. The latent heat capacity of the composite PCM decreased with increase in GO content. The melting temperatures were almost the same regardless of the GO/PEG ratios used, while the crystallization temperature first increased and then decreased for a high content of GO. However, the effect on the thermal conductivity was not presented.

He et al. [92] prepared a series of shape stable PEG with GNPs (contents ranged from 0.5 to 2.0 wt.%) via a simple melt blending method. The GNPs were selected as conductive fillers to enhance the thermal conductivity of the shape stable PCM. The thermal conductivity of the shape stable with 2.0 wt% GNPs presented was determined to be as high as 0.67 W/(m K), which was 131 % higher than that of the pristine PCM. The significant increase in thermal conductivity was attributed to the fact when the GNPs are uniformly dispersed in the PEG/unsaturated polyester resin (UPR) matrix, the different layers of graphene form a high thermal conductivity network. Moreover, the large specific surface area of the GNPs reduces significantly the interfacial thermal resistance between the GNPs and the PCM matrix, and consequently, phonons can travel more rapidly. Also, the results showed that the latent heat capacity of the shape stabilized PCM with GNPs was not compromised by the presence of GPNs, because the latent heat capacity of the composite PCM was in accordance with an approximately 80 wt.% loading of pristine PCM and can be utilized for LHTES applications. However, the slight decrease in the latent heat capacity is due to the interactions between PEG and the GNPs which can limit the mobility of PEG molecular chains during the process of crystallization, resulting in a decrease in the crystallization of PEG.

Recently Mehrali et al. [93] have dispersed nitrogen-doped graphene (NDG) in liquid PA using various mass fractions (1.0–5.0 wt.%) and high power ultrasonication, in order to stabilize the shape and enhance the thermal conductivity of PA. For 3.0 wt.% of NGD, the shape stabilized material presented an enhancement of 250% in thermal conductivity and a slight loss of latent heat

capacity (3.3%). However, the thermal conductivity did not increase linearly with increasing NDG loading and the reason suggested for this way the arrangement of the layer structures in NDGs which influences the interaction between PA and NDGs. In another study Mehrali [94] reported the preparation of a shape-stabilized PCM of PA/GO prepared by vacuum impregnation method as well. In this case, the thermal conductivity of the composite PA/GO was improved in 385% and the latent heat capacity was decreased in 50% (composite prepared using 50.11 wt% of PA in GO sheets). The results obtained showed that the pores of GO sheets act as supporting material for PA protecting it. Therefore, the ensuing SSPCM material presented high conductivity, good chemical stability and high thermal reliability.

For the production of active solar LHTES, Xia and Zhang [95] studied the thermal conductivity and the latent heat capacity performances of acetamide (AC)/EG composite with 10 wt% of EG content. The addition of EG provided the thermal conduction path in AC (thermal conductivity enhancement of the composite) and consequently enhanced the heat transfer in the inner part of AC, but the latent heat capacity decreased nearly 30.00 kJ/kg compared to that of pristine PCM. The presence of the EG limited the natural convection of the PCM during the heat storage process while enhancing the thermal conductivity of the AC/EG composite and reduced the mass fraction of the PCM (latent heat capacity decrease). However, the work focused exclusively on the quantitative increase of the thermal properties of the AC/EG composite comparatively to pristine PCM and not on the reason(s) for that increase or decrease. Li et al. [96] prepared a novel shape-stabilized composite PCM for thermal energy storage and provided some new insights into phase change behaviour of organic PCM in nano confined geometries. In this study, stearic acid/graphene oxide (SA/GO) composites were prepared by incorporation of SA in the interlayer spaces of the multilayers of GO, based on the capillary action and interfacial interaction. Experiments were carried out using various SA/GO mass ratios of 1.0, 2.0 and 3.0, respectively. The SA/GO composite prepared using the SA/GO mass ratio of 1.0 yielded a decrease of 40% in latent heat capacity, and a significant decrease of the melting point and freezing point relative to those of pristine SA due to the confinement effect of nanoscale spaces. Yet, the effect on the thermal conductivity was not discussed.

Three fatty acid eutectics of capric acid (CA) and lauric acid (LA), capric acid and palmitic acid (PA), and capric acid and stearic acid (SA) were prepared through melt-blending followed by ultrasonication were prepared by Cai et al. [97] prepared. Thereafter, polyamide 6 (PA6) nanofibers and PA6/EG composite nanofibers with 10.0 wt.% expanded graphite (EG) were prepared by electrospinning; then composite PCM with fatty acid eutectics absorbed in and/or supported by the overlaid mats of electrospun nanofibers (e.g., PA6 and PA6/EG) were explored for

energy storage and release. The addition of EG increased the latent heat capacity of composite PCM and improved energy storage/release rates of fatty acids (e.g., CA and SA) during phase transition which was attributed to high heat transfer of EG in composite PCM. The results indicated that the phase transition temperatures as well as the latent heat capacity values of melting and crystallization for individual fatty acids increased with the increase of molecular length/size. However, the effect on the thermal conductivity was not discussed.

Tang et al. [98] prepared a SSPCM with a low melting point (around 20ºC) using capric and lauric acid (as PCM) using different mass ratios of EG (used as heat transfer intensifier and shape stabilized container of PCM). The latent heat capacity of the SSPCM decreased (not significantly) with the increase of the mass ratio of the PCM, except when the SSPCM had already reached saturation (slightly drop). In this case, the PCM was just deposited on the surface of EG or filled into the spaces between the stacks of EG sheets. The thermal conductivity of the SSPCM achieved a significant improvement with increase of the mass ratio of EG added, because the large amount of porous EG structure acted as carrier during the heat transmission process.

Although the effect of pore size and geometry of the support was thought to affect the performance of PCM, direct comparisons could not be established because materials with distinct porosity are normally associated with different surface characteristics, namely chemical composition. To address this problem, the study carried out by Wang et al.[99] brought a clearer understanding of the effect of porosity on latent heat capacity. Using three carbon porous materials (EG, active carbon and ordered mesoporous carbon) and PEG as PCM the authors guaranteed that the surface characteristics were basically the same and were able to assess the actual effect of pore dimensions and geometry. The results obtained proved that the use of EG affords higher latent heat capacity due to the larger dimensions of its pores. As a result, PEG chains have the ability to crystallize and melt whilst the reduced dimensions of micropores of active carbon prevent crystallization and the polymer is actually amorphous. In brief, the use of support materials with larger pores (i.e. in the micrometer range) helps reducing heat losses (i.e. latent heat capacity) by minimizing the interactions with the support. The results for this experimental research were very similar to those reported by Tang et al. [98], the use of CNs with large amount of pore structure helps to the thermal transmission of SSPCM.

2.5. Enhancement of the thermal properties of PCM by the encapsulation method

The encapsulation method consists in confining the PCM as a core covered by a shell of another type of material (see Figure 7). Sometimes, an additional air pocket is provided inside the core part to accommodate for the change in volume during phase change process. The classification of encapsulation techniques is dependent on the size of the capsules: macroencapsulation (1mm to greater than 1cm), microencapsulation (1μm to 1mm) and nanoencapsulation (less than 1μm) [32,100–102].

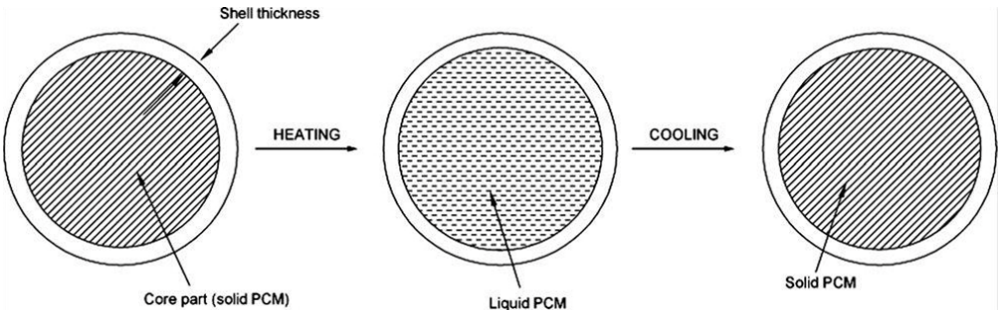

Figure 7: Structure and working principle of the encapsulation of PCM. Reproduced with permission from Elsevier [102]

For the use of PCM in building components, the encapsulation of the PCM is an advantage because, if not encapsulated, they may interact with the building structure and change the properties of the matrix materials. Moreover, leakage may be a problem over the lifetime use of non-encapsulated PCM. Additionally, encapsulation has the benefit of increasing the surface area for heat transfer, therefore increasing the thermal conductivity of the LHTES, increasing the compatibility of the PCM with storage materials, reducing the risk of corrosion and minimizing the effect of volume change during phase change.

As previously referenced, one of the ways to improve the thermal properties of the PCM, namely latent heat capacity and thermal conductivity, involves the encapsulation of the PCM with shell materials with high thermal conductivity. In the subsequent sub-sections information of various experimental studies regarding the enhancement of the thermal properties of encapsulated PCM are provide as well as highlights of possible future research directions.

2.5.1. Micro and Nano Encapsulation

To facilitate the integration capabilities of PCM into existing and new products, some commercial products base their solutions on microencapsulated PCM. PCM

microcapsules consist of microscopic capsules, commonly a polymer, with a diameter of some micrometers [103,104]. These capsules have a spherical shape and the PCM is enclosed inside the microcapsule [105]. The material selection for the polymer capsule has to ensure the absence of chemical reactions between the microcapsules and the building materials [103,106,107].

There are many techniques available to successfully encapsulate PCM such as: coacervation, suspension, emulsion, condensation or polyaddition polymerization (chemical processes) or spray drying (physical process) [18,108–111] that can be coupled in the process. Considering the studies already reported, urea-formaldehyde (UF) resin, melamine-formaldehyde (MF) resin, urea-melamine-formaldehyde (UMF) resin [112,113], polyurethanes (PU), poly(methyl metracrylate) (PMMA) [109,114] and poly(vinyl chloride) (PVC) [115,116] are usually selected as the microcapsule shell material [3,18,26].

Polymeric shells bring some disadvantages such as flammability, poor thermal and chemical stability, and low heat conductivity. So, recent studies have focused on developing inorganic shell materials with high thermal conductivity, chemical and thermal stability and flame retardancy [117]. Yet, these approaches have revealed lower encapsulation efficiency in comparison with to the organic shells.

Table 7 lists the results of relevant research studies regarding microencapsulation of PCM. For example, the use of calcium carbonate shell material (inorganic shell) presented 30-40% of encapsulation efficiency and thermal conductivity in the range of 1.0-1.3 (W/mK). Also, the use of silica as shell material (inorganic shell) presented 40-80% of encapsulation efficiency and thermal conductivity in the range of 0.4-0.8 (W/mK). In order to establish a direct comparison this table was filled with information taken directly from the references and evidences the lack of information regarding thermal conductivity results of microencapsulation of PCM in the case of organic shell.

For microencapsulated PCM the encapsulation efficiency (%) is calculated using equation (4).

$$\text{Encapsulation efficiency } (\%) = \frac{\Delta H_{m,microPCM} + \Delta H_{c,microPCM}}{\Delta H_{m,PCM} + \Delta H_{c,PCM}} \times 100\% \quad (4)$$

Where $\Delta H_{m,microPCM}$ and $\Delta H_{c,microPCM}$ represents the melting and cooling latent heat capacity of the microencapsulated PCM, respectively; $\Delta H_{m,PCM}$ and $\Delta H_{c,PCM}$

represents the melting and cooling latent heat capacity of the pristine PCM, respectively [118].

Table 7: Microencapsulated PCM

Core Material	Shell Material	Melting temp. (°C)	Latent heat (kJ/kg)	Thermal conductivity (W/mK)	Encapsulation efficiency (%)	Ref.
n-Octadecane	Calcium carbonate	29.19	84.37	1.264	40.04	[117]
n-Eicosane	Calcium carbonate	37.29	86.13	1.057	37.93	[119]
n-tetradecane	Calcium carbonate	-	58.54	0.610	25.86	[120]
Paraffin (RT28)	Calcium carbonate	23.33	105.80	0.714	59.4	[121]
Paraffin (RT44)	Calcium carbonate	51.30	177.5	0.657	68.8	[122]
Paraffin	Calcium carbonate	20.48	16.58	-	20.80	[123]
n-Octadecane	Silica	27.10	184.90	0.457	86.12	[124]
Paraffin	Silica	58.37	165.68	-	87.55	[125]
n-Nonadecane	Silica	25.80	74.78	0.650	41.12	[126]
n-Octadecane	Silica	27.96	87.46	0.891	41.83	[127]
n-Octacosane	PMMA	50.60	86.40	-	42.86	[128]
capric–stearic eutectic mixture	PMMA	20.20	116.25	0.190	65.80	[129]
n-Eicosane: n-Tetracosane (1:2)	PMMA	35.49	153.37	-	57.74	[130]
Docosane	PMMA	41.0	54.6	-	28	[109]
n-heptadecane	PMMA	18.2	81.5	-	38	[114]
Stearic acid	PMMA	55.3	102.1	-	52.2	[131]
Decanoid acid	UF MF MUF	33.12 31.03 31.56	129.47 34.25 61.32	-	78.87 18.25 36.66	[112]
Octanoic acid	UF MF MUF	17.12 14.99 16.11	93.95 25.58 63.32	-	61.23 11.19 38.40	[113]
n-Octadecane	PU	29.8	117.5	-	94.9	[132]
Butyl stearate	PU	22.3	80.6	-	73.95	[133]
Paraffin	PVC	32.1	120.7	-	61.83	[115]
Hydrated salt (sodium sulfate decahydrate)	PVC	35.9	194.6	-	-	[116]

The early studies referred the use of silica as shell material prepared by oil-in-water emulsion [134] and via a sol-gel process [125,135]. Li et al. and Fang et al.[13,75,136] reported the preparation and energy storage properties of PCM microcapsules based on paraffin cores and a silica shell material via *in situ* polycondensation [117]. Figure 8 shows the steps involved in the preparation of paraffin microencapsulated SiO_2 PCM [124,137].

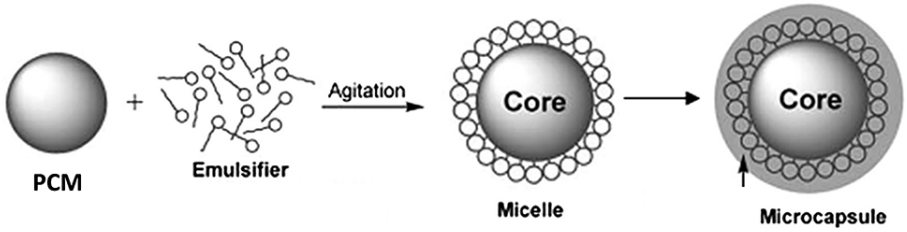

Figure 8: Schematic representation of the preparation of silica microencapsulated PCM. Reproduced with permission from Elsevier [124].

Recent studies of Cao et al. reported the microencapsulation of paraffin and fatty acid with TiO_2 by sol gel method [138,139]. Also, hybrid (organic and inorganic) materials have been an issue of interest due to the potential of combining distinct properties of these materials. Pan et al.[140] reported an encapsulation method for palmitic acid (PA) with aluminium hydroxide shell.

However, few studies have reported the encapsulation of PCM with the incorporation of CNs. Borreguero et al. [141] encapsulated paraffin RT27 with and without CNFs using spray drying process, and low density poly(ethylene-ethylvinylacetate) as shell and obtained an encapsulation yield of 49%. Furthermore, based on the results obtained for the thermal properties of the ensuing composites, they concluded that the presence of CNFs enhanced the thermal conductivity and stiffness of microcapsules and maintained the latent heat capacity.

The microencapsulation of PCM (n-hexadecane) with double-walled shells (polystyrene/graphene oxide) was carried out resourcing to Pickering emulsion templating by Zhang et al. [142]. The encapsulated PCM presented similar high latent heat capacity (183.1 J/g) in comparison with the pristine PCM value (236.5 J/g). The results indicated that the encapsulation ratio of n-hexadecane was as high as 78%. The encapsulated PCM showed good thermal performance, owing to the presence of graphene oxide on the surface protecting the core material from leakage and evaporation. However, the effect on the thermal conductivity was not discussed.

During the course of this PhD thesis, Wang et al. [143] have reported the development of a microencapsulated PCM (paraffin) with double layer network,

incorporating calcium carbonate microcapsules with different mass fractions (10.0, 20.0 and 30.0 wt.%) of EG. The calcium carbonate shells were the first layer network of the paraffin core and EG formed the second layer percolated network for enhancement on heat transfer and thermal stability. Interestingly, the microencapsulated PCM with 20.0 wt.% of EG enhanced the heat transfer (309 % increase in thermal conductivity with 20.7 % decrease in latent heat capacity) more effectively compared to the others. This is because of effective carbon network structure was formed in the microencapsulated PCM with 20.0 wt.% of EG which significantly increases the heat transfer areas. Microcapsules based paraffin and calcium carbonate with different CNs (flake graphite, EG and GNs) for improved thermal conductivity were also developed by Wang et al. [144]. The results showed that the thermal conductivity was increased up to 70.0 times of the pristine paraffin when the microencapsulated PCM contains 20 wt% of GNs and the changes in latent heat capacity were negligible. Hereinto, GNs is considered an excellent carbon filler in view of its low cost, large specific surface area, inherent superior thermal conductivity and ability to form a network structure with less filler contents. Jiang et al. [145] prepared microencapsulated PCM (paraffin) with calcium carbonate shells modified with GO. The results indicated that the addition of GO contributed to improving the heat storage capacity of microencapsulated PCM with calcium carbonate. When the GO content was 1.0 wt %, the encapsulation ratio of microencapsulated PCM was as high as 73.19%, and the leakage rate was reduced by 89.6% compared to the microencapsulated PCM with calcium carbonate without GO, and the thermal conductivity was improved significantly.

In what concerns the nanoencapsulation of PCM there are only few studies in the literature referring to experimental work. For example, Fang et al. [146] nanoencapsulated polystyrene/n-dotriacontane composite by a ultrasonically initiated miniemulsion polymerization method to prepare a PCM for thermal energy storage. The synthesized composite nanocapsules with uniform spherical core/shell structure and z-average particle size of 168.2 nm, showed an excellent encapsulation efficiency (61.23%) and a similar high latent heat capacity (174.8 J/g) for the nanoencapsulated PCM in comparison with the pristine PCM value (285.5 J/g). In other words, the amount of n-dotriacontane in the nanoencapsulated PCM is about 61% which is higher than the ratio of PCM in raw materials of nanoencapsulated PCM, indicating that part of the styrene monomers did not polymerize. Yet, the effect on the thermal conductivity was not presented.

Sari et al. [129] synthesized micro/nano capsules of poly(methyl methacrylate) capric–stearic eutectic mixture using emulsion polymerization and the particle size distribution analysis indicated that the mean diameter of the capsules was 1.3 μm and 28.1% part of the capsules can be characterized as nano-sized spheres. The

results showed that the encapsulation efficiency was 65.8% and the high latent heat capacity (116.2 J/g) of the encapsulated PCM in comparison with pristine PCM values (176.7 J/g). In turn, the thermal conductivity values of pristine PCM and micro/nano encapsulated PCM were 0.19 W/mK and 0.15 W/mK, respectively. By taking into account both results (latent heat capacity and thermal conductivity), it can be concluded that the micro/nano encapsulated PCM showed similar values comparatively to pristine PCM. Yet, smaller PCM particles having larger surface to volume ratio were associated with significantly higher energy transfer efficiency.

Finally, Konuklu et al. [147] synthesized a series of four nanocapsules containing *n*-alkanes (C_nH_{2n+2}), namely *n*-tetradecane (TD), *n*-pentadecane (PD), *n*-hexadecane (HD) and *n*-heptadecane (HP), in poly(styrene-co-ethylacrylate) using emulsion copolymerization. The results showed that the best core material:shell polymer ratio was 3:1 for this study and the maximum encapsulation efficiencies were 79%, 69%, 87%, 81% for TD, PD, HD, and HP, respectively. However, the effect on the thermal conductivity was not discussed.

2.5.2. Macro Encapsulation

The simplest phase change material encapsulation method is the macroencapsulation, which comprises the inclusion of the PCM in some form of package or container such as tubes, pouches, spheres, panels, etc. These containers can serve directly as heat exchangers and be incorporated into building construction solutions.

The macroencapsulation method allows accommodating large PCM quantities and the macrocapsules can have different shapes according to the building element in which they are incorporated. Besides these advantages, macrocapsules improves the thermal performance of the PCM (depending on the type of core material), improve material compatibility with the surrounding, creating a barrier and containing the external volume change of PCM [32,107,148].

Table 8 summarizes the materials that can be considered as suitable shell materials for high temperature applications. This table was filled in with information taken directly from each reference.

Table 8: Macroencapsulation of materials with high thermal energy stability

Core Material	Shell Material	Thermal stability temp in test (°C)	Theoretical melting point (°C)	Reference of research
Paraffin wax	PVC	70	52	[149]
Paraffin wax	Steel	36	18	[150]
Paraffin wax (n-eicosane) (OM35)	Steel	60.2	36-38 35	[151]
Paraffin wax	Aluminium	54	27-29	[152]
Paraffin wax (RT18) (SP29)	Aluminium	40-45	17-19 28-30	[153]
Paraffin wax	PVC Copper	-	25	[154]
Paraffin wax	Stainless steel	-	1400	[155]
Hydrated salt	Polyethylene Aluminium	51	24-34	[156]
Molten salt	Stainless steel 304L/carbon steel 1018	>470	-	[157]
Molten salt	Metallic-ceramic	300-800	-	[158]
Lead	Nickel	400	1455	[159]
Copper	Nickel	>1100	-	[160]
Copper	Chromium-nickel	>1150	-	[161]
Magnesium chloride	Stainless steel 304L	>750	-	[162]

Some applications of the PCM macroencapsulation include: bricks and blocks for external and compartment walls [150,163–165][125, 136-138], air conditioning system and heat exchangers [166,167], flooring systems [168–170], ceiling/roof panels [171,172] and ventilated façade systems (inside air gap) [173,174].

2.6. Conclusions

Thermal energy storage systems based on the latent heat capacity of phase change materials is an efficient method to store thermal energy. This has been the topic of extensive research for several years and several strategies have been considered to overcome the drawbacks associated with the use of PCM in order to widen the potential of this technology. This review outlines the research related to the use of carbon nanostructures to overcome constrains associated with the use of PCM such as their low thermal conductivity and high melting temperatures of some

materials. Furthermore, it also complies information on the currently available shell materials used for encapsulating PCM and to provide the analysis about the influence of the nature shell materials on the thermal properties of the ensuing PCM composites. The following main conclusions taken from the contributions considered regarding the combination of PCM/CNs and encapsulated PCM for thermal energy storage are:

- A number of reports focus solely on the effect of nanocomposites containing PCM and CNs on the thermal properties (thermal conductivity and/or latent heat capacity) relative to the pristine PCM but a correlation of those effects with the performance of the ensuing latent heat thermal heat system is rarely presented;

- The incorporation of CNs in PCM improves the thermal conductivity and generally does not affect significantly the latent heat capacity, keeping it within acceptable levels for LHTES applications. For most cases the reduction in latent heat capacity observed ranges between -16% and 13%. Indeed, increasing the load content of CNs is associated with a lower content of PCM hence, the latent heat capacity of composites is normally lower than that of pristine PCM. Yet, this reduction can be compensated by the fact that CNs increase the thermal conductivity hence, the overall response of the system is faster;

- The effect of CNs on the thermal conductivity of CNs/PCM composites depends on their surface area which is related to their size, shape and porosity, good dispersion and orientation. Among the CNs reported, GNPs and EG seem to have the greatest beneficial effect over thermal conductivity. In the case of GNPs, this is due to their two-dimensional planar structure which reduces filler/matrix thermal interface resistance whilst ensuring better dispersion due to their reduced dimensions, but in the case of the EG, due to the due to its worm-like structure which created more heat conductions links;

- As regards the effect of CNs on the latent heat capacity of composites, increasing mass fraction of CNs causes a reduction of this property, whilst strong surface interactions tend to improve it;

- SSPCM composites with CNs show significantly higher thermal conductivity (40% to 8000%) compared to pristine PCM and prevent leakage during the phase change process of the PCM. The latent heat capacity of SSPCM composites with CNs depends on a variety of aspects whose understanding allows the design of composites by fine tuning the characteristics of CNs. In particular, the pore size and geometry are critical as phenomena associated with molecular thermal mobility and inner pressure are highly dependent on the volume available. Indeed, confinement effects at sub-nanoscale bring rather different results from those expected from classical thermodynamics.

Additionally, the chemical characteristics of the surface can also be tuned in order to modulate the intermolecular forces between the PCM and support;

- The micro and nano encapsulation of PCM encapsulation of PCM with inorganic and organic shells has been widely explored. Whilst inorganic shells are preferred due to their high thermal conductivity, chemical and thermal stability and flame retardancy, their encapsulation efficiency is lower than that obtained using organic shells. Nevertheless, for practical purposes macro encapsulations of PCM using a metallic shell is the most commonly used due to the low cost, the availability of these materials and the easy fabrication (macro-scale). Just few recent researches was study the development of a microencapsulated PCM with different mass fractions of CNs as a solution to explore in the future.

From this review it is unquestionable that the combination of PCM with CNs offers interesting possibilities to enhance thermal energy storage. In this review, the effects of the shell materials for encapsulation on PCM thermal properties were evaluated and showed. Yet, despite of the promising results that have been achieved but there is still a long path to go in terms of fully understanding the improvement of the energy storage properties and thermal conductivity of the composites as a result of adding CNs to PCM, by encapsulation of the PCM and more systematic studies are still required to select and/or develop tailor made solutions for thermal energy storage. The review indicate that the majority of research has focused exclusively on the quantitative increase on the thermal properties of the nanocomposites and not on the reason(s) for that increase.

CHAPTER 3

3. Development of polyurethane foam incorporating phase change material for thermal energy storage

This chapter was submitted in the Journal of Energy Storage and part of this chapter was published in Journal of Ciência & Tecnologia dos Materiais

Amaral, C.; Pinto, S.C.; Silva, T; Mohseni, F.; Amaral, J.S.; Amaral, V.S.; Marques, P.A.A.P.; Barros-Timmons, A.; Vicente, R. (2019) – Development of polyurethane foam incorporating phase change material for thermal energy storage – Journal of Energy Storage, Elsevier (in 1st revision)

Amaral, C.; Vicente, R.; Eisenblätter, J.; Marques, P.A.A.P. (2017) – Thermal characterization of polyurethane foams with phase change material – Journal of Ciência & Tecnologia dos Materiais, Elsevier, Vol. 29, Issue 2, May-August 2017, 10.1016/j.ctmat.2016.06.015, pp. 1-7. https://doi.org/10.1016/j.ctmat.2016.06.015.

Abstract

The major aim of the present study is to improve the thermal characteristics of polyurethane foams (PUFs) that have been almost exclusively used for thermal insulation purposes but can also play a role in potential thermal energy storage components as a matrix material.

To overcome the low thermal conductivity of the of PUFs matrix, a synthesized phase change material (PCM) based on paraffin and calcium carbonate ($CaCO_3$) has been developed to enhance the thermal conductivity and thus achieve a more effective charging and discharging process. The synthesized PCM (PCM@$CaCO_3$) exhibited a good phase change performance with significant thermal storage capacity and thermal stability compared to commercial based PCM (PCM@BASF).

Different PUFs formulations incorporating PCM (PCM@$CaCO_3$ and PCM@BASF) were used to produce PUFs panels (rigid and soft PUFs panels). The thermal conductivity of the PUFs panels was measured using the transient plane heat source method (HotDisk Analyser, TPS 2500 S) and the thermal flux meter method (steady-state method). The results obtained revealed that, regardless of the method used, the thermal conductivity profile has a similar increasing trend before and after the bounds of the PCM phase change transition zone, whilst during PCM phase transition both methods showed a decreasing trend of the thermal conductivity as the temperature increased.

In addition, this work presents and discusses the limitation of the HotDisk method to analyse panels composed by multilayers.

Keywords: calcium carbonate ($CaCO_3$); phase change material (PCM); polyurethane foam (PUFs); thermal conductivity; layered structured composite panels.

3.1. Introduction

Thermal energy storage (TES) systems are foreseen as a promising approach to improve the energy efficiency in buildings through reducing the energy consumption without compromising indoor thermal comfort and indoor air quality in buildings, and for that reason have gained significant attention amongst the research community in the last decade [5,175]. A fundamental action to increase the energy efficiency of new and refurbished buildings is improving the external envelope solutions based on passive cooling and heating strategies. The use of PCM improve the insulation capacity and increase the energy storage of building components such as: glazing solutions, enclosure façade and partitions walls, ceilings, doors and others [9,11,176], for storing thermal energy and having a thermal regulation effect by charging and discharging large amounts of latent heat during the phase change process [35,37,41,177].

To enhance the integration and compatibility of PCM into new building solutions and components, encapsulation is presently a well-developed technology which shows great potential for using pristine PCM [103,177]. Encapsulation consists in confining the PCM as a core covered by a more conductive shell of another material. In some solutions, due to the change in volume during phase change process an additional air pocket is left inside the core part to accommodate for that phenomenon. [101,102]. The most common type of material for microencapsulating are polymer based solutions which should inhibit chemical reaction between the microcapsules and the surrounding matrix building materials in with they are incorporated [175]. Nevertheless, polymeric shells have some disadvantages such as flammability, poor thermal and chemical stability and low heat conductivity. Therefore, recent studies have focused on developing inorganic shell material with higher thermal conductivity, chemical and thermal stability, coupled to flame retardancy properties [113,175].

The improvement of the thermal performance of the latent heat thermal energy storage (LHTS) systems includes various techniques, such as using fins and extended surfaces, applying different types of PCM in the same solution, encapsulation with higher thermal conductivity shell material, incorporation of materials with higher thermal conductivity into the PCM mix, such as the addition of high thermal conductive nanoparticles [25,26,178,179]. Du et al. [180] studied the improvement of the charge/discharge rate of the PCM-metal foams composite used in LHTES. It was shown that the effective thermal diffusivity and effective thermal conductivity were improved by more than 21 times due to the embedding of metal foams in the PCM. Klemm et al. [181] evaluated a new concept of LHTS combining a PCM with metallic fibre structures in a PCM solar module. The results

showed that, compared to the solar module without PCM, even a small volume share of metallic fibre structure incorporation (i.e. 10 %), is enough to achieve a considerable heat transfer that leads to the reduction of the peak temperature of the solar module for a daily cycle by approximately 20 K. Mayilvelnathan et al. [73] researched the thermal conductivity enhancement resulting from dispersing three different mass fractions (0,1 %, 0.5 % and 1.0 %) of graphene particles into the PCM matrix and concluded that the thermal conductivity of PCM was enhanced with the increase of the weight fraction of graphene due to its high thermal conductivity. The addition of 1 wt.% of graphene led to 53.1 % increase in thermal conductivity with only 6.1 % decrease in latent heat enthalpy. Jiang et al. [145] prepared microencapsulated PCM with calcium carbonate shells modified with graphene oxide using a modified self-assembly method. This microencapsulated PCM proved to have higher thermal conductivity and better mechanical properties than the microencapsulated PCM with calcium carbonate shells prepared without graphene oxide.

In comparation with other thermal insulation materials, polyurethane foams (PUFs) exhibit excellent thermal insulation properties, lower thermal conductivity, good mechanical and chemical stability and lower manufacturing cost. PUFs are widely used as insulation layers incorporated or associated to opaque building envelope solutions. These cellular materials are made by reacting polyols with isocyanates with the proper amount of catalysts, additives and blowing agents [84,176,182–184]. The incorporation of PCM into PUFs to improve the thermal performance was presented and discussed by many authors [84,185–187]. You et al. [185] studied the performance of soft PUFs containing different types and content of PCM. For the same PCM content, the efficiency of the enthalpy of the PUFs fabricated with PCM *n*-octadecane is lower than that of the foams fabricated with PCM *n*-nonadecane and PCM *n*-eicosane. As the PCM *n*-octadecane content is increased, the heat storage and thermo-regulation capacity of PUFs become greater. Gama et al. [187] researched the thermal insulating properties of the PUFs using PCM (2.5-10.0 % (wt/wt)) and expandable graphite (EG) (0.5-1.50 % (wt/wt)). It was concluded that the use of PCM disrupted the cellular structure of the composite foams, improved the heat storage capacity of these materials and the incorporation of EG caused a substantial increase of the thermal conductivity and density of the ensuing foams which limited their thermal energy storage capability.

In fact, recently various works have reported methods to microencapsulate PCM materials with enhanced thermal conductivity using $CaCO_3$ [117,119–122] as well as $CaCO_3$ modified with carbon nanoparticles. [143–145], however, the incorporation of the ensuing materials in panels, i.e. in LHTES systems. Therefore,

in the present study a method to synthetize a PCM based on paraffin and $CaCO_3$ has been developed, which was then incorporated into PUFs formulations ro produce two different types of PUFs panels with and without PCM. These panels where then thoroughly characterized in respect to their structure, morphology, phase change properties, thermal stability and thermal conductivity resourcing to Fourier transform infrared (FTIR) spectroscopy, scanning electron microscopy (SEM), differential scanning calorimetry (DSC), thermogravimetric analysis (TGA), transient plane heat source method (HotDisk Analyser, TPS 2500 S) and thermal flux meter method (steady-state method). This study focuses on the experimental work to fully characterize the thermal conductivity with the temperature range (before and after the limits/bounds of the PCM phase change transition zone) of PUFs panels with and without PCM and the comparison of both methods of measurement used for this purpose (transient plane heat source method and thermal flux meter method), identifying trends and constraints, whilst gaining new insights on thermal characteristics of PUFs with the incorporation of PCM.

Furthermore, in terms of the energy storage, the synthesized PCM (PCM@$CaCO_3$) formulation proved to obtain a more effective charging and discharging process in comparison to the commercial PCM solution as a result of the higher thermal conductivity which allows the rapid heat transfer throughout PUFs panels despite of its lower latent heat storage capacity.

3.2. Materials and Methods

3.2.1. Phase change materials (PCM)

3.2.1.1. PCM Micronal®DS 5001X (PCM@BASF)

Microencapsulated PCM (PCM@BASF) powder purchased from BASF (Ludwigshafen, Germany) was used in this study, (Micronal®DS 5001X). It contains paraffin wax with a melting point of 26°C as the core material and a shell of PMMA (poly(methyl methacrylate)).

3.2.1.2. PCM with calcium carbonate (PCM@$CaCO_3$)

The PCM with $CaCO_3$ were synthesized using paraffin RT18HC (main peak of melting point: 18ºC) purchased from Rubitherm (Germany). The surfactant sodium dodecyl sulphate (SDS) was purchased from TCI (Belgium) and the sodium carbonate (Na_2CO_3) was supplied by Panreac (Spain). The calcium chloride ($CaCl_2$) and petroleum ether were supplied by Chem-Lab (Belgium).

PCM@$CaCO_3$ containing paraffin were prepared by the sol-gel method in O/W emulsion using SDS as surfactant. In a two-neck round-bottom flask, 50 g of paraffin RT were added to 250 mL of an SDS solution (2 wt.%) and vigorously stirred with a mechanical stirrer (CAT R100SD overhead stirrer with a polytetrafluoroethylene (PTFE) half-moon blade) at 1000 rpm for 10 min. Then, the mixing power was reduced to 250 rpm and 375 mL of an aqueous solution of $CaCl_2$ (145 g/L) were added dropwise using a dropping funnel. The mixture was continuously stirred at 750 rpm for 2 h in order to form a stable O/W emulsion. Subsequently, 250 mL of an aqueous solution of Na_2CO_3 (300 g/L) was added dropwise (dropping funnel addition), under slow and continuous agitation of 250 rpm and the reaction took place for more 3 h. The temperature was maintained constant during all process at 35 ºC, using a water bath. The final product was washed several times with petroleum ether and water and collected by vacuum filtration. Finally, the PCM@$CaCO_3$ were dried in an oven at 50 ºC, for 18 h.

3.2.1.3. Characterization of PCM

To evaluate the behaviour of PCM (PCM@BASF and PCM@$CaCO_3$), it was taken into account the tests referred in the literature review. The selected experimental characterization tests were: *i)* FTIR analysis; *ii)* SEM analysis; *iii)* density; i*v)* energy storage properties; *v)* thermal gravimetric analysis; *vi)* thermal conductivity.

The chemical composition of PCM@BASF and PCM@$CaCO_3$ were identified by spectroscopic analyses performed on a KBr disk using a Fourier transform infrared (FTIR) spectroscopy. The FTIR spectra of PCM were performed with a Mattson 7000 galaxy series spectrophotometer. All data were recorded at room temperature, in the range 350 to 4000 cm^{-1}, with a resolution of 8 cm^{-1} and 64 scans.

The morphology and structure (shape and size) of the PCM were analysed by scanning electron microscopy (SEM). A small piece of each specimen was placed on a metal support by means of double-sided adhesive carbon tape and sputter-coated with carbon prior to the analysis. The SEM analysis was carried out with Hitachi SU 70 Bruker scanning electron microscope at an accelerating voltage of 15.0 kV.

The bulk density of a powder is the ratio of the mass of an untapped powder specimen and its volume including the contribution of the interparticle void volume. Hence, the bulk density was determined according to [188].

To characterize the energy storage properties of the PCM@BASF and PCM@$CaCO_3$ (melting temperature and enthalpy), a dynamic scanning calorimeter (DSC 4000, PerkinElmer) was used, at a heating rate of 5 ºC/min, in the range of

10 ºC to 50º C under a nitrogen atmosphere. This test is essential to characterize the energy storage properties of the PCM@BASF and PCM@$CaCO_3$.

The thermal stability of both PCM was evaluated by thermal gravimetric analysis (TGA). A thermogravimetric analyzer, TG 449 F3 Jupiter, Netzsch was used, at a scanning rate of 10 ºC/min, in the temperature range of 30–600 ºC, under a nitrogen atmosphere.

The thermal conductivity was measured using a Hot Disk Analyser, TPS 2500 S, and a special specimen holder (a cylinder) for powder specimens. This cylinder is composed of four pieces, which when assembled seal a two-sided Hot Disk sensor in the middle of the PCM to be tested. The final piece on the top applies pressure to the set-up and minimizes the change of air pockets around the sensor. The tests were performed at 10±0.5 ºC (PCM solid state) and 20±0.5 ºC (PCM liquid state), and the mean values of thermal conductivity were obtained from four readings for each specimen.

3.2.2. Polyurethane foam incorporating PCM

In this study, the PCM (PCM@BASF and PCM@$CaCO_3$) were then incorporated in PUF´s formulations to yield PUF´s panels: rigid PUFs panels and PUFs composite panels. The production of the panels was made in Fraunhofer Institute for Chemical Technology, ICT laboratory (Germany).

3.2.2.1. Rigid PUFs panels

In Table 9 the weight in (wt/wt), scaled to 100 parts of polyol, of the rigid PUFs (RPU) formulations are listed.

Table 9: RPU panels formulations (scaled to 100 parts of polyol)

Material	**Parts**
Polyol	100
Isocyanate	130
Additives (catalyst etc.)	1.3
Melamine	20
PCM (5.0wt%)	12.5

The rigid PUFs (RPU) was prepared using 100 parts of polyol 463 RG 48 and 130 parts of isocyanate (Puronate 900/1) was purchased from Rühl. Both components were mixed for 10 s with a blade stirrer at 2000 rotations/second. Afterwards the mixture was put in a foaming mould under a fume hood until final foaming. The foam remained at room temperature for at least 24 h before performing out any

measurement, to insure complete reaction between polyol and isocyanate. The PCM (PCM@BASF or PCM@$CaCO_3$) and flame retardant (melamine was purchased from Sigma-Aldrich) were incorporated in the polyol fraction prior to the PUFs formation by mixing for 55 s. To avoid high shear forces, a blade stirrer with a lower rotation rate (1000 rotations/second) that does not touch the bottom of the beaker was used. According to the Figure 9 the mixture was immediately transferred into the mould.

Figure 9: Scheme of the RPU panel production

Additionally, according to Amaral et al. [183] the experimental results were used to determine the optimal wt% of PCM to add to the RPU, which was 5.0 wt%. To evaluate the influence of PCM in the RPU foam layer, the following experimental characterization tests were carried out over 3 types of specimens with dimensions according to Figure 10:

- RPU without PCM (designated as RPU);
- RPU with 5.0 wt% PCM@BASF (designated as RPU_5PCM@BASF);
- RPU with 5.0 wt% PCM@$CaCO_3$ (designated as RPU_5PCM@$CaCO_3$).

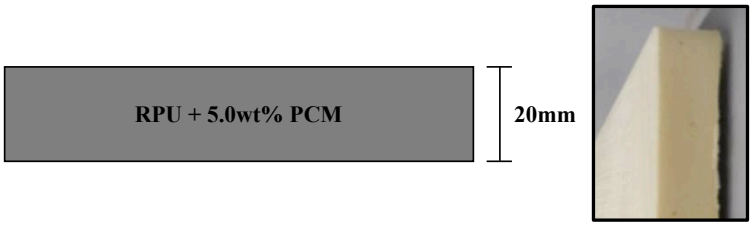

Figure 10: Scheme of the RPU panels

3.2.2.2. PUFs composite panels

In the following Table 10 the weight in (wt/wt), scaled to 100 parts of polyol, of the PUFs composite panels formulations are listed.

Layer	Material	Parts
RPU foam	Polyol	100
	Isocyanate	130
	Additives (catalyst etc.)	1.3
	Melamine	20
	PCM (1.8wt%)	4.5
SPU foam	Polyol	100
	Isocyanate	27
	Additives (catalyst etc.)	1.1
	Aerosil 200	0.5
	Melamine	20
	PCM (1.8wt%)	2.7

Table 10: PU composite panels formulations (scaled to 100parts of polyol)

The PUFs composite panels are composed of three-layered structured composite of rigid foam (RPU) and soft foam (SPU) (see Figure 13). The first layer is a soft foam with PCM, this layer offers a first acoustic insulation function of the PUFs panel and will be compressed against a backing surface when installed, covering defects and protrusions. The second layer is the rigid foam with PCM and will have the thermal insulation function and assure the mechanical stability of the PUFs panel. Finally, the soft foam layer without PCM, serves as a protection to adjacent layers against mechanical forces.

The production of the PUFs composite panels underwent three different steps shown in Figure 11. The first step was the production of the rigid foam layer, which is the middle layer of the finished panel. The next step was the production of the soft foam layer without PCM and to connect this layer to the rigid foam, this layer had to be roughen up, so that the soft and rigid foam stick together. The third and final step was the production of the last soft foam layer containing PCM. The thickness and the position of the layers is shown in Figure 13.

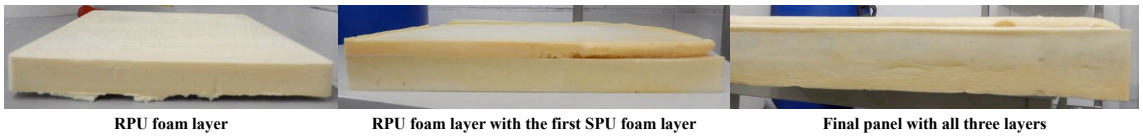

Figure 11: Scheme of the PUFs composite panel production

Starting with the rigid foam, the first step was the weighing of all the materials in a 400 mL cardboard cup starting with the polyol 463 RG 48, then the melamine (purchased from Sigma-Aldrich) and the PCM and the mixture is stirred for 1 minute. In the next step the isocyanate (Puronate 900/1) (purchased from Rühl) was added and then the mixture is stirred again for at least 15 seconds, till everything seems homogeneous and finally the mixture is placed as fast as possible into the moulding apparatus which will then be closed for 15 minutes.

Using the spacer (see Figure 12) the layer dimensions are adjusted to the defined dimensions. The next step was the addition of the first soft foam layer without PCM. First of all, the surface of the rigid foam has to be roughened. Therefore, the surface receives a preparation with a wire brush and afterwards the panel is positioned inside the mould with the rough treated surface facing upwards.

Next the soft foam materials are prepared, weighed and stirred in an identical manner and for a time similar as the rigid foam. The polyol EP 3408 and the isocyanate (PURONAT 947) was purchased from Rühl, the melamine purchased from Sigma-Aldrich and the PCM (PCM@BASF or PCM@$CaCO_3$) was purchased from BASF and produce according to section 3.2.1.2. The mixture will be added on top of the rigid foam and the mould apparatus will be closed also for 15 minutes.

After adjusting the dimension for the third layer, the procedure is very similar to the addition of the first soft foam layer. The already added soft foam will face the bottom of the mould so that the roughen rigid foam surface faces upwards. The mixture will then be added and set in the closed mould apparatus for 15 minutes to finish the three-panel composition.

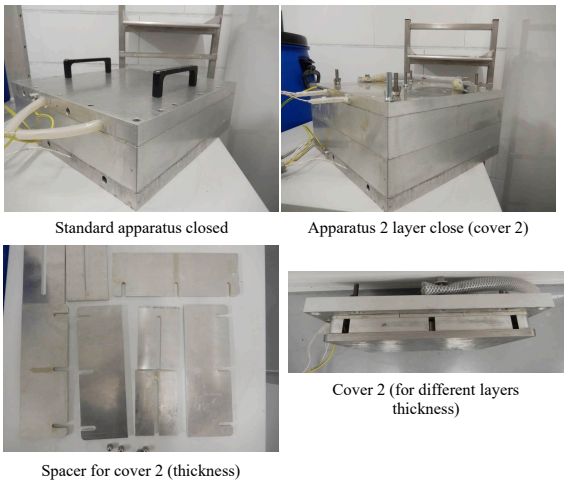

Figure 12: Apparatus of the PUFs composite panel production

Additionally, according to Gomez et al.[189] the numerical analysis was used to determine the optimal wt% of PCM to add to the PUFs composite (with RPU and SPU). The determined values were 1.8 wt% of PCM for the PUFs composite. To evaluate the influence of PCM in the PUFs composite layers, the following experimental characterization tests were carried out over 3 types of specimens with configuration and dimensions according to Figure 13:

- PUFs (with RPU and SPU) without PCM (designated as PU);
- PUFs (with RPU and SPU) with 1.8 wt% PCM@BASF (designated as PU_1.8PCM@BASF);
- PUFs (with RPU and SPU) with 1.8 wt% PCM@$CaCO_3$ (designated as PU_1.8PCM@$CaCO_3$).

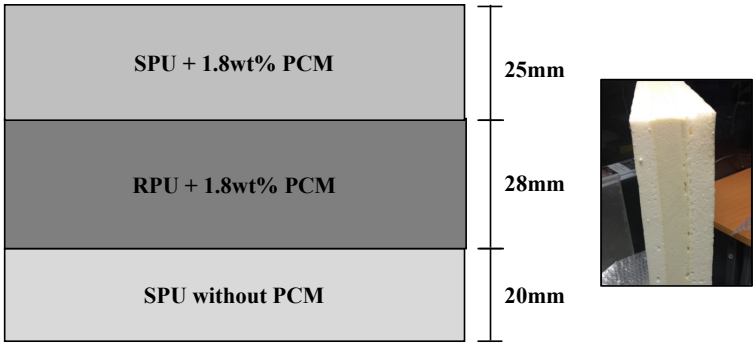

Figure 13: Scheme of the PU composite panels

3.2.2.3. Characterization of PUFs panels

To evaluate the influence of PCM in the PUFs panels, the selected experimental characterization tests were carried out over all the produced panels: *i)* SEM analysis; *ii)* density; *iii)* energy storage properties; i*v)* thermal conductivity.

The cellular structure (shape and size) of the PUFs were analysed by SEM according to the section 3.2.1.3.

PUFs specimens (50×50×thickness mm^3) were cut and weighed to determine the density. Densities were determined dividing the weight of the specimens by their respective calculated volume. The values presented correspond to the average density determined for 9 specimens of each PUFs panel. The density of the PUFs panels was used to determine if the PCM incorporated process influences the PUFs foam density.

To characterize the energy storage properties of the PUFs panels (melting temperature and enthalpy), a dynamic scanning calorimeter (DSC 4000, PerkinElmer) was used according to section 3.2.1.3. This test is essential to characterize the energy storage properties of the PUFs panels and useful for to determinate the PCM content ($\%_{PCM}$) incorporated into the PUFs, according the following Equation (5):

$$\%_{PCM} = \frac{\Delta H_{m,PCM}}{\Delta \mathrm{H}_{m,PUFs}} \times 100 \quad (5)$$

Where, $\Delta H_{m,PCM}$ is the latent heat of the PCM for melting curve and $\Delta H_{m,PUFs}$ is the latent heat of the PUFs for melting.

The thermal conductivity of the PUFs panels was measured using the Hot Disk Transient Plane Source (TPS) technique [190]. The method is based on a planar sensor made of a patterned nickel element, between two thin layers of insulated material, like Kapton or mica. By passing current through the nickel element, and simultaneously measuring its resistivity, the sensor acts as both heater and thermometer. By fitting the transient heating curve, estimates of thermal conductivity and diffusivity are obtained, and specific heat calculated from the former two. The method is standardised in ISO 22007-2 [191]. The type of the sensor used in this measurement approach consists of a nickel/Kapton sensor, which was placed between two similar specimens with dimensions of 40 × 40 mm (width x length) and thickness of the real specimens (see Figure 10). Hot Disk measurements of the PUFs composite panels were not performed, as the composite (layered rigid and soft foam) structure of the material prevents accurate

measurements with this technique. The uncertainty of the final thermal conductivity was obtained directly from the TPS equipment and the value is ±0.00005 W/m.K.

The hot box approach is based on the steady-state method. This method consists in a simple hot box configuration composed by two closed chambers with controlled temperature and relative humidity conditions: one of the chambers is at low and constant temperature (cold chamber) and the other, the measuring chamber, is placed at higher and constant temperature (warm chamber). Between the two compartments or chambers there is a mounting ring with the wall specimen or panel to be tested, as presented on

Figure 14. The procedures, the schemes, the materials, have been previously defined Amaral et al. elsewhere [176].

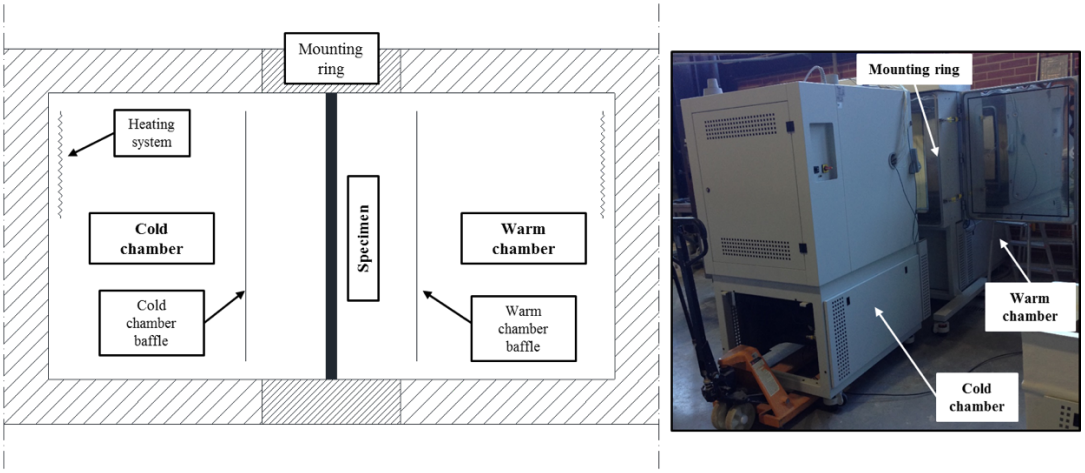

Figure 14: Scheme of the hot box Setup [176]

The thermal conductivity (λ) is calculated according the Fourier´s Law, using Equation (6):

$$\lambda = \frac{q \times s}{\Delta T} \tag{6}$$

Where, q is the measured heat flux (W/m²) on the face of the wall specimen, s is the thickness of the wall specimen (meters) and ΔT is the temperature difference between the two wall specimens faces (°C). The sensors were calibrated and the uncertainty of each of them is ± 0.01 °C (temperature sensor), ±0.1 W/m^2 (heat flux sensor) and ±0.01 mm (calliper for specimen thickness). The uncertainty of the final thermal conductivity was associated to the propagation of uncertainty of

indirect experimental measurements. The calculation of the uncertainty propagation for the thermal conductivity is ±0.017 W/m.K, according to Ricklefs et al. [192].

The thermal conductivity was calculated for different setup temperatures on the cold and warm chambers, using the same thermal amplitude value of 10 ºC and 50 % of RH. The thermal conductivity was calculated for the following setup temperatures: {2;12}, {4;14}, {6;16}, {…}, {26;36}, {28;38} and {30;40} (which means: {temperature of the cold chamber in ºC; temperature of the warm chamber in ºC}). The total amount of temperature steps carried out in these experimental setups was 15, and the measurement time for each temperature step was 6 hours.

The most important advantage of the use of hot box approach for thermal conductivity measurements is the possibility to measure layered structured specimens.

3.3. Results and Discussion

3.3.1. Phase change materials (PCM)

3.3.1.1. Morphology and microstructure

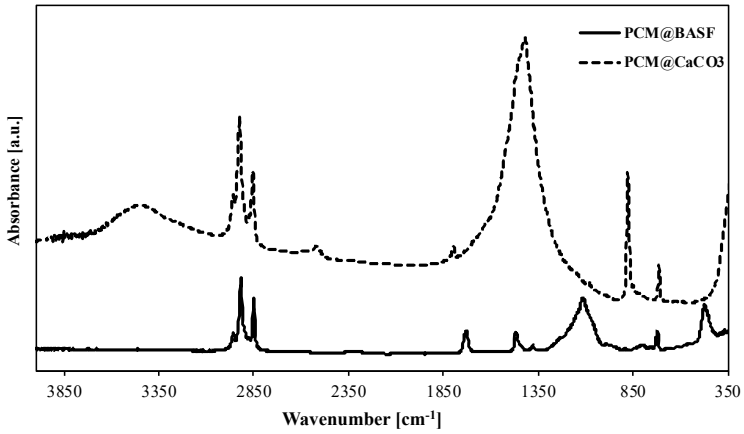

Figure 15: FTIR of PCM@BASF and PCM@$CaCO_3$.

The chemical compositions of the commercial PCM@BASF and the synthesized PCM@$CaCO_3$ were confirmed by FTIR, as shown in Figure 15.

For the commercial PCM@BASF the FTIR spectrum shows peaks from 2956 cm^{-1} to 2849 cm^{-1} that correspond to the aliphatic C–H stretching vibration. The vibration at 1730 cm^{-1} is attributed to the carbonyl group of acrylate, while the absorption peak at 1465 cm^{-1} is associated with the C–H bending vibration, and the absorption

peak at 1114 cm^{-1} can be assigned to the C–O stretching of the ester group of PMMA used as encapsulating material.

For the synthesized PCM@$CaCO_3$ the vibrational bands at 877 cm^{-1} can be assigned to a carbonate out-of-plane stretching vibration. The presence of an absorption peak at 711 cm^{-1} is attributed to the in-plane bending vibration of O−C−O in calcite. The presence of a broad band at 1417 cm^{-1} represents the asymmetric stretch of carbonate ions, which is an indicative of the existence of CO_3^{2-}. FTIR spectra also reveal two intensive absorption peaks at 2925 and 2855 cm^{-1}, which are associated with the alkyl C-H stretching vibrations of methyl and methylene groups and these bands are characteristic of paraffin.

The PCM morphology was analysed by SEM. Figure 16(a) shows the morphology and the size of the PCM@BASF particles. The PCM@BASF specimens consists on microspheres of approximately 300-50 μm in diameter, which in turn are made of multiple spheres with diameters approximately 7-2 μm each. PCM@$CaCO_3$ specimens exhibit a quasi-spherical and rhombohedral morphology (Figure 16(b)). The formation of a rhombohedral particles may be ascribed to the spontaneous steric compression during the crystallization of the calcium carbonate in calcite form. This specimen is constituted by agglomerates of microparticles and nanoparticles (particle size approximately 7 μm – 55 nm).

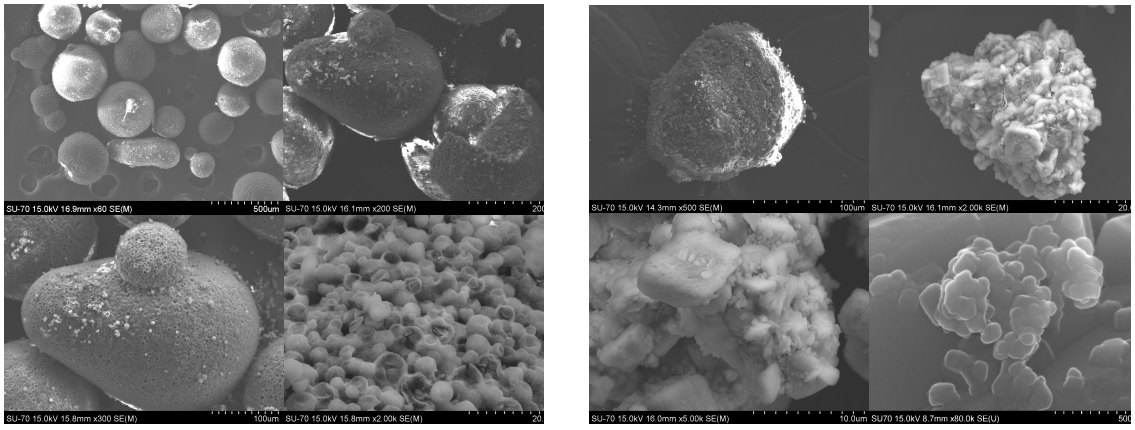

(a) (b)

Figure 16: SEM images with different magnifications of (a) commercial PCM@BASF and (b) synthesized PCM@$CaCO_3$.

According to the Table 11, the synthesized PCM@$CaCO_3$ increase in density compared to the commercial PCM@BASF. The results of the commercial PCM@BASF are in the agreement with the technical data sheet of the supplier (density between 250 kg/m^3 and 350 kg/m^3) [193]. The increase of the synthesized PCM@$CaCO_3$ density is related with the presence of the $CaCO_3$. The values presented correspond

to the average bulk density determined for 4 specimens for each type of PCM (PCM@BASF and PCM@$CaCO_3$).

Table 11: Bulk density of the PCM

Specimen	Density (kg/m³)
PCM@BASF	345.59 ± 3.65
PCM@$CaCO_3$	503.36 ± 4.39

3.3.1.2. Thermal properties

Table 12 summarizes the results of the transition temperature ($T_{t,m}$), the melting temperature (T_m) and the latent heat (ΔH_m) values of the specimens for melting curve. The measurements were made using three specimens for each type of PCM.

Table 12: DSC results of the commercial PCM@BASF and the synthesized PCM@$CaCO_3$

Specimens	Melting		
	Transition temperature $T_{t,m}$ (°C)	Melting temperature T_m (°C)	Melting latent heat ΔH_m (J/g)
PCM@BASF	25.36±0.04	27.55±0.10	97.85±14.64
PCM@$CaCO_3$	23.37±0.65	25.84±0.44	59.56±11.78

According to the data listed in Table 12, the commercial PCM@BASF has considerably higher phase change enthalpy in comparison with the synthesized PCM@$CaCO_3$, because the PCM@$CaCO_3$ has less amount of paraffin compared to the PCM@BASF. This indicates that the commercial PCM@BASF can store more latent heat when phase change occurs.

Figure 17 shows the thermal stability of the commercial PCM@BASF and the synthesized PCM@$CaCO_3$.

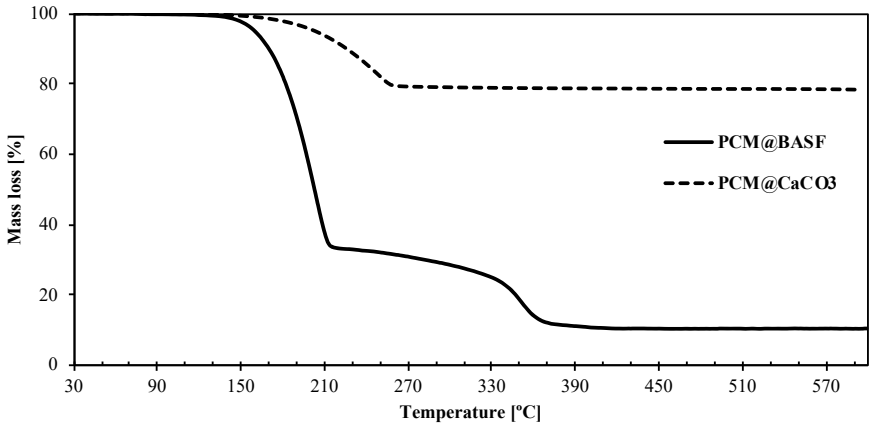

Figure 17: TGA of PCM@BASF and PCM@$CaCO_3$.

As observed in the TGA of PCM@BASF, thermal degradation takes place in two stages. The first one corresponds to the decomposition of the paraffin wax between 110 and 210 °C. The second mass loss is attributed to the shell material (PMMA) with an onset temperature around 330 °C. This behaviour is in accordance with the Giro-Paloma et al. [194].

For the synthesized PCM@$CaCO_3$ the first stage of weight loss, between 180 and 230ºC, is ascribed to the decomposition of PCM paraffin and the degradation of $CaCO_3$. From the above TGA curve for PCM@$CaCO_3$, this material contains about 20 % paraffin and 80 % $CaCO_3$ and a thermal stabilization of the paraffin occurs as it begins to degrade later compared to the PCM@BASF. Thus, PCM@$CaCO_3$ is more stable material than PCM@BASF in terms of thermal stability.

Compared to Shi et al. [123] the TGA curves are quite similar to the synthesized PCM@$CaCO_3$, the specimens show a two-step degradation process, the temperatures at maximum weight loss rate are significantly improved up to 215 ºC at least. Such a rapid weight loss is due to the evaporation of paraffin and high temperature decomposition of $CaCO_3$, and finally the residues are calcium oxide (above 600 ºC).

Table 13: Thermal conductivity results of the commercial PCM@BASF and the synthesized PCM@$CaCO_3$ at different temperatures.

Specimens	**Thermal conductivity (W/mk)**	
	10±0.5°C	**20±0.5°C**
PCM@BASF	0.083±0.000	0.121±0.009
PCM@$CaCO_3$	0.970±0.000	1.051±0.003

The thermal conductivities of the PCM@BASF and PCM@$CaCO_3$ are summarized in Table 13. The commercial PCM@BASF and the synthesized PCM@$CaCO_3$ in the solid state (at 10±0.5 °C) show a thermal conductivity as low as in the liquid state (at 20±0.5 °C). Nevertheless, PCM@$CaCO_3$ has considerably higher thermal conductivity when compared to PCM@BASF. These results confirm that the PCM@$CaCO_3$ composite shows a high thermal conductivity.

3.3.2. Polyurethane foam incorporating phase change material

3.3.2.1. Rigid PUFs panels (RPU)

Figure 18 shows the SEM images at a magnification of 50× of three different RPU foams.

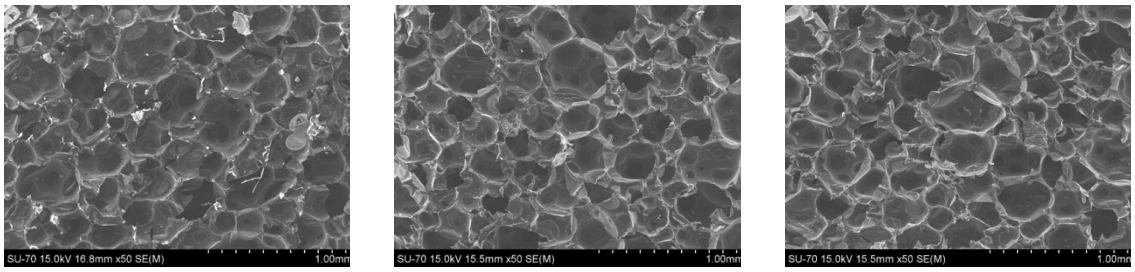

(a) RPU (b) RPU_5PCM@BASF (c) RPU_5PCM@$CaCO_3$

Figure 18: SEM images of the RPU panels

In Figure 18(a) it can be seen that the RPU foam without PCM present the typical polyhedral closed-cell structure. When the PCM are added to the foaming system, the closed cells tend generally to be smaller size (see Table 14), which is induced by the nucleating character of the added PCM [183,195,196]. However, the presence of PMC in the RPU foams does not change significantly the size and shape of the foam cell structure according to Figure 18. The behaviour was similar for both types of the PCM. These results confirm the PCM content (only 5 wt.%) was not enough to change the cellular structure of the foams.

Table 14: Physical properties of the RPU panels

Specimen	**Density (kg/m^3)**	**Average cell size (μm)**
RPU	81.411±1.553	350.780±84.766
RPU_5PCM@BASF	88.864±1.035	283.913±74.655
RPU_5PCM@$CaCO_3$	93.249±1.473	273.733±80.029

According to the Table 14, it was observed that the foam density increased with the incorporation of the PCM because the fillers are denser materials. which in in agreement with what has been reported in the literature density [27,186,197,198].

Table 15 summarizes the results of the transition temperature ($T_{t,m}$), the melting temperature (T_m) and the latent heat (ΔH_m) values of the specimens for the melting curve. The measurements were made using three specimens for each panels' composition.

Table 15: DSC results of the RPU panels

Specimens	**Melting**			**$\%_{m,PCM}$**
	Transition temperature $T_{t,m}$ (°C)	**Melting temperature T_m (°C)**	**Melting latent heat ΔH_m (J/g)**	
RPU_5PCM@BASF	22.31±0.04	23.54±0.08	6.16±1.22	6.3
RPU_5PCM@$CaCO_3$	21.22±0.35	22.97±0.16	2.81±0.37	4.7

According to the Table 15 and Table 12, it can be seen that the RPU foams with PCM (RPU_5PCM@BASF and RPU_5PCM@$CaCO_3$) have an endothermic peak in the process of heating with a small decrease in range of values to the PCM. For the RPU_5PCM@BASF the range decreases 3 ºC compared to the commercial PCM@BASF and for the RPU_5PCM@$CaCO_3$ the range decreases 2 ºC compared to the synthesized PCM@$CaCO_3$, due to the effect of the flame retardant melamine.

The PCM content ($\%_{PCM}$) incorporated in the RPU foams calculated according the Equation (1) is within the expected value (5.0 wt.%) for the both panels. However, the RPU_5PCM@BASF shows the highest latent heat storage capacity (6.12 J/g corresponding to 6.3 wt.%) compared to the RPU_5PCM@$CaCO_3$ (2.81 J/g corresponding to 4.7 wt.%). This indicates that the RPU_5PCM@BASF can store more latent heat.

Figure 19 illustrates the thermal conductivity versus temperature results of the RPU panels specimens with or without PCM using the Hot Disk approach. Temperature increasing (range 6–40 °C), followed by temperature decreasing (range 40–6 °C) measurements were performed.

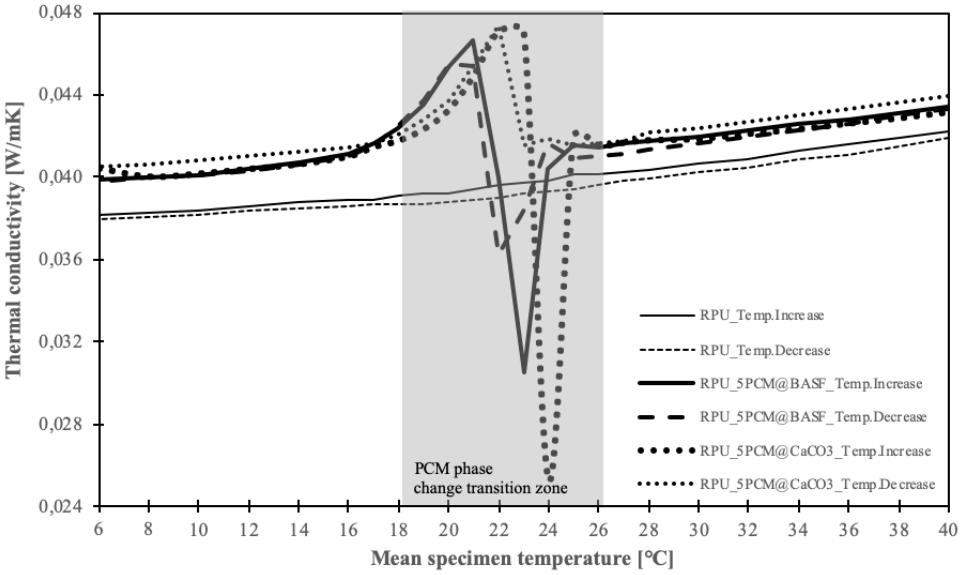

Figure 19: Thermal conductivity versus mean temperature of RPU panels

The specimen with no PCM shows a steady increase of thermal conductivity with temperature. This trend is also observed in all specimens with PCM, away from the phase transition interval (18 ºC – 26 ºC). It is interesting to note that there is a small, but observable increase of thermal conductivity of the RPU_5PCM@$CaCO_3$ specimen compared to RPU_5PCM@BASF. This is expected due to the higher thermal conductivity of PCM@$CaCO_3$ (see Table 13) which allows faster heat transfer throughout the RPU foam. Within the phase transition interval, the thermal conductivity measurements reflect the heat absorption/release process of the PCM. Consequently, the nickel sensor is influenced by the cooling/heating effect from the phase change, which will shift the transient, resulting in this singularity-like temperature behaviour.

Figure 20 and Figure 21 show the experimental data of the thermal conductivity versus mean specimen surfaces temperature for the RPU panels (without and with PCM) using the hot box approach.

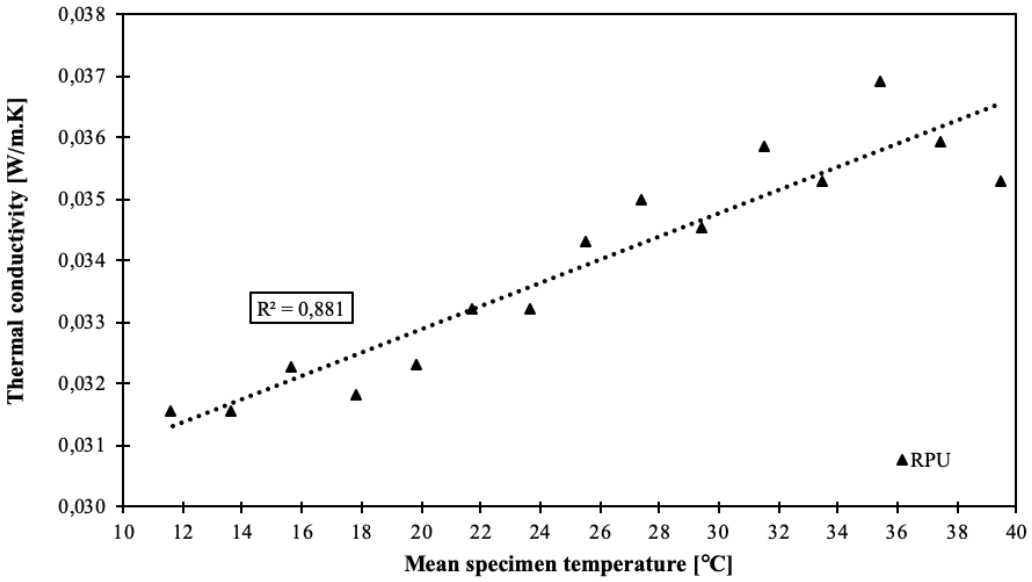

Figure 20: Thermal conductivity as function of the mean RPU (without PCM) surface temperature (adapted from [176])

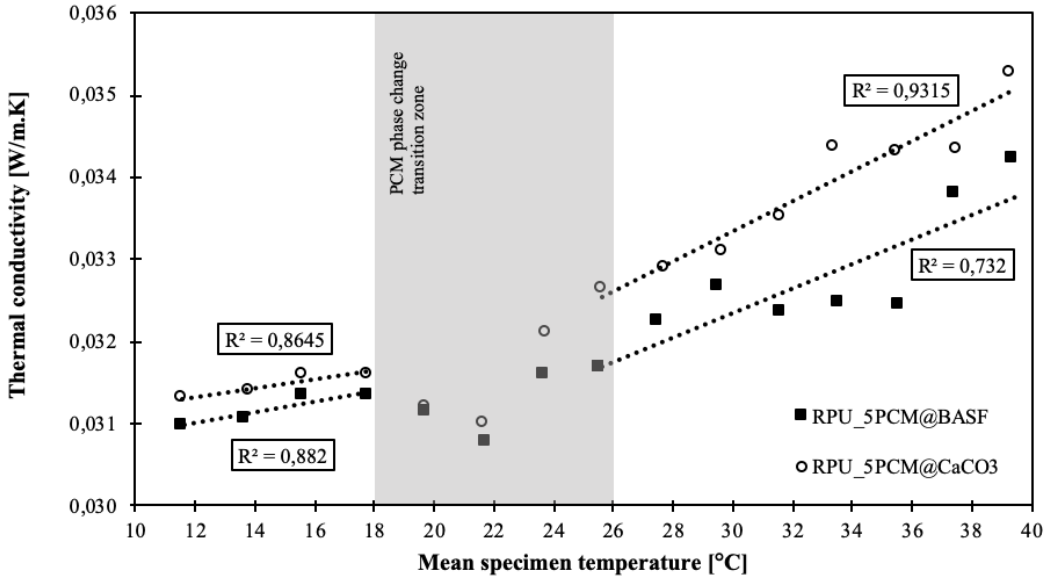

Figure 21: Thermal conductivity as function of the mean RPU (with PCM) surface temperature

According to Figure 20, for the RPU panel without PCM, it can be observed that the value of the thermal conductivity increases linearly with a square correlation (R^2) of 0.881 with the surface temperature increase, as expected Amaral et al. [176]. The values of the thermal conductivity were between 0.0315 W/m.K (at 11.64 ºC) and 0.0369 W/m.K (at 39.48 ºC).

Figure 21 shows the results for the thermal conductivity as function of the mean surface temperature for the RPU panels with PCM (RPU_5PCM@BASF and

RPU_5PCM@$CaCO_3$). For both panels the thermal conductivity profile shows a similar behaviour to that of the RPU foam without PCM when the mean specimen surface temperature is below and above the phase change transition range (18 °C to 26 °C). In this case, the thermal conductivity increases with the surface temperature increase and the R^2 was between 0.7320 and 0.9315, which demonstrates that the regression line fits reasonably the experimental data. However, the RPU_5PCM@$CaCO_3$ has higher values compared to the RPU_5PCM@BASF, which is the expected behaviour. This enhancement of RPU_5PCM@$CaCO_3$ is attributed to the high thermal conductivity of the PCM@$CaCO_3$ (see Table 13) which allows the rapid heat transfer throughout RPU foam.

During PCM phase change transition the value of the thermal conductivity decreases in the RPU foams in the phase change temperature range (18 °C to 26 °C). It was observed a decreasing trend with the increasing mean temperature of the specimen. According to Amaral et al. [176] and Wang et al. [199], this behaviour is due to the coexistence of the PCM in two physical states (solid and liquid) in the phase change temperature range and was influenced by the temperature rise, as well as by the phase change fraction of the PCM. Also, in this case (during PCM phase change transition) the RPU_5PCM@$CaCO_3$ revealed higher thermal conductivity values compared to the RPU_5PCM@BASF.

3.3.2.2. PU composite panels

Figure 22 shows SEM micrographs of the different layers of PU composite cell structure at a magnification of 30×. For the RPU layer when the PCM were added to the foaming system, the cell diameter was smaller and irregular than that without PCM. The phenomenon is induced by the "nucleation" function and is in agreement with the rule that, in general, added powder filling will reduce the cell diameter. Although the percentage of PCM is lower than in the RPU panels, in this case the phenomenon was observed, and may be related to the fact that the production methods are distinct. For the SPU layer, the presence of the PCM cause the irregularity of the size and shape of the cellular structure of the SPU foams. Moreover, the diameters of the cells became larger when the PCM were added. This was caused by the adding of PCM. The behaviour was similar in the both types of the PCM.

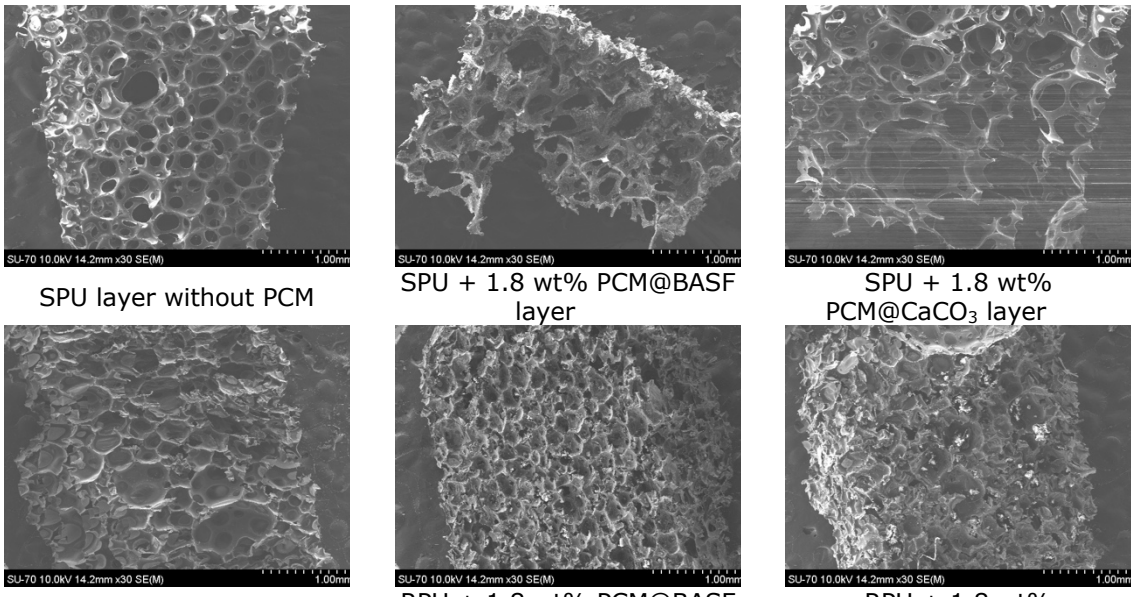

SPU layer without PCM | SPU + 1.8 wt% PCM@BASF layer | SPU + 1.8 wt% PCM@$CaCO_3$ layer

RPU layer without PCM | RPU + 1.8 wt% PCM@BASF layer | RPU + 1.8 wt% PCM@$CaCO_3$ layer

Figure 22: SEM images of the different layers of PU composite panels

Table 16: Density of the PU composite panels

Layer specimen	**Density (kg/m^3)**
SPU without PCM	78.581±0.733
SPU_1.8PCM@BASF	95.969±3.846
SPU_1.8PCM@$CaCO_3$	110.541±1.564
RPU without PCM	88.889±3.409
RPU_1.8PCM@BASF	107.339±2.682
RPU_1.8PCM@$CaCO_3$	113.590±2.274

According to Table 16, it was observed that the results are in the agreement with those in Table 14. The foam density (for the SPU layer and RPU layer) increased with the incorporation of the PCM because the fillers are denser materials.

Table 17 summarizes the results of the transition temperature ($T_{t,m}$), the melting temperature (T_m) and the latent heat (ΔH_m) values of the specimens for melting curve. The measurements were made using three specimens for each layer (SPU and RPU) composition.

Table 17: DSC results of the PU composite panels

Layer specimens	Melting			$\%_{m,PCM}$
	Transition temperature $T_{t,m}$ (°C)	Melting temperature T_m (°C)	Melting latent heat ΔH_m (J/g)	
SPU_1.8PCM@BASF	23.68±0.30	24.79±0.83	1.66±0.12	1.7
SPU_1.8PCM@$CaCO_3$	20.80±0.14	22.79±0.16	1.11±0.36	1.9
RPU_1.8PCM@BASF	23.98±0.42	25.11±0.34	1.76±0.23	1.8
RPU_1.8PCM@$CaCO_3$	20.72±0.16	22.58±0.21	1.03±0.47	1.7

The results in Table 17 are in agreement with the results obtained for the RPU panels (see Table 15) in section 3.3.1.2. For the SPU layer and RPU layer of the PU composite panels, it can be seen that the PU layers with PCM have an endothermic peak in the process of heating with a small decrease in the range of values to the PCM (PCM@BASF and PCM@$CaCO_3$) due to the effect of the flame retardant melamine. The PCM content ($\%_{PCM}$) incorporated in the RPU foams calculated according the Equation (1) is within the expected value (1.8 wt.%) for each layer (SPU and RPU) both panels.

Hot Disk measurements of the PU composite panels were not performed, as the composite (layered rigid and soft foam) structure of the material prevents accurate measurements with this technique.

Figure 23 and Figure 24 show the experimental data of the thermal conductivity versus mean specimen surfaces temperature for the PU composite panels (without and with PCM) using the hot box approach.

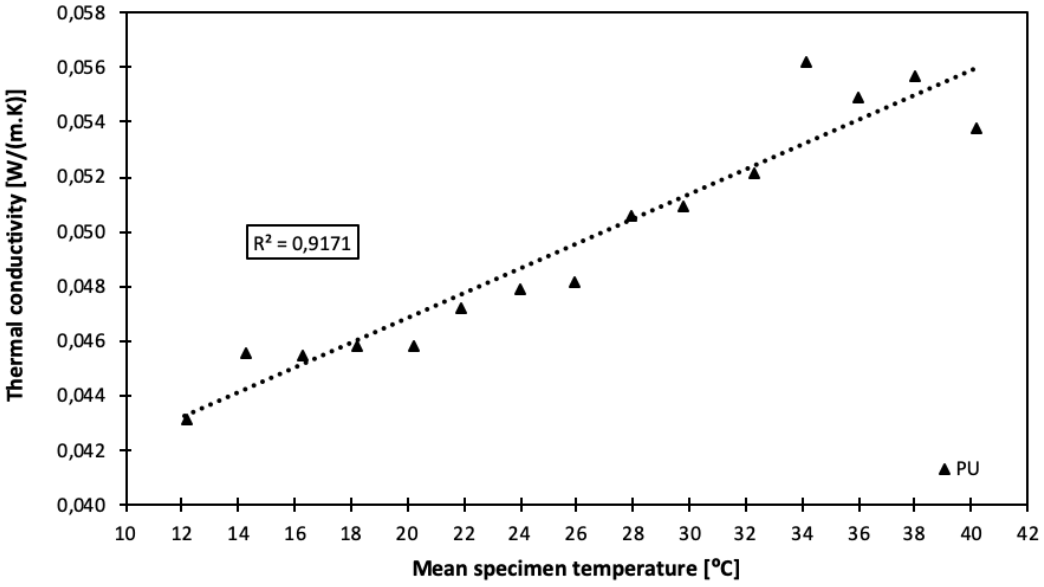

Figure 23: Thermal conductivity as function of the mean PU (without PCM) surface temperature.

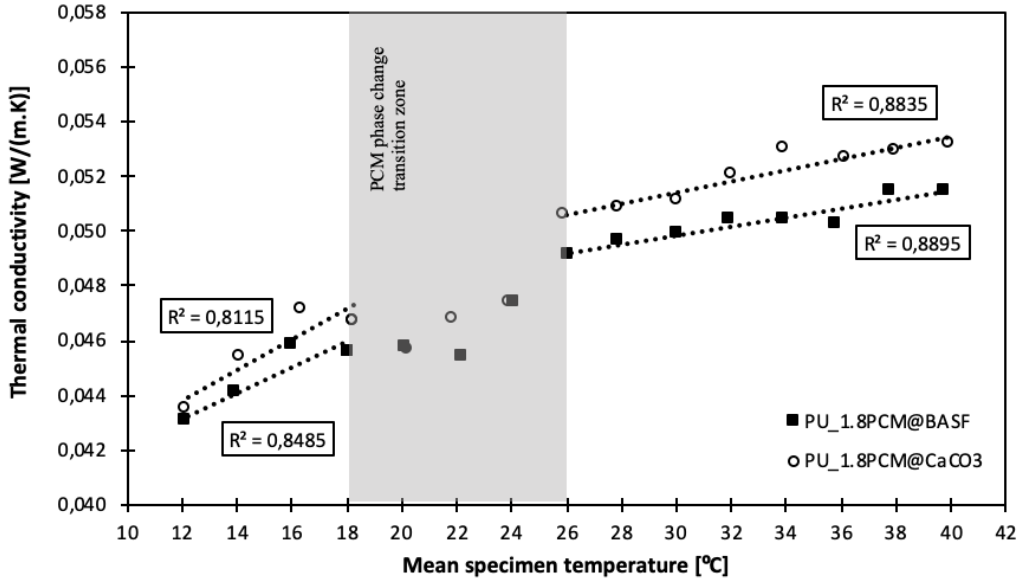

Figure 24: Thermal conductivity as function of the mean PU (with PCM) surface temperature

The results obtained for the PU composite panel without PCM (see Figure 23) are in agreement with the results obtained for the RPU panel without PCM (see Figure 20). The thermal conductivity increases with the surface temperature increase. The R^2 was 0.917, which demonstrates that the regression line fits the experimental data. The values of the thermal conductivity were between 0.0431 W/m.K (for 12.10 ºC) and 0.0538 W/m.K (for 40.15 ºC).

Figure 24 shows the results for the thermal conductivity as function of the mean surface temperature for the PU composite panels with PCM (PU_1.8PCM@BASF and

PU_1.8PCM@$CaCO_3$). For the PU composite panels, the thermal conductivity profile shows a similar behaviour for the RPU panels when the mean specimen surface temperature was below, during and above of the phase change transition range (18 °C to 26 °C). Below and above of the phase change transition range, the thermal conductivity increases with the surface temperature increase and the PU_1.8PCM@$CaCO_3$ has higher values compared to the PU_1.8PCM@BASF. During PCM phase change transition the value of the thermal conductivity decreases with the presence of the PCM in the PU composite foams and there was a decreasing trend with the increasing mean temperature of the specimen.

3.4. Conclusions

In the present study, different PUFs panels (rigid PUFs, a layered structured composite of rigid and soft foam) were produced using standard PUFs synthesis. To overcome the low thermal conductivity of the PUFs matrix, a method to prepare PCM based on paraffin and calcium carbonate has been developed. The PCM (both synthesized and commercial) were then incorporated in PU formulations to yield PU panels.

The following main conclusions taken are:

- The synthesized PCM@$CaCO_3$ increase in density and thermal conductivity compared to the commercial PCM@BASF. However, the commercial PCM@BASF has considerably higher phase change enthalpy then the synthesized PCM@$CaCO_3$.

- Comparing the experimental results obtained for RPU panels and PUFs composite panels with and without PCM, it was observed that the presence of PCM led to an increase in density (by the incorporation of denser fillers) and small changes in cell structure (induced by the "nucleation" process).

- The hot disk and hot box approaches were used to assess the thermal conductivity of RPU panels with and without PCM. However, for the PUFs composite panels it was not possible to use the hot disk method to determine the thermal conductivity because it was a panel with multilayers (hot disk limitation).

- The experimental results show that the values of thermal conductivity for temperatures below and above the PCM phase change transition zone increase with the increasing temperature. However, during the PCM phase change transition a decreasing trend of the thermal characteristics with increasing temperature is observed. This behaviour was similar for both types of PCM (PCM@BASF and PCM@$CaCO_3$) and for both types of panels (RPU panel and PUFs composite panel).

- Results revealed that panels with PCM@$CaCO_3$ have higher thermal conductivity values compared to the panels with PCM@BASF, due to the high thermal conductivity of PCM@$CaCO_3$ which allows the rapid heat transfer throughout the PUFs.

This experimental study presents the promising results of the synthesized PCM@$CaCO_3$ compared to the commercial PCM@BASF and the incorporation of this PCM into the PUFs panels. Optimization of the content of PCM and the PCM position in a PUFs panel needs further research, including other issues such as thermal performance evaluation.

CHAPTER 4

4. Comparative analysis of thermal conductivity characterization approaches

This chapter was published in the Journal of Energy and Building

Amaral, C., Vicente, R., Ferreira, V., Silva, T. (2017) – Polyurethane foams with microencapsulated phase change material: Comparative analysis of thermal conductivity characterization approaches – Journal of Energy and Building, Elsevier, vol. 153, pp. 392-402 (IF2017=4.067; IF5y=4.599) http://dx.doi.org/10.1016/j.enbuild.2017.08.019

Abstract

The use of thermal insulation materials is regarded as the most effective passive measure of energy savings in buildings. Rigid polyurethane foams (RPU) are commonly used as the insulation layers of opaque building envelope solutions, as well as for other applications in the field of transportation, textile industry and electrical appliances, accounting for almost one-third of the polyurethane market. In the assessment of the energy performance of buildings, insulation materials, such as RPU foams have good insulating properties (low thermal conductivity), however their thermal performance can be enhanced by the incorporation of phase change materials (PCM). In this work, three different approaches (flux meter approach, the guarded hot plate approach and the transient plane source approach) are presented to determine the thermal conductivity of RPU foams with and without the incorporation of PCM based on steady state method and transient method. In addition, this work presents and discusses the comparison between measurements carried out using the three approaches revealing the important factors that should be considered to determinate the thermal conductivity of the RPU foams with PCM, particularly in the temperature range during PCM phase change transition (solid/liquid state).

Keywords: guarded hot plate; hot box heat flux meter; phase change material PCM; rigid polyurethane foams (RPU); thermal conductivity; transient plane source.

4.1. Introduction

Energy consumption in the residential, commercial and public services sector is responsible for consuming 40% of the total final energy use of the European Union (EU) [1–4]. Therefore, it is necessary that the energy consumption of buildings decreases, but without compromising the living standards and thermal indoor comfort requirements [5].

Thermal energy storage (TES) systems have gained much attention in the last decade, particularly as a potential approach to improve the energy efficiency in buildings. In this context, phase change materials (PCM) appear as a potential solution to increase the thermal efficiency in buildings since they can store more energy, in the latent form, than the typical sensible energy stored by most common building materials [6,7,29,31].

The main advantage of the integration of latent heat thermal energy storage systems (LHTES) using PCM into building solutions is the high storage density for small temperature intervals and when coupled with other active systems can increase the energy efficiency in new and refurbished buildings [7–10,41,175]. This storage capacity increases the building thermal inertia, and it is expected to contribute to solving the time mismatch between the energy supply and demand.

One of the most used solutions, to improve the thermal behaviour of building envelopes and enhance the building indoor thermal regulation, is the use of thermal insulation materials. Rigid polyurethane foams (RPU) are one of the most well-known material that are used in a wide range of different sectors, such as medicine transportation, decoration and appliances and also in the building sector, mainly as insulation layers incorporated into opaque envelope building solutions [84,200]. Compared with others known typically insulating materials, RPU are highly competitive, because of their good thermal and physical properties, such as: *i)* low thermal conductivity, ii) high mechanical and chemical stability and *iii)* their compatibility and easy form to be incorporated into others façade materials [84]. Furthermore, besides the good insulation properties that the RPU foams have, their thermoregulation capacity can be improved using PCM [185,186,201,202]. In this case, the introduction of PCM will provide an extra heat capacity to the building solution, storing and releasing more energy and keeping the good RPU thermal properties [84].

As referred above, the external envelope of a building plays a fundamental role in its energy efficiency. However, the thermal properties evaluation of building components requires a high level of care and several methods are available.

Thermal conductivity is one of the most fundamental parameters in the assessment of the energy consumption in buildings [203,204], because heat transfer occurs at a lower rate across materials of low thermal conductivity than across materials of high thermal conductivity.

Typical thermal conductivity values for RPU foams are between 0.02 and 0.05 W/mK and variation of the thermal conductivity values is related to several factors. Zhang et al. [205] presented an experimental study of the thermal conductivity of PU foams under various environments, discussing the effect of factors such as temperature, humidity, water uptake, alternate high and low temperature, long time storage at high temperature and gas pressure of the atmosphere. For instance, they have concluded that thermal conductivity of RPU foam increases non-monotonically with temperature and increases as high as 10–18% in moist air. Estravís et al. [206] studied the relationship between cellular structure and thermal conductivity of the RPU foams with infused nanoclays. The thermal conductivity of the foam is reduced after the addition of nanoclays. Marcovich et al. [207] showed that the unfavourable changes of thermal conductivity was an effect of the foam's cellular structure, mainly attributed to the closed cell content.

According to most references, there are many different forms to estimate and calculate the thermal conductivity, however these forms can be divided into two main methods: the steady-state and transient (non-steady-state) method [4,208,209]. To estimate the thermal conductivity using the steady-state method, the temperature imposed to the material surface is kept constant, so that it does not change over time. One advantage of this method is the simple and direct signal analysis. For the calculation of the thermal conductivity using the transient method, the measurements are made during a variable heating process. The sensor imposes a small electric signal in the specimen and the distribution of this signal is analysed and measured. Hereafter, the thermal conductivity is calculated using mathematical approaches, so this method is more difficult to use [199,204,209].

Wang et al. [199] investigated the influence of the temperature as well as the amount of the phase change fraction on the thermal conductivity of the composite wall with PCM based on a steady-state method. A good positive linear relationship was obtained between the thermal conductivity and the increasing temperature for the liquid and solid PCM state. However, in the temperature range during PCM phase change transition (solid/liquid state) the thermal conductivity was negatively proportional to the increasing content of the phase-changed fraction. Eddhahak-Ouni et al. [210] presented the experimental analysis of the influence of temperature and PCM mass percentage on the thermal conductivity of the concrete with PCM by the transient method(hot-disk apparatus), but the study was only

carried out within the temperature range that the incorporated PCM were in liquid state. The results showed that the thermal conductivity decreased slightly with the increasing temperature of the specimens. Ye et al. [211] studied the performance of the thermal conductivity of the shape-stabilized PCM by a steady-state method (a laser flash apparatus). The experimental study was carried out when the PCM was in both the solid and the liquid states and, the results showed a decreasing trend of thermal conductivity of the shape-stabilized when the PCM was in liquid state compared with that in solid state.

This work presents and tests two different methods to calculate the thermal conductivity of RPU foams with and without PCM. The comparison between measurements on the RPU foams with and without PCM specimens showed that there are important factors that must be considered in the determination of the thermal conductivity of the RPU foams with PCM, particularly in the melting/phase change transition range of PCM. Therefore, for a better understanding of these issues, this work focuses firstly on the thermal conductivity of RPU foams without PCM, then on the thermal conductivity of RPU foams with PCM, including a comparative analysis for the three approaches. To evaluate the influence of PCM incorporated into the PU foam in terms of the thermal conductivity, it was taken into account the tests referred in the literature review. The selected experimental characterization tests were: i) hot box heat flux meter approach, ii) guarded hot plate approach, and iii) transient plane source approach. The main aim of this work is to get new insights on the thermal conductivity measurements of RPU foams with PCM using these three different approaches, especially in the temperature range during PCM phase change transition (solid/liquid state).

4.2. Materials and approaches

4.2.1. Description of the specimens

Microencapsulated PCM powder purchased from BASF (Ludwigshafen, Germany) was used in this study, (Micronal® DS 5001 X). It contains paraffin wax with a melting point of 26°C as the core material and a shell of PMMA (poly(methyl methacrylate)). The polyurethane (PU) main components Purotherm 463 RG 48 (polyol) and puronate 900 (isocyanate) of the PU foam formulation were purchased from Rühl Puromer GmbH (Friedrichsdorf, Germany). The polyol includes different proportions of bio-polyols, catalyst and stabilizers. Melamine (99%) was used as flame retardant was purchased from SIGMA ALDRICH (Munich, Germany) as a fine power.

The standard PU foam was prepared using 100 parts of polyol (Purotherm 463 RG 48) and 130 parts of isocyanate (puronate 900). Both components were mixed for 10 seconds with a blade stirrer at 2000 rotations / second. Afterwards the mixture was put in a foaming mould under a fume hood until final foaming. The foam remained at room temperature for at least 24 h before performing out any measurement, to ensure complete reaction between polyol and isocyanate. The PCM (up to 12.5 parts = 5%) and flame retardant (melamine) were incorporated in the polyol fraction prior to the PU foam formation by mixing for 55 sec. To avoid high shear forces, a blade stirrer with a lower rotation rate (1000 rotations/second) that does not touch the bottom of the beaker was used.

Additionally, according to Amaral et al. [183] the experimental results were used to determine the optimal wt% of PCM to add to the RPU, which was 5.0 wt%. To evaluate the influence of PCM (Micronal® DS 5001 X) in the PU foam layer, the following experimental characterization tests were carried out over 2 specimens:

- Rigid PU foam with melamine and without PCM (designated as RPU);
- Rigid PU foam with melamine and with 5.0wt% PCM (designated as RPU_5PCM).

To characterize the energy storage properties of the pristine microencapsulated PCM and RPU_5PCM foam specimens (melting and solidification temperature and enthalpy), a dynamic scan calorimeter (DSC 4000, PerkinElmer) was used, at a heating and cooling rate of 1 ºC/min, in the range of 10 ºC to 50 ºC under a nitrogen atmosphere. Table 18 summarize the results of specific heat capacity versus temperature for the PCM and RPU_5PCM foam specimens and the latent heat, ΔH (J/g) values for melting and solidification curves. The measurements were made using three specimens for each composition (PCM pristine and RPU_5PCM foam).

Table 18: DSC results of the PCM and RPU_5PCM foam specimens

Specimens	**Melting**		
	Transition temperature $T_{t,m}$ (°C)	**Melting temperature T_m (°C)**	**Melting latent heat ΔH_m (J/g)**
PCM	25.36±0.04	27.55±0.10	97.85±14.64
RPU_5PCM	22.31±0.04	23.54±0.08	6.16±1.22

4.2.2. Hot box heat flux meter (HB-HFM)

The HB-HFM approach is based on the steady-state method. This method consists in a relatively stable thermal environment using a simple hot box setup [199,212,213], as presented in Figure 25. Each hot box configuration has two closed compartments/chambers with controlled conditions: one of the chambers is at low and constant temperature (cold chamber) and the other, the measuring chamber, is placed at higher and constant temperature (warm chamber). Between the two compartments or chambers there is a mounting ring with the wall specimen or panel to be tested [199,203,208]. This procedures are defined in the EN ISO 8990 standard [214].

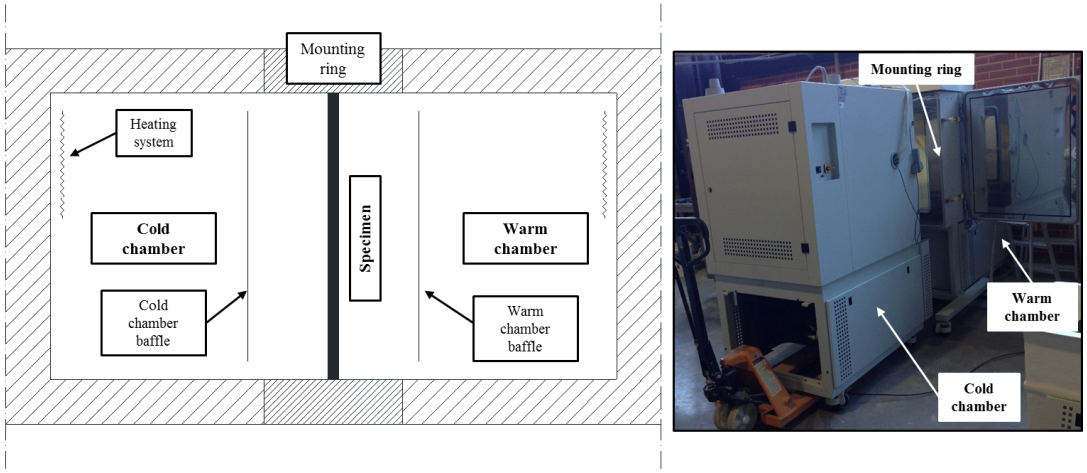

Figure 25: Scheme of the hot box setup

The dimensions of the specimens for thermal properties evaluation are 800x650 mm (HxL in Figure 26) with 20 mm thickness. These dimensions are conditioned by the hot box ring structure geometry (maximum internal dimensions are 800x650x390 mm). The specimen divides the two chambers of the hot box setup, the cold and the warm chamber. Both climatic chambers (Fitoclima 300 ECP20) are manufactured by Aralab with a range temperature from -20 °C to +100ºC ±0.5ºC and a range of relative humidity (RH) of 10% to 98%±2%RH. The internal dimensions are: 800 mm height, 650 mm width, and 600 mm length. The mounting ring was also manufactured by Aralab and is made of the same materials of the climatic chambers. The cold and warm baffles are simple plywood boards.

The indoor temperatures in the chambers, the wall specimen heat fluxes and temperatures on both faces were monitored using: two Hukseflux type HFP01 sensors, twelve PT100 probes and sixteen T type thermocouples. The measured data were collected using the following data loggers; two ICP I-7015P, and two ICP-DAS–I-7018-CR).

Figure 26 presents the sensors position on the specimen (with the same configuration on both sides). Eight T type thermocouples and one heat flux meter were mounted on the external surface of the specimen (cold chamber side). On the internal surface of the specimen, there were eight thermocouples type-T and one heat flux meter in the same position on the opposite side.

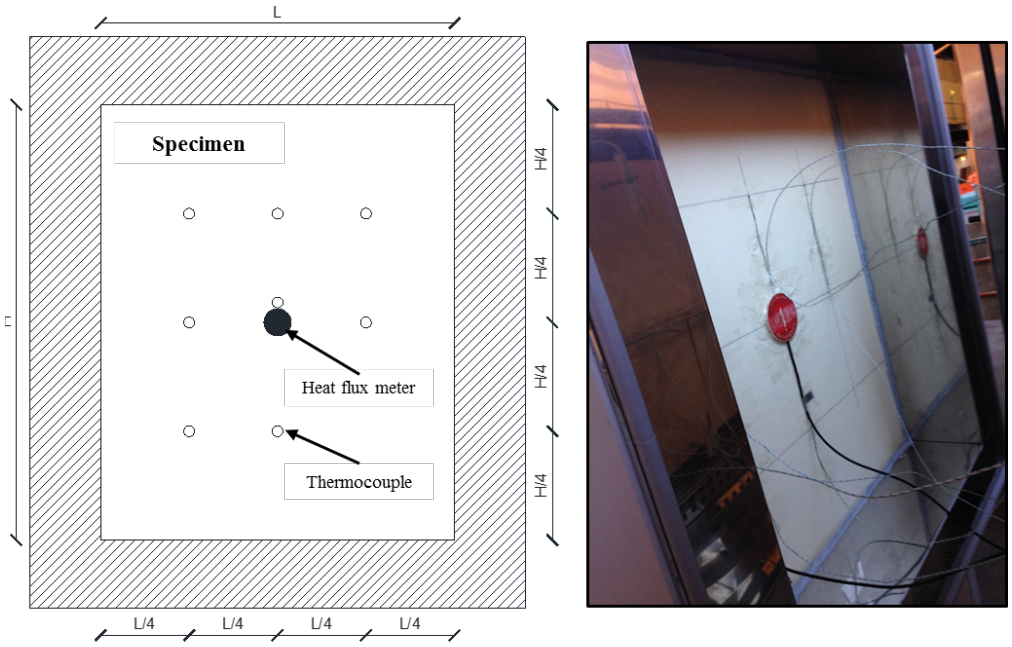

Figure 26: Specimen ring mounting and sensor positioning.

Figure 27 presents five PT100 probes at a distance of 150 mm from the specimen (cold and warm chambers) and one PT100 probe was placed in the middle of the chamber (cold chamber side). In the warm chamber side, six PT100 probes were positioned in the same relative positions on the opposite side.

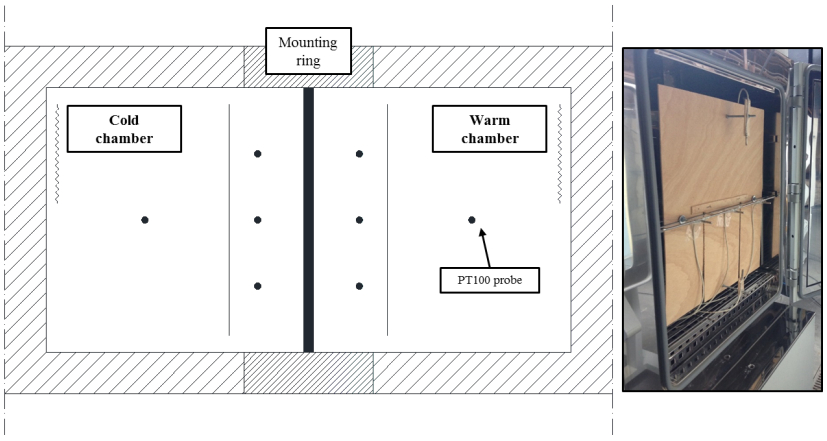

Figure 27: Schematic layout of the PT100 probes in the chambers

The sensors were calibrated and the uncertainty of each of them is ±0.01 °C (temperature sensor) and ±0.1 W/m^2 (heat flux sensor). The measurements were recorded continuously each 5 minutes up to the total testing time of 6 hours.

The thermal conductivity (λ) is calculated according the Fourier´s Law, using equation (6) in the section 3.2.1.6. The thickness of the wall specimen was measured using a pachymeter and the uncertainty is ±0.01 mm.

The uncertainty of the final thermal conductivity was associated with the propagation of uncertainty in indirect experimental measurements. The calculation of the uncertainty propagation for the thermal conductivity is ±0.017 W/m.K, according to Ricklefs et al. [192].

The thermal conductivity was calculated for different setup temperatures on the cold and warm chambers, using the same thermal amplitude value of 10 ºC and 50% of RH. The thermal conductivity was calculated for the following setup temperatures: {2;12}, {4;14}, {6;16}, {…}, {26;36}, {28;38} and {30;40} (which means:{temperature of the cold chamber in ºC; temperature of the warm chamber in ºC}. The total amount steps carried out in these experimental measurements was 15, and the time at each temperature difference step was 6 hours (see Figure 30).

4.2.3. Guarded hot plate (GHP)

Both for the pristine rigid PU foam, as well as the rigid PU foam with the addition of PCM the thermal conductivity was measured at Fraunhofer ICT using an oneplate-thermal conductivity analyser Lambda-Meter EP500 from Lambda-Messtechnik Dresden Germany (see Figure 28). The thermal conductivity test tool λ-Meter EP500 is based on the guarded hot plate approach. Using this tool the absolute values of thermal conductivity and thermal resistance for insulation materials, construction materials and other products can be calculated [215,216].

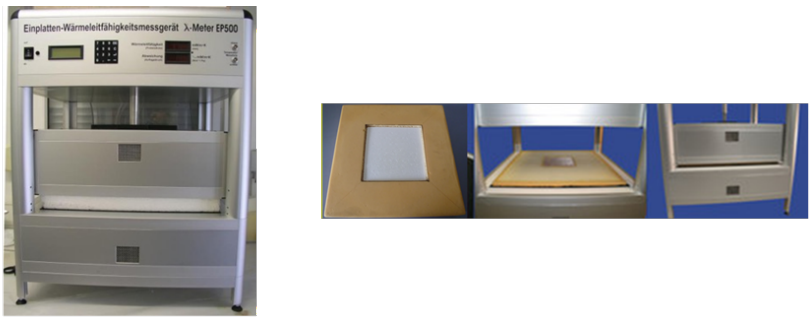

(a) – Lambda-Meter EP500 Equipment (b) – Specimen preparation apparatus and insertion in a stencil

Figure 28: Lambda-Meter EP500 Lambda-Messtechnik Dresden Germany

To determinate the thermal conductivity, the measurement is performed according to the DIN 52612 standard [217,218] and the existing approach uses the equation (7) as follows:

$$\lambda = \frac{q \times s}{t_w - t_k} \tag{7}$$

Where, q is the average heat flux through the specimen in W/m² , calculated using the equation (8); s is the average thickness of the specimen in m; t_w is the average temperature of the specimen surface on the heating plate in °C; t_k is the average temperature of the specimen surface on the cooling plate in °C.

$$q = \frac{q_w + q_k}{2} \tag{8}$$

Where, q_w is the heat flux between the specimen and heating plate in W/m²; q_k is the heat flux between the specimen and cooling plate in W/m². The uncertainty of the final thermal conductivity was obtained directly from the GHP equipment and their value is ±0.05 mW/m.K.

Before carrying out measurements, the specimens are firstly stored for 48 h at 23 °C and 50% relative humidity. For the measurements the specimen is clamped between the two measuring plates (upper and lower) and to these are applied a temperature difference of 10 K and a pressure of 2500 Pa. The measured temperatures should be between 0 and 50 °C. In the present study, temperatures of 10, 25 and 40 °C were applied to the upper plate. The determination of the thermal conductivity is measured, when its value does not change more than 1% for at least one hour.

4.2.4. Transient plane source (TPS)

The measurements were carried out according the ISO 22007-2:2008 [191] test approach procedure for the determination of thermal conductivity. Figure 29 shows the apparatus (Hot Disk Analyser, TPS 2500 S) used to measure the thermal conductivity by a transient plane heat source approach suitable for testing homogeneous and isotropic materials.

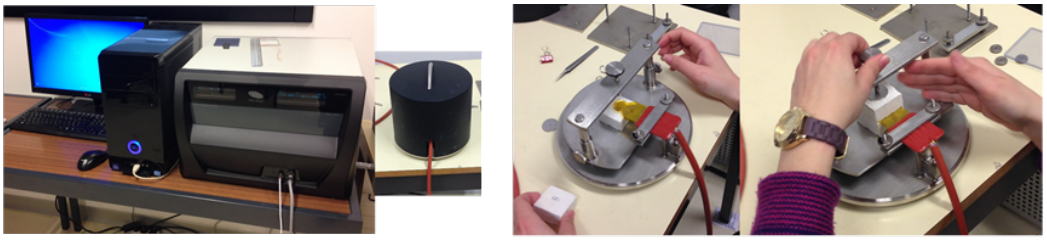

(a) – TPS 2500 S Equipment (b) – Specimen preparation apparatus and sensor positioning

Figure 29: Thermal conductivity measurement using the TPS approach

The type of the sensor used in this measurement consists of a thin nickel foil folded in a double spiral pattern, which is involved between two thin layers of Kapton polyimide protective films. This sensor is positioned between two similar specimens with dimensions of 40x40 mm and a thickness of 18 mm (the specimens may have other dimensions and shapes).

The variation in the sensor resistance *R(t) is* calculated using equation (9) [204,209,219] and is directly related to the electrical heat current that passes through the nickel spiral during the measurement and that creates an increase in temperature *ΔT(t)* of the sensor as function of time:

$$R(t) = R_0[1 + \alpha \Delta T(t)] \tag{9}$$

Where, R_0 is the initial nickel electrical resistance at initial time (t=0), a is the temperature coefficient of the resistance of the nickel foil.

The energy generated (in the form of heat) spreads and dissipates through the specimen on each side at a rate that is dependent on the thermal transport characteristics of the specimen material. Another important parameter is the temperature increase of the sensor $\overline{\Delta T_{(\tau)}}$ and can be obtained using equation (10):

$$\overline{\Delta T_{(\tau)}} = P_0\left(\pi^{3/2} a.\lambda\right)^{-1} D_{(\tau)} \tag{10}$$

Where, P_0 is the total output of power from the sensor, a is the overall sensor radius in mm, λ is the thermal conductivity of the specimen that is being measured and $D_{(\tau)}$ is a dimensionless time dependent function with the variable τ, defined by equation (11):

$$\tau = (t/\theta)^{1/2} \tag{11}$$

Where, t is the time measured from the start of the transient heating in sec. and θ is the characteristic time, which depends both on the parameters of the sensor and the specimen, as defined by the equation (12):

$$\theta = a^2/\kappa \tag{12}$$

Where, κ is the thermal diffusivity of the specimen in mm^2/s.

These parameters can accurately be calculated by a computational algorithm based on Hot Disk Thermal analyser software. In order to calculate the thermal conductivity correctly, a series of computational plots of $\Delta T(t)$ versus $D_{(\tau)}$ are usually made for a range of κ values. The correct value of κ will result in a straight line for the $\Delta T(t)$ versus $D_{(\tau)}$ according to Solórzano et al. [219].

The uncertainty of the final thermal conductivity was obtained directly from the TPS equipment and their value is ±0.00005 W/m.K.

The experiments involved measuring the thermal conductivity of the specimens at different temperatures in the range 6-40 ºC with a step of 2 ºC, except those in the temperature range before and after the phase change transition of PCM (16-28 ºC) which used a step of 1 ºC. The measurements were made using temperature increase and temperature decrease following the procedure as described above.

4.3. Results and discussion

4.3.1. Hot box heat flux meter (HB-HFM) results

Figure 30 presents the experimental results of the temperatures on both wall specimens faces. This result shows good agreement overtime, which eliminates misleading accidental error of the calculation. From the analysis in the warm chamber, the air and the surface temperatures on the wall specimen are similar, which means there is a high stability of the air temperature control as shown in Figure 30. The cold chamber presents also similar results, but not as good as the warm chamber.

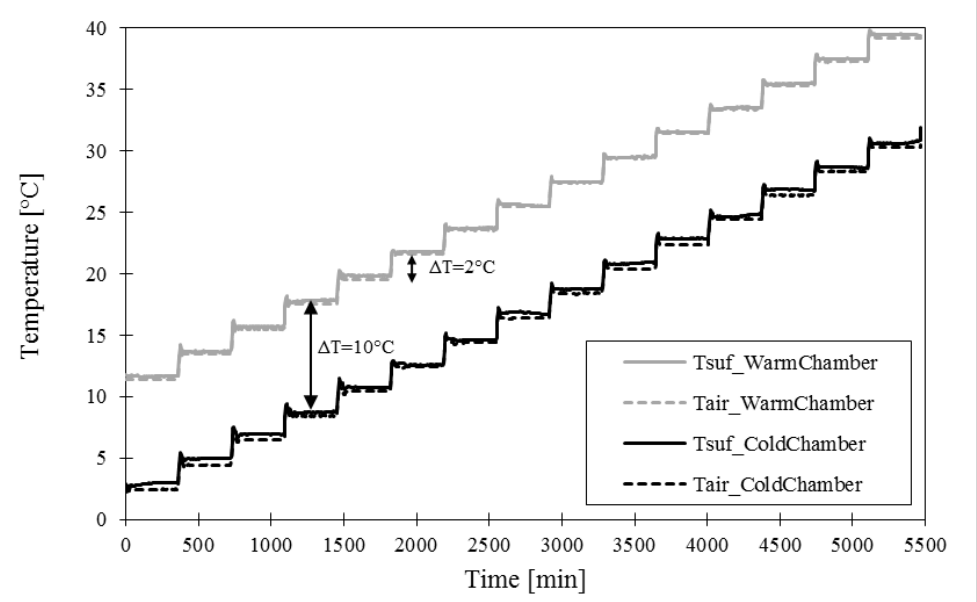

Figure 30: Experimental temperature results in the cold chamber and warm chamber (specimen surface and environmental air)

Therefore, it can be observed that the temperature measurements present extreme values when the temperature step is changed (at the end of each temperature step). So, for measuring the thermal conductivity, it was not taken into account the temperature values of the first and last hour for each step, which means that 4 hours of each step was considered to calculate the thermal conductivity. For each step of any 4 hours, the thermal conductivity were determined considering the five highest values of heat flux and surface temperatures of the last hour of each step (in the cold and warm chambers).

Figure 31 shows the experimental data of the thermal conductivity versus mean specimen surfaces temperature for the RPU foam without PCM. It can be observed a correlation between the values of the thermal conductivity and the surface temperatures. The square correlation coefficient (R^2) was 0.881, which demonstrates that the regression line fits well the experimental data. The values of the calculated thermal conductivity values were between 0.0315 and 0.0369 W/m.K, for a mean surface temperatures range of 11.64 ºC to 39.48 ºC.

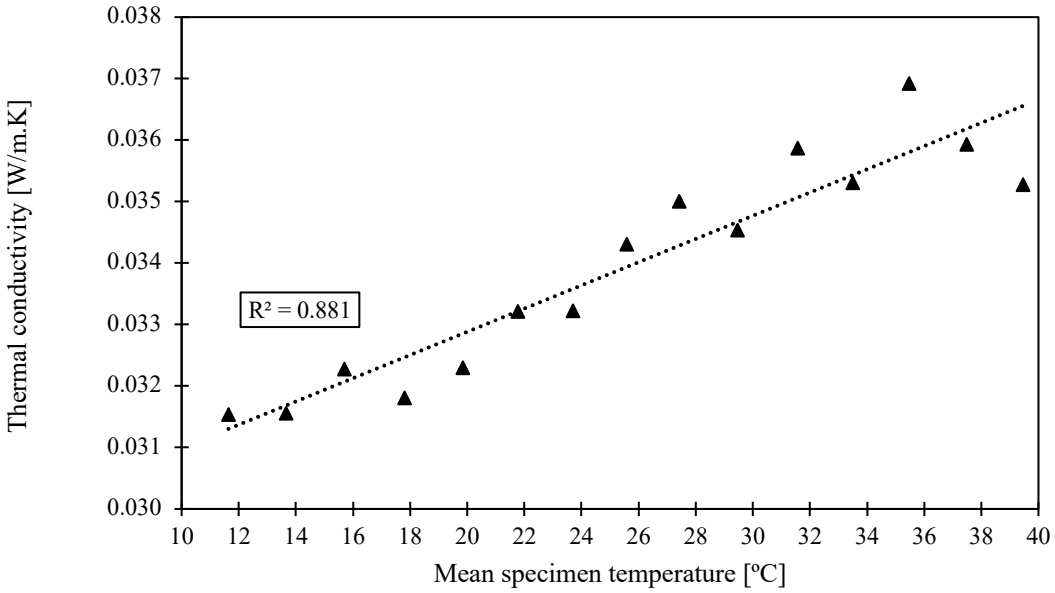

Figure 31: Thermal conductivity as a function of the mean specimen surface temperature (RPU foam)

Figure 32 shows the experimental data of the thermal conductivity versus mean specimen surface temperature for the RPU foam with PCM. The measurements exhibited a significant different behaviour from the RPU foam without PCM. The thermal conductivity profile shows a similar increasing trend when the mean specimen surface temperature was below and above of the phase change transition range (20 °C to 26 °C). However, during the phase change transition, when the PCM was neither solid nor liquid (mushy zone), the results of the thermal conductivity present some discrepancies. Outside the mushy zone, the R^2 was 0.882 and 0.732 respectively, which demonstrates that the regression line fits reasonably well the experimental data. The thermal conductivity values obtained for the PCM solid state were between 0.0310 and 0.0313 W/m.K for a mean specimen surface temperature range of 11.61 ºC to 15.64 ºC. For the PCM on liquid state the thermal conductivity were between 0.0322 and 0.0342 W/m.K for a mean specimen surface temperature range of 27.50 ºC to 39.44 ºC.

During PCM phase change transition there was a decreasing trend with the increasing mean temperature of the specimen and main conclusions are: *i)* as the solid/liquid phase change temperature range of the RPU_5PCM foam was about 22-24 ºC, part of the RPU foam would experience phase change when temperature rises from 20 ºC to 26 ºC and *ii)* the RPU foam with PCM were simultaneously influenced by temperature rise as well as the phase change fraction of the PCM incorporated, and *iii)* using HB-HFM approach there are some restrictions to carry out a quantitative analysis of the influence on thermal conductivity brought the solid and liquid phase change effect. Restrictions concerns about the positive effect of

the increasing temperature on the thermal conductivity when the PCM phase changes from solid to liquid and about the increasing phase change fraction (liquid fraction) of the PCM that would affect the thermal conductivity. The quantitative analysis is difficult because the restrictions take effect simultaneously.

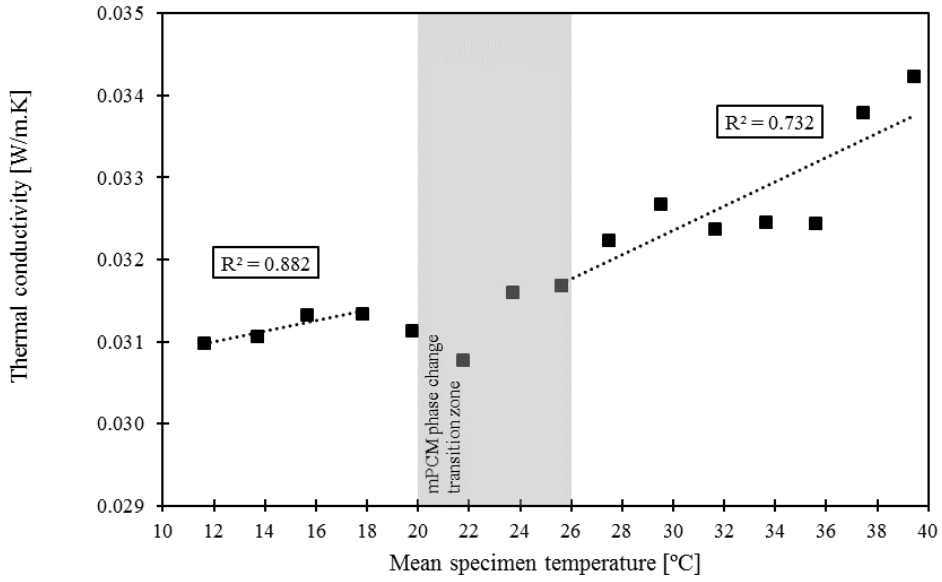

Figure 32: Thermal conductivity as a function of the mean specimen surface temperature (RPU_5PCM foam)

In addition, the temperature rise has a similar influence on the thermal conductivity of the RPU foam with and without PCM outside the boundaries of the phase change temperature range. However, the value of the thermal conductivity decreases with the presence of the PCM in the RPU foams in the phase change temperature range, as expected.

Wang X. et al [199] also observed the decrease trend of the thermal conductivity values on the wall with PCM during the PCM phase change transition (using the time steady-state method). This behaviour was checked because the mushy zone on the PCM, where two physical states coexist (solid and liquid) was influenced by the temperature rise and as well as by the phase change fraction of the PCM. However, when the specimens with PCM were in solid and liquid states, there was a good positive linear relationship between the thermal conductivity with the increasing temperature, even though redundant and for the sake of recording reliable data, the heat flux was measured using one heat flux meter on each side at the middle of the specimen. The most important advantage of the use of HB-HFM approach for thermal conductivity measurements is that the thickness and dimensions of the specimens can be higher than the other approaches. Also, with this approach it is possible to quantify the potential as a thermal regulator of indoor temperatures,

reducing the temperature peaks and decreasing the temperature swing through the PCM capacity to store and release energy.

4.3.2. Guarded hot plate (GHP) results

Figure 33 shows the thermal conductivity values for the RPU foams at 10 ºC (PCM solid state), 25 ºC (PCM solid/liquid phase change) and 40 ºC (PCM liquid state).

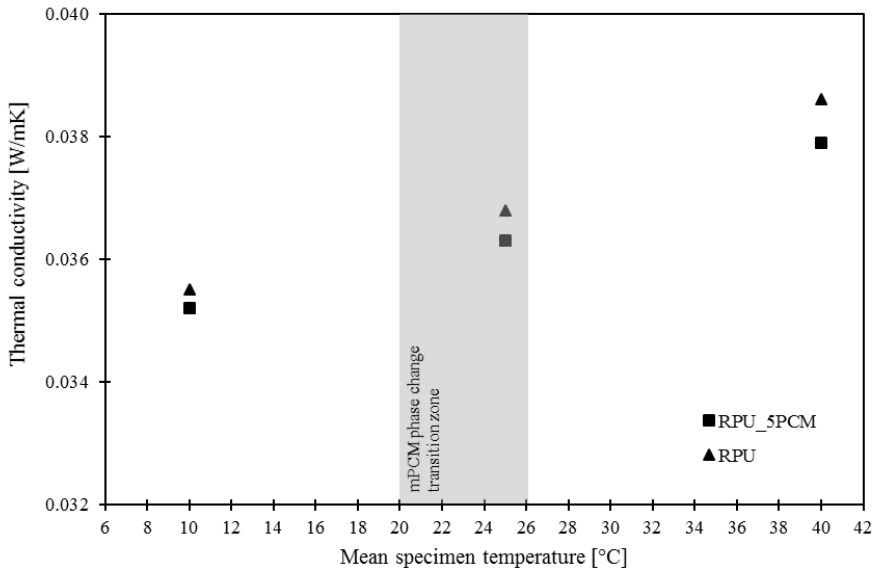

Figure 33: Thermal conductivity of RPU foams using guarded hot plate approach (measured at 10, 25 and 40 ºC)

The measurements show that the thermal conductivity increases with increasing temperature. This behaviour was similar in the solid state, liquid state and in the solid/liquid phase change temperature state, in spite of the fact that there was only one measurement in each PCM temperature state, since the measurements for the defined temperatures are out or at the limit of the phase change temperature range. The addition of PCM does not seem to have significant influence on the thermal conductivity of the RPU foams. To confirm this trend (where thermal conductivity increases with increasing temperature) it would be necessary to measure more temperature points in each PCM state. Only one point in each PCM temperature state (solid, solid/liquid and liquid state) is not enough.

In the great majority of studies, the information about the influence of the temperature on thermal conductivity values of the specimens with PCM promoted by GHP approach is not available during the PCM phase change transition. The researchers only showed the thermal conductivity values when the specimens with PCM was in solid and liquid states. However, Ricklefs et al. [192] presented the

thermal conductivity of cement composites containing PCM measured during the PCM phase change transition. The study indicates that the effective thermal conductivity of cement-PCM composites was not affected appreciably by the occurrence of PCM phase change. This can be attributed to the fact that the temperature range considered was relatively narrow (10–50 ºC) although representative of real conditions and was necessary more temperature points during the PCM phase change transition.

The GHP approach was the first extensively used method in this field, and is still used, yet it has some drawbacks related to the specimen size (it is required a 200x200 mm minimum size), and the contact area between the measuring plates and the specimen surface (the unevenness of the specimen surface is identified as a major source of error).

4.3.3. Transient plane source (TPS) results

Figure 34 summarizes the results for thermal conductivity versus temperature for the RPU foams specimens with or without PCM. Two different kinds of measurements have been carried out. The first part of the experiments involved measuring the thermal conductivity with temperature increase (range 6-40 ºC) and the second part involved measuring the thermal conductivity with temperature decrease (range 40-6 ºC). This covers the practical range of use in summer Mediterranean climates [220–223].

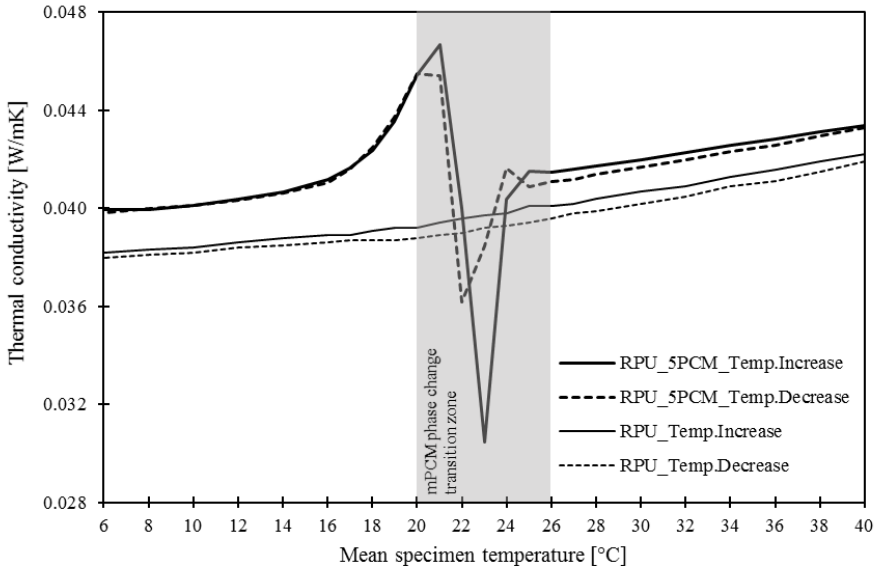

Figure 34: Thermal conductivity versus mean temperature of RPU foams using the TPS approach

In the temperature range before and after the phase change transition (20 °C to 26 °C) of the PCM, the thermal conductivity values are near to those expected for the RPU foams. The measurements show that, the thermal conductivity increases with increasing temperature and decrease with decreasing temperature. The relation becomes practically linear for temperatures outside the boundaries of the phase change transition range.

It can be observed that the value of the thermal conductivity increases with the presence of the PCM in the RPU foams. The behaviour of the thermal conductivity versus mean temperature for the RPU foams is similar for the measurements when the temperature is increased and decreased.

The thermal conductivity profile showed a similar increasing trend before and after the boundaries of the PCM phase change transition zone (the PCM is in the solid or liquid state). During PCM phase transition there was a decreasing trend with the increasing of temperature. The solid/liquid phase change temperature range of the RPU_5PCM foam was about 22-24 ºC and part of the specimen would experience phase change when temperature rose from 20 ºC to 26 ºC. As a result, the nickel sensor measures a cooling or heating effect from the phase change, which will shift the transient and the result in this singularity-like temperature behaviour. The drop in thermal conductivity profile is directly linked to the drop in thermal diffusivity in this phase change temperature range.

In order to establish a direct comparison between this study and other studies it became clear the lack of information regarding thermal conductivity measurements of composites with PCM during PCM phase change transition using TPS approach (transient method). However, Ling et al. [69] studied the effect of the temperature on the thermal conductivity of a composite PCM with expanded graphite across the PCM phase change transition. When the composite PCM was in solid and liquid states, there was negligible difference of the thermal conductivity values. But, it was noticeable that thermal conductivity nearly doubles within the PCM phase change temperature range. This increasing trend in thermal conductivity may be attributed to PCM superior capability of keeping the temperature constant during phase change transition. In addition, during the PCM phase change transition there was a slight decreasing trend with the increasing temperature of the specimen similar to the present work. The TPS approach has some constrains for the thermal conductivity measurements with specimens incorporating PCM. The measure is a combination of energy being transferred through the material and the energy stored or released in the phase change. The thermal conductivity is affected very slightly and can be estimated by interpolating from a point before, to a point after the phase change.

4.3.4. Comparison between approaches – Main findings

The comparative analysis between the three test approaches for thermal conductivity measurements was for RPU foams with and without PCM at the 10 ºC (PCM solid state), 25 ºC (PCM solid/liquid phase change) and 40 ºC (PCM liquid state). In the case of the HB-HFM approach the thermal conductivity measurements were taken as the mean specimen surface temperature at 11.6 ºC (PCM solid state), 25.6 ºC (PCM solid/liquid phase change) and 39.5 ºC (PCM liquid state). The results are shown in

Figure 35 for the three approaches. The results do not take into account correction factors, according to the ISO 10456, since the main target is to compare in relative terms the results from the different measurement approaches.

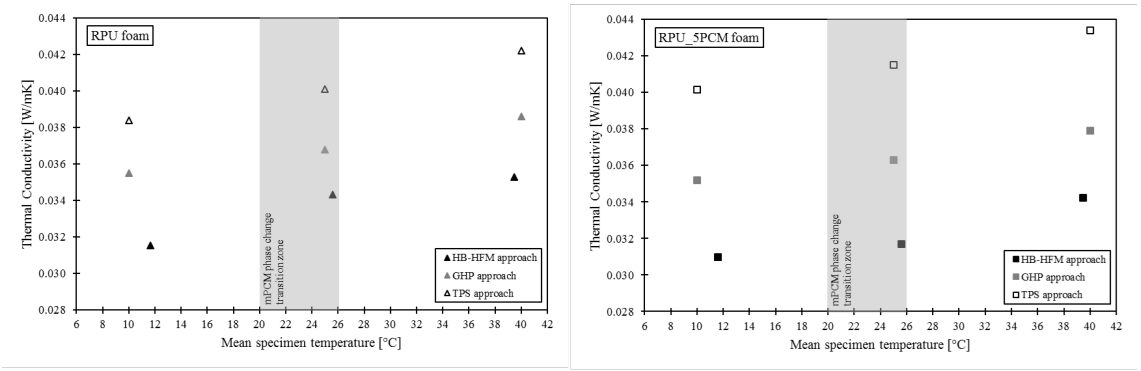

Figure 35: Comparison of thermal conductivity at 10 ºC, 25 ºC and 40 ºC for all approaches (HB-HFM, GHP and TPS): (a) for RPU foam without PCM; (b) for RPU foam with 5wt% PCM

The results show that the enhancement in thermal conductivity of the RPU foams with and without PCM increased with temperature. Using the HB-HFM approach and GHP approach, the value of the thermal conductivity of the RPU foam with PCM comparatively to the RPU foam without PCM is lower in respect to the TPS approach. However, the addition of the PCM does not seem to have significantly influence on the thermal conductivity of the RPU foams, because the variance on the thermal conductivity (in relation of the RPU foam without PCM) obtained for the PCM solid state were approximately -1.78% for the HB-HFM approach, -0.85% for the GHP approach and 4.97% for the TPS approach. For the PCM on solid/liquid state the variance of the thermal conductivity was -7.65% for the HB-HFM approach, -1.36% for the GHP approach and 3.75% for the TPS approach. Finally, for the PCM in the liquid state the variance on the thermal conductivity was -2.97% for the HB-HFM approach, -1.81% for the GHP approach and 3.29% for the TPS approach. These small differences are more evident in the TPS approach perhaps because the effect of the thermal resistance at the contact interfaces between the specimens and the sensor are more significant relative to the other approaches. One other reason may

be due to the effect of the homogeneity and isotropy of the RPU foam in the presence of PCM.

From a theoretical point of view, when incorporating 5 wt% of a material with higher thermal conductivity (in this case the PCM) into a 95 wt% material with very low thermal conductivity (RPU foam), the resulting composite material (RPU foam with PCM) should have a slightly higher conductivity. In the present study, this trend behaviour was not evident.

In addition, in the phase change transition zone (20 ºC to 26 ºC) just for the HB-HFM approach it was clear a decreasing trend of the thermal conductivity value for the RPU foam with PCM comparatively to the RPU foam without PCM. In other approaches, it was not possible to see this trend, because the temperature at 25 ºC is nearer to the upper limit of the phase change, with the PCM going to its liquid state. Hence, it´s possible that the PCM was already in the total liquid state at 25 ºC as show in section 4.3.1 and 4.3.3.

4.4. Conclusions

The present study highlights the evaluation and comparison of the thermal conductivity of RPU foams with and without PCM using three different approaches: *i)* the thermal flux meter approach (steady-state method), *ii)* the guarded hot plate (GHP) approach and *iii)* the transient plane source (TPS) approach (transient methods). The results showed that the three approaches present similar values of thermal conductivity for temperatures below and above the PCM phase change transition zone (variance on the thermal conductivity between -1.81% and 4.97%). However during the PCM phase change transition zone there are important factors that should be considered to determine the thermal conductivity. Nevertheless, the TPS approach presents the higher values of thermal conductivity values for the RPU foams with and without PCM.

The following main conclusions taken from the presented research are:

- The temperature had a similar influence on thermal conductivity (increase) of the RPU foam with and without PCM when in solid and liquid state. However, the value of the thermal conductivity decreases with the presence of the PCM in the RPU foams using the HB-HFM and GHP approaches. However, the TPS approach, the value of the thermal conductivity slightly increases with the presence of the PCM in the RPU foams;

- During PCM phase change transition a decreasing trend of the thermal conductivity with the increasing temperature is observed. The temperature range of the solid/liquid phase change of the RPU_5PCM foam was about 22-

24 ºC, however melting actually starts earlier and finishers later (being the whole temperature range from 20 ºC to 26 ºC). Therefore, the thermal conductivity measured is lower;

- The thermal conductivity of the RPU foam with PCM was simultaneously influenced by the temperature increase as well as by the phase change fraction of the PCM. This behaviour was clearly observed using the HB-HFM and TPS approach, because in these two approaches the experiments involved measuring the thermal conductivity of the specimens at different temperatures in the 2-40 ºC range (range temperature that represent all the PCM phases);

- The most important advantage of the use of HB-HFM approach for thermal conductivity measurements is that the thickness and dimensions of the specimens can be higher than the other approaches. However, it is recommended to use more than one heat flux meter on each side of the specimen;

- Using the GHP approach, the influence of the addition of PCM into RPU foams on the thermal conductivity could not be observed, since the measurements were made only for temperatures 10 ºC, 25 ºC and 40 ºC. One important factor is the measurement temperatures which must be representative of all PCM phases (solid, solid/liquid and liquid phase). Also, the unevenness of the specimen surface is identified as another major source of error;

- The TPS approach has some constrains for the thermal conductivity measurements with specimens incorporating PCM. The measurement is a combination of energy being transferred through the material and the energy stored or released in the phase change;

- The three approaches presented a good correlation of the experimental data to calculate the thermal conductivity of RPU foams with and without PCM, when in the liquid and solid state, but some testing constraints and factors were identified when determining the thermal conductivity of the specimens for the phase change zone. It is important to try a quantitative analysis of the simultaneous influence on the thermal conductivity of temperature rise as well as the phase change fraction of the PCM incorporated during the phase change zone;

- Overall, this study confirmed that the HB-HFM approach gives more reliable thermal information of the RPU foams with PCM;

- Based on the DSC analysis and thermal conductivity measurements for different approaches, the results reveal that the thermal characteristics of RPU foams are enhanced by the presence of the PCM.

Promising results have been achieved but there is still a long path to go in terms of thermal conductivity measurements of the RPU foams with PCM, particularly during PCM phase transition stage using steady-state and transient methods. It is important to identify the coupling effect of the temperature rise and the phase change fraction of the PCM on the thermal conductivity value. This study is interesting and that is worth considering further studies on behaviour of the thermal conductivity values during the PCM phase change transition.

CHAPTER 5

5. Experimental and numerical analysis on thermal performance of polyurethane foams panels incorporating phase change material

This chapter is in preparation for submission in the Journal of Energy, Elsevier.

Abstract

Phase change materials (PCM) incorporated into the building envelope solutions of new and existing buildings, can decrease the building energy demand and improve the thermal comfort of indoor environments through enhancing the thermal energy storage capacity of the building envelope skins. Typically, the use of thermal insulation materials is regarded as one of the most effective means of energy conservation in buildings. Thus, rigid polyurethane (RPU) foams are widely used as insulation layers incorporated or associated to opaque building envelope solutions. The RPU foams have good insulating properties but their potential thermal regulation capacity can be enhanced by the incorporation of PCM. The main goal of the present work is to assess the thermal characteristics of RPU panels with PCM incorporated and to quantify their potential as thermal regulators of indoor spaces, reducing the temperature peaks and decreasing the temperature swing through the PCM capacity to store and release energy.

The hot box heat flux meter method is used to evaluate the thermal performance of the RPU panel with PCM incorporation. The experimental setup, which is based on the steady-state method possible to establish resourcing to climatic chambers, creates a relatively stable thermal environment to asses reliably the thermal characteristics. The comparison of the experimental results obtained for RPU panels with and without PCM is presented. The presence of PCM revealed to lead to a thermal amplitude reduction of about 4 ºC for the peak maximum temperature and 1 ºC for the peak minimum temperature.

Furthermore, numerical simulations were carried out to evaluate the performance of the use of PCM over a wider range of conditions and operating modes. A numerical simulation model was used (ANSYS-FLUENT) and validated using the experimental data in static and dynamic conditions. The numerical simulation carried out is foreseen as an essential decision and design tool to evaluate the potential of the PCM incorporation in different operating conditions and its impact over energy consumption and thermal comfort in buildings.

Keywords: phase change material (PCM), rigid polyurethane (RPU), insulation panels, thermal conductivity, thermal performance, numerical simulations.

5.1. Introduction

As growing demand of thermal comfort levels in buildings has risen increasingly, consequently increasing the energy consumption. The energy consumption of buildings has increased by 40% during the last two decades. Residential, commercial and public sector are responsible for the consumption of approximately 40% of all energy sources and approximately 40% of the total CO_2 emissions [1–4,103]. Nowadays, thermal energy storage (TES) systems are essential for reducing dependency on fossil fuels, contributing to a more efficient environmentally benign energy use. TES systems provides new means of thermal energy management by improving the energy efficiency in buildings [5,29,175]. Phase change materials (PCM) which are classified as latent heat thermal energy storage (LHTES) materials are suitable for TES applications. PCM besides storing thermal energy can have a thermal regulation effect in building components into which they are incorporated, by charging and discharging large amounts of latent heat during the phase change process [35,37,41,177]. The use of PCM in LHTES systems has attracted attention in new and refurbished buildings, because PCM offer high energy storage density per unit weight within a small temperature difference in comparison with sensible heat storage systems [224,225].

Presently, the most commonly used thermal insulation material used in building envelopes for assuring building indoor thermal regulation, are rigid polyurethane foams (RPU) [176,186,226]. The combination of RPU foams and PCM is the focus of increasing attention in trying to couple/combine the advantages of thermal insulation and thermal energy storage materials. The incorporation of the PCM into RPU foams is a possible form to provide extra heat capacity to the building solutions, storing and releasing more energy without compromising the good RPU thermal properties [28,84]. Various works have indicated that an appropriate amount of PCM incorporated in RPU foams would enhance the thermal energy storage capacity of these materials. The quality of RPU with PCM is highly dependent on: the distribution and spatial dispersion of PCM particles into the RPU foam matrix, the type and quantity of PCM used, the chemical and physical compatibility of the chosen PCM with RPU matrix, the types of catalyst, the blowing agent and any other agents used in the foaming process [225,227–229].

The list of studies and research topics driven by the use of PCM into building systems is very extensive, therefore the main reviewed works, herein, focus on their use in opaque building envelopes solutions. The opaque building envelope (façades) assure two main functions: first, they are the barriers that separate the building's interior from the external environment; and second, more than any other building component, they create the image of the building. High-performance

sustainable façades can be defined as exterior enclosures that use the least possible amount of energy to maintain a comfortable indoor environment, which promotes the health and productivity of the building's occupants. This means that sustainable façades are not simply barriers between interior and exterior; rather, they are building systems that protect and can or should respond to the building's external environment [1,2,8,35,36,40,103,230–234]. For example, the direct incorporation of PCM in opaque building solutions has reached a level of development that commercially based solutions are available, such as wallboards, concrete blocks, and/or other wall components (e.g., hollowed bricks).

Many studies have been carried out on these types of opaque solutions, focusing on the position of arrangement of the PCM inside the building solutions and their impact over heat fluxes during the day.

Fateh et al. [235] developed a detailed dynamic model validate with several experimental tests in order to determinate the effects of PCM (position) in insulation layers of lightweight walls. The results show that, the maximum reduction of heat consumption, is about 15%, when PCM are located in positions designated as three and four, which are approximately in the middle of the wall solution. In addition, this specific kind of insulation layer generates a delay of the maximum heat flux that is about two hours. Lee et al. [236] studied the orientation effect on the thermal performance of a thin PCM layer using of the plug-and-play walls concept for testing walls through the Energy Plus. The results showed that the average daily heat transfer reductions were 27.4% and 10.5% for south and west facing walls, respectively, and the average heat flux reductions when the heat fluxes of the control walls were at their peaks were 67.0% and 80.2% for the same orientations, respectively. The average time delays of the peak heat fluxes were 3 h and 2 h when the thin PCM layer were integrated in the south and west walls, respectively. The interior surface temperatures of the retrofit panels were more constant than those of the control panels when the thin PCM layer was integrated. Jin et al. [237] evaluated a dynamic model of walls with and without PCM and estimated the optical PCM location. The optimal PCM location was closer to the interior surface of the wall with the increase of the interior surface temperature of the wall. Sharifi et al. [238] studied the evaluation of the efficiency of PCM incorporated in gypsum boards on improving the thermal performance of buildings subjected to the real temperature profiles of different cities, resourcing to computational simulations. The efficiency of PCM is completely dependent on the applied temperature and the PCM do not have high efficiency in areas with high temperature fluctuations. Also, increasing the amount of the utilized PCM leads to diminishing returns on efficiency. Errebai et al. [239] presented experimental and numerical a new solution for improvement of thermal behaviour of a plasterboards with PCM microencapsulated. It consists of

perforating the panel with several small holes yielding a greater contact surface area with the surrounding air. Results show that the perforated panels produce an augmentation in heat absorption (100%) and release (175%) compared to a standard panel without holes. The absorbed and released heat flux values have a direct relationship with the ratio of the panel thickness to the holes spacing. Izquierdo-Barrientos et al. [240] developed a one-dimensional transient heat transfer model using a finite difference method to investigate the impact of PCM in external building walls. The results showed that there is no significant reduction in the total heat lost during winter regardless of the wall orientation or PCM transition temperature. Higher differences were observed in the heat gained during the summer period, due to the elevated solar radiation fluxes. The high thermal inertia of the wall implies that the inclusion of a PCM layer increases the thermal load during the day while decreasing the thermal load during the night.

This herein research describes an experimental test resourcing to the hot box heat flux meter method used to assess the thermal characteristics of RPU panels with and without PCM (two different types of PCM microencapsulated: commercial and synthetized with calcium carbonate) and to quantify the potential as a thermal regulator of indoor spaces, reducing the temperature peaks and decreasing the temperature swing through the PCM capacity to store and release energy. Further on it is described a numerical 2D model of the panels tested with the same boundary conditions to compare experimental and simulated data for both types of panels. Once validated the numerical model different temperatures amplitudes and RPU panel thickness where simulated to asses different operating conditions

5.2. Experimental apparatus

5.2.1. Materials and description of the RPU panels

The microencapsulated PCM powder and synthetized PCM with $CaCO_3$ was purchased and synthetized according to the section 3.2.1 of Chapter 3.

In this study, the PCM solutions (PCM@BASF and PCM@$CaCO_3$) were then incorporated into rigid PUF´s (RPU) formulations to yield RPU panels. The production of the panels was carried out at the Fraunhofer Institute for Chemical Technology, ICT laboratory (Germany) according to the procedure described in Amaral et al. [176].

To evaluate the influence of PCM in the RPU panels, the experimental characterization tests were carried out over 3 types of specimens with 20 mm of thickness according to Figure 36:

- RPU without PCM (designated as RPU);
- RPU with 5.0 wt% PCM@BASF (designated as RPU_5PCM@BASF);
- RPU with 5.0 wt% PCM@$CaCO_3$ (designated as RPU_5PCM@$CaCO_3$).

Figure 36: RPU panels aspect

Table 19 lists the principal properties of the pristine PCM and three types of RPU panels produced, particularly the density, the transition temperature ($T_{t,m}$), the melting temperature (T_m) as well as the latent heat (ΔH_m) values of the specimens for the melting curve and the PCM content ($\%_{PCM}$) incorporated into the RPU panels according the following Equation (5) in the section 3.2.1.6:

Table 19: Properties of the PCM solely and the three types of RPU panels

Specimens	**Density (kg/m³)**	**Melting**			**$\%_{m,PCM}$**
		Transition temp. $T_{t,m}$ (°C)	**Melting temp. T_m (°C)**	**Melting latent heat ΔH_m (J/g)**	
PCM@BASF	345.588±3.645	25.36±0.04	27.55±0.10	97.85±14.64	-
PCM@$CaCO_3$	503.359±4.386	23.37±0.65	25.84±0.44	59.56±11.78	-
RPU	81.411±1.553	-	-	-	-
RPU_5PCM@BASF	88.864±1.035	22.31±0.04	23.54±0.08	6.16±1.22	6.3
RPU_5PCM@$CaCO_3$	93.249±1.473	21.22±0.35	22.97±0.16	2.81±0.37	4.7

Figure 37, 38 and 39 illustrate the thermal conductivity, specific heat and thermal diffusivity versus temperature results of the RPU panels specimens with or without PCM using the Hot Disk approach [176,190,191]. The temperature testing range was from 6 to 40 ºC), and each sample/specimen was tested for heating cycle (temperature increase) and cooling cycle (temperature decrease).

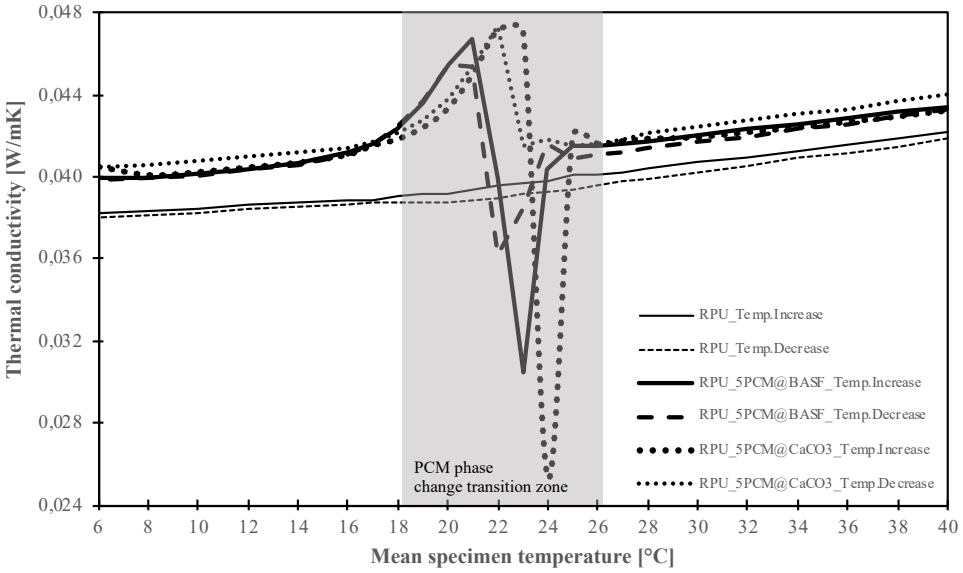

Figure 37: Thermal conductivity versus mean temperature of RPU panels [from section 3.3.2.1 of chapter 3, Figure 19]

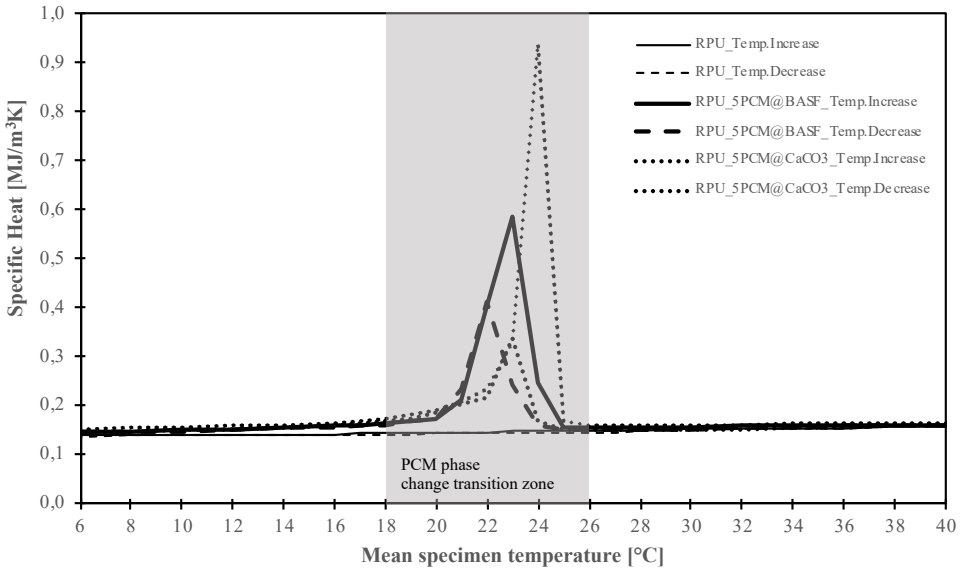

Figure 38: Specific heat versus mean temperature of RPU panels

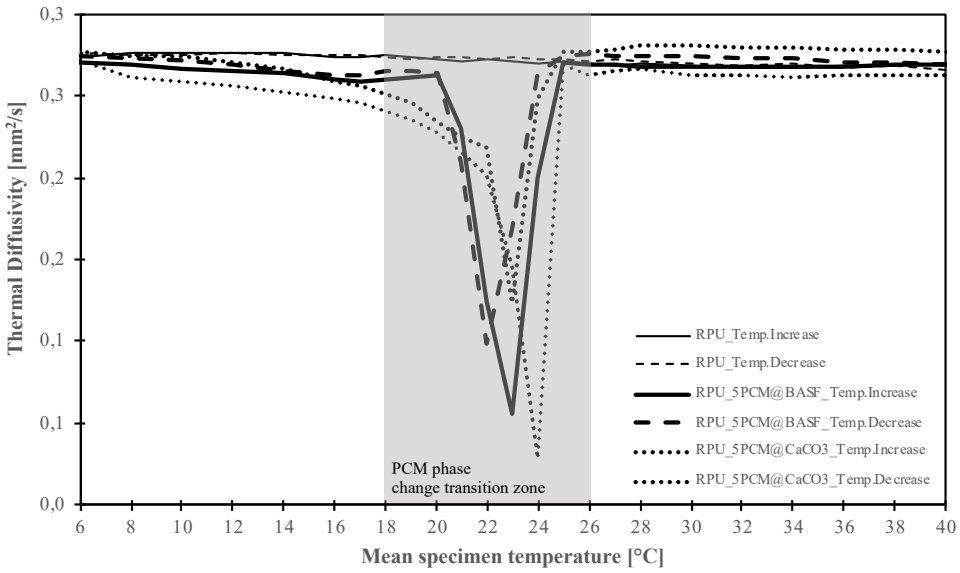

Figure 39: Thermal diffusivity versus mean temperature of RPU panels

5.2.2. Hot box approach

The hot box approach is based on the steady-state method [199,208,213]. This method consists in a simple hot box configuration composed by two closed chambers with controlled temperature and relative humidity conditions: one of the chambers is at low and constant temperature (cold chamber) and the other, the metering chamber, is placed at higher and constant temperature (warm chamber). Between the two chambers there is a mounting ring in which the wall specimen or panel to be tested, this case the RPU panel. The procedures, the schemes, the materials, have been previously defined in Amaral et. al. elsewhere [176].

Figure 40 (a) presents the sensors positioning (heat flux meters and thermocouples) on each specimen surface (with same configuration on both sides). Figure 40 (b) presents five PT100 probes at a distance of 150 mm from the specimen/RPU panel and one PT100 probe was placed in the middle of the chamber. In the cold chamber, six PT100 probes were positioned oppositely in the same relative position in respect to the warm chamber (mirror).

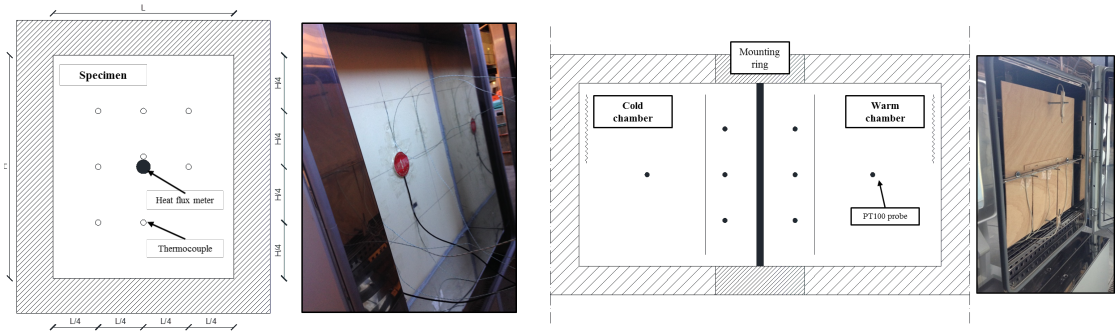

(a) (b)

Figure 40: Schematic layout and sensor positioning in: (a) specimen ring mounting; (b) chambers.

5.2.3. Experimental results

5.2.3.1. Temperature amplitude

For evaluating the reduction of temperature amplitude between the warm and cold chambers, the temperature of the cold chamber was left to free float temperature conditions and the temperature of the warm chamber was set to impose a temperature curve profile between 12 °C and 52 °C for 24 hours during four cycle measurements (see Figure 41). This temperature profile covers the practical range of maximum temperature amplitude for Mediterranean climates. Experimental results for the temperature profiles for the chambers and surface temperature are shown in Figure 41 for the RPU panel without PCM. The air temperature measurements inside the warm chamber are very similar to the specimen/RPU panel surface temperature measurements on the warm side, however inside the cold chamber the results reveal a small difference, but more significant difference of these temperatures. These differences are due to the free float temperature condition of this chamber in comparison to the warm chamber, in which a strong convection is imposed for metering the chamber.

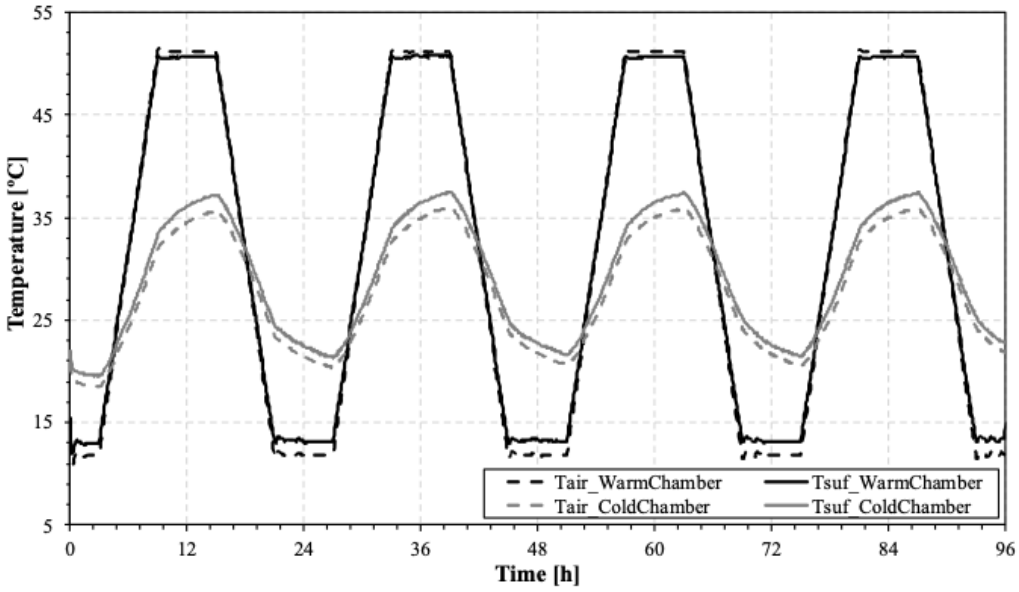

Figure 41: Temperature profiles of the RPU panel without PCM for the 4 days cycle

The Figure 42 shows compares the mean air temperature in the cold chamber for the RPU panels without and with PCM (RPU, RPU_5PCM@BASF and RPU_5PCM@$CaCO_3$). For the RPU_5PCM@BASF, comparing the temperature curves (exterior conditions-warm chamber and indoor conditions-cold chamber) results it can be observed that the thermal amplitude reduction corresponds to a reduction of 2 ºC for the peak maximum temperature and buffering of about 1 °C for the peak minimum temperature. For the RPU_5PCM@$CaCO_3$, the thermal amplitude reduction corresponds to a reduction of about 3.5 ºC for the peak maximum temperature and buffering of about 1 °C for the peak minimum temperature.

So, comparing the experimental results obtained for RPU with and without PCM, it is noticeable the impact of the PCM incorporation led to a thermal amplitude reduction of about 1-2 ºC for the RPU_5PCM@BASF and about 1-3.5 ºC for the RPU_5PCM@$CaCO_3$.

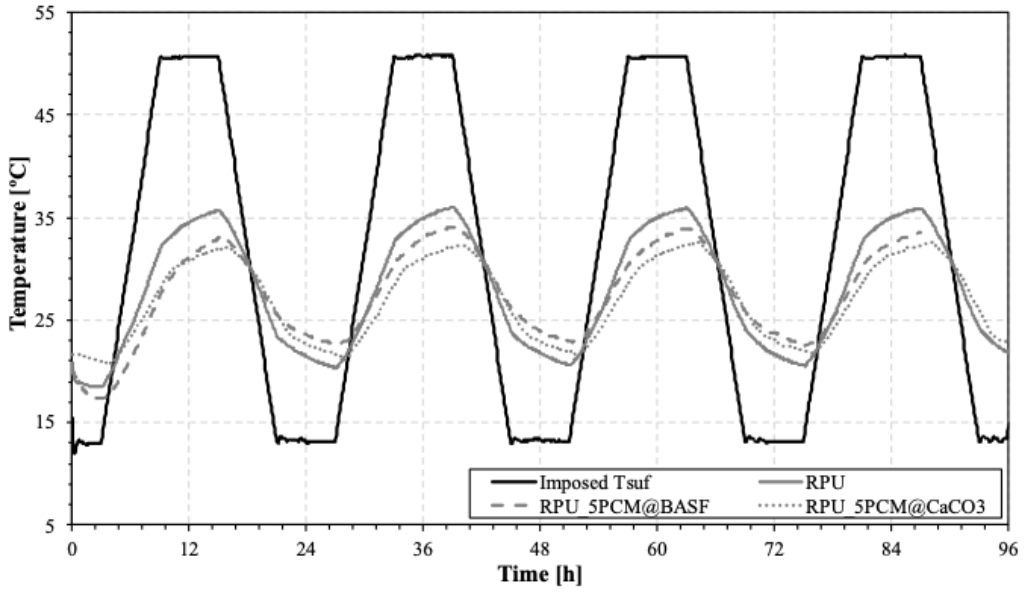

Figure 42: Comparison of the mean air temperature profiles of the RPU panels for the 4 days cycle.

5.3. Numerical models

The numerical models and following simulations were carried out to evaluate the thermal performance of each RPU panels, using the experimental data shown in the previous sections. In order to calibrate and validate the numerical models, a geometrical model of an experimental setup test was used. Following are presented and discussed the numerical definitions, validation and main optimization results.

5.3.1. Numerical definitions

The 2D models were built with the Solidworks software – as plain surfaces – and the modelled file was exported to ANSYS DesignModeler v19 to simulate the experimental transient thermal tests according to the hot box approach (see dimensions and experimental setup in previous section 5.2.2). Due to the symmetry of the geometry, material and boundary conditions and in order to reduce computational effort, the cold chamber was not considered, and the imposed conditions were applied on the external surface of the tested RPU panels, as shown in Figure 43. The chamber wall is composed by three layers: an inner galvanized steel sheeting, rockwool insulation and an external zinc sheeting and protection. The thickness of these three layers are 1.5 mm, 125 mm and 1.5 mm respectively. The internal air is modelled as a fluid in laminar regime.

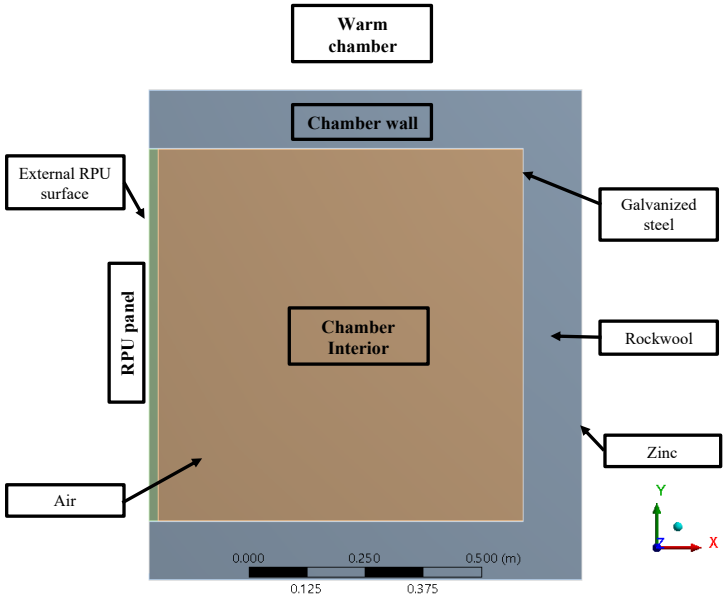

Figure 43: Numerical model, materials and boundary conditions

The materials, thickness and thermal properties of the RPU panels are listed in Table 19. The thermal conductivity, specific heat and thermal diffusivity versus mean specimen temperature for the RPU panels without and with PCM used was obtained from Figure 37, Figure 38 and Figure 39 in section 5.2.1. The material properties of the chamber walls and the internal air are shown in Table 20.

Table 20: Material properties of the chamber walls and air

Material	**Thickness (mm)**	**Density (kg/m^3)**	**Thermal conductivity (W/m.K)**	**Specific heat (J/kg^oC)**
Galvanized steel	1.5	7833	54	465
Rockwool	125	70	0.0375	840
Zinc	1.5	7144	112.2	384.3
Interior air	-	7833	54	465

The creation of the model mesh was done selecting the CFD physic preference and the Fluent solver, that enables the default values of the mesh properties. To improve the element quality, it was used refinement controls for the smallest domains and also quadrilateral method control for all domains. Refinement control at the following elements was used: RPU panel, chamber wall (composed by three layers: an inner galvanized steel sheeting, rockwool insulation and an external zinc sheeting) and inner chamber. The final mesh geometry is presented in Figure 44.

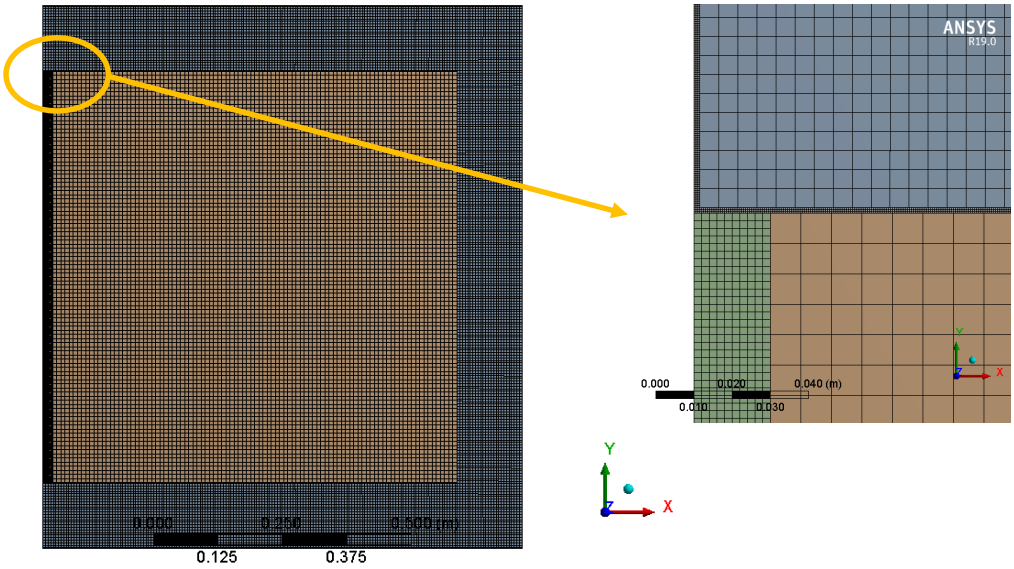

Figure 44: Model mesh – overall geometry and close-up to the boundary conditions

The temperatures of the warm chamber were monitored at three points according to the experimental schematic layout and sensor positioning (see Figure 40). These temperature probes are located at mid-height of the chamber, and considering an x-axis referential position from the external face, they are positioned at 20, 249 and 504 mm respectively (as shown in Figure 43). The imposed conditions used on the external face was the experimental temperature profile measured on the on warm surface of the RPU panels (between 12 °C and 52 °C for 24 hours for a total of 4 complete cycles) according to Figure 42.

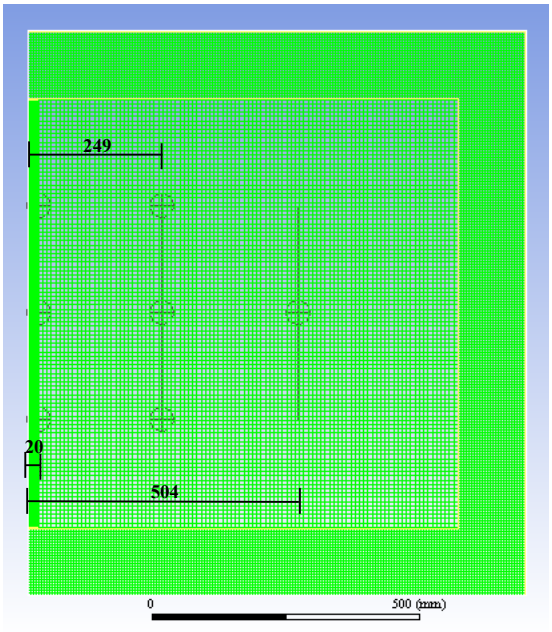

Figure 45: Measured and monitored points positioning of the numerical model

5.3.2. Numerical validation with experimental results

The input of the numerical model is the experimental surface temperature curve of the warm side chamber and the room temperature variation (around the chambers in laboratory conditions). The former is a trapezoidal temperature profile that ranges between 12°C and 52°C; with a period equal to one day cycle (24h) with 6 hours steps. A total number of 4 days cycles were runned. The laboratory room temperature in which the chambers are installed is around 22°C±2ºC for the case of RPU and RPU_5PCM@BASF. For the RPU_5PCM@$CaCO_3$, the profile room temperature was used the real room temperature measured with a PT100 probe during the experimental tests (around the chambers in laboratory conditions). A temperature contour example is shown in Figure 46 that corresponds to a time step when the imposed temperature on the outer RPU panel surface is maximum (at 52 ºC) for the RPU, RPU_5PCM@BASF and RPU_5PCM@$CaCO_3$.

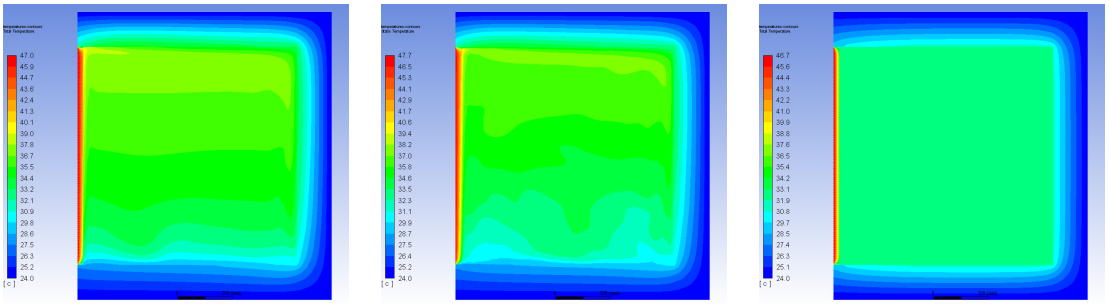

(a) (b) (c)

Figure 46: Temperature contour for maximum imposed temperature on the outer surface, 52ºC for: (a) RPU, (b) RPU_5PCM@BASF and (c) RPU_5PCM@$CaCO_3$

The numerical output to be compared is the temperature curve in the cold chamber in free float mode, the average temperature plot is taken from a mean value of the PT 100 probes positioned 150 away from the RPU panels as shown in Figure 40 (b). Figure 47, 48 and 49 presents the numerical and experimental temperature curves for each model: RPU, RPU_5PCM@BASF and RPU_5PCM@$CaCO_3$. These temperatures profiles were created from the indoor average values of each point/probes in the cold chamber.

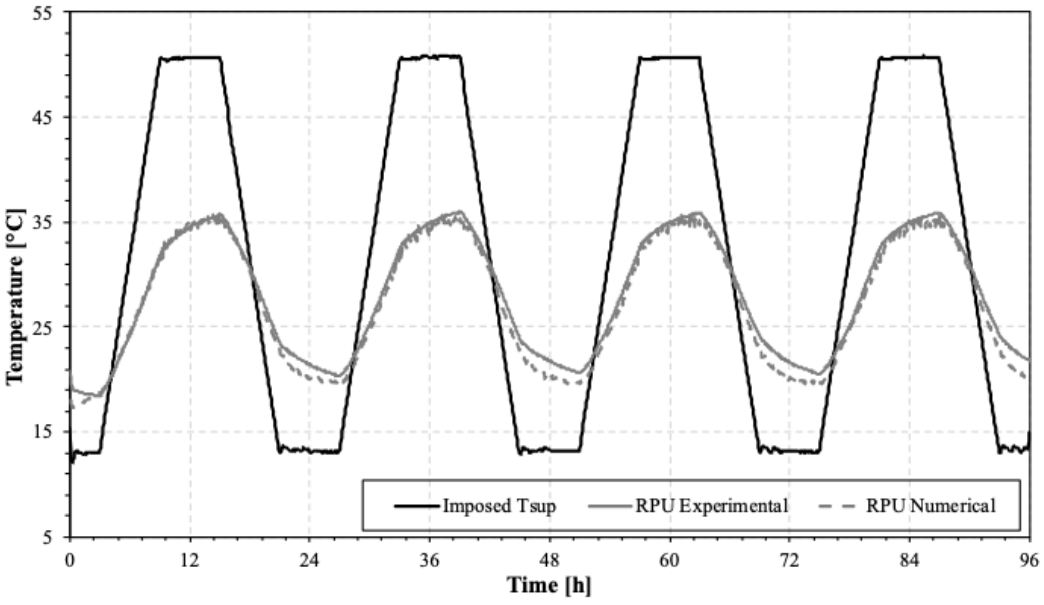

Figure 47: Temperature curve comparison (experimental data and numerical simulation) for the RPU

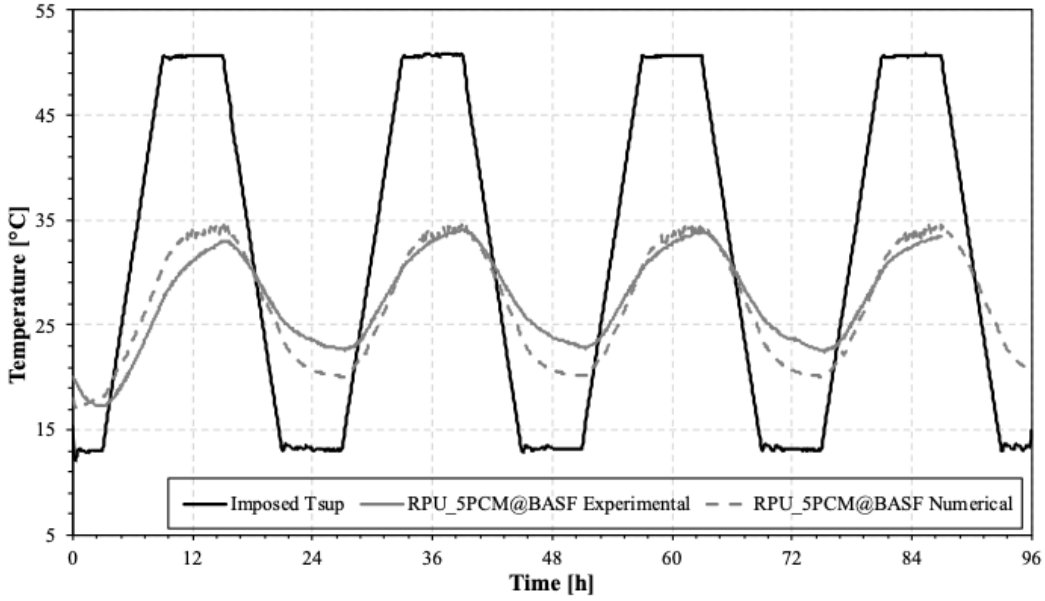

Figure 48: Temperature curve comparison (experimental data and numerical simulation) for the RPU_5PCM@BASF

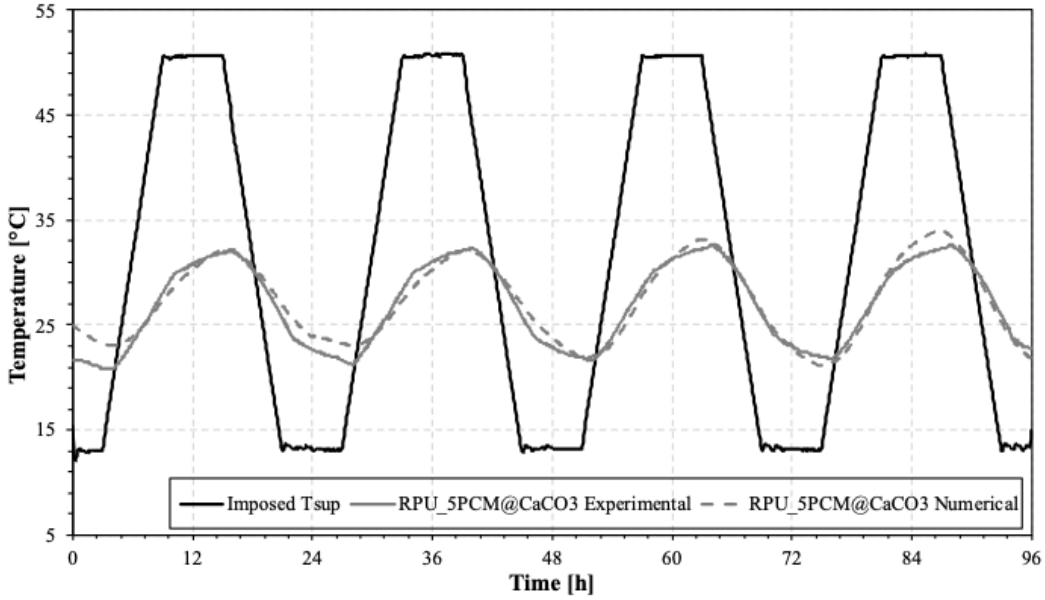

Figure 49: Temperature curve comparison (experimental data and numerical simulation) for the RPU_5PCM@$CaCO_3$

The goodness-of-fit (GOF) criteria and correlation factor, R^2, were used as criteria to validate the numerical models accuracy.

5.3.2.1. Goodness-of-fit (GOF) criteria

The GOF [241] indicator is related to the calculation of the following dimensionless indexes for the optimised model. The methodology followed involves the following equations:

1) RMSE – root mean square error

This index was the objective function used in the optimization process with an evolutionary algorithm. RMSE is a measure of the variability of the data. In this present study the difference in paired data points is calculated and squared hourly.

$$RMSE = \sqrt{\frac{1}{n}\sum_{i=1}^{n}(M_i - S_i)^2} \tag{13}$$

Where S_i represents the measured values of experimental apparatus and M_i the temperature values of the numerical model for each instance "*i*". The "*n*" represents the total number of values for the interval considered.

2) NBME (%) – Normalized mean bias error

The NMBE compares the mean values of the experimental data with the simulated data and normalizes with the data of the mean experimental data. This statistical index is presented in percentage.

$$NMBE = \frac{\sum_{i=1}^{n}(M_i - S_i)}{n \times \overline{M_i}} \times 100 \tag{14}$$

Where $\overline{M_i}$ is the average of the measured data values for the considered period "*n*". The NMBE gives the perception of how close the numerical results are to the experimental data.

3) CV RMSE (%) – Coefficient of Variation of the Root Mean Square Error

This index quantifies how well a model fits the data by capturing offsetting errors between measured and simulated data.

$$CV\ RMSE = \frac{\sqrt{\frac{1}{n}\sum_{i=1}^{n}(M_i - S_i)^2}}{\overline{M_i}} \times 100 \quad (15)$$

4) GOF (%) – Goodness of Fit

$$GOF\ (\%) = \frac{\sqrt{2}}{2} \times \sqrt{NMBE^2 + CV\ RMSE^2} \quad (16)$$

Once calculated the GOF indicator, lower values of this statistical indicator represent the parameters that provides a closer match between measured data and simulated results.

Table 21 presents the calculated statistical indexes for each type of RPU panel with and without PCM. For each index, the results that present the best agreement between the experimental and numerical data are presented below:

Table 21: Statistical indexes for each testing period

Statistical Index	**RPU panel**		
	RPU	**RPU_5PCM@BASF**	**RPU_5PCM@$CaCO_3$**
RMSE	0.80	2.61	0.97
CVRMSE	2.84	9.48	3.54
NMBE	0.56	0.06	1.04
GOF	2.05	6.70	2.61

Cipriano et al. [241] proposed a new procedure of the GOF criteria. This procedure can be used to calibrate building energy simulation models of real testing under indoor free-floating conditions. According to Cipriano et al. [241] a GOF lower than 11% is recommended for trial agreement, so the overall results of the selected period present favourable GOF values for the all RPU panels (see Table 21).

5.3.2.2. Correlation factor, R^2

Another approach to evaluate the agreement between the experimental and numerical data is the average of the correlation factor, R^2, of a scatter plot with experimental and simulated results for each model: RPU, RPU_5PCM@BASF and RPU_5PCM@$CaCO_3$, which is presented in Figure 50.

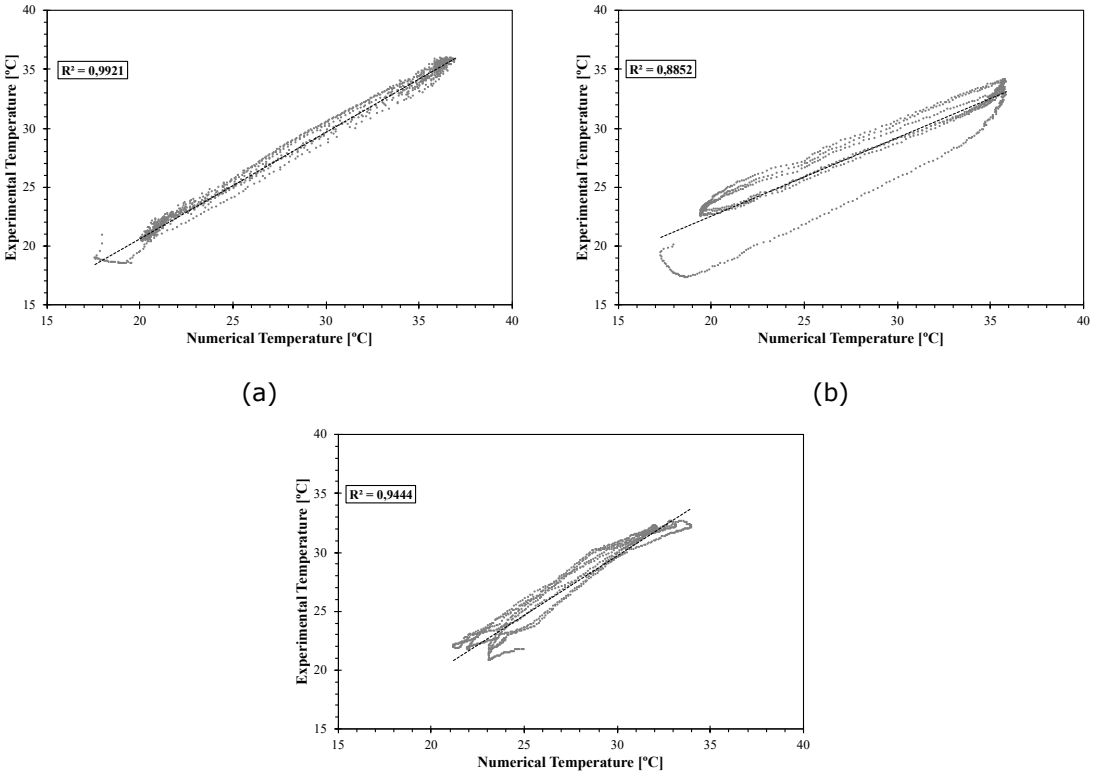

Figure 50: Experimental temperatures Vs. Numerical temperatures for the (a) RPU, (b) RPU_5PCM@BASF and (c) RPU_5PCM@$CaCO_3$.

The results comparison between the numerical models and the experimental testing presented a good agreement with a correlation factor, R^2, of 0.9921, 0.8852 and 0.9444 for the RPU, RPU_5PCM@BASF and RPU_5PCM@$CaCO_3$ models respectively. However, comparing the experimental and numerical results obtained for the RPU_5PCM@BASF, it was observed that for peak temperature values the results revealed more deviation (more evident in the case of minimum temperatures). This deviation in the case of the RPU_5PCM@BASF may be due to the way the room temperature was recorded and taken in the simulation (22°C±2ºC). For the RPU and RPU_5PCM@$CaCO_3$ models, the laboratory room temperature profile was monitored continuously, using a PT 100 probe during the whole 4 day experimental testing cycle and this data was used as input in the numerical model leading to a very fairly good agreement between numerical and experimental results.

5.3.3. Numerical results

Once the model is considered validated in comparison with the experimental data, in order to evaluate the function and performance of the PCM incorporated into the RPU panels and to analyse their optimum working conditions, a parametric

analysis was carried out. The input variables defined were: i) the thickness of the RPU panel and ii) imposed surface temperature profile. These variables can range as follows:

- RPU panel thickness: 20mm and 30mm.
- Imposed surface temperature profile of trapezoidal form between: 12°C and 52°C (Amplitude = 40ºC); 15°C and 45°C (Amplitude = 30ºC); 15°C and 35°C (Amplitude = 20ºC) according to Figure 51.

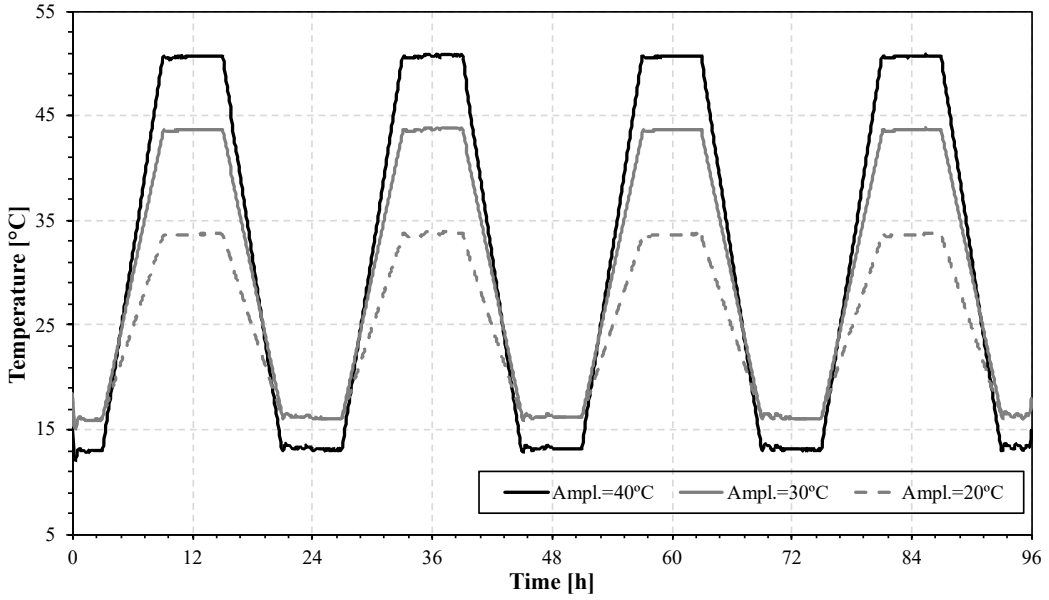

Figure 51: Imposed surface temperature profiles with different amplitudes (40 ºC, 30 ºC and 20 ºC)

Each timestep of the numerical model represents 5 minutes, so for the equivalent of 4 testing days a total of 1152 timestep were considered. Combining the two variables and the three types of RPU panels (RPU, RPU_5PCM@BASF and RPU_5PCM@$CaCO_3$) there are 18 combinations to be studied, this is, to be runned.

5.3.3.1. Temperature results

Table 22 presents the comparison of the mean air temperature profiles of each type of RPU panel with and without PCM combining the two variables (panel thickness and surface temperature amplitude imposed) for the 4 days cycle.

Table 22: Comparison of the mean air temperature profiles of the RPU panels for the 4 days cycle

Imposed surface temperature profile	RPU panel thickness: 20 mm	RPU panel thickness: 30 mm
Ampl. = 40 ºC	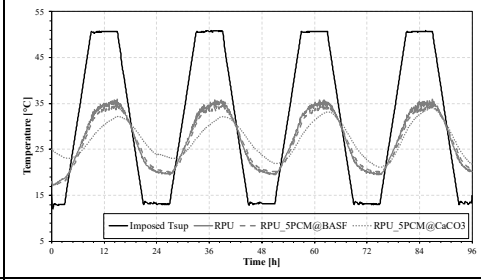	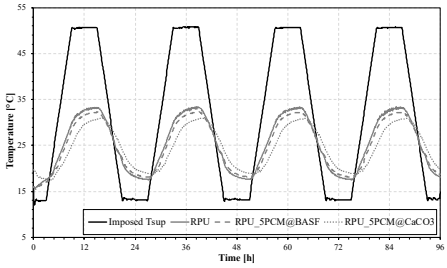
Ampl. = 30 ºC	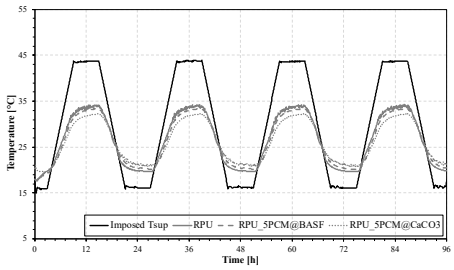	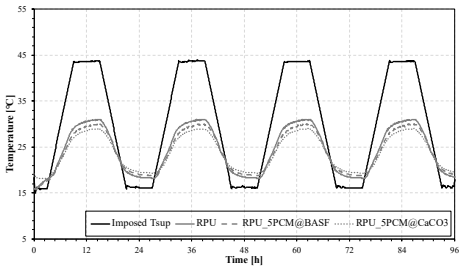
Ampl. = 20 ºC	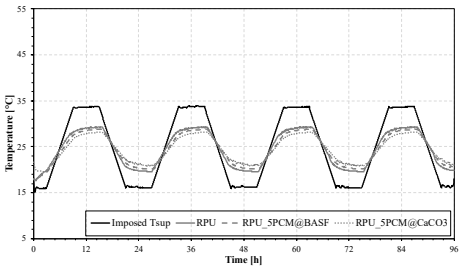	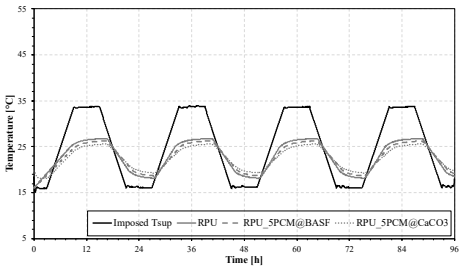

According to the results presented in Table 22, the different RPU panels with 20 mm and 30 mm of thickness present slight differences since the PCM content incorporated into the RPU panels is quite low and equal (5.0 wt%). However, a more significant difference amongst the panels is noteworthy, the thermal amplitude reduction due to the presence of PCM is well observed for the RPU_5PCM@$CaCO_3$ panel, due to the high thermal conductivity of synthetized PCM@$CaCO_3$ which allows for a more effective and faster heat transfer throughout the RPU compared to the commercial PCM@BASF.

However, when the amplitude of the imposed surface temperature profile decreases, the thermal amplitude reduction also decreases in the case of the panels that incorporate PCM. For the imposed temperature amplitude of 20 ºC it was observed that the panels with PCM led to a less significant reduction of the temperature swing in comparison to the other two (ΔT=30 and 40ºC). These results reflect that the heat absorption/release process of the PCM is more efficient for

higher temperature amplitudes of the imposed surface temperature profile. It is also noteworthy, that for the case of the PCM@$CaCO_3$ RPU panel for the imposed amplitude of 40 ºC, the temperature profiles reveal a delay/offset of the peak temperature (maximum and minimum) about 2 to 3 hours.

5.3.3.2. Temperature difference results

To better assess and understand the impact of the PCM incorporation over the thermal amplitude reduction between the reference RPU panel and the RPU 5PCM@BASF and RPU 5PCM@$CaCO_3$, it is presented in Table 23 the results of the temperature difference between these for each time step of the third day cycle (between 48h-72h). The 24 day cycle (48h-72h) was selected taking into account the stabilization of the numerical model results. The results are given for 20o and 30mm panel thickness and three imposed surface temperature profiles.

Table 23: Comparison of the temperature differences of the RPU panels with and without PCM for 24h period

Imposed surface temperature profile	RPU panel thickness: 20 mm	RPU panel thickness: 30 mm
Ampl. = 40 ºC	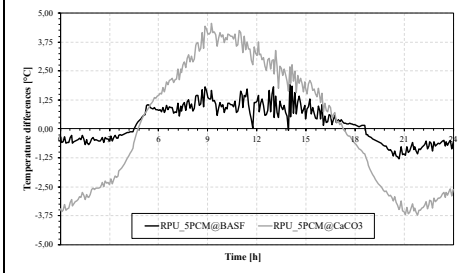	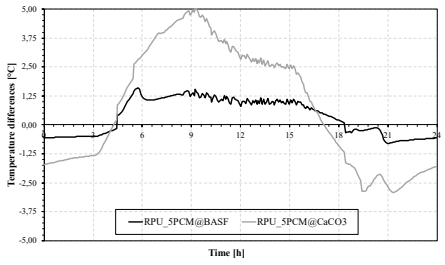
Ampl. = 30 ºC	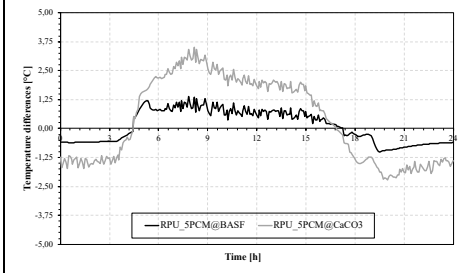	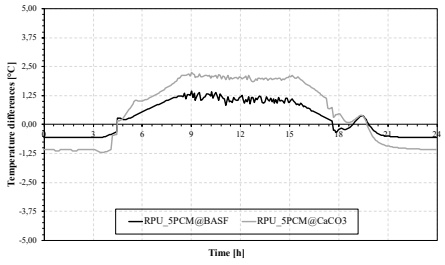
Ampl. = 20 ºC	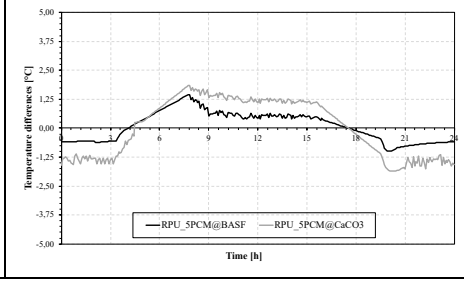	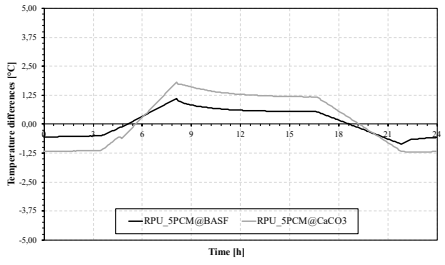

Comparing the numerical results in terms of the thermal amplitude reduction obtained for RPU panels with and without PCM, it was observed that the PCM led to a thermal amplitude reduction ranging from 1.0 to 5.0 ºC for the peak maximum temperature and 0.5 to 3.75 ºC for the peak minimum temperature. The thermal amplitude reduction is more evident for the RPU_5PCM@$CaCO_3$ panel and for the imposed surface temperature profile of 40ºC amplitude (imposed mean temperature is near 32°C), since the synthetized PCM@$CaCO_3$ has a higher thermal conductivity compared to the commercial PCM@BASF. The thermal response is smoothened out by the PCM melting and solidifying process that is influenced by imposed mean temperature. The behaviour is considered more effective when the input mean temperature is near 32°C (corresponding to an amplitude 40 ºC, between 12ºC and 52ºC). Therefore, the efficiency of the RPU panels incorporating PCM is not exclusively dependent on the presence/quantity of PCM (equivalent in %wt in all cases) but also by the imposed temperature profile and the thermal properties of the PCM.

5.4. Conclusions

The work presented and discussed the role and impact of the incorporation of PCM into RPU panels. The thermal characteristics and the potential thermal regulation effect was firstly assessed by means of laboratory testing (by hot box heat flux meter method) and then carried out additional evaluation through calibrated 2D numerical models resourcing to ANSYS Fluent.

According the experimental results it was observed that the incorporated PCM can lead to a thermal amplitude reduction of about 2-1 ºC for the RPU_5PCM@BASF and about 4-2 ºC for the RPU_5PCM@$CaCO_3$ (peak maximum temperature- peak minimum temperature).

Then numerical models were considered validated comparing the numerical results with the experimental data for which a good agreement was obtained using statistical indexes. The calibrated numerical model was then used to evaluate the impact of the PCM incorporated into the panel under a wider range and combined conditions.

A parametric analysis with more than 18 combinations was carried out to better understand the thermal conditions that could lead to the best performance of the RPU panels incorporating PCM. The best behaviour of the RPU panel with PCM was registered when the external and internal mean temperature are nearer to the melting peak temperature of the PCM. The thermal amplitude reduction due to the PCM is more significant for the case of the RPU_5PCM@CaCO3 panel, due to its

higher thermal conductivity of synthetized PCM@CaCO3 which allows for a more rapid heat transfer when compared to the commercial PCM@BASF in the charging and discharging process. Overall the results have shown that the PCM can have a thermal regulation effect in the melting and solidifying phases.

Further numerical modelling is still needed to tackle optimization of PCM quantity/content, melting temperature ranges, latent heat capacity and the optimal panel thickness. From the numerical modelling point of view the combination of different PCM with different melting temperatures should be considered.

CHAPTER 6

6. Development of structural layer PVC incorporating phase change material for thermal energy storage

This chapter was submitted in the Journal of Applied Thermal Engineering

Amaral, C.; Gama, N.; Mohseni, F.; Amaral, J.S.; Amaral, V.S.; Marques, P.A.A.P.; Barros-Timmons, A.; Vicente, R. (2019) – Development of structural layer PVC incorporating phase change material for thermal energy storage – Journal of Applied Thermal Engineering, Elsevier (under review)

Abstract

The use of poly(vinyl chloride) (PVC) structural layer incorporating phase change materials (PCM) for latent heat thermal energy storage (LHTES) has become more attractive in the recent years compared other supporting materials. In this study, PVC layers with different types of PCM were prepared by blending and compression moulding method. Two types of synthesized PCM one based on paraffin and calcium carbonate (PCM@$CaCO_3$) and the other on paraffin, silica and graphene oxide (PCM@SiGO) have been developed to enhance the thermal conductivity of the PVC matrix and thus achieve a more effective charging and discharging process. PVC layers prepared with commercial PCM (PCM@BASF) were also prepared for comparison.

SEM images and the DSC results reveal that the PVC layers with PCM have homogeneous constitution and that most PCM particles are undamaged. The shell material (in the case of PCM@BASF) and the shape stability (in the case of synthesized PCM@$CaCO_3$ and PCM@SiGO) prevent leakage of molten paraffin during the PVC layer production.

The thermal conductivity profile of the PVC layer without PCM have a decreasing trend with the increasing of temperature using a transient plane heat source method (HotDisk Analyser, TPS 2500 S) and thermal flux meter method (steady-state method). However, for PVC layers with PCM the thermal conductivity profile shows a different behaviour when the mean specimen surface temperature is below the phase change transition temperature range (increasing trend). During phase change transition (18 °C to 26 °C), the thermal conductivity presents two distinct trends. First, the thermal conductivity reveals a decreasing trend with the increasing mean temperature of the specimen and afterwards an increasing trend. But, when the mean specimen surface temperature is above the phase change transition temperature range, the thermal conductivity profile shows a decreasing trend, independently of the PCM origin.

Finally, the mechanical properties of PVC layers were assessed and the results obtained revealed that the incorporation of PCM in the PVC matrix has a significant impact on the mechanical performance of the composites, especially on the elongation at break.

Keywords: phase change material (PCM); poly(vinyl chloride) (PVC); thermal conductivity; structural layer.

6.1. Introduction

The building and industrial sectors generate pollution and consume natural resources being one of the major energy consumers taking up to 40 % of the overall energy consumption [1–4]. Therefore, thermal energy storage (TES) systems are a useful tool for improve the energy efficiency and decrease energy consumption, without compromising thermal comfort and indoor air quality in buildings [5,175]. The most attractive TES system is the latent heat storage because of high storage density and small temperature change from storage to release. In latent heat thermal energy storage (LHTES) systems, energy is stored during melting and released during freezing of a phage change material (PCM). Therefore, the use of PCM can increase the energy storage of building components [9,11,176] for storing thermal energy and having a thermal regulation effect by charging and discharging large amounts of latent heat during the phase change process [35,37,41,177]. Thus, it contributes to the time mismatch between the energy supply and demand.

PCM are divided into two main categories: organic and inorganic. This classification depends on different chemical properties. These types of materials have been studied during the last 40 years, including mainly hydrated salts, paraffin waxes, fatty acids and eutectics mixtures of organic and non-organic compounds. The paraffin was found to be widely used for LHTS systems [35–37,41]. However, the low thermal conductivity of PCM limits the use of the full potential of these materials since it slows down the heat transfer process associated to the charging and discharging process. The strategies to improve the thermal properties of PCM [175] include: the incorporation of high thermal conductivity nanofillers or other additives [12–14], the PCM micro/nano encapsulation with shell material with higher thermal conductivity [18,19,103,113,177] and the shape stabilization of the PCM with high thermal conductivity supporting materials [15–17]. Vivekananthan M. and Amirtham V. [73] researched the thermal conductivity enhancement through the dispersing of three different mass fraction (0,1 %, 0.5 % and 1.0 %) of graphene particles into the PCM matrix. It was concluded that the thermal conductivity of PCM was enhanced with the increase in weight fraction of graphene due to its high thermal conductivity (the addition of 1 wt.% of graphene led to 53.1 % increase in thermal conductivity with only 6.1 % decrease in latent heat enthalpy). Mehrali et al. [17] studied a new shape stable composite PCM prepared by vacuum impregnation of paraffin within graphene oxide (GO) sheets. The composite PCM contained 48.3 wt.% of paraffin without leakage of melted PCM and therefore this composite was found to be a shape stable with a thermal conductivity enhancement of 230%. The decrease in latent heat capacity values was 50% (in acceptable level for LHTES applications for composite PCM in this study). Jiang et

al. [145] prepared microencapsulated PCM with calcium carbonate ($CaCO_3$) shells modified with GO using a modified self-assembly method. This microencapsulated PCM had higher thermal conductivity and better mechanical properties than the microencapsulated PCM with $CaCO_3$ shells prepared without GO.

A shape stabilized PCM is composed of working substance (prevents the melted phase from leaking so the whole system remains in solid state) and supporting material (prevents the melted phase from leaking). There is a variety of supporting materials used for shape stabilization of PCM which mainly includes polymer matrix, porous materials and nanomaterials [28,99]. Poly(vinyl chloride) (PVC) has been explored by some researchers both, as shell material in the PCM microencapsulated or as a supporting material in the shape stabilized PCM. Feldman et al. [242] studied the possibility of developing shape stabilized PCM based on PVC and fatty acids. Jin et al. [243] prepared microencapsulated PCM as latent heat storage medium and PVC/wood flour compound as supporting material for the application of potential LHTES. Chen et al. [115] studied the development of PVC macro capsules that encapsulated paraffin directly by coating multiple layers of polyamide, silica or polydopamine. The prepared composite not only solves the problems of paraffin leaking and hysteresis of phase transition, but also has a high phase change enthalpy. Wang et al. [116] explored a simply and environment-friendly method for the preparation micro/nano PCM encapsulated with PVC shell with excellent energy storage performance. However, adding microencapsulated and shape stabilized PCM into PVC layer used for LHTES applications has not been investigated so far.

In this study, PVC layers with different types of PCM as latent heat storage and PVC layers as structural matrix were prepared by blending and compression moulding. Two types of shape stable PCM based on paraffin and calcium carbonate (PCM@$CaCO_3$) and other on paraffin, silica and graphene oxide (PCM@SiGO) have been developed to enhance the thermal conductivity and to achieve a more effective charging and discharging process of the PVC layer. The PVC layers produced where thoroughly characterized in respect to their structure, morphology, mechanical and thermal properties, using different scanning methods (SEM, EDS and EDX), tensile mechanical analyses, differential scanning calorimetry (DSC), thermogravimetric analysis (TGA), transient plane heat source method (HotDisk Analyser, TPS 2500 S) and thermal flux meter method (steady-state method). This experimental work particularly focuses on promising results of the synthesized PCM@$CaCO_3$ and PCM@SiGO compared to the commercial PCM@BASF and the incorporation of these PCM into PVC layers for the potential LHTES applications.

6.2. Materials and Methods

6.2.1. Phase change materials (PCM)

6.2.1.1. PCM Micronal®DS 5001X (PCM@BASF)

Microencapsulated PCM (PCM@BASF) powder purchased from BASF (Ludwigshafen, Germany) was used in this study according to the section 3.2.1.1 of chapter 3.

6.2.1.2. PCM with calcium carbonate (PCM@$CaCO_3$)

The PCM with $CaCO_3$ was synthesized according to the section 3.2.1.2 of Chapter 3 of this PhD thesis.

6.2.1.3. PCM with silica and graphene oxide (PCM@SiGO)

The PCM with silica and GO was synthesized using paraffin RT18HC (main peak of melting point: 18ºC) purchased from Rubitherm (Germany). Octadecylamine (OCA) and hydrochloric acid (HCl) were purchased from Sigma-Aldrich. The GO water dispersion was commercially obtained from Graphenea (Spain). Tetraethyl orthosilicate (TEOS) was purchased from Acros Organics and the surfactant Pluronic F-127 was purchased from BASF.

In order to improve compatibility between paraffin and GO, the alkylamination method was used. This method has the purpose of chemically modifying the GO surface. The aliphatic amine used was octadecylamine (OCA). OCA solution in ethanol was added to a water dispersion of GO 4mg/mL. The reaction was conducted at room temperature (RT) during 24 h. Then 0.1 wt% of GO with OCA (GO_OCA) was dispersed in paraffin. In a beaker, 20 g paraffin were added to 20 mg of GO_OCA and vigorously stirred with a mechanical stirrer (CAT R100SD overhead stirrer equipped with a polytetrafluoroethylene (PTFE) half-moon blade) at 1300 rpm during 40 min. The mixture was then stirred at ultrasonic bath during 120 min. The temperature was maintained constant during the whole process at 35 ºC (to ensure the dispersion was liquid), using a water bath.

PCM@SiGO containing paraffin was synthesized through the interfacial polycondensation of silica precursors at 3.0 of pH. An oil solution was prepared by mixing 15 g of paraffin with GO_OCA and 16 mL of TEOS in a beaker with agitation at 500 rpm during 45 min. An O/W emulsion was formed by dropping the oil solution into 150 mL aqueous solution containing 0,75 g of F-127 surfactant with agitation at 500 rpm, and then emulsification was carried out in a round-bottom flask and

vigorously stirred with a mechanical stirrer at 650 rpm for 45 min. Subsequently, the HCl aqueous solution with concentration of 2.0 mol/L was used as catalyst to initiate the condensation of silica hydrolysates, and it was added dropwise into the emulsion at a stirring rate of 250 rpm, until a 3.0 pH value was obtained using a pH meter from drop to drop. Then, the emulsion was continuously stirred at 500 rpm during 48 h to complete the condensation. The temperature was maintained constant during all process at 35ºC, using a water bath. The final product was washed several times using ethanol aqueous solution with the concentration of 30 wt% and collected by vacuum filtration. Finally, the PCM@SiGO was dried in an oven at 50 ºC, during 72h.

6.2.1.4. Characterization of PCM

To evaluate the success of the functionalization of the GO with OCA the selected experimental characterization tests were: *i)* FTIR analysis and *ii)* thermal gravimetric analysis. To evaluate the behaviour of PCM (PCM@BASF, PCM@$CaCO_3$ and PCM@SiGO), the selected experimental characterization tests were: *i)* FTIR analysis; *ii)* SEM and EDS analysis; *iii)* density; i*v)* energy storage properties; *v)* thermal gravimetric analysis.

The Fourier transform infrared (FTIR) spectra of GO and GO_OCA specimens were collected on a Perkin Elmer FTIR System Spectrum BX Spectrometer equipped with a single horizontal Golden Gate ATR cell. All data were recorded at room temperature, in the range 4000 to 500 cm^{-1} by accumulating 32 scans with a resolution of 4 cm^{-1}. The chemical composition of PCM was identified by spectroscopic analyses performed on a KBr disk using a FTIR spectroscopy. The FTIR spectra were performed on a Mattson 7000 galaxy series spectrophotometer. All data were recorded at room temperature, in the range 350 to 4000 cm^{-1} with a resolution of 8 cm^{-1} and 64 scans.

The morphology (shape and size) of the PCM were analysed by scanning electron microscopy (SEM) coupled with energy dispersive spectroscopy (EDS). A small piece of each specimen was placed on a metal support by means of double-sided adhesive carbon tape and sputter-coated with carbon prior to the analysis. The SEM analysis were carried out with Hitachi SU 70 Bruker scanning electron microscope at an accelerating voltage of 15.0 kV. The EDS spectra were performed using a Tabletop Microscope TM4000Plus from Hitachi equipped with Bruker Quantax 75.

The bulk density of a powder is the ratio of the mass of an untapped powder specimen and its volume including the contribution of the interparticle void volume. Hence, the bulk density was determined according to [188].

To characterize the energy storage properties of the PCM (melting temperature and enthalpy), a dynamic scanning calorimeter (DSC 4000, PerkinElmer) was used, during a heating rate of 5 ºC/min, in the range of 10 ºC to 50 ºC under a nitrogen atmosphere. DSC was calibrated with indium (heating rate of 5 ºC/min, in the range of 30 to 170 ºC) prior to the measurement and the specimens were accurately weighted into an aluminium capsule (pans and covers). This test is essential to characterize the energy storage properties of the PCM.

The thermal stability of GO, GO_OCA and the PCM was evaluated by thermal gravimetric analysis (TGA). A thermogravimetric analyzer, TG 449 F3 Jupiter, Netzsch was used, during a scanning rate of 10 ºC/min, in the temperature range of 30–600 ºC, under a nitrogen flux of 200 mL/min.

6.2.2. Structural Layer (PVC) incorporating PCM

In this study, the PCM (PCM@BASF, PCM@$CaCO_3$ and PCM@SiGO) were then incorporated in PVC formulation to yield PVC structural layers.

6.2.2.1. Structural layer (PVC)

The different PCM were prepared according to the section 6.2.1. The PVC layers production resulted from the experimental research of Gama et al. [244,245] using 100 parts of PVC resin (VICIR S1200 with *K* value of 70) supplied by Cires (Portugal), 60 parts of plasticizer DOTP (dioctyl terephthalate) were supplied by Eastman, 10 parts of ESBO (epoxidized soybean oil) supplied by Galata chemicals and 2 parts of stabilizer Ca/Zn (FI 240 CZ) were supplied by Markstat.

The PVC blend was mixed with PCM (5.0 wt%) in a high-speed mixer and the composite films (PVC structural layer incorporating PCM) were produced using a hot press (CARVER model 3851-0) at 150 ºC, using 3 tons of pressure, during 10 min.

Preliminary experimental studies were carried out to determine the maximum wt% of PCM to add to the PVC layer to achieve a structurally sound layer without visual defects. It should be noted that only commercial PMC@BASF was used in these preliminary experimental studies, because it is the PCM that had in largest quantities. The preliminary experimental studies consisted in incorporating different PCM content (2.5, 5.0, 7.5 and 10.0 wt%) into the PVC matrix. By visual observation and handling of the specimens produced the value of 5.0 wt% was defined to move forward, since the specimens with PCM content above 5.0 wt% were brittle and cracked (see Figure 52).

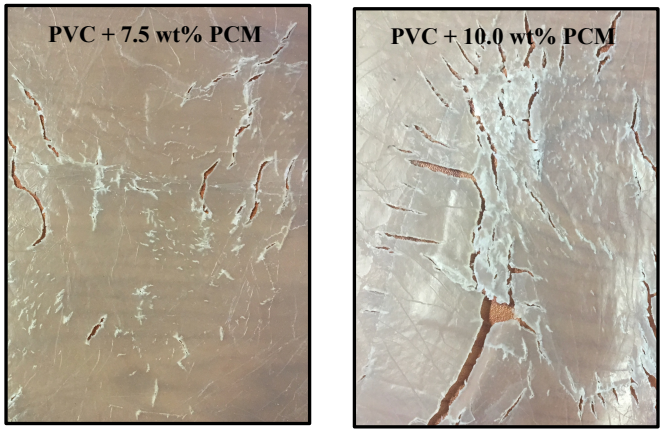

Figure 52: Cracks in PVC layer with 7.5 and 10.0 wt% of PCM content

To evaluate the influence of PCM in the PVC layer, the following experimental characterization tests were carried out over 4 types of specimens with dimensions according to Figure 10 and Table 24.

Table 24: Designation of the PVC layers

Name	**PVC layers**
PVC	PVC layer without PCM
PVC_5PCM@BASF	PVC layer with 5.0 wt% PCM@BASF
PVC_5PCM@$CaCO_3$	PVC layer with 5.0 wt% PCM@$CaCO_3$
PVC_5PCM@SiGO	PVC layer with 5.0 wt% PCM@SiGO

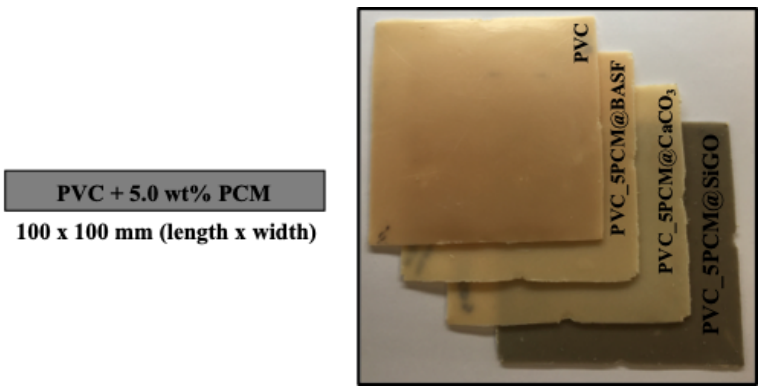

Figure 53: Scheme of the PVC layer

6.2.2.2. Characterization of PVC layer

To evaluate the influence of PCM in the PVC layer, the selected experimental characterization tests were carried out: *i)* SEM and EDS analysis; *ii)* density; *iii)* mechanical properties; i*v)* energy storage properties; *v)* thermal conductivity.

The morphology (shape and size) and the composition (element types and contents) of the PVC layers were analysed by SEM and EDS. The SEM images and EDS spectra were performed using a Tabletop Microscope TM4000Plus from Hitachi equipped with Bruker Quantax 75.

PVC specimens (50×50×thickness mm^3) were cut and weighed to determine the density. Densities were determined dividing the weight of the specimens by their respective calculated volume. The values presented correspond to the average density determined for 9 specimens of each PVC layer. The density of the PVC layers was used to determine if the PCM incorporated process influences the PVC layer density.

Tensile mechanical analyses of PVC layers (50x1x10 mm^3) were performed using a SHIMADZU AGS-X using a load cell of 1.0 kN and a deformation rate of 20.0 mm min^{-1}. Three specimens of each PVC layer were tested.

To characterize the energy storage properties of the PVC layers (melting temperature and enthalpy), a dynamic scanning calorimeter (DSC 4000, PerkinElmer) was used according to section 6.2.1.4. This test is essential to characterize the energy storage properties of the PVC layers and useful to determinate the PCM content ($\%_{PCM}$) incorporated in the PVC layers, according the following Equation (17):

$$\%_{PCM} = \frac{\Delta H_{m,\mathrm{PCM}}}{\Delta \mathrm{H}_{m,PVC}} \times 100 \qquad (17)$$

Where, $\Delta H_{m,PCM}$ is the latent heat of the PCM for melting curve and $\Delta H_{m,PVC}$ is the latent heat of the PVC layers for melting.

The hot box test is based on the steady-state method. This method consists in a simple hot box configuration composed by two closed chambers with controlled temperature and relative humidity conditions: one of the chambers is at low and constant temperature (cold chamber) and the other, the measuring chamber, is placed at higher and constant temperature (warm chamber). Between the two compartments or chambers there is a mounting ring with the wall specimen or panel to be tested, as presented on

Figure 14. The procedures, the schemes and the materials have been previously defined by Amaral et al. elsewhere [176]. However, due to the PVC specimens small dimensions (100x100 mm) it was necessary to place an XPS (extruded polystyrene) panel with 20 mm of thickness in the mounting ring to support the frame the

openings to position the PVC specimens. Four holes were opened in the XPS panel to position and distance the PVC specimens according to Figure 54.

Figure 54 presents the sensors position on the specimen (in the cold and warm chambers sides). Four type-T thermocouples and four heat flux meters were mounted on the internal surface (warm chamber side) of the PVC specimen and one thermocouple type-T on the internal surface of the XPS panel (in the middle of the panel). On the internal surface (cold chamber side) of the PVC specimen, there were five eight thermocouple type-T in the same position on the opposite side.

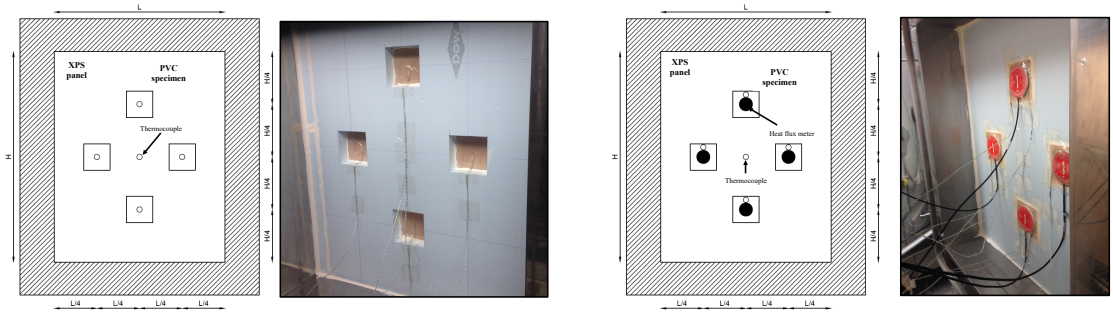

(a) Cold chamber (b) Warm chamber

Figure 54: Specimen ring mounting and sensor positioning.

The schematic layout of the PT100 probes in the chambers can be found elsewhere [176], where five PT100 probes at a distance of 150 mm from the specimen (cold and warm chambers) and one PT100 probe placed in the middle of the chamber (cold chamber side). In the warm chamber side, six PT100 probes were positioned in the same relative positions to the opposite side.

The thermal conductivity (λ) is calculated according the Fourier´s Law, using equation (6) in the section 3.2.1.6.

The thermal conductivity was calculated for different setup temperatures on the cold and warm chambers, using the same thermal amplitude value of 10 ºC and 50 % of RH. The thermal conductivity was calculated for the following setup temperatures: {2;12}, {4;14}, {6;16}, {…}, {26;36}, {28;38} and {30;40} (which means: {temperature of the cold chamber in ºC; temperature of the warm chamber in ºC}). The total number of temperature steps carried out in these experimental setups was 15, and the measurement time for each temperature step was 6 hours.

The most important advantage of the use of hot box test for thermal conductivity measurements is the possibility to measure thin specimens.

The thermal conductivity of the PVC layer without PCM was measured using the Hot Disk Transient Plane Source (TPS) technique [190]. The method is based on a planar sensor made of a patterned nickel element, between two composite thin layers of PVC material, like Kapton or mica. By passing current through the nickel element, and simultaneously measuring its resistivity, the sensor acts as both heater and thermometer. By fitting the transient heating curve, estimates of thermal conductivity and diffusivity are obtained, and specific heat calculated from the former two. The method is standardised in ISO 22007-2 [191]. The type of sensor used in this measurement test consists of a nickel/Kapton sensor, which was placed between two similar composite thin layers. Each composite thin layer consists of 4 layers with dimensions of 40 × 40 mm (width x length) and thickness of the real specimens, this technique was only used to validate the thermal conductivity vs specimen temperature behaviour of the PVC without PCM using the hot box test. Therefore, hot disk measurements of the PVC layers with PCM were not performed.

6.3. Results and Discussion

6.3.1. Phase change materials (PCM)

6.3.1.1. GO functionalization with OCA

Figure 55 (a) shows the FTIR spectra of functionalized GO with OCA, as well as the characteristics bands of simple GO. The disappearance of the hydroxyl (OH) bands characteristics of GO, together with the appearance of well-defined CH bands indicates the presence of aliphatic chain. The results suggest the successfully functionalization.

Figure 55 (b) shows TGA curves of GO, functionalized GO and the aliphatic amine (OCA). The weight loss at about 100ºC is associated with the loss of the adsorbed water and at 200ºC is due to de decomposition of oxygen-containing groups. For higher temperatures, 250-450ºC, it can be observed an abrupt loss of weight that is caused by the decomposition of the aliphatic chain.

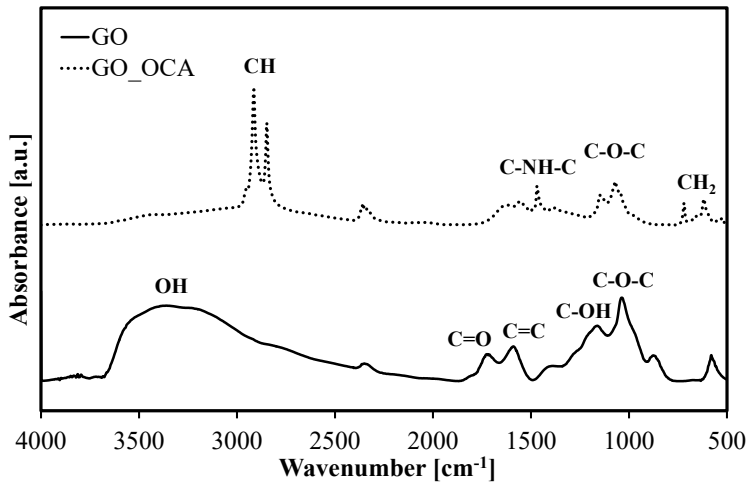

(a)

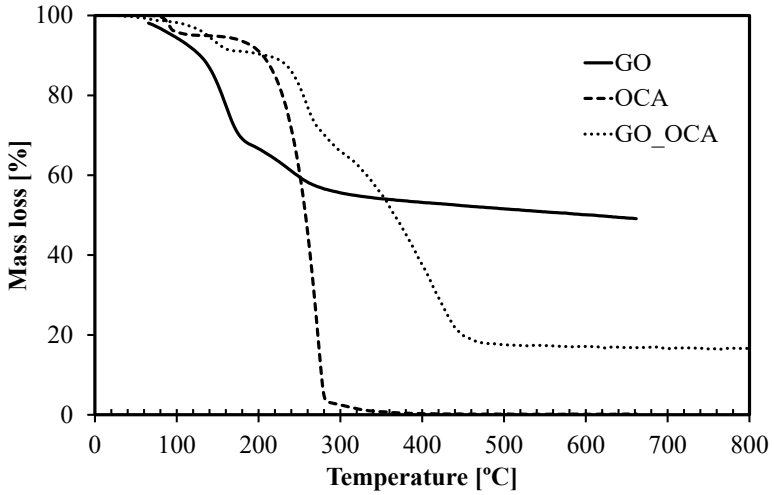

(b)

Figure 55: FTIR (a) and TGA thermograms (b) of GO and GO_OCA.

Based on FTIR and TGA analysis, the GO functionalization with OCA seems to have been successfully achieved. Interestingly, the thermal stability of GO_OCA was improved, and the degradation pattern significantly changed when compared to that of GO and GO_OCA. This may be due to a synergist effect.

6.3.1.2. Chemical composition, morphology and microstructure of PCM

The chemical compositions of the commercial PCM@BASF, the synthesized PCM@$CaCO_3$ and PCM@SiGO were confirmed by FTIR, as shown in Figure 56.

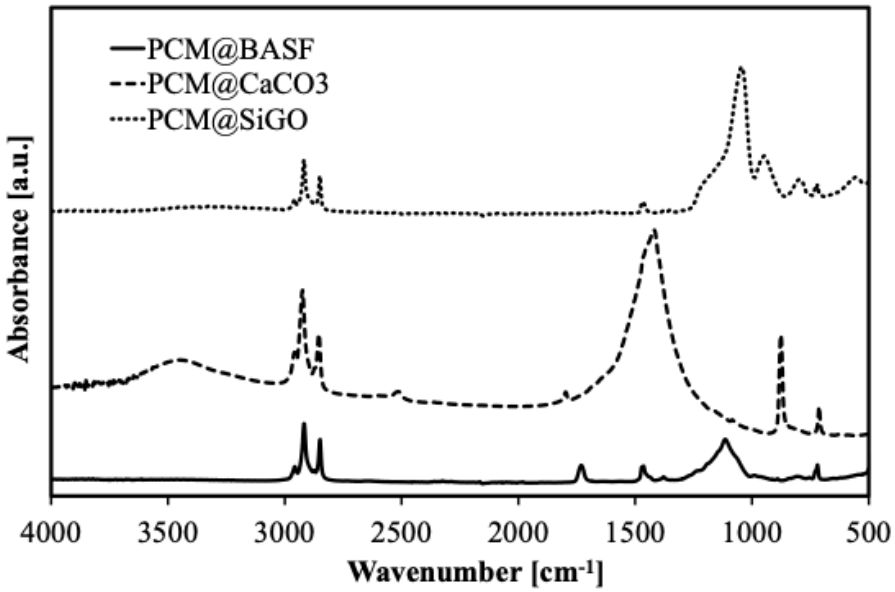

Figure 56: FTIR of PCM@BASF, PCM@$CaCO_3$ and PCM@SiGO.

For the commercial PCM@BASF the FTIR spectrum shows peaks from 2956 cm^{-1} to 2849 cm^{-1} that correspond to the aliphatic C–H stretching vibration. The vibration at 1730 cm^{-1} is attributed to the carbonyl group of the acrylate, while the absorption peak at 1465 cm^{-1} is associated with the C–H bending vibration, and the absorption peak at 1114 cm^{-1} can be assigned to the C–O stretching of the ester group of PMMA used as encapsulating material.

For the synthesized PCM@$CaCO_3$ the vibrational bands at 877 cm^{-1} can be assigned to a carbonate out-of-plane stretching vibration. The presence of an absorption peak at 711 cm^{-1} is attributed to the in-plane bending vibration of O–C–O in calcite. The presence of a broad band at 1417 cm^{-1} represents the asymmetric stretch of carbonate ions, which is an indicative of the presence of CO_3^{2-}. FTIR spectra also reveal two intensive absorption peaks at 2925 and 2855 cm^{-1}, which are associated with the alkyl C-H stretching vibrations of methyl and methylene groups which bands are characteristic of paraffin.

For the synthesized PCM@SiGO the FTIR spectrum shows peaks from 2956 cm^{-1} to 2849 cm^{-1} that correspond to the aliphatic C–H stretching vibration (characteristic of paraffin). The peak at 1460 cm^{-1}corresponds to bending vibration resulting due to the CH_2 absorption vibration. In turn the peaks at 1044 cm^{-1} are attributed to the asymmetrical stretching vibration of Si-O, while the peaks at 795 cm^{-1} and 424 cm^{-1} are due to the symmetrical stretching vibration of Si-O. The most intense band at 1044 cm^{-1} is due to asymmetric stretching of the Si–O–Si bonding which normally appears between 1200 and 1000 cm^{-1} confirms the presence of silica in the specimen.

The PCM morphology was analysed by SEM. Figure 57(a) shows the morphology and the size of the PCM@BASF particles. The PCM@BASF specimen consists of microspheres of approximately 300-50 μm in diameter, which in turn are made of multiple spheres with diameters approximately 7-2 μm each. PCM@$CaCO_3$ specimen exhibits a quasi-spherical and rhombohedral morphology (Figure 57(b)). The formation of rhombohedral particles may be ascribed to the spontaneous steric compression during the crystallization of the calcium carbonate in calcite form. This specimen is constituted by agglomerates of microparticles and nanoparticles (particle size approximately 7 μm – 55 nm). The morphology and detailed microstructure of the PCM@SiGO is shown in Figure 57(c). It is evident the presence of the silica microspheres (20-2 μm) with some free nanoparticles (200-20 nm) deposited on their surface forming a rough and porous silica microsphere.

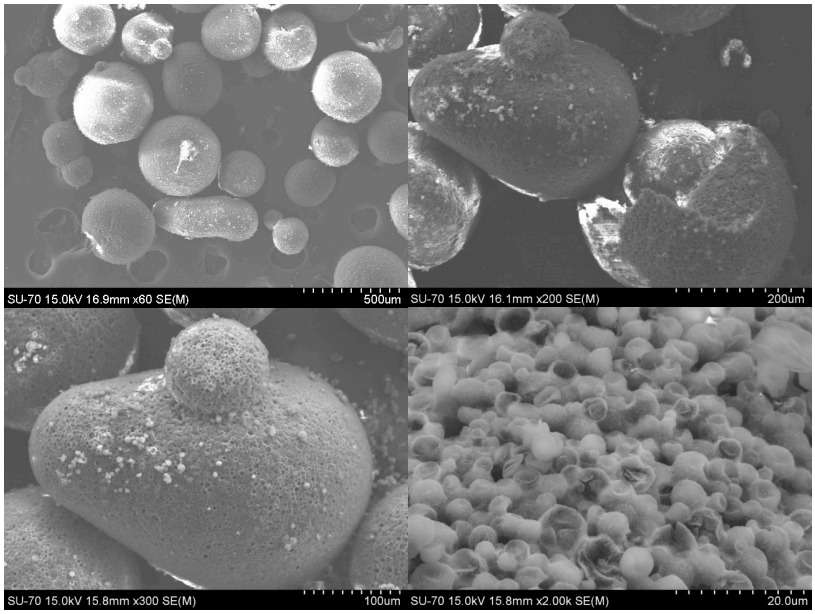

(a)

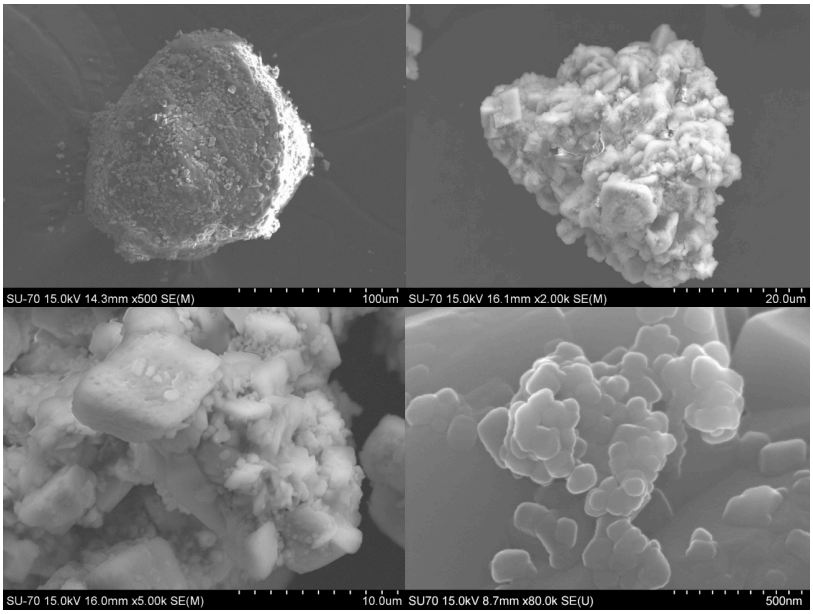

(b)

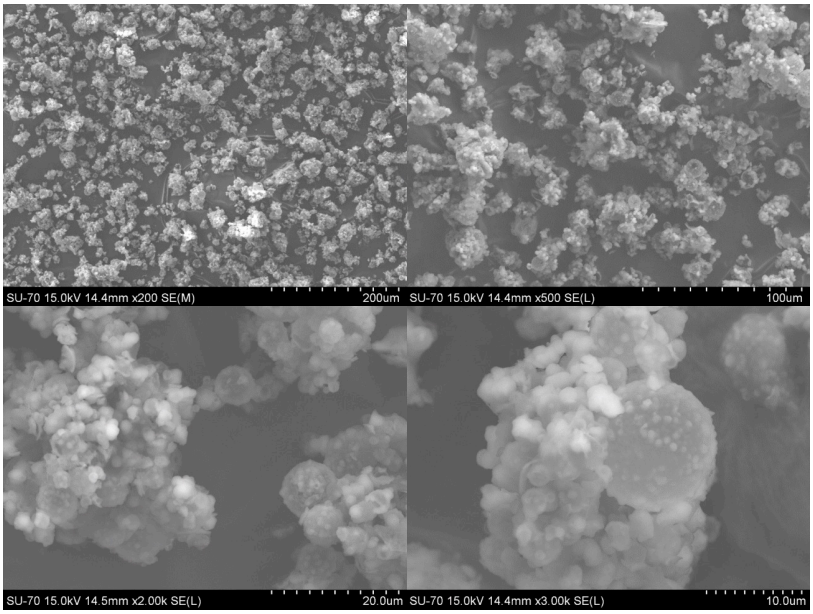

(c)

Figure 57: SEM images with different magnifications of (a) PCM@BASF, (b) PCM@$CaCO_3$ and (c) PCM@SiGO.

Figures 58, 59 and 60 show all the information collected by SEM and coupled techniques (SEM, EDX spectra and element mapping) for all PCM specimens. The results revealed the presence of a small amount of aluminium (Al) in all PCM specimens, due to the support where the specimens are placed.

For the commercial PCM@BASF the results (see Figure 58) revealed that the major components are carbon (C) and oxygen (O) due to the presence of paraffin. The presence of silicon (Si) and sodium (Na) may be included in the polymer (PMMA)

formulation as silica (SiO_2) according to Giro-Paloma et al. [194]. As observed in the Figure 59 , the synthetized PCM@$CaCO_3$ exhibited the presence of carbon (C), oxygen (O) and calcium (Ca) due to the presence of paraffin and calcium carbonate ($CaCO_3$). The small amount of sodium (Na) results from the fact that during their synthesis the sodium carbonate was used. As expect and according to Figure 60, the synthetized PCM@SiGO showed the presence of carbon (C), oxygen (O) and silicon (Si) due to the presence of paraffin and silica. The presence of GO is only inferred due to the nature of its chemical composition.

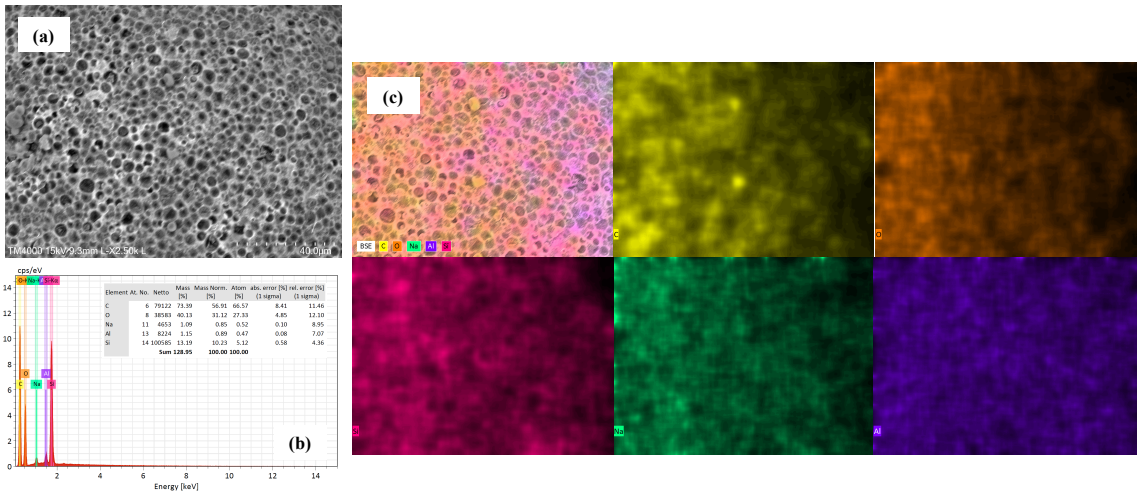

Figure 58: Commercial PCM@BASF scanned (a) SEM (b) EDX spectra and (c) element mapping.

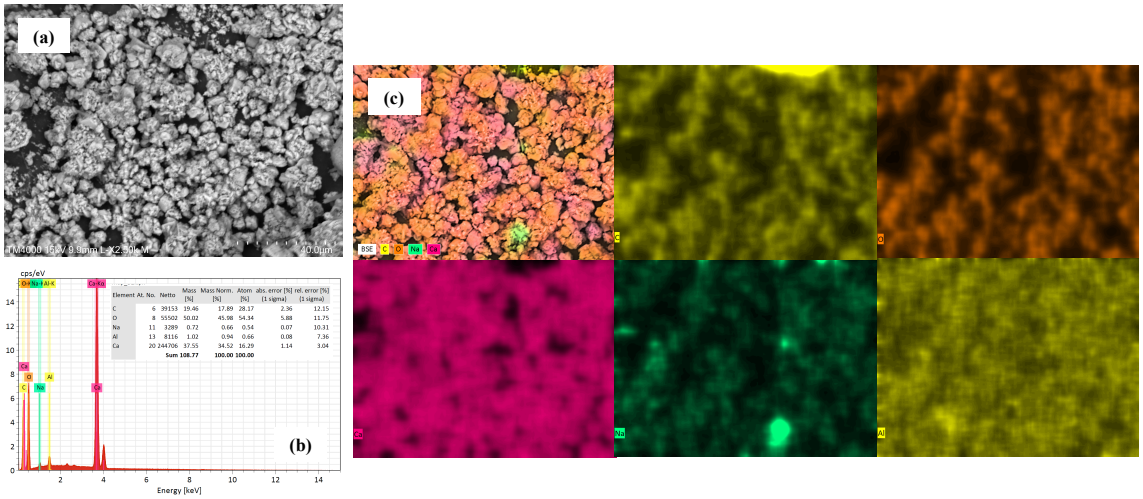

Figure 59: Synthetized PCM@$CaCO_3$ scanned (a) SEM (b) EDX spectra and (c) element mapping.

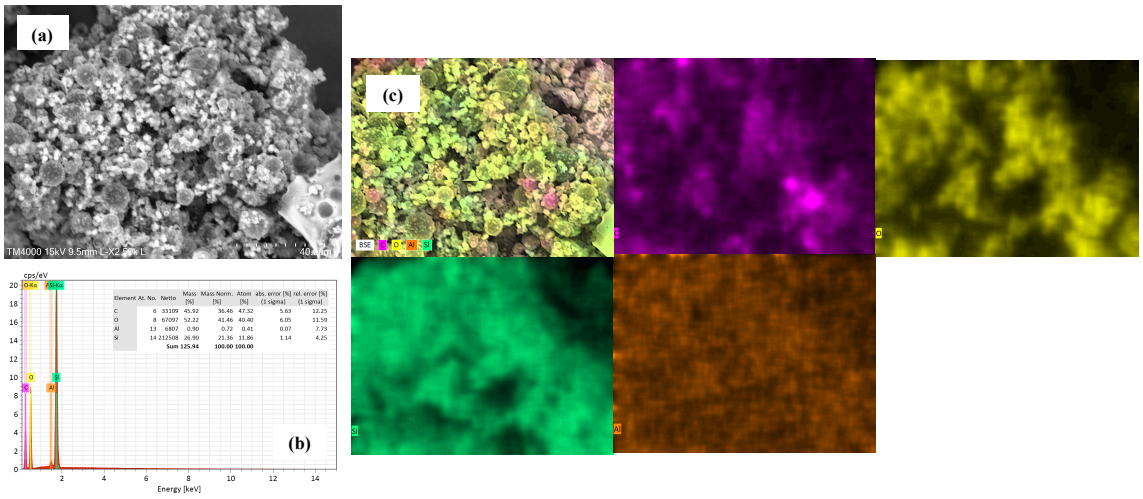

Figure 60: Synthetized PCM@SiGO scanned (a) SEM (b) EDX spectra and (c) element mapping.

In view of the relevance that density has on the physical properties of materials, the density of the PCM was determined and the results are presented in Table 25. The values presented correspond to the average bulk density determined for 4 specimens for each type of PCM.

As is can be observed, the density of the synthesized PCM@$CaCO_3$ is higher than that of commercial PCM@BASF. However, the synthesized PCM@SiGO has a very low density compared to the other two types of PCM. The results of the commercial PCM@BASF are in agreement with the technical data sheet of the supplier (density between 250 kg/m^3 and 350 kg/m^3) [193]. The increase in density of the synthesized PCM@$CaCO_3$ is related with the presence of the $CaCO_3$. It is important to stress that for the synthetized PCM formulation, the same type of paraffin (RT18HC) and the same ratio of paraffin/$CaCO_3$ (50/50) in case of PCM@$CaCO_3$ formulation and of paraffin/TEOS in case of PCM@SiGO formulation, were used. Interestingly, the presence of silica and GO in the synthetized PCM@SiGO lead to a considerable reduction of the density when compared to the presence of the $CaCO_3$ in the synthetized PCM@$CaCO_3$. This may be due to various factors. On one hand the molar mass of $CaCO_3$ (100.087 g/mol) is higher than that of SiO_2 (60.08 g/mol). On the other hand, the present of the GO in the PCM@SiGO has the effect of "expansion" forming more porous structures (consequently lighter) despite of the low GO concentration. In fact, this result agrees with the more porous morphology of this specimen show in Figure 16(c).

Table 25: Bulk density of the PCM

Specimens	Density (kg/m^3)
PCM@BASF	345.59±3.65
PCM@$CaCO_3$	503.36±4.39
PCM@SiGO	119.93±3.51

6.3.1.3. Thermal properties

Table 26 summarizes the results of the transition temperature ($T_{t,m}$), melting temperature (T_m) and latent heat (ΔH_m) values of the specimens obtained from the melting curve. The measurements were made using three specimens for each type of PCM and averaged.

Table 26: DSC results of the PCM

Specimens	Melting		
	Transition temperature $T_{t,m}$ (°C)	Melting temperature T_m (°C)	Melting latent heat ΔH_m (J/g)
PCM@BASF	25.36±0.04	27.55±0.10	97.85±14.64
PCM@$CaCO_3$	23.37±0.65	25.84±0.44	59.56±11.78
PCM@SiGO	23.35±0.64	25.79±0.39	56.41±9.69

As expected, the commercial PCM@BASF has considerably higher phase change enthalpy in comparison with the synthesized PCM@$CaCO_3$ and PCM@SiGO, because the synthesized PCM have less amount of paraffin. This indicates that the commercial PCM@BASF can store more latent heat when the phase change occurs. In turn, the results of both synthesized PCM@$CaCO_3$ and PCM@SiGO are very similar, because in their formulation the same type of paraffin (RT18HC) and the same ratio (50/50) of paraffin/$CaCO_3$ in case of PCM@$CaCO_3$ and paraffin/TEOS in case of PCM@SiGO were used.

Figure 61 shows the thermal stability of the commercial PCM@BASF, and of the synthesized PCM@$CaCO_3$ and PCM@SiGO.

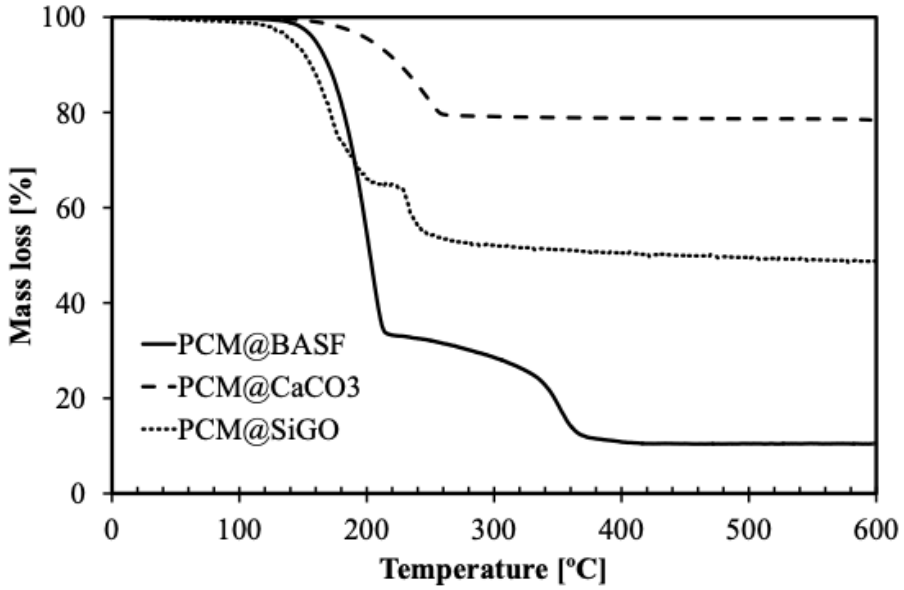

Figure 61: TGA of PCM@BASF, PCM@CaCO3 and PCM@SiGO.

As observed in the PCM@BASF thermogram, the thermal degradation takes place in two stages. The first one corresponds to the decomposition of the paraffin wax between 110 and 210 °C and the second mass loss is attributed to the decomposition of the shell material (PMMA) with an onset temperature around 330°C. This behaviour is in accordance with the Giro-Paloma et al. [194].

For the synthesized PCM@$CaCO_3$, the first drop of mass loss, between 180 and 230 ºC, is ascribed/due to the decomposition of PCM paraffin and the degradation of $CaCO_3$. Compared to Shi et al. [123] the TGA curves are quite similar to the synthesized PCM@$CaCO_3$ results, showing a one-step degradation process. The temperatures of maximum weight loss rate are significantly increased to about 215ºC. Such a sudden weight loss is due to the evaporation of paraffin and high temperature decomposition of $CaCO_3$, and finally the residues are calcium oxide (above 600ºC).

As regards the PCM@SiGO, the mass loss takes place in two steps, little step may be associated with release of water bound with the SiO_2. The drastic mass loss starting at around 100ºC until 220ºC, is attributed to the evaporation of PCM paraffin and the degradation of silica. According to Zhang et al. [246] the TGA curves are quite similar to the synthesized PCM@SiGO, but the mass loss of the shape-stabilized PCM with paraffin and silica undergo only one step process. The paraffin components in the composite shape stabilized PCM reveal the initiation of their decomposition when the temperature exceeded 150 °C regardless of matrices and stopped/seized/slowed down after 220 °C. It is observed a sharp mass loss

around 200 °C caused by the decomposition of organic paraffin corresponding to the degradation process.

In summary, all PCM (the commercial and the synthesized) have perfect thermal stability below 100 °C, which is way above the utilization envisaged for these materials. It can also be seen that the synthesized PCM@$CaCO_3$ and PCM@SiGO decompose more slowly than the commercial PCM@BASF.

6.3.2. Structural layer (PVC) incorporating phase change material

Having prepared and characterized the PCM, these materials were blended with PVC and layers of PVC were prepared and characterized.

6.3.2.1. Morphology and mechanical properties

Figures 62 – 65 show PVC layers with and without PCM images obtained by SEM and coupled techniques (SEM, EDX spectra and element mapping).

The PVC without PCM results (see Figure 62) revealed that the major component is carbon (C) and show a small amount of chlorine (Cl), due to the presence of PVC resin. The presence of calcium (Ca) and oxygen (O) are due to the thermal stabilizers Ca/Zn and $CaCO_3$. As observed in Figures 63 – 68, PVC, the PVC_5PCM@BASF, the PVC_5PCM@$CaCO_3$ and the PVC_5PCM@SiGO layers exhibited the presence of the same components. However, the PVC_5PCM@BASF and PVC_5PCM@SiGO layers showed the presence of silicon (Si) due to the presence of silica (SiO_2) in the PCM formulation. The PVC_5PCM@$CaCO_3$ layer revealed a greater amount of the calcium (Ca) due to the presence of calcium carbonate ($CaCO_3$) in the PCM synthesis. This is in accordance with components of the PVC and PCM formulations (see section 6.3.1.2).

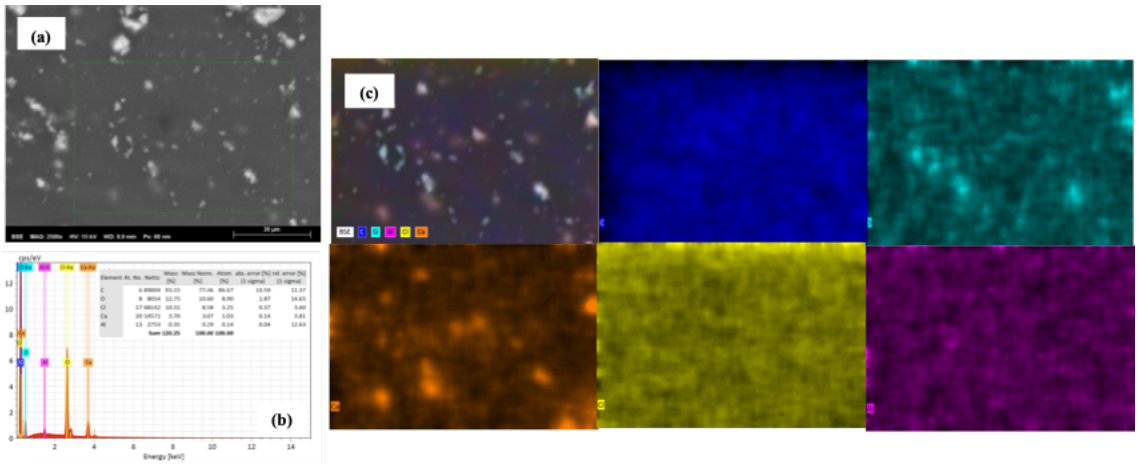

Figure 62: PVC layer scanned (a) SEM (b) EDX spectra and (c) element mapping.

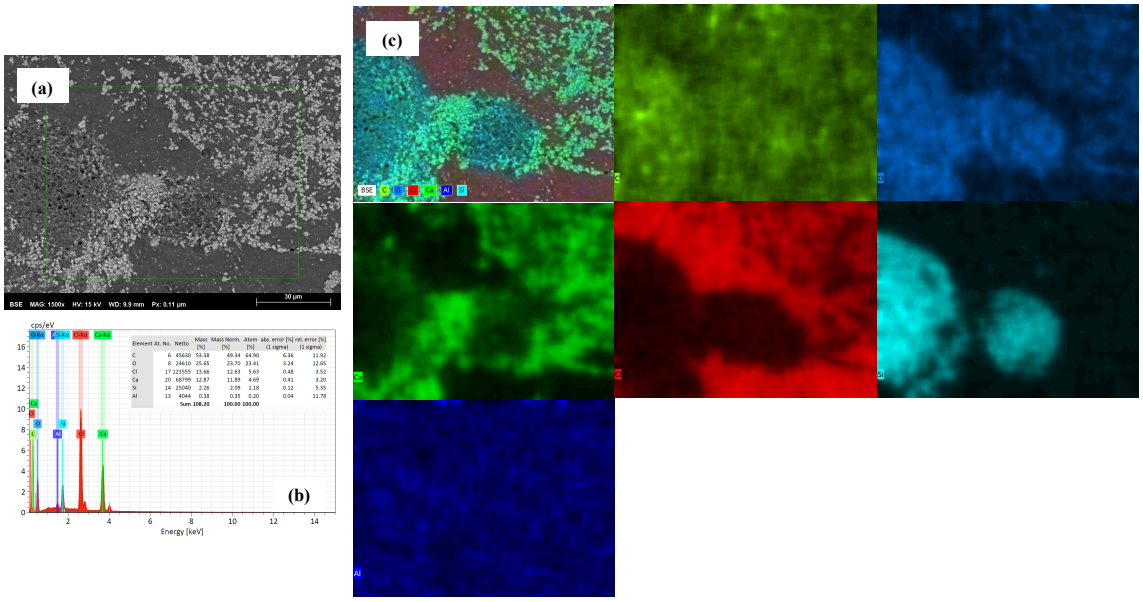

Figure 63: PVC_5PCM@BASF layer scanned (a) SEM (b) EDX spectra and (c) element mapping.

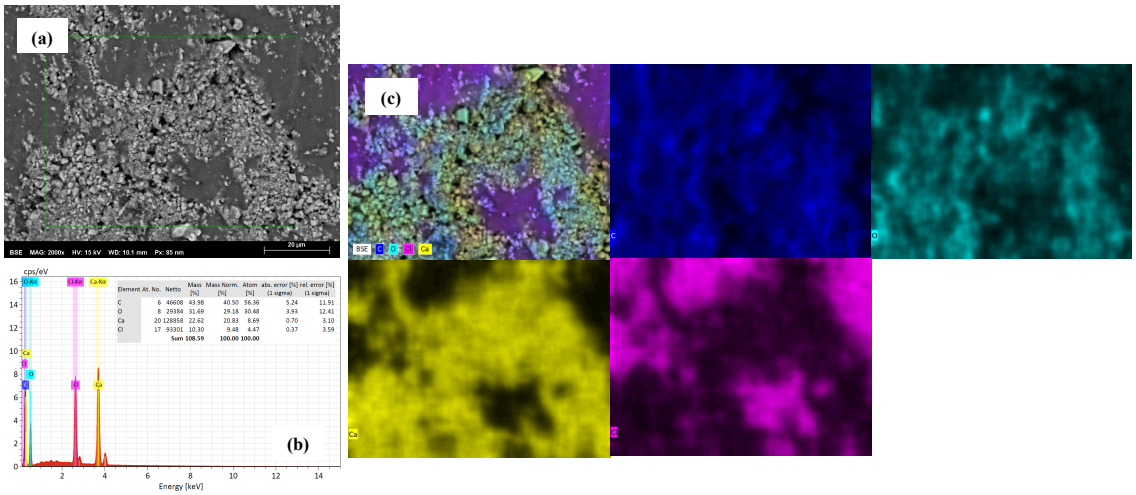

Figure 64: PVC_5PCM@$CaCO_3$ layer scanned (a) SEM (b) EDX spectra and (c) element mapping.

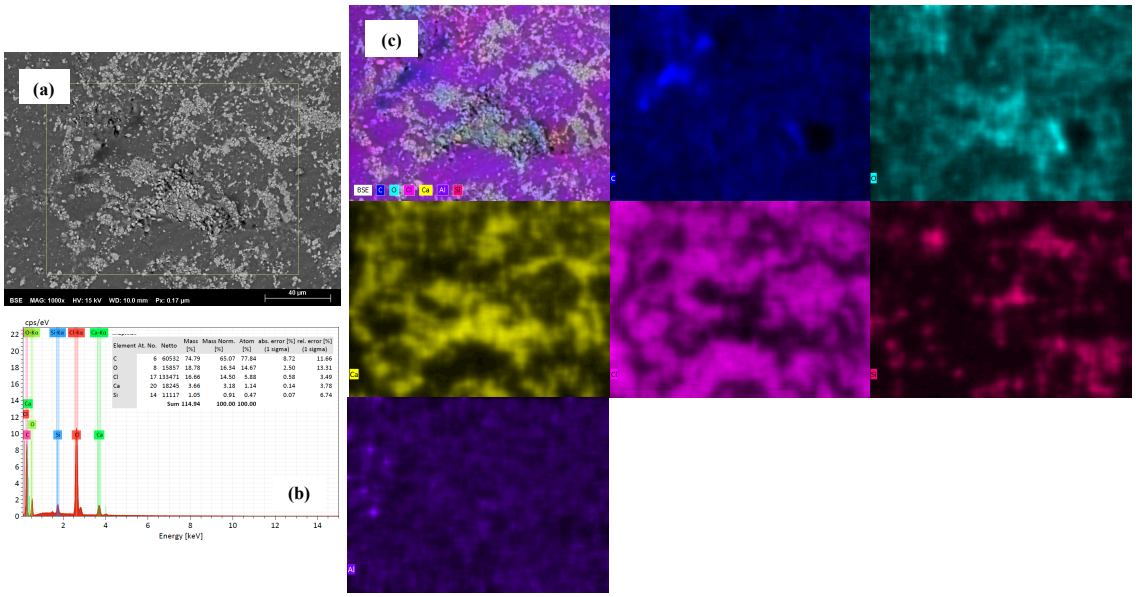

Figure 65: PVC_5PCM@SiGO layer scanned (a) SEM (b) EDX spectra and (c) element mapping.

According to the Table 27, the density of the PVC layers increased with the incorporation of the PCM because the fillers are denser materials. The PVC density is in agreement with those reported in the literature for this PVC formulation (density between 1.15 g/cm^3 and 1.23 g/cm^3) [244,245]. According to the Table 27, it can also be observed that the density of the PVC layers increased with the incorporation of the PCM, since the PCM are denser materials. A similar trend was reported by Michel et al. [229]. Moreover, the fact that the density of PVC_5PCM@SiGO layer is lower than that of the others PCM used is also reflected in the density of the ensuing PVC layers.

Prior to measuring the mechanical properties of the PVC based layers, the density and the thickness were measured. The results are summarized in Table 27.

Table 27: Thickness, density and mechanical properties of the PVC layers with and without PCM

Specimen	Thickness (kg/m³)	Density (kg/m³)	Elongation at break (%)	Maximum tension (Pa)	Young´s Modulus (MPa)
PVC	1.042 ± 0.008	1256.02 ± 15.47	69.7 ± 18.2	2410.8 ± 262.7	7890.8 ± 249.8
PVC_5PCM@BASF	1.124 ± 0.044	1296.67 ± 10.79	54.2 ± 14.6	1769.8± 361.4	7251.5 ± 586.3
PVC_5PCM@$CaCO_3$	1.137 ± 0.044	1325.38 ± 15.88	34.0 ± 1.0	1403.0 ± 130.7	6892.0 ± 186.6
PVC_5PCM@SiGO	1.147 ± 0.028	1275.71 ± 18.26	38.0 ± 7.2	1337.3 ± 215.8	5866.8 ± 259.3

Next, the mechanical properties of the different PVC layers were assessed. Table 27 and Figure 66 show the tensile behaviour of the PVC layer with and without PCM. It can be seen clearly that the presence of PCM can greatly decrease the elongation at break, the maximum tension and the Young´s modulus (tensile modulus). The reduction of the mechanical performance of materials with the addition of PCM was already reported in literature by Eddhahak-Ouni et al. [210]. This decrease is more pronounced when the synthetized PCM was incorporated in the PVC matrix (PVC_5PCM@$CaCO_3$ and PVC_5PCM@SiGO layers). However, the PVC_5PCM@SiGO layer shows slightly higher elongation at break value than the PVC_5PCM@$CaCO_3$ layer. This may be due to the presence of the GO (high modulus) which has the effect of elongation up to the breaking strain despite of its low GO concentration, or due to the lower density or better dispersion of this additive in the PVC matrix.

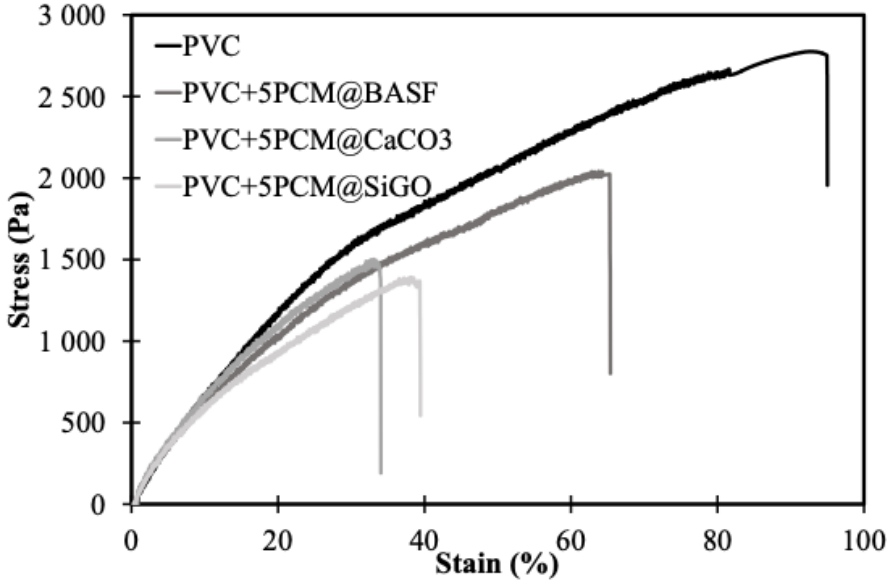

Figure 66: Stress – Strain curves the PVC layers without and with PCM

6.3.2.2. Thermal properties

The thermal performance of the PVC layers was assessed by DSC and the results obtained are summarized in Table 28. Table 28 summarizes the results of the transition temperature ($T_{t,m}$), melting temperature (T_m) and latent heat (ΔH_m) values of the specimens measured on the melting curve. The measurements were made using three specimens for each layer composition and averaged.

Table 28: DSC results of the PVC layers with PCM

Specimens	Melting			$\%_{PCM}$
	Transition temperature $T_{t,m}$ (°C)	Melting temperature T_m (°C)	Melting latent heat ΔH_m (J/g)	
PVC_5PCM@BASF	23.39±0.16	24.93±0.16	4.25±0.82	4.3
PVC_5PCM@$CaCO_3$	23.98±0.43	24.96±1.13	3.16±0.90	5.3
PVC_5PCM@SiGO	23.35±0.64	25.07±0.29	2.66±0.29	4.7

According to the Tables 26 and 28 it can be seen that the PVC layers with PCM (PVC_5PCM@BASF, PVC_5PCM@$CaCO_3$ and PVC_5PCM@SiGO) reveal an endothermic peak in the process of heating with a small decrease in range of values. For the PVC_5PCM@BASF layer the range decreases 2º C compared to the commercial PCM@BASF. The range of PVC_5PCM@$CaCO_3$ and PVC_5PCM@SiGO layers decreases 0.5 ºC compared to the synthesized PCM@$CaCO_3$ and PCM@SiGO, due to the effect of the PVC formulation and PVC layer production.

The PCM content ($\%_{PCM}$) incorporated in the PVC layer was calculated according the Equation (1) is within the expected value (5.0 wt.%) for the all layers. This indicates there was no significant loss of PCM during the PVC layer production process. The PVC_5PCM@BASF layer shows the highest latent heat storage capacity (4.25 J/g corresponding to 4.3 wt.%) compared to the PVC_5PCM@$CaCO_3$ layer (3.18 J/g corresponding to 5.3 wt.%) and PVC_5PCM@SiGO layer (2.66 J/g corresponding to 4.7 wt.%).

Next, the thermal conductivity of the PVC layers was measured. Figure 67 illustrates the thermal conductivity versus temperature results of the PVC layer without PCM using the hot disk test.

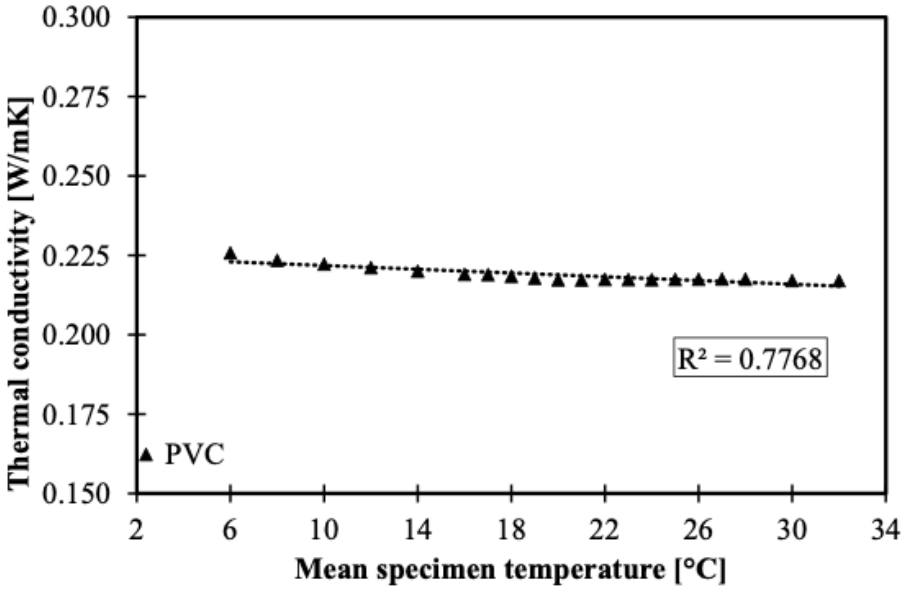

Figure 67: Thermal conductivity versus mean temperature of PVC layer without PCM

The PVC specimen without PCM shows a steady decrease of thermal conductivity as the surface temperature increases. It can be observed that the value of the thermal conductivity decreases linearly with a square correlation (R^2) of 0.7768, as expected according to the Figure 20 using the hot box test. The values of the thermal conductivity were between 0.22579 W/m.K (at 6 ºC) and 0.21708 W/m.K (at 32 ºC). These results are consistent with the results obtained for the hot box test. However, hot disk measurements of the PVC layers with PCM were not performed.

Figures 68 and 69 show the experimental data of thermal conductivity versus mean specimen surfaces temperature for the PVC panels (with and without PCM) using the hot box test.

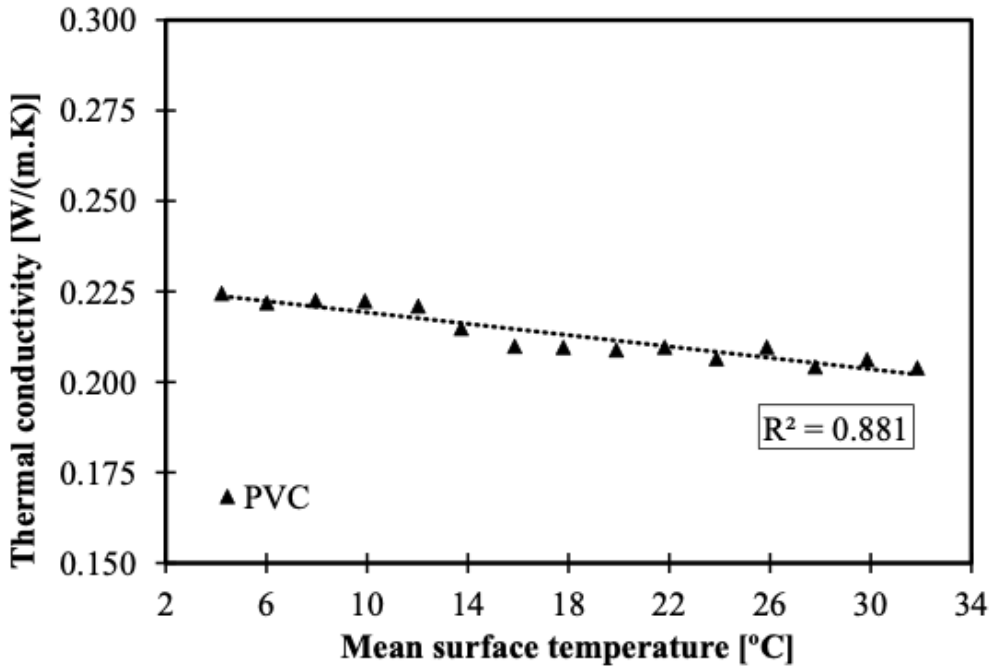

Figure 68: Thermal conductivity as a function of the mean PVC (without PCM) surface temperature

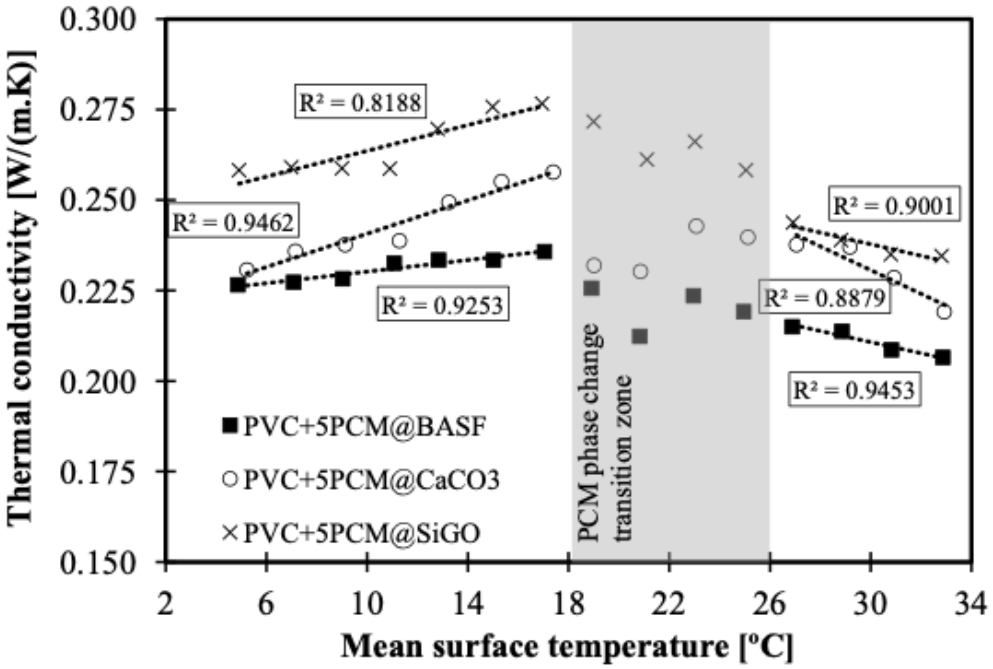

Figure 69: Thermal conductivity as a function of the mean PVC (with PCM) surface temperature

According to Figure 68, for the PVC layer without PCM, it can be observed that the value of the thermal conductivity decreases linearly (with a square correlation (R^2) of 0.881) as the surface temperature increase, as expected according to the

Figure 67 using the hot disk test. The values of the thermal conductivity were between 0.2245 W/m.K (at 4.22 ºC) and 0.2039 W/m.K (at 31.85 ºC).

Figure 69 shows the results obtained for the thermal conductivity as a function of the mean surface temperature for the PVC layers with PCM (PVC_5PCM@BASF, PVC_5PCM@$CaCO_3$ and PVC_5PCM@SiGO). For the PVC layers with PCM the thermal conductivity profile shows a different behaviour to that of the PVC layer without PCM when the mean specimen surface temperature is below and above the phase change transition range (18 °C to 26 °C). When the mean specimen surface temperature is below the phase change transition range, the thermal conductivity increases as the surface temperature increase and the R^2 was between 0.8188 and 0.9462, which demonstrates that the regression line fits reasonably well with the experimental data. But, when the mean specimen surface temperature is above the phase change transition range, the thermal conductivity profile shows a similar behaviour to that of the PVC layer without PCM. In this case, the thermal conductivity decreases as the surface temperature increase and the R^2 was between 0.8879 and 0.9453, which demonstrates that the regression line fits reasonably the experimental data. However, the PVC_5PCM@SiGO has higher values compared to the PVC_5PCM@$CaCO_3$ and PVC_5PCM@BASF, which have the expected behaviour. This enhancement of PVC_5PCM@SiGO is attributed to the high thermal conductivity of synthetized component the PCM@SiGO (the presence of GO) which allows the rapid heat transfer throughout PVC layer.

During PCM phase change transition (temperature range between 18 °C and 26 °C) the thermal conductivity profile of the PVC layers with PCM follows two different trends. First, a reduction was observed and then an increase with the increasing mean temperature of the specimen. According to Amaral et al. [176] and Wang et al. [199] (although an experimental study of polyurethane foams), this behaviour is due to the coexistence of the PCM in two physical states (solid and liquid) in the phase change temperature range and was influenced by the temperature rise, as well as by the phase change fraction of the PCM. Also, in this case (during PCM phase change transition) the PVC_5PCM@SiGO layer revealed higher thermal conductivity values compared to the PVC_5PCM@$CaCO_3$ and PVC_5PCM@BASF layers due to the higher thermal conductivity of GO.

6.4. Conclusions

In this study a method to prepare PCM based on paraffin, silica and GO has been developed. This novel PCM, together with a commercial PCM and a PCM containing $CaCO_3$ have been fully characterized and then successfully incorporated into PVC layers.

The following main conclusions can be taken:

- To improve the compatibility between paraffin and GO, GO was first functionalized with OCA. FTIR and TGA analysis confirmed the successful functionalization.

- The density of the synthesized PCM@$CaCO_3$ is higher than that of the commercial PCM@BASF and synthesized PCM@SiGO. Interestingly, the presence of the silica and GO in the synthetized PCM@SiGO considerably reduced the density of this material when compared to the presence of the $CaCO_3$ in the synthetized PCM@$CaCO_3$.

- SEM and the DSC results reveal that most PCM particles in the PVC layers with PCM are undamaged. Thus, both the shell (in the case of commercial PCM@BASF) and the shape stable (in the case of synthesized PCM@$CaCO_3$ and PCM@SiGO) prevent molten paraffin from leakage during the PVC layer production.

- Comparing the experimental results obtained for PVC layers with and without PCM, it was observed that the presence of PCM led to an increase in density (by the incorporation of denser fillers) and a decrease of the mechanical properties (the PCM particles create break points in PVC matrix).

- The experimental results show that the thermal conductivity decreases linearly as the surface temperature increases for the PVC layer without PCM using the hot box and hot disk tests.

- For PVC layers with PCM the thermal conductivity profile shows a different behaviour to that of the PVC layer without PCM when the mean specimen surface temperature is below and above the phase change transition range. When the mean specimen surface temperature is below of the phase change transition range, the thermal conductivity increases as the surface temperature increases. But, when the mean specimen surface temperature is above of the phase change transition range, the thermal conductivity profile shows a similar behaviour to that of the PVC layer without PCM. However, during PCM phase change transition, the thermal conductivity profile of the PVC layers with PCM follows two trends. First, it was observed a reduction and then an increase with the increasing mean temperature of the specimen.

This experimental study presents promising results of the synthesized PCM@CaCO3 and PCM@SiGO compared to the commercial PCM@BASF and their incorporation into the PVC layers shows potential LHTES applications. Optimization of the production of PVC layers with PCM and of the content of PCM in a PVC layer still needs further research.

CHAPTER 7

7. Final remarks and future work

7.1. Final comments

Presently, the environmental concerns and the energy efficiency are two widely compatible main research topics. The building sector appears as one of the major energy consumers, so, it is necessary that their energy consumption is minimized, but without compromising thermal comfort and indoor air quality in the buildings, which is the concept of energy efficiency. In this context, the use of phase change materials (PCM) in building solutions and components arises as a potential solution to increase the thermal efficiency in buildings, either new or refurbished, since they can storage more energy, in latent form, than the typical sensible energy stored by common construction materials. PCM helps to reduce the thermal temperature peaks, decrease the temperature swing through the PCM capacity to store and release energy and have a significant potential as a passive strategy with a thermal regulator effect of the indoor temperature assuring good comfort levels. Despite their many advantages, one important drawback of these materials is their low thermal conductivity, that limits the full potential use of these materials because it slows down the heat transfer response associated to the charging and discharging processes.

The main goal of this PhD thesis was to research and develop innovative building solutions with the incorporation of synthetized PCM based on nanofillers and other additives to enhance the thermal conductivity and thus achieve a more effective charging and discharging process. Then, the goal was to incorporate these solutions into different polymeric matrices (PUFs foams and PVC films). The evaluation of the thermal performance of different PUFs formulations incorporating first, commercial microencapsulated PCM and second, synthetized PCM based on paraffin and calcium carbonate, for comparison were carried out. Alternatively, to PUFs, work was also developed on PVC structural layer incorporating commercial PCM and the two synthetized PCM.

The main conclusions could be summarized by:

- According to the literature review a number of reports focus solely on the effect of nanocomposites containing PCM and carbon based nanostructures (CNs) on the thermal properties (thermal conductivity and/or latent heat capacity) relative to the pristine PCM but a correlation of those effects with the performance of the ensuing latent heat thermal heat system is rarely presented. The incorporation of CNs in PCM matrix improves the thermal conductivity and generally does not affect significantly the latent heat capacity (keeping it within acceptable levels for LHTES applications) and the effects depends on CNs surface area which is related to their size, shape and porosity, good dispersion and orientation. Also, the shape stabilized PCM

composites with CNs show significantly higher thermal conductivity and prevent leakage during the phase change process of the PCM. Just few recent researches reported the development of a microencapsulated PCM with different mass fractions of CNs as a solution to explore in terms of thermal conductivity and/or latent heat capacity. However, the micro and nano encapsulation of PCM with inorganic and organic shells has been widely explored;

- The synthesized PCM with calcium carbonate increase the density and thermal conductivity compared to the commercial PCM. However, the commercial PCM (PCM@BASF) has considerably higher phase change enthalpy than the synthesized PCM with calcium carbonate (PCM@$CaCO_3$). When the PCM were incorporated into PUFs panels, the results revealed that panels with PCM@$CaCO_3$ have higher thermal conductivity values compared to the panels with PCM@BASF, due to the high thermal conductivity of PCM@$CaCO_3$ which allows the rapid heat transfer throughout the PUFs. In addition, the experimental results show that the values of thermal conductivity for temperatures below and above the PCM phase change transition zone increase with the increasing temperature. However, during the PCM phase change transition a decreasing trend of the thermal characteristics with increasing temperature was observed. This behaviour is due to the coexistence of the PCM in two physical states (solid and liquid) in the phase change temperature range and was influenced by the temperature rise, as well as by the phase change fraction of the PCM;
- The three different testing approaches (flux meter approach, the guarded hot plate approach and the transient plane source approach) presented to determine the thermal conductivity of rigid PUF´s (RPU) with and without the incorporation of PCM based on steady state method and transient method, presented a good correlation of the experimental data when in the liquid and solid state, but some testing constraints and factors were identified when determining the thermal conductivity of the specimens for the phase change zone. It is important to try a quantitative analysis of the simultaneous influence on the thermal conductivity of temperature rise as well as the phase change fraction of the PCM incorporated during the phase change zone. Overall, the experimental campaign targeted on thermal conductivity assessment, confirmed that the hot box heat flux meter approach gives more reliable thermal information on the RPU with PCM;
- In addition, the present PhD thesis present and discusses the RPU panel that incorporates PCM and its performance validation and evaluation. The thermal characteristics and the potential as thermal regulator of indoor spaces has been determined by means of laboratory testing (by hot box heat flux meter approach) and numerical simulation (using ANSYS). Comparing the experimental results obtained for the exterior and indoor temperatures, it was observed that the presence of PCM led to a thermal amplitude reduction of about 2-1 ºC for the RPU_5PCM@BASF and about 4-2 ºC for the RPU_5PCM@$CaCO_3$ (peak maximum temperature- peak minimum

temperature) compared to the RPU panel without PCM. A numerical model has been developed to evaluate the effectiveness of the PCM incorporated into the panel under a wide range and combination of conditions. The behaviour of the RPU panel was optimum when the external mean temperature and the internal are near the melting peak temperature of the PCM. The thermal amplitude reduction caused by the presence of PCM was more significant for the RPU_5PCM@$CaCO_3$ panel, due to the high thermal conductivity of synthetized PCM@$CaCO_3$ which allows the rapid heat transfer throughout the RPU compared to the commercial PCM@BASF. The thermal properties of PCM influence the panels performance and was related with the amplitude temperature that proves that it can have a thermal regulation function in the melting and solidifying, this was the charging and discharging process;

- A method to prepare PCM based on paraffin, silica and graphene oxide (GO) has been developed and together with a commercial PCM and a PCM containing $CaCO_3$ have been fully characterized and then successfully incorporated into PVC layers. The results reveal that most PCM particles in the PVC layers with PCM are undamaged. Thus, both the shell (in the case of commercial PCM@BASF) and the shape stable (in the case of synthesized PCM@$CaCO_3$ and PCM@SiGO) prevent molten paraffin from leakage during the PVC layer production. For PVC layers with PCM the thermal conductivity profile shows a different behaviour to that of the PVC layer without PCM when the mean specimen surface temperature is below and above the phase change transition range. When the mean specimen surface temperature is below of the phase change transition range, the thermal conductivity increases as the surface temperature increases. However, when the mean specimen surface temperature is above of the phase change transition range, the thermal conductivity profile shows a similar behaviour to that of the PVC layer without PCM. However, during PCM phase change transition, the thermal conductivity profile of the PVC layers with PCM follows two trends. First, it was observed a reduction and then an increase with the increasing mean temperature of the specimen.

This PhD thesis has brought forward some promising results for the synthesized PCM@CaCO3 and PCM@SiGO compared to the commercially available PCM@BASF and their incorporation into the different polymeric matrices (PUFs and PVC) shows their potential for LHTES applications.

7.2. Further work

Research work in modelling and optimization of energy efficient buildings and new building solutions resorting to the nanotechnology and nanosciences is a steady, evolutive and growing trend. As a result of the research work performed

herein many other opportunities were identified for further exploration. Thus, some recommendations and research topics are suggested for future work:

- Despite of the promising results that have been achieved, there is still a long path to go in terms of fully understanding the improvement of the energy storage properties and thermal conductivity of the composites as a result of adding CNs to PCM, by encapsulation of the PCM and more systematic studies are still required to select and/or develop tailor made solutions for thermal energy storage;
- Optimization of the content of PCM and the PCM position in a PUFs panel, including other issues such as thermal performance evaluation;
- It is important to identify the coupling effect of the temperature rise and the phase change fraction of the PCM on the thermal conductivity value. This study is interesting and therefore it is worth considering further studies on behaviour of the thermal conductivity values during the PCM phase change transition;
- From the numerical modelling point of view, it should be carried out studies for combining PCM with different contents and melting temperatures. The process of ongoing research will tackle complement issues such as the energy performance assessment of the RPU panel to optimize the PCM quantity, melting temperatures, latent heat capacity and the optimal RPU thickness;
- Carry out more numerical studies adding new variables and parameters, such as: different testing locations and building orientation;
- Optimization of the production of PVC layers with PCM and of the content of PCM in a PVC layer still needs further research;
- Performing the life cycle assessment (LCA) and life cycle cost (LCC) of the different PCM building solutions;
- Carry out an experimental campaign in a real building environment to evaluate the thermal regulation effect of the PCM building solutions.

References

References

[1] N. Soares, J.J. Costa, a. R. Gaspar, P. Santos, Review of passive PCM latent heat thermal energy storage systems towards buildings' energy efficiency, Energy Build. 59 (2013) 82–103. doi:10.1016/j.enbuild.2012.12.042.

[2] L. Pérez-Lombard, J. Ortiz, C. Pout, A review on buildings energy consumption information, Energy Build. 40 (2008) 394–398. doi:https://doi.org/10.1016/j.enbuild.2007.03.007.

[3] K. Pielichowska, K. Pielichowski, Phase change materials for thermal energy storage, Prog. Mater. Sci. 65 (2014) 67–123. doi:10.1016/j.pmatsci.2014.03.005.

[4] S.A. Memon, Phase change materials integrated in building walls: A state of the art review, Renew. Sustain. Energy Rev. 31 (2014) 870–906. doi:10.1016/j.rser.2013.12.042.

[5] E. Asadi, M.G. da Silva, C.H. Antunes, L. Dias, Multi-objective optimization for building retrofit strategies: A model and an application, Energy Build. 44 (2012) 81–87. doi:https://doi.org/10.1016/j.enbuild.2011.10.016.

[6] I. Dincer, On thermal energy storage systems and applications in buildings, Energy Build. 34 (2002) 377–388. doi:http://dx.doi.org/10.1016/S0378-7788(01)00126-8.

[7] D. Zhou, C.Y. Zhao, Y. Tian, Review on thermal energy storage with phase change materials (PCMs) in building applications, Appl. Energy. 92 (2012) 593–605. doi:10.1016/j.apenergy.2011.08.025.

[8] M. Pomianowski, P. Heiselberg, Y. Zhang, Review of thermal energy storage technologies based on PCM application in buildings, Energy Build. 67 (2013) 56–69. doi:http://dx.doi.org/10.1016/j.enbuild.2013.08.006.

[9] L.F. Cabeza, A. Castell, C. Barreneche, A. de Gracia, A.I. Fernández, Materials used as PCM in thermal energy storage in buildings: A review, Renew. Sustain. Energy Rev. 15 (2011) 1675–1695. doi:10.1016/j.rser.2010.11.018.

[10] E. Osterman, V. V Tyagi, V. Butala, N.A. Rahim, U. Stritih, Review of PCM based cooling technologies for buildings, Energy Build. 49 (2012) 37–49. doi:http://dx.doi.org/10.1016/j.enbuild.2012.03.022.

[11] E. Rodriguez-Ubinas, B.A. Arranz, S.V. Sánchez, F.J.N. González, Influence of the use of PCM drywall and the fenestration in building retrofitting, Energy Build. 65 (2013) 464–476. doi:https://doi.org/10.1016/j.enbuild.2013.06.023.

[12] G. Raam Dheep, a. Sreekumar, Influence of nanomaterials on properties of latent heat solar thermal energy storage materials – A review, Energy Convers. Manag. 83 (2014) 133–148. doi:10.1016/j.enconman.2014.03.058.

[13] L.-W. Fan, X. Fang, X. Wang, Y. Zeng, Y.-Q. Xiao, Z.-T. Yu, X. Xu, Y.-C. Hu, K.-F. Cen, Effects of various carbon nanofillers on the thermal conductivity and energy storage properties of paraffin-based nanocomposite phase change materials, Appl. Energy. 110 (2013) 163–172. doi:10.1016/j.apenergy.2013.04.043.

[14] P. Mantilla Gilart, Á. Yedra Martínez, M. González Barriuso, C. Manteca Martínez, Development of PCM/carbon-based composite materials, Sol. Energy Mater. Sol. Cells. 107 (2012) 205–211. doi:10.1016/j.solmat.2012.06.014.

[15] Y.P. Zhang, K.P. Lin, R. Yang, H.F. Di, Y. Jiang, Preparation, thermal performance and application of shape-stabilized PCM in energy efficient buildings, Energy Build. 38 (2006) 1262–1269. doi:10.1016/j.enbuild.2006.02.009.

[16] G.-Q. Qi, C.-L. Liang, R.-Y. Bao, Z.-Y. Liu, W. Yang, B.-H. Xie, M.-B. Yang, Polyethylene glycol based shape-stabilized phase change material for thermal energy storage with ultra-low content of graphene oxide, Sol. Energy Mater. Sol. Cells. 123 (2014) 171–177. doi:10.1016/j.solmat.2014.01.024.

[17] M. Mehrali, S.T. Latibari, M. Mehrali, H.S.C. Metselaar, M. Silakhori, Shape-stabilized phase change materials with high thermal conductivity based on paraffin/graphene oxide composite, Energy Convers. Manag. 67 (2013) 275–282. doi:10.1016/j.enconman.2012.11.023.

[18] a. Jamekhorshid, S.M. Sadrameli, M. Farid, A review of microencapsulation methods of phase change materials (PCMs) as a thermal energy storage (TES) medium, Renew. Sustain. Energy Rev. 31 (2014) 531–542. doi:10.1016/j.rser.2013.12.033.

[19] C.Y. Zhao, G.H. Zhang, Review on microencapsulated phase change materials (MEPCMs): Fabrication, characterization and applications, Renew. Sustain. Energy Rev. 15 (2011) 3813–3832. doi:10.1016/j.rser.2011.07.019.

[20] L. Liu, D. Su, Y. Tang, G. Fang, Thermal conductivity enhancement of phase change materials for thermal energy storage: A review, Renew. Sustain. Energy Rev. 62 (2016) 305–317. doi:https://doi.org/10.1016/j.rser.2016.04.057.

[21] N.I. Ibrahim, F.A. Al-Sulaiman, S. Rahman, B.S. Yilbas, A.Z. Sahin, Heat transfer enhancement of phase change materials for thermal energy storage applications: A critical review, Renew. Sustain. Energy Rev. 74 (2017) 26–50. doi:https://doi.org/10.1016/j.rser.2017.01.169.

[22] X. Huang, G. Alva, Y. Jia, G. Fang, Morphological characterization and applications of phase change materials in thermal energy storage: A review, Renew. Sustain. Energy Rev. 72 (2017) 128–145. doi:https://doi.org/10.1016/j.rser.2017.01.048.

[23] Z. Qiu, X. Ma, P. Li, X. Zhao, A. Wright, Micro-encapsulated phase change material (MPCM) slurries: Characterization and building applications, Renew. Sustain. Energy Rev. 77 (2017) 246–262. doi:https://doi.org/10.1016/j.rser.2017.04.001.

[24] Y.E. Milián, A. Gutiérrez, M. Grágeda, S. Ushak, A review on encapsulation techniques for inorganic phase change materials and the influence on their thermophysical properties, Renew. Sustain. Energy Rev. 73 (2017) 983–999. doi:https://doi.org/10.1016/j.rser.2017.01.159.

[25] M. Al-Maghalseh, K. Mahkamov, Methods of heat transfer intensification in PCM thermal storage systems: Review paper, Renew. Sustain. Energy Rev. 92 (2018) 62–94. doi:https://doi.org/10.1016/j.rser.2018.04.064.

[26] F. Rodríguez-Cumplido, E. Pabón-Gelves, F. Chejne-Jana, Recent developments in the synthesis of microencapsulated and nanoencapsulated phase change materials, J. Energy Storage. 24 (2019) 100821. doi:https://doi.org/10.1016/j.est.2019.100821.

[27] H. Gao, J. Wang, X. Chen, G. Wang, X. Huang, A. Li, W. Dong, Nanoconfinement effects on thermal properties of nanoporous shape-stabilized composite PCMs: A review, Nano Energy. 53 (2018) 769–797. doi:https://doi.org/10.1016/j.nanoen.2018.09.007.

[28] M.M. Umair, Y. Zhang, K. Iqbal, S. Zhang, B. Tang, Novel strategies and supporting materials applied to shape-stabilize organic phase change materials for thermal energy storage–A review, Appl. Energy. 235 (2019) 846–873. doi:https://doi.org/10.1016/j.apenergy.2018.11.017.

[29] I. Dinçer, M. Rosen, Thermal energy storage : systems and applications, Wiley, New Jersey, EUA, 2011.

[30] K.A.R. Ismail, J.R. Henŕíquez, Thermally effective windows with moving phase change material curtains, Appl. Therm. Eng. 21 (2001) 1909–1923. doi:10.1016/s1359-4311(01)00058-8.

[31] N. Zhu, Z. Ma, S. Wang, Dynamic characteristics and energy performance of buildings using phase change materials: A review, Energy Convers. Manag. 50 (2009) 3169–3181.

[32] H. Mehling, L.F. Cabeza, Heat and cold storage with PCM : an up to date introduction into basics and applications, Springer, Berlin, Germany, 2008.

[33] M.H.M. Isa, X. Zhao, H. Yoshino, Preliminary Study of Passive Cooling Strategy Using a Combination of PCM and Copper Foam to Increase Thermal Heat Storage in Building Facade, Sustainability. 2 (2010) 2365–2381. doi:10.3390/su2082365.

[34] B.P. Jelle, Traditional, state-of-the-art and future thermal building insulation materials and solutions – Properties, requirements and possibilities, Energy Build. 43 (2011) 2549–2563. doi:10.1016/j.enbuild.2011.05.015.

[35] R. Baetens, B.P. Jelle, A. Gustavsen, Phase change materials for building applications: A state-of-the-art review, Energy Build. 42 (2010) 1361–1368. doi:http://dx.doi.org/10.1016/j.enbuild.2010.03.026.

[36] V.V. Tyagi, D. Buddhi, {PCM} thermal storage in buildings: A state of art, Renew. Sustain. Energy Rev. 11 (2007) 1146–1166. doi:http://dx.doi.org/10.1016/j.rser.2005.10.002.

[37] A. Sharma, V. V Tyagi, C.R. Chen, D. Buddhi, Review on thermal energy storage with phase change materials and applications, Renew. Sustain. Energy Rev. 13 (2009) 318–345. doi:http://dx.doi.org/10.1016/j.rser.2007.10.005.

[38] Y. Yuan, N. Zhang, W. Tao, X. Cao, Y. He, Fatty acids as phase change materials: A review, Renew. Sustain. Energy Rev. 29 (2014) 482–498. doi:10.1016/j.rser.2013.08.107.

[39] M.K. Rathod, J. Banerjee, Thermal stability of phase change materials used in latent heat energy storage systems: A review, Renew. Sustain. Energy Rev. 18

(2013) 246–258. doi:http://dx.doi.org/10.1016/j.rser.2012.10.022.

[40] P. Tatsidjodoung, N. Le Pierrès, L. Luo, A review of potential materials for thermal energy storage in building applications, Renew. Sustain. Energy Rev. 18 (2013) 327–349. doi:http://dx.doi.org/10.1016/j.rser.2012.10.025.

[41] T. Silva, R. Vicente, F. Rodrigues, Literature review on the use of phase change materials in glazing and shading solutions, Renew. Sustain. Energy Rev. 53 (2016) 515–535. doi:https://doi.org/10.1016/j.rser.2015.07.201.

[42] M. Farid, A review on phase change energy storage: materials and applications, Energy Convers. Manag. 45 (2004) 1597–1615. doi:10.1016/j.enconman.2003.09.015.

[43] M. Scarselli, P. Castrucci, M. De Crescenzi, Electronic and optoelectronic nano-devices based on carbon nanotubes, J. Phys. Condens. Matter. 24 (2012) 313202. http://stacks.iop.org/0953-8984/24/i=31/a=313202.

[44] H. Dai, Carbon nanotubes: opportunities and challenges, Surf. Sci. 500 (2002) 218–241. doi:http://dx.doi.org/10.1016/S0039-6028(01)01558-8.

[45] R. Sengupta, M. Bhattacharya, S. Bandyopadhyay, A.K. Bhowmick, A review on the mechanical and electrical properties of graphite and modified graphite reinforced polymer composites, Prog. Polym. Sci. 36 (2011) 638–670. doi:http://dx.doi.org/10.1016/j.progpolymsci.2010.11.003.

[46] M.J. Allen, V.C. Tung, R.B. Kaner, Honeycomb Carbon: A Review of Graphene, Chem. Rev. 110 (2010) 132–145. doi:10.1021/cr900070d.

[47] D. Jariwala, V.K. Sangwan, L.J. Lauhon, T.J. Marks, M.C. Hersam, Carbon nanomaterials for electronics, optoelectronics, photovoltaics, and sensing., Chem. Soc. Rev. 42 (2013) 2824–60. doi:10.1039/c2cs35335k.

[48] D.R. Dreyer, R.S. Ruoff, C.W. Bielawski, From conception to realization: an historial account of graphene and some perspectives for its future., Angew. Chem. Int. Ed. Engl. 49 (2010) 9336–44. doi:10.1002/anie.201003024.

[49] K. Chen, S. Song, D. Xue, Beyond graphene: materials chemistry toward high performance inorganic functional materials, J. Mater. Chem. A. 3 (2015) 2441–2453. doi:10.1039/C4TA06989G.

[50] P.A.A.P. Marques, G. Gonçalves, S. Cruz, N. Almeida, M.K. Singh, J. Grácio, A.C.M. Suosa, Functionalized Graphene Nanocomposites, 2011. doi:17097.

[51] P. Wick, A.E. Louw-Gaume, M. Kucki, H.F. Krug, K. Kostarelos, B. Fadeel, K.A. Dawson, A. Salvati, E. Vázquez, L. Ballerini, M. Tretiach, F. Benfenati, E. Flahaut, L. Gauthier, M. Prato, A. Bianco, Classification Framework for Graphene-Based Materials, Angew. Chemie Int. Ed. 53 (2014) 7714–7718. doi:10.1002/anie.201403335.

[52] A. Bianco, H.-M. Cheng, T. Enoki, Y. Gogotsi, R.H. Hurt, N. Koratkar, T. Kyotani, M. Monthioux, C.R. Park, J.M.D. Tascon, J. Zhang, All in the graphene family - A recommended nomenclature for two-dimensional carbon materials, CARBON Carbon. 65 (2013) 1–6.

[53] G. Goncalves, P.A.A.P. Marques, C.M. Granadeiro, H.I.S. Nogueira, M.K. Singh, J. Grácio, Surface Modification of Graphene Nanosheets with Gold Nanoparticles: The Role of Oxygen Moieties at Graphene Surface on Gold Nucleation and Growth, Chem. Mater. 21 (2009) 4796–4802. doi:10.1021/cm901052s.

[54] G. Goncalves, P.A.A.P. Marques, A. Barros-Timmons, I. Bdkin, M.K. Singh, N. Emami, J. Gracio, Graphene oxide modified with PMMA via ATRP as a reinforcement filler, J. Mater. Chem. 20 (2010) 9927–9934. doi:10.1039/C0JM01674H.

[55] R. Garg, N. Dutta, N. Choudhury, Work Function Engineering of Graphene, Nanomaterials. 4 (2014) 267–300. doi:10.3390/nano4020267.

[56] A. Nieto, D. Lahiri, A. Agarwal, Synthesis and properties of bulk graphene nanoplatelets consolidated by spark plasma sintering, Carbon N. Y. 50 (2012) 4068–4077. doi:http://dx.doi.org/10.1016/j.carbon.2012.04.054.

[57] P.-C. Ma, N.A. Siddiqui, G. Marom, J.-K. Kim, Dispersion and functionalization of carbon nanotubes for polymer-based nanocomposites: A review, Compos. Part A Appl. Sci. Manuf. 41 (2010) 1345–1367. doi:http://dx.doi.org/10.1016/j.compositesa.2010.07.003.

[58] A. Dorri Moghadam, E. Omrani, P.L. Menezes, P.K. Rohatgi, Mechanical and tribological properties of self-lubricating metal matrix nanocomposites reinforced by carbon nanotubes (CNTs) and graphene – A review, Compos. Part B Eng. 77 (2015) 402–420. doi:http://dx.doi.org/10.1016/j.compositesb.2015.03.014.

[59] S. Goenka, V. Sant, S. Sant, Graphene-based nanomaterials for drug delivery and tissue engineering, J. Control. Release. 173 (2014) 75–88. doi:http://dx.doi.org/10.1016/j.jconrel.2013.10.017.

[60] L. Qiu, Y. Ouyang, Y. Feng, X. Zhang, Review on micro/nano phase change materials for solar thermal applications, Renew. Energy. 140 (2019) 513–538. doi:https://doi.org/10.1016/j.renene.2019.03.088.

[61] V. Kumaresan, R. Velraj, S.K. Das, The effect of carbon nanotubes in enhancing the thermal transport properties of PCM during solidification, Heat Mass Transf. 48 (2012) 1345–1355. doi:10.1007/s00231-012-0980-3.

[62] S. Shaikh, K. Lafdi, K. Hallinan, Carbon nanoadditives to enhance latent energy storage of phase change materials, J. Appl. Phys. 103 (2008) 094302. doi:10.1063/1.2903538.

[63] S. Kim, L.T. Drzal, High latent heat storage and high thermal conductive phase change materials using exfoliated graphite nanoplatelets, Sol. Energy Mater. Sol. Cells. 93 (2009) 136–142. doi:10.1016/j.solmat.2008.09.010.

[64] Y.-J. Chen, D.-D. Nguyen, M.-Y. Shen, M.-C. Yip, N.-H. Tai, Thermal characterizations of the graphite nanosheets reinforced paraffin phase-change composites, Compos. Part A Appl. Sci. Manuf. 44 (2013) 40–46. doi:10.1016/j.compositesa.2012.08.010.

[65] Z.-T. Yu, X. Fang, L.-W. Fan, X. Wang, Y.-Q. Xiao, Y. Zeng, X. Xu, Y.-C. Hu, K.-F. Cen, Increased thermal conductivity of liquid paraffin-based suspensions in the presence of carbon nano-additives of various sizes and shapes, Carbon N. Y. 53

(2013) 277–285. doi:10.1016/j.carbon.2012.10.059.

[66] Y. Cui, C. Liu, S. Hu, X. Yu, The experimental exploration of carbon nanofiber and carbon nanotube additives on thermal behavior of phase change materials, Sol. Energy Mater. Sol. Cells. 95 (2011) 1208–1212. doi:10.1016/j.solmat.2011.01.021.

[67] J. Wang, H. Xie, Z. Xin, Thermal properties of paraffin based composites containing multi-walled carbon nanotubes, Thermochim. Acta. 488 (2009) 39–42. doi:10.1016/j.tca.2009.01.022.

[68] A. Elgafy, K. Lafdi, Effect of carbon nanofiber additives on thermal behavior of phase change materials, Carbon N. Y. 43 (2005) 3067–3074. doi:10.1016/j.carbon.2005.06.042.

[69] Z. Ling, J. Chen, T. Xu, X. Fang, X. Gao, Z. Zhang, Thermal conductivity of an organic phase change material/expanded graphite composite across the phase change temperature range and a novel thermal conductivity model, Energy Convers. Manag. 102 (2015) 202–208. doi:https://doi.org/10.1016/j.enconman.2014.11.040.

[70] M. Joseph, V. Sajith, Graphene enhanced paraffin nanocomposite based hybrid cooling system for thermal management of electronics, Appl. Therm. Eng. 163 (2019) 114342. doi:10.1016/J.APPLTHERMALENG.2019.114342.

[71] F. Yavari, H.R. Fard, K. Pashayi, M.A. Ra, A. Zamiri, Z. Yu, R. Ozisik, T. Borca-tasciuc, N. Koratkar, Enhanced Thermal Conductivity in a Nanostructured Phase Change Composite due to Low Concentration Graphene Additives, (2011) 8753–8758.

[72] L.-W. Fan, Z.-Q. Zhu, Y. Zeng, Y.-Q. Xiao, X.-L. Liu, Y.-Y. Wu, Q. Ding, Z.-T. Yu, K.-F. Cen, Transient performance of a PCM-based heat sink with high aspect-ratio carbon nanofillers, Appl. Therm. Eng. 75 (2015) 532–540. doi:http://dx.doi.org/10.1016/j.applthermaleng.2014.10.050.

[73] M. Vivekananthan, V.A. Amirtham, Characterisation and thermophysical properties of graphene nanoparticles dispersed erythritol PCM for medium temperature thermal energy storage applications, Thermochim. Acta. 676 (2019) 94–103. doi:https://doi.org/10.1016/j.tca.2019.03.037.

[74] H. Babaei, P. Keblinski, J.M. Khodadadi, Thermal conductivity enhancement of paraffins by increasing the alignment of molecules through adding CNT/graphene, Int. J. Heat Mass Transf. 58 (2013) 209–216. doi:10.1016/j.ijheatmasstransfer.2012.11.013.

[75] X. Fang, L.-W. Fan, Q. Ding, X. Wang, X.-L. Yao, J.-F. Hou, Z.-T. Yu, G.-H. Cheng, Y.-C. Hu, K.-F. Cen, Increased Thermal Conductivity of Eicosane-Based Composite Phase Change Materials in the Presence of Graphene Nanoplatelets, Energy & Fuels. 27 (2013) 4041–4047. doi:10.1021/ef400702a.

[76] J. Wang, H. Xie, Z. Xin, Y. Li, Increasing the thermal conductivity of palmitic acid by the addition of carbon nanotubes, Carbon N. Y. 48 (2010) 3979–3986. doi:10.1016/j.carbon.2010.06.044.

[77] T. Li, J.-H. Lee, R. Wang, Y.T. Kang, Enhancement of heat transfer for thermal

energy storage application using stearic acid nanocomposite with multi-walled carbon nanotubes, Energy. 55 (2013) 752–761. doi:10.1016/j.energy.2013.04.010.

[78] S. Yu, S.-G. Jeong, O. Chung, S. Kim, Bio-based PCM/carbon nanomaterials composites with enhanced thermal conductivity, Sol. Energy Mater. Sol. Cells. 120 (2014) 549–554. doi:10.1016/j.solmat.2013.09.037.

[79] Y. Yuan, N. Zhang, T. Li, X. Cao, W. Long, Thermal performance enhancement of palmitic-stearic acid by adding graphene nanoplatelets and expanded graphite for thermal energy storage: A comparative study, Energy. 97 (2016) 488–497. doi:https://doi.org/10.1016/j.energy.2015.12.115.

[80] M. He, L. Yang, W. Lin, J. Chen, X. Mao, Z. Ma, Preparation, thermal characterization and examination of phase change materials (PCMs) enhanced by carbon-based nanoparticles for solar thermal energy storage, J. Energy Storage. 25 (2019) 100874. doi:https://doi.org/10.1016/j.est.2019.100874.

[81] J. Wang, H. Xie, Z. Xin, Y. Li, L. Chen, Enhancing thermal conductivity of palmitic acid based phase change materials with carbon nanotubes as fillers, Sol. Energy. 84 (2010) 339–344. doi:10.1016/j.solener.2009.12.004.

[82] L. Feng, J. Zheng, H. Yang, Y. Guo, W. Li, X. Li, Preparation and characterization of polyethylene glycol/active carbon composites as shape-stabilized phase change materials, Sol. Energy Mater. Sol. Cells. 95 (2011) 644–650. doi:10.1016/j.solmat.2010.09.033.

[83] A. Mills, M. Farid, J.R. Selman, S. Al-Hallaj, Thermal conductivity enhancement of phase change materials using a graphite matrix, Appl. Therm. Eng. 26 (2006) 1652–1661. doi:10.1016/j.applthermaleng.2005.11.022.

[84] N. Sarier, E. Onder, Thermal characteristics of polyurethane foams incorporated with phase change materials, Thermochim. Acta. 454 (2007) 90–98. doi:https://doi.org/10.1016/j.tca.2006.12.024.

[85] Z. Zhang, X. Fang, Study on paraffin/expanded graphite composite phase change thermal energy storage material, Energy Convers. Manag. 47 (2006) 303–310. doi:10.1016/j.enconman.2005.03.004.

[86] L. Xia, P. Zhang, R.Z. Wang, Preparation and thermal characterization of expanded graphite/paraffin composite phase change material, Carbon N. Y. 48 (2010) 2538–2548. doi:10.1016/j.carbon.2010.03.030.

[87] Y. Zhong, S. Li, X. Wei, Z. Liu, Q. Guo, J. Shi, L. Liu, Heat transfer enhancement of paraffin wax using compressed expanded natural graphite for thermal energy storage, Carbon N. Y. 48 (2010) 300–304. doi:10.1016/j.carbon.2009.09.033.

[88] M. Li, A nano-graphite/paraffin phase change material with high thermal conductivity, Appl. Energy. 106 (2013) 25–30. doi:10.1016/j.apenergy.2013.01.031.

[89] J.-N. Shi, M.-D. Ger, Y.-M. Liu, Y.-C. Fan, N.-T. Wen, C.-K. Lin, N.-W. Pu, Improving the thermal conductivity and shape-stabilization of phase change materials using nanographite additives, Carbon N. Y. 51 (2013) 365–372. doi:10.1016/j.carbon.2012.08.068.

[90] J. Xiang, L.T. Drzal, Investigation of exfoliated graphite nanoplatelets (xGnP) in improving thermal conductivity of paraffin wax-based phase change material, Sol. Energy Mater. Sol. Cells. 95 (2011) 1811–1818. doi:10.1016/j.solmat.2011.01.048.

[91] S. Ye, Q. Zhang, D. Hu, J. Feng, Core-shell-like structured graphene aerogel encapsulating paraffin: shape-stable phase change material for thermal energy storage, J. Mater. Chem. A. 3 (2015) 4018–4025. doi:10.1039/C4TA05448B.

[92] L. He, H. Wang, F. Yang, H. Zhu, Preparation and properties of polyethylene glycol/unsaturated polyester resin/graphene nanoplates composites as form-stable phase change materials, Thermochim. Acta. 665 (2018) 43–52. doi:https://doi.org/10.1016/j.tca.2018.04.012.

[93] M. Mehrali, S. Tahan Latibari, M. Mehrali, T.M.I. Mahlia, E. Sadeghinezhad, H.S.C. Metselaar, Preparation of nitrogen-doped graphene/palmitic acid shape stabilized composite phase change material with remarkable thermal properties for thermal energy storage, Appl. Energy. 135 (2014) 339–349. doi:http://dx.doi.org/10.1016/j.apenergy.2014.08.100.

[94] M. Mehrali, S.T. Latibari, M. Mehrali, T.M. Indra Mahlia, H.S. Cornelis Metselaar, Preparation and properties of highly conductive palmitic acid/graphene oxide composites as thermal energy storage materials, Energy. 58 (2013) 628–634. doi:10.1016/j.energy.2013.05.050.

[95] L. Xia, P. Zhang, Thermal property measurement and heat transfer analysis of acetamide and acetamide/expanded graphite composite phase change material for solar heat storage, Sol. Energy Mater. Sol. Cells. 95 (2011) 2246–2254. doi:10.1016/j.solmat.2011.03.031.

[96] B. Li, T. Liu, L. Hu, Y. Wang, S. Nie, Facile preparation and adjustable thermal property of stearic acid–graphene oxide composite as shape-stabilized phase change material, Chem. Eng. J. 215–216 (2013) 819–826. doi:10.1016/j.cej.2012.11.077.

[97] Y. Cai, C. Gao, T. Zhang, Z. Zhang, Q. Wei, J. Du, Y. Hu, L. Song, Influences of expanded graphite on structural morphology and thermal performance of composite phase change materials consisting of fatty acid eutectics and electrospun PA6 nanofibrous mats, Renew. Energy. 57 (2013) 163–170. doi:10.1016/j.renene.2013.01.044.

[98] X. Tang, B. Zhu, M. Xu, W. Zhang, Z. Yang, Y. Zhang, G. Yin, D. He, H. Wei, X. Zhai, Shape-stabilized phase change materials based on fatty acid eutectics/expanded graphite composites for thermal storage, Energy Build. 109 (2015) 353–360. doi:https://doi.org/10.1016/j.enbuild.2015.09.074.

[99] C. Wang, L. Feng, W. Li, J. Zheng, W. Tian, X. Li, Shape-stabilized phase change materials based on polyethylene glycol/porous carbon composite: The influence of the pore structure of the carbon materials, Sol. Energy Mater. Sol. Cells. 105 (2012) 21–26. doi:https://doi.org/10.1016/j.solmat.2012.05.031.

[100] P. Schossig, H.M. Henning, S. Gschwander, T. Haussmann, Micro-encapsulated phase-change materials integrated into construction materials, Sol. Energy Mater. Sol. Cells. 89 (2005) 297–306. doi:http://dx.doi.org/10.1016/j.solmat.2005.01.017.

[101] R. Jacob, F. Bruno, Review on shell materials used in the encapsulation of phase change materials for high temperature thermal energy storage, Renew. Sustain. Energy Rev. 48 (2015) 79–87. doi:https://doi.org/10.1016/j.rser.2015.03.038.

[102] P.B. Salunkhe, P.S. Shembekar, A review on effect of phase change material encapsulation on the thermal performance of a system, Renew. Sustain. Energy Rev. 16 (2012) 5603–5616. doi:https://doi.org/10.1016/j.rser.2012.05.037.

[103] F. Kuznik, D. David, K. Johannes, J.-J. Roux, A review on phase change materials integrated in building walls, Renew. Sustain. Energy Rev. 15 (2011) 379–391. doi:http://dx.doi.org/10.1016/j.rser.2010.08.019.

[104] P.A. Maldonado, Application of passive thermal energy storage in buildings using PCM and awnings, (n.d.).

[105] P.A. Maldonado, L.F. Cabeza, M. Medrano, Application of Passive Thermal Energy Storage in Buildings Using PCM and Awnings, (2011). http://books.google.pt/books?id=12xpMwEACAAJ.

[106] S. Drissi, T.-C. Ling, K.H. Mo, A. Eddhahak, A review of microencapsulated and composite phase change materials: Alteration of strength and thermal properties of cement-based materials, Renew. Sustain. Energy Rev. 110 (2019) 467–484. doi:https://doi.org/10.1016/j.rser.2019.04.072.

[107] V.V. Rao, R. Parameshwaran, V.V. Ram, PCM-mortar based construction materials for energy efficient buildings: A review on research trends, Energy Build. 158 (2018) 95–122. doi:https://doi.org/10.1016/j.enbuild.2017.09.098.

[108] V.V. Tyagi, S.C. Kaushik, S.K. Tyagi, T. Akiyama, Development of phase change materials based microencapsulated technology for buildings: A review, Renew. Sustain. Energy Rev. 15 (2011) 1373–1391. doi:10.1016/j.rser.2010.10.006.

[109] C. Alkan, A. Sarı, A. Karaipekli, O. Uzun, Preparation, characterization, and thermal properties of microencapsulated phase change material for thermal energy storage, Sol. Energy Mater. Sol. Cells. 93 (2009) 143–147. doi:10.1016/j.solmat.2008.09.009.

[110] A. Hassan, M. Shakeel Laghari, Y. Rashid, Micro-Encapsulated Phase Change Materials: A Review of Encapsulation, Safety and Thermal Characteristics, Sustainability. 8 (2016) 1046. http://www.mdpi.com/2071-1050/8/10/1046.

[111] E. Alehosseini, S.M. Jafari, Micro/nano-encapsulated phase change materials (PCMs) as emerging materials for the food industry, Trends Food Sci. Technol. 91 (2019) 116–128. doi:https://doi.org/10.1016/j.tifs.2019.07.003.

[112] Y. Konuklu, H.O. Paksoy, M. Unal, S. Konuklu, Microencapsulation of a fatty acid with Poly(melamine–urea–formaldehyde), Energy Convers. Manag. 80 (2014) 382–390. doi:10.1016/j.enconman.2014.01.042.

[113] Y. Konuklu, M. Unal, H.O. Paksoy, Microencapsulation of caprylic acid with different wall materials as phase change material for thermal energy storage, Sol. Energy Mater. Sol. Cells. 120 (2014) 536–542. doi:10.1016/j.solmat.2013.09.035.

[114] A. Sarı, C. Alkan, A. Karaipekli, Preparation, characterization and thermal

properties of PMMA/n-heptadecane microcapsules as novel solid–liquid microPCM for thermal energy storage, Appl. Energy. 87 (2010) 1529–1534. doi:10.1016/j.apenergy.2009.10.011.

[115] Y. Chen, L. Zhao, Y. Shi, Preparation of polyvinyl chloride capsules for encapsulation of paraffin by coating multiple organic/inorganic layers, J. Taiwan Inst. Chem. Eng. 77 (2017) 177–186. doi:https://doi.org/10.1016/j.jtice.2017.04.046.

[116] Y. Wang, S. Ge, B. Huang, Z. Zheng, A simple route to PVC encapsulated Na2SO4·10H2O nano/micro-composite with excellent energy storage performance, Mater. Chem. Phys. 223 (2019) 723–726. doi:https://doi.org/10.1016/j.matchemphys.2018.11.075.

[117] S. Yu, X. Wang, D. Wu, Microencapsulation of n-octadecane phase change material with calcium carbonate shell for enhancement of thermal conductivity and serving durability: Synthesis, microstructure, and performance evaluation, Appl. Energy. 114 (2014) 632–643. doi:10.1016/j.apenergy.2013.10.029.

[118] P.K. Singh Rathore, S.K. Shukla, N.K. Gupta, POTENTIAL OF MICROENCAPSULATED PCM FOR ENERGY SAVINGS IN BUILDINGS: A CRITICAL REVIEW, Sustain. Cities Soc. (2019) 101884. doi:https://doi.org/10.1016/j.scs.2019.101884.

[119] S. Yu, X. Wang, D. Wu, Self-Assembly Synthesis of Microencapsulated n-Eicosane Phase-Change Materials with Crystalline-Phase-Controllable Calcium Carbonate Shell, Energy & Fuels. 28 (2014) 3519–3529. doi:10.1021/ef5005539.

[120] Y. Fang, T. Zou, X. Liang, S. Wang, X. Liu, X. Gao, Z. Zhang, Self-assembly Synthesis and Properties of Microencapsulated n-Tetradecane Phase Change Materials with a Calcium Carbonate Shell for Cold Energy Storage, ACS Sustain. Chem. Eng. 5 (2017) 3074–3080. doi:10.1021/acssuschemeng.6b02758.

[121] T. Wang, S. Wang, R. Luo, C. Zhu, T. Akiyama, Z. Zhang, Microencapsulation of phase change materials with binary cores and calcium carbonate shell for thermal energy storage, Appl. Energy. 171 (2016) 113–119. doi:https://doi.org/10.1016/j.apenergy.2016.03.037.

[122] Z. Jiang, W. Yang, F. He, C. Xie, J. Fan, J. Wu, K. Zhang, Microencapsulated Paraffin Phase-Change Material with Calcium Carbonate Shell for Thermal Energy Storage and Solar-Thermal Conversion, Langmuir. 34 (2018) 14254–14264. doi:10.1021/acs.langmuir.8b03084.

[123] J. Shi, X. Wu, R. Sun, B. Ban, J. Li, J. Chen, Synthesis and performance evaluation of paraffin microcapsules with calcium carbonate shell modulated by different anionic surfactants for thermal energy storage, Colloids Surfaces A Physicochem. Eng. Asp. 571 (2019) 36–43. doi:https://doi.org/10.1016/j.colsurfa.2019.03.029.

[124] H. Zhang, X. Wang, D. Wu, Silica encapsulation of n-octadecane via sol–gel process: A novel microencapsulated phase-change material with enhanced thermal conductivity and performance, J. Colloid Interface Sci. 343 (2010) 246–255. doi:http://dx.doi.org/10.1016/j.jcis.2009.11.036.

[125] G. Fang, Z. Chen, H. Li, Synthesis and properties of microencapsulated paraffin

composites with SiO2 shell as thermal energy storage materials, Chem. Eng. J. 163 (2010) 154–159. doi:10.1016/j.cej.2010.07.054.

[126] F. He, X. Wang, D. Wu, Phase-change characteristics and thermal performance of form-stable n-alkanes/silica composite phase change materials fabricated by sodium silicate precursor, Renew. Energy. 74 (2015) 689–698. doi:http://dx.doi.org/10.1016/j.renene.2014.08.079.

[127] F. He, X. Wang, D. Wu, New approach for sol–gel synthesis of microencapsulated n-octadecane phase change material with silica wall using sodium silicate precursor, Energy. 67 (2014) 223–233. doi:http://dx.doi.org/10.1016/j.energy.2013.11.088.

[128] A. Sarı, C. Alkan, A. Karaipekli, O. Uzun, Microencapsulated n-octacosane as phase change material for thermal energy storage, Sol. Energy. 83 (2009) 1757–1763. doi:http://dx.doi.org/10.1016/j.solener.2009.05.008.

[129] A. Sarı, C. Alkan, A.N. Özcan, Synthesis and characterization of micro/nano capsules of PMMA/capric–stearic acid eutectic mixture for low temperature-thermal energy storage in buildings, Energy Build. 90 (2015) 106–113. doi:http://dx.doi.org/10.1016/j.enbuild.2015.01.013.

[130] A. Sarı, C. Alkan, C. Bilgin, Micro/nano encapsulation of some paraffin eutectic mixtures with poly(methyl methacrylate) shell: Preparation, characterization and latent heat thermal energy storage properties, Appl. Energy. 136 (2014) 217–227. doi:http://dx.doi.org/10.1016/j.apenergy.2014.09.047.

[131] T. Zhang, M. Chen, Y. Zhang, Y. Wang, Microencapsulation of stearic acid with polymethylmethacrylate using iron (III) chloride as photo-initiator for thermal energy storage, Chinese J. Chem. Eng. 25 (2017) 1524–1532. doi:https://doi.org/10.1016/j.cjche.2017.04.013.

[132] J.-F. Su, L.-X. Wang, L. Ren, Z. Huang, X.-W. Meng, Preparation and characterization of polyurethane microcapsules containing n-octadecane with styrene-maleic anhydride as a surfactant by interfacial polycondensation, J. Appl. Polym. Sci. 102 (2006) 4996–5006. doi:10.1002/app.25001.

[133] S. Lu, T. Shen, J. Xing, Q. Song, J. Shao, J. Zhang, C. Xin, Preparation and characterization of cross-linked polyurethane shell microencapsulated phase change materials by interfacial polymerization, Mater. Lett. 211 (2018) 36–39. doi:https://doi.org/10.1016/j.matlet.2017.09.074.

[134] L.Y. Wang, P.S. Tsai, Y.M. Yang, Preparation of silica microspheres encapsulating phase-change material by sol-gel method in O/W emulsion., J. Microencapsul. 23 (2006) 3–14. doi:10.1080/02652040500286045.

[135] M. Li, Z. Wu, J. Tan, Properties of form-stable paraffin/silicon dioxide/expanded graphite phase change composites prepared by sol–gel method, Appl. Energy. 92 (2012) 456–461. doi:10.1016/j.apenergy.2011.11.018.

[136] M. Li, M. Chen, Z. Wu, Enhancement in thermal property and mechanical property of phase change microcapsule with modified carbon nanotube, Appl. Energy. 127 (2014) 166–171. doi:10.1016/j.apenergy.2014.04.029.

[137] H. Zhang, S. Sun, X. Wang, D. Wu, Fabrication of microencapsulated phase

change materials based on n-octadecane core and silica shell through interfacial polycondensation, Colloids Surfaces A Physicochem. Eng. Asp. 389 (2011) 104–117. doi:http://dx.doi.org/10.1016/j.colsurfa.2011.08.043.

[138] L. Cao, F. Tang, G. Fang, Synthesis and characterization of microencapsulated paraffin with titanium dioxide shell as shape-stabilized thermal energy storage materials in buildings, Energy Build. 72 (2014) 31–37. doi:10.1016/j.enbuild.2013.12.028.

[139] L. Cao, F. Tang, G. Fang, Preparation and characteristics of microencapsulated palmitic acid with TiO2 shell as shape-stabilized thermal energy storage materials, Sol. Energy Mater. Sol. Cells. 123 (2014) 183–188. doi:10.1016/j.solmat.2014.01.023.

[140] L. Pan, Q. Tao, S. Zhang, S. Wang, J. Zhang, S. Wang, Z. Wang, Z. Zhang, Preparation, characterization and thermal properties of micro-encapsulated phase change materials, Sol. Energy Mater. Sol. Cells. 98 (2012) 66–70. doi:10.1016/j.solmat.2011.09.020.

[141] a. M. Borreguero, J.L. Valverde, J.F. Rodríguez, a. H. Barber, J.J. Cubillo, M. Carmona, Synthesis and characterization of microcapsules containing Rubitherm®RT27 obtained by spray drying, Chem. Eng. J. 166 (2011) 384–390. doi:10.1016/j.cej.2010.10.055.

[142] Y. Zhang, X. Zheng, H. Wang, Q. Du, Encapsulated phase change materials stabilized by modified graphene oxide, J. Mater. Chem. A. 2 (2014) 5304. doi:10.1039/c3ta15242a.

[143] T. Wang, S. Wang, L. Geng, Y. Fang, Enhancement on thermal properties of paraffin/calcium carbonate phase change microcapsules with carbon network, Appl. Energy. 179 (2016) 601–608. doi:https://doi.org/10.1016/j.apenergy.2016.07.026.

[144] T. Wang, Y. Jiang, J. Huang, S. Wang, High thermal conductive paraffin/calcium carbonate phase change microcapsules based composites with different carbon network, Appl. Energy. 218 (2018) 184–191. doi:https://doi.org/10.1016/j.apenergy.2018.02.108.

[145] Z. Jiang, W. Yang, F. He, C. Xie, J. Fan, J. Wu, K. Zhang, Modified Phase Change Microcapsules with Calcium Carbonate and Graphene Oxide Shells for Enhanced Energy Storage and Leakage Prevention, ACS Sustain. Chem. Eng. 6 (2018) 5182–5191. doi:10.1021/acssuschemeng.7b04834.

[146] Y. Fang, X. Liu, X. Liang, H. Liu, X. Gao, Z. Zhang, Ultrasonic synthesis and characterization of polystyrene/n-dotriacontane composite nanoencapsulated phase change material for thermal energy storage, Appl. Energy. 132 (2014) 551–556. doi:http://dx.doi.org/10.1016/j.apenergy.2014.06.056.

[147] Y. Konuklu, H.O. Paksoy, M. Unal, Nanoencapsulation of n-alkanes with poly(styrene-co-ethylacrylate) shells for thermal energy storage, Appl. Energy. 150 (2015) 335–340. doi:http://dx.doi.org/10.1016/j.apenergy.2014.11.066.

[148] P.K.S. Rathore, S.K. Shukla, Potential of macroencapsulated PCM for thermal energy storage in buildings: A comprehensive review, Constr. Build. Mater. 225 (2019) 723–744. doi:https://doi.org/10.1016/j.conbuildmat.2019.07.221.

[149] Y. Chen, S. Zhang, Q. Zhang, Y. Chen, Y. Zhang, Composite phase change materials prepared by encapsuling paraffin in PVC macrocapsules, Thermochim. Acta. 578 (2014) 10–14. doi:http://dx.doi.org/10.1016/j.tca.2013.12.018.

[150] R. Vicente, T. Silva, Brick masonry walls with PCM macrocapsules: An experimental approach, Appl. Therm. Eng. 67 (2014) 24–34. doi:http://dx.doi.org/10.1016/j.applthermaleng.2014.02.069.

[151] R. Saxena, D. Rakshit, S.C. Kaushik, Phase change material (PCM) incorporated bricks for energy conservation in composite climate: A sustainable building solution, Sol. Energy. 183 (2019) 276–284. doi:https://doi.org/10.1016/j.solener.2019.03.035.

[152] T. Silva, R. Vicente, F. Rodrigues, A. Samagaio, C. Cardoso, Development of a window shutter with phase change materials: Full scale outdoor experimental approach, Energy Build. 88 (2015) 110–121. doi:http://dx.doi.org/10.1016/j.enbuild.2014.11.053.

[153] E. Meng, H. Yu, B. Zhou, Study of the thermal behavior of the composite phase change material (PCM) room in summer and winter, Appl. Therm. Eng. 126 (2017) 212–225. doi:https://doi.org/10.1016/j.applthermaleng.2017.07.110.

[154] M.. Z. Medina D., A Comparative Heat Transfer Examination of Structural Insulated Panels (SIPs) With and Without Phase Change Materials (PCMs) Using a Dynamic Wall Simulator., (2008).

[155] J. Wei, Y. Kawaguchi, S. Hirano, H. Takeuchi, Study on a PCM heat storage system for rapid heat supply, Appl. Therm. Eng. 25 (2005) 2903–2920. doi:http://dx.doi.org/10.1016/j.applthermaleng.2005.02.014.

[156] X. Jin, M.A. Medina, X. Zhang, On the importance of the location of PCMs in building walls for enhanced thermal performance, Appl. Energy. 106 (2013) 72–78. doi:http://dx.doi.org/10.1016/j.apenergy.2012.12.079.

[157] Y. Zheng, W. Zhao, J.C. Sabol, K. Tuzla, S. Neti, A. Oztekin, J.C. Chen, Encapsulated phase change materials for energy storage – Characterization by calorimetry, Sol. Energy. 87 (2013) 117–126. doi:10.1016/j.solener.2012.10.003.

[158] A.K. Mathur, R.B. Kasetty, Thermal energy storage system comprising encapsulated phase change material, (2012). http://www.google.com/patents/US20120018116.

[159] N. Maruoka, T. Akiyama, Thermal stress analysis of PCM encapsulation for heat recovery of high temperature waste heat, J. Chem. Eng. Japan. 36 (2003) 794–798. doi:10.1252/jcej.36.794.

[160] N. Maruoka, K. Sato, J. Yagi, T. Akiyama, Development of PCM for Recovering High Temperature Waste Heat and Utilization for Producing Hydrogen by Reforming Reaction of Methane, ISIJ Int. 42 (2002) 215–219. doi:10.2355/isijinternational.42.215.

[161] G. Zhang, J. Li, Y. Chen, H. Xiang, B. Ma, Z. Xu, X. Ma, Encapsulation of copper-based phase change materials for high temperature thermal energy storage, Sol. Energy Mater. Sol. Cells. 128 (2014) 131–137.

doi:http://dx.doi.org/10.1016/j.solmat.2014.05.012.

[162] W. Zhao, Y. Zheng, J.C. Sabol, K. Tuzla, S. Neti, A. Oztekin, J.C. Chen, High temperature calorimetry and use of magnesium chloride for thermal energy storage, Renew. Energy. 50 (2013) 988–993. doi:http://dx.doi.org/10.1016/j.renene.2012.08.036.

[163] E.M. Alawadhi, Thermal analysis of a building brick containing phase change material, Energy Build. 40 (2008) 351–357. doi:10.1016/j.enbuild.2007.03.001.

[164] A. Castell, I. Martorell, M. Medrano, G. Pérez, L.F. Cabeza, Experimental study of using PCM in brick constructive solutions for passive cooling, Energy Build. 42 (2010) 534–540. doi:10.1016/j.enbuild.2009.10.022.

[165] T. Silva, R. Vicente, N. Soares, V. Ferreira, Experimental testing and numerical modelling of masonry wall solution with PCM incorporation: A passive construction solution, Energy Build. 49 (2012) 235–245. doi:10.1016/j.enbuild.2012.02.010.

[166] J.M. Marín, B. Zalba, L.F. Cabeza, H. Mehling, Improvement of a thermal energy storage using plates with paraffin–graphite composite, Int. J. Heat Mass Transf. 48 (2005) 2561–2570. doi:http://dx.doi.org/10.1016/j.ijheatmasstransfer.2004.11.027.

[167] N.H.S. Tay, M. Belusko, F. Bruno, Designing a PCM storage system using the effectiveness-number of transfer units method in low energy cooling of buildings, Energy Build. 50 (2012) 234–242. doi:http://dx.doi.org/10.1016/j.enbuild.2012.03.041.

[168] I. Cerón, J. Neila, M. Khayet, Experimental tile with phase change materials (PCM) for building use, Energy Build. 43 (2011) 1869–1874. doi:10.1016/j.enbuild.2011.03.031.

[169] L. Royon, L. Karim, A. Bontemps, Thermal energy storage and release of a new component with PCM for integration in floors for thermal management of buildings, Energy Build. 63 (2013) 29–35. doi:http://dx.doi.org/10.1016/j.enbuild.2013.03.042.

[170] J.C. Kurnia, A.P. Sasmito, S. V Jangam, A.S. Mujumdar, Improved design for heat transfer performance of a novel phase change material (PCM) thermal energy storage (TES), Appl. Therm. Eng. 50 (2013) 896–907. doi:http://dx.doi.org/10.1016/j.applthermaleng.2012.08.015.

[171] S. Álvarez, L.F. Cabeza, A. Ruiz-Pardo, A. Castell, J.A. Tenorio, Building integration of PCM for natural cooling of buildings, Appl. Energy. 109 (2013) 514–522. doi:http://dx.doi.org/10.1016/j.apenergy.2013.01.080.

[172] M. Koschenz, B. Lehmann, Development of a thermally activated ceiling panel with PCM for application in lightweight and retrofitted buildings, Energy Build. 36 (2004) 567–578. doi:10.1016/j.enbuild.2004.01.029.

[173] A. de Gracia, L. Navarro, A. Castell, Á. Ruiz-Pardo, S. Álvarez, L.F. Cabeza, Thermal analysis of a ventilated facade with PCM for cooling applications, Energy Build. 65 (2013) 508–515. doi:http://dx.doi.org/10.1016/j.enbuild.2013.06.032.

[174] G. Diarce, A. Urresti, A. García-Romero, A. Delgado, A. Erkoreka, C. Escudero, Á.

Campos-Celador, Ventilated active façades with PCM, Appl. Energy. 109 (2013) 530–537. doi:http://dx.doi.org/10.1016/j.apenergy.2013.01.032.

[175] C. Amaral, R. Vicente, P.A.A.P. Marques, A. Barros-Timmons, Phase change materials and carbon nanostructures for thermal energy storage: A literature review, Renew. Sustain. Energy Rev. 79 (2017). doi:10.1016/j.rser.2017.05.093.

[176] C. Amaral, R. Vicente, V.M. Ferreira, T. Silva, Polyurethane foams with microencapsulated phase change material: Comparative analysis of thermal conductivity characterization approaches, Energy Build. 153 (2017). doi:10.1016/j.enbuild.2017.08.019.

[177] B. Li, T. Liu, L. Hu, Y. Wang, L. Gao, Fabrication and Properties of Microencapsulated Paraffin@SiO2 Phase Change Composite for Thermal Energy Storage, ACS Sustain. Chem. Eng. 1 (2013) 374–380. doi:10.1021/sc300082m.

[178] N.S. Dhaidan, J.M. Khodadadi, Improved performance of latent heat energy storage systems utilizing high thermal conductivity fins: A review, J. Renew. Sustain. Energy. 9 (2017) 034103. doi:10.1063/1.4989738.

[179] S. Jegadheeswaran, S.D. Pohekar, Performance enhancement in latent heat thermal storage system: A review, Renew. Sustain. Energy Rev. 13 (2009) 2225–2244. doi:https://doi.org/10.1016/j.rser.2009.06.024.

[180] Y. Du, Y. Ding, Towards improving charge/discharge rate of latent heat thermal energy storage (LHTES) by embedding metal foams in phase change materials (PCMs), Chem. Eng. Process. Process Intensif. 108 (2016) 181–188. doi:https://doi.org/10.1016/j.cep.2016.08.003.

[181] T. Klemm, A. Hassabou, A. Abdallah, O. Andersen, Thermal energy storage with phase change materials to increase the efficiency of solar photovoltaic modules, Energy Procedia. 135 (2017) 193–202. doi:https://doi.org/10.1016/j.egypro.2017.09.502.

[182] C. Liu, Y. Long, J. Xie, X. Xie, Towards green polyurethane foams via renewable castor oil-derived polyol and carbon dioxide releasing blowing agents from alkylated polyethylenimines, Polymer (Guildf). 116 (2017) 240–250. doi:https://doi.org/10.1016/j.polymer.2017.03.079.

[183] C. Amaral, R. Vicente, J. Eisenblätter, P.A.A.P. Marques, Thermal characterization of polyurethane foams with phase change material, Cienc. e Tecnol. Dos Mater. 29 (2017). doi:10.1016/j.ctmat.2016.06.015.

[184] N. V Gama, R. Silva, F. Mohseni, A. Davarpanah, V.S. Amaral, A. Ferreira, A. Barros-Timmons, Enhancement of physical and reaction to fire properties of crude glycerol polyurethane foams filled with expanded graphite, Polym. Test. 69 (2018) 199–207. doi:https://doi.org/10.1016/j.polymertesting.2018.05.012.

[185] M. You, X. Zhang, X. Wang, L. Zhang, W. Wen, Effects of type and contents of microencapsuled n-alkanes on properties of soft polyurethane foams, Thermochim. Acta. 500 (2010) 69–75. doi:https://doi.org/10.1016/j.tca.2009.12.013.

[186] C. Yang, L. Fischer, S. Maranda, J. Worlitschek, Rigid polyurethane foams incorporated with phase change materials: A state-of-the-art review and future

research pathways, Energy Build. 87 (2015) 25–36. doi:https://doi.org/10.1016/j.enbuild.2014.10.075.

[187] N. Gama, C. Amaral, T. Silva, R. Vicente, J. Coutinho, A. Barros-Timmons, A. Ferreira, N.V. Gama, C. Amaral, T. Silva, R. Vicente, J.A.P. Coutinho, A. Barros-Timmons, A. Ferreira, Thermal Energy Storage and Mechanical Performance of Crude Glycerol Polyurethane Composite Foams Containing Phase Change Materials and Expandable Graphite, Materials (Basel). 11 (2018) 1896. doi:10.3390/ma11101896.

[188] O.D. Neikov, N.A. Yefimov, Chapter 1 - Powder Characterization and Testing, in: O. Neikov, S. Naboychenko, N.V.B.T.-H. of N.-F.M.P. (Second E. Yefimov (Eds.), Elsevier, Oxford, 2019: pp. 3–62. doi:https://doi.org/10.1016/B978-0-08-100543-9.00001-4.

[189] F.J. Gomez, C. Amaral, R. Vicente, Experimental and numerical analysis on thermal performance of multifunctional façade containing PCM, Bern, 2017.

[190] S.E. Gustafsson, Transient plane source techniques for thermal conductivity and thermal diffusivity measurements of solid materials, Rev. Sci. Instrum. 62 (1991) 797–804. doi:10.1063/1.1142087.

[191] ISO 22007-2: Plastics - Determination of thermal conductivity and thermal diffusivity - Part 2: Transient plane heat source (hot disc) method, (2015). https://www.iso.org/standard/61190.html.

[192] A. Ricklefs, A.M. Thiele, G. Falzone, G. Sant, L. Pilon, Thermal conductivity of cementitious composites containing microencapsulated phase change materials, Int. J. Heat Mass Transf. 104 (2017) 71–82. doi:https://doi.org/10.1016/j.ijheatmasstransfer.2016.08.013.

[193] BASF, Micronal® PCM: Intelligent Temperatura Management for Buildings, (2008). www.micronal.de.

[194] J. Giro-Paloma, G. Oncins, C. Barreneche, M. Martínez, A.I. Fernández, L.F. Cabeza, Physico-chemical and mechanical properties of microencapsulated phase change material, Appl. Energy. 109 (2013) 441–448. doi:https://doi.org/10.1016/j.apenergy.2012.11.007.

[195] A.M. Borreguero, J.F. Rodríguez, J.L. Valverde, R. Arevalo, T. Peijs, M. Carmona, Characterization of rigid polyurethane foams containing microencapsulated Rubitherm® RT27: catalyst effect. Part II, J. Mater. Sci. 46 (2011) 347–356. doi:10.1007/s10853-010-4824-6.

[196] A.M. Borreguero, J.L. Valverde, T. Peijs, J.F. Rodríguez, M. Carmona, Characterization of rigid polyurethane foams containing microencapsulated Rubitherm® RT27. Part I, J. Mater. Sci. 45 (2010) 4462–4469. doi:10.1007/s10853-010-4529-x.

[197] R. Verdejo, R. Stämpfli, M. Alvarez-Lainez, S. Mourad, M.A. Rodriguez-Perez, P.A. Brühwiler, M. Shaffer, Enhanced acoustic damping in flexible polyurethane foams filled with carbon nanotubes, Compos. Sci. Technol. 69 (2009) 1564–1569. doi:https://doi.org/10.1016/j.compscitech.2008.07.003.

[198] N.V. Gama, C. Amaral, T. Silva, R. Vicente, J.A.P. Coutinho, A. Barros-Timmons,

A. Ferreira, Thermal energy storage and mechanical performance of crude glycerol polyurethane composite foams containing phase change materials and expandable graphite, Materials (Basel). (2018). doi:10.3390/ma11101896.

[199] X. Wang, H. Yu, L. Li, M. Zhao, Research on temperature dependent effective thermal conductivity of composite-phase change materials (PCMs) wall based on steady-state method in a thermal chamber, Energy Build. 126 (2016) 408–414. doi:https://doi.org/10.1016/j.enbuild.2016.05.058.

[200] A. Demharter, Polyurethane rigid foam, a proven thermal insulating material for applications between +130°C and −196°C, Cryogenics (Guildf). 38 (1998) 113–117. doi:https://doi.org/10.1016/S0011-2275(97)00120-3.

[201] C.P.D. Bryant G. Yvonne, Moldable foam insole with reversible enhanced thermal storage properties, 1996.

[202] M.L. Nuckols, Analytical modeling of a diver dry suit enhanced with micro-encapsulated phase change materials, Ocean Eng. 26 (1999) 547–564. doi:https://doi.org/10.1016/S0029-8018(98)00001-8.

[203] F. Asdrubali, G. Baldinelli, Thermal transmittance measurements with the hot box method: Calibration, experimental procedures, and uncertainty analyses of three different approaches, Energy Build. 43 (2011) 1618–1626. doi:http://dx.doi.org/10.1016/j.enbuild.2011.03.005.

[204] S.A. Al-Ajlan, Measurements of thermal properties of insulation materials by using transient plane source technique, Appl. Therm. Eng. 26 (2006) 2184–2191. doi:https://doi.org/10.1016/j.applthermaleng.2006.04.006.

[205] H. Zhang, W.-Z. Fang, Y.-M. Li, W.-Q. Tao, Experimental study of the thermal conductivity of polyurethane foams, Appl. Therm. Eng. 115 (2017) 528–538. doi:https://doi.org/10.1016/j.applthermaleng.2016.12.057.

[206] S. Estravís, J. Tirado-Mediavilla, M. Santiago-Calvo, J.L. Ruiz-Herrero, F. Villafañe, M.Á. Rodríguez-Pérez, Rigid polyurethane foams with infused nanoclays: Relationship between cellular structure and thermal conductivity, Eur. Polym. J. 80 (2016) 1–15. doi:https://doi.org/10.1016/j.eurpolymj.2016.04.026.

[207] N.E. Marcovich, M. Kurańska, A. Prociak, E. Malewska, K. Kulpa, Open cell semi-rigid polyurethane foams synthesized using palm oil-based bio-polyol, Ind. Crops Prod. 102 (2017) 88–96. doi:https://doi.org/10.1016/j.indcrop.2017.03.025.

[208] C. Buratti, E. Belloni, L. Lunghi, M. Barbanera, Thermal Conductivity Measurements By Means of a New `Small Hot-Box' Apparatus: Manufacturing, Calibration and Preliminary Experimental Tests on Different Materials, Int. J. Thermophys. 37 (2016) 47. doi:10.1007/s10765-016-2052-2.

[209] Y. He, Rapid thermal conductivity measurement with a hot disk sensor: Part 1. Theoretical considerations, Thermochim. Acta. 436 (2005) 122–129. doi:https://doi.org/10.1016/j.tca.2005.06.026.

[210] A. Eddhahak-Ouni, S. Drissi, J. Colin, J. Neji, S. Care, Experimental and multi-scale analysis of the thermal properties of Portland cement concretes embedded with microencapsulated Phase Change Materials (PCMs), Appl. Therm. Eng. 64 (2014) 32–39. doi:https://doi.org/10.1016/j.applthermaleng.2013.11.050.

[211] H. Ye, L. Long, H. Zhang, R. Zou, The performance evaluation of shape-stabilized phase change materials in building applications using energy saving index, Appl. Energy. 113 (2014) 1118–1126. doi:https://doi.org/10.1016/j.apenergy.2013.08.067.

[212] X. Meng, Y. Gao, Y. Wang, B. Yan, W. Zhang, E. Long, Feasibility experiment on the simple hot box-heat flow meter method and the optimization based on simulation reproduction, Appl. Therm. Eng. 83 (2015) 48–56. doi:https://doi.org/10.1016/j.applthermaleng.2015.03.010.

[213] C. Guattari, L. Evangelisti, P. Gori, F. Asdrubali, Influence of internal heat sources on thermal resistance evaluation through the heat flow meter method, Energy Build. 135 (2017) 187–200. doi:https://doi.org/10.1016/j.enbuild.2016.11.045.

[214] European Standard EN ISO 8990 - Thermal insulation, determination of steady-state thermal transmission properties, calibrated and guarded hot box, (1994).

[215] T. Kobari, J. Okajima, A. Komiya, S. Maruyama, Development of guarded hot plate apparatus utilizing Peltier module for precise thermal conductivity measurement of insulation materials, Int. J. Heat Mass Transf. 91 (2015) 1157–1166. doi:https://doi.org/10.1016/j.ijheatmasstransfer.2015.08.044.

[216] C.S. Sanjaya, T.-H. Wee, T. Tamilselvan, Regression analysis estimation of thermal conductivity using guarded-hot-plate apparatus, Appl. Therm. Eng. 31 (2011) 1566–1575. doi:https://doi.org/10.1016/j.applthermaleng.2011.01.007.

[217] M.H. Rausch, K. Krzeminski, A. Leipertz, A.P. Fröba, A new guarded parallel-plate instrument for the measurement of the thermal conductivity of fluids and solids, Int. J. Heat Mass Transf. 58 (2013) 610–618. doi:https://doi.org/10.1016/j.ijheatmasstransfer.2012.11.069.

[218] Standard: DIN 52612-2, Tesing of thermal insulating materials; determination of thermal conductivity by means of the guarded hot plate apparatus; conversion of the measured values for building applications, Dtsch. Inst. Fur Normung E.V. (German Natl. Stand. (1984).

[219] E. Solórzano, J.A. Reglero, M.A. Rodríguez-Pérez, D. Lehmhus, M. Wichmann, J.A. de Saja, An experimental study on the thermal conductivity of aluminium foams by using the transient plane source method, Int. J. Heat Mass Transf. 51 (2008) 6259–6267. doi:https://doi.org/10.1016/j.ijheatmasstransfer.2007.11.062.

[220] M.C. Peel, B.L. Finlayson, T.A. McMahon, Updated world map of the Köppen-Geiger climate classification, Hydrol. Earth Syst. Sci. 11 (2007) 1633–1644. doi:10.5194/hess-11-1633-2007.

[221] F. Giorgi, P. Lionello, Climate change projections for the Mediterranean region, Glob. Planet. Change. 63 (2008) 90–104. doi:https://doi.org/10.1016/j.gloplacha.2007.09.005.

[222] S. Somot, F. Sevault, M. Déqué, M. Crépon, 1st century climate change scenario for the Mediterranean using a coupled atmosphere–ocean regional climate model, Glob. Planet. Change. 63 (2) (2008) 112–126.

[223] E. Hertig, J. Jacobeit, Downscaling future climate change: Temperature scenarios for the Mediterranean area, Glob. Planet. Change. 63 (2008) 127–131.

doi:https://doi.org/10.1016/j.gloplacha.2007.09.003.

[224] M. Costa, D. Buddhi, A. Oliva, Numerical simulation of a latent heat thermal energy storage system with enhanced heat conduction, Energy Convers. Manag. 39 (1998) 319–330. doi:https://doi.org/10.1016/S0196-8904(96)00193-8.

[225] S.A. Mohamed, F.A. Al-Sulaiman, N.I. Ibrahim, M.H. Zahir, A. Al-Ahmed, R. Saidur, B.S. Yılbaş, A.Z. Sahin, A review on current status and challenges of inorganic phase change materials for thermal energy storage systems, Renew. Sustain. Energy Rev. 70 (2017) 1072–1089. doi:https://doi.org/10.1016/j.rser.2016.12.012.

[226] P. Glouannec, B. Michel, G. Delamarre, Y. Grohens, Experimental and numerical study of heat transfer across insulation wall of a refrigerated integral panel van, Appl. Therm. Eng. 73 (2014) 196–204. doi:https://doi.org/10.1016/j.applthermaleng.2014.07.044.

[227] A. Tinti, A. Tarzia, A. Passaro, R. Angiuli, Thermographic analysis of polyurethane foams integrated with phase change materials designed for dynamic thermal insulation in refrigerated transport, Appl. Therm. Eng. 70 (2014) 201–210. doi:https://doi.org/10.1016/j.applthermaleng.2014.05.003.

[228] F. Souayfane, F. Fardoun, P.-H. Biwole, Phase change materials (PCM) for cooling applications in buildings: A review, Energy Build. 129 (2016) 396–431. doi:https://doi.org/10.1016/j.enbuild.2016.04.006.

[229] B. Michel, P. Glouannec, A. Fuentes, P. Chauvelon, Experimental and numerical study of insulation walls containing a composite layer of PU-PCM and dedicated to refrigerated vehicle, Appl. Therm. Eng. 116 (2017) 382–391. doi:https://doi.org/10.1016/j.applthermaleng.2016.12.117.

[230] Z. Hu, W. He, J. Ji, S. Zhang, A review on the application of Trombe wall system in buildings, Renew. Sustain. Energy Rev. 70 (2017) 976–987. doi:https://doi.org/10.1016/j.rser.2016.12.003.

[231] M. Kenisarin, K. Mahkamov, Passive thermal control in residential buildings using phase change materials, Renew. Sustain. Energy Rev. 55 (2016) 371–398. doi:https://doi.org/10.1016/j.rser.2015.10.128.

[232] X. Wang, Y. Zhang, W. Xiao, R. Zeng, Q. Zhang, H. Di, Review on thermal performance of phase change energy storage building envelope, Chinese Sci. Bull. 54 (2009) 920–928. doi:10.1007/s11434-009-0120-8.

[233] D.N. Nkwetta, F. Haghighat, Thermal energy storage with phase change material—A state-of-the art review, Sustain. Cities Soc. 10 (2014) 87–100. doi:https://doi.org/10.1016/j.scs.2013.05.007.

[234] T.-C. Ling, C.-S. Poon, Use of phase change materials for thermal energy storage in concrete: An overview, Constr. Build. Mater. 46 (2013) 55–62. doi:https://doi.org/10.1016/j.conbuildmat.2013.04.031.

[235] A. Fateh, F. Klinker, M. Brütting, H. Weinläder, F. Devia, Numerical and experimental investigation of an insulation layer with phase change materials (PCMs), Energy Build. 153 (2017) 231–240. doi:https://doi.org/10.1016/j.enbuild.2017.08.007.

[236] K.O. Lee, M.A. Medina, X. Sun, On the use of plug-and-play walls (PPW) for evaluating thermal enhancement technologies for building enclosures: Evaluation of a thin phase change material (PCM) layer, Energy Build. 86 (2015) 86–92. doi:https://doi.org/10.1016/j.enbuild.2014.10.020.

[237] X. Jin, M.A. Medina, X. Zhang, Numerical analysis for the optimal location of a thin PCM layer in frame walls, Appl. Therm. Eng. 103 (2016) 1057–1063. doi:https://doi.org/10.1016/j.applthermaleng.2016.04.056.

[238] N.P. Sharifi, A.A.N. Shaikh, A.R. Sakulich, Application of phase change materials in gypsum boards to meet building energy conservation goals, Energy Build. 138 (2017) 455–467. doi:https://doi.org/10.1016/j.enbuild.2016.12.046.

[239] F. Boudali Errebai, S. Chikh, L. Derradji, Experimental and numerical investigation for improving the thermal performance of a microencapsulated phase change material plasterboard, Energy Convers. Manag. 174 (2018) 309–321. doi:https://doi.org/10.1016/j.enconman.2018.08.052.

[240] M.A. Izquierdo-Barrientos, J.F. Belmonte, D. Rodríguez-Sánchez, A.E. Molina, J.A. Almendros-Ibáñez, A numerical study of external building walls containing phase change materials (PCM), Appl. Therm. Eng. 47 (2012) 73–85. doi:https://doi.org/10.1016/j.applthermaleng.2012.02.038.

[241] J. Cipriano, G. Mor, D. Chemisana, D. Pérez, G. Gamboa, X. Cipriano, Evaluation of a multi-stage guided search approach for the calibration of building energy simulation models, Energy Build. 87 (2015) 370–385. doi:https://doi.org/10.1016/j.enbuild.2014.08.052.

[242] D. Feldman, M.M. Shapiro, P. Fazio, A heat storage module with a polymer structural matrix, Polym. Eng. Sci. 25 (1985) 406–411. doi:10.1002/pen.760250705.

[243] X. Jin, J. Li, P. Xue, M. Jia, Preparation and characterization of PVC-based form-stable phase change materials, Sol. Energy Mater. Sol. Cells. 130 (2014) 435–441. doi:https://doi.org/10.1016/j.solmat.2014.07.013.

[244] N. Gama, R. Santos, B. Godinho, R. Silva, A. Ferreira, Triacetin as a Secondary PVC Plasticizer, J. Polym. Environ. 27 (2019) 1294–1301. doi:10.1007/s10924-019-01432-z.

[245] N. V Gama, R. Santos, B. Godinho, R. Silva, A. Ferreira, Methyl Acetyl Ricinoleate as Polyvinyl Chloride Plasticizer, J. Polym. Environ. 27 (2019) 703–709. doi:10.1007/s10924-019-01383-5.

[246] Y. Zhang, S. Zheng, S. Zhu, J. Ma, Z. Sun, M. Farid, Evaluation of paraffin infiltrated in various porous silica matrices as shape-stabilized phase change materials for thermal energy storage, Energy Convers. Manag. 171 (2018) 361–370. doi:https://doi.org/10.1016/j.enconman.2018.06.002.